Cloning, expression, purification, biochemical, functional and structure characterization of pectin methylesterase (*Ct*PME) from family 8 Carbohydrate Esterase (CE8) from *Clostridium thermocellum* ATCC 27405 and its applications in textile and food industry

PhD Thesis

by

Vikky Rajulapati

September 2019

DEPARTMENT OF BIOSCIENCES AND BIOENGINEERING

INDIAN INSTITUTE OF TECHNOLOGY GUWAHATI

GUWAHATI – 781039, ASSAM, INDIA

Cloning, expression, purification, biochemical, functional and structure characterization of pectin methylesterase (*Ct*PME) from family 8 Carbohydrate Esterase (CE8) from *Clostridium thermocellum* ATCC 27405 and its applications in textile and food industry

A Thesis

Submitted in partial fulfillment of the requirements for the Degree of

Doctor of Philosophy

by

Vikky Rajulapati

Under supervision of

Professor Arun Goyal

September 2019

DEPARTMENT OF BIOSCIENCES AND BIOENGINEERING
INDIAN INSTITUTE OF TECHNOLOGY GUWAHATI
GUWAHATI – 781039, ASSAM, INDIA

INDIAN INSTITUTE OF TECHNOLOGY GUWAHATI

DEPARTMENT OF BIOSCIENCES & BIOENGINEERING

STATEMENT

I do hereby declare that the content embodied in this thesis entitled as **"Cloning, expression, purification, biochemical, functional and structure characterization of pectin methylesterase (*Ct*PME) from family 8 Carbohydrate Esterase (CE8) from *Clostridium thermocellum* ATCC 27405 and its applications in textile and food industry"** is the result of investigations carried out by me in the Carbohydrate Enzyme Biotechnology Laboratory, Department of Biosciences and Bioengineering, Indian Institute of Technology Guwahati, Guwahati, India under the guidance of Professor Arun Goyal.

In keeping with the general practice of reporting scientific observations, due acknowledgements have been made wherever the work described is based on the findings of other investigators.

September, 2019

Vikky Rajulapati
(136106031)

INDIAN INSTITUTE OF TECHNOLOGY GUWAHATI

DEPARTMENT OF BIOSCIENCES & BIOENGINEERING

CERTIFICATE

It is certified that the work described in this thesis entitled **"Cloning, expression, purification, biochemical, functional and structure characterization of pectin methylesterase (*Cf*PME) from family 8 Carbohydrate Esterase (CE8) from *Clostridium thermocellum* ATCC 27405 and its applications in textile and food industry"** by **Vikky Rajulapati (Roll No. 136106031)** for the award of degree of Doctor of Philosophy is an authentic record of the results obtained from the research work carried out under my supervision at the Carbohydrate Enzyme Biotechnology Laboratory, Department of Biosciences & Bioengineering, Indian Institute of Technology Guwahati, Guwahati, India and this work has not been submitted elsewhere for a degree.

Dr. Arun Goyal *(MTech, PhD)*
(FAMI, FBRS, FABAP, FNABS, FNAAS, FIFIB)
Professor
(Thesis Supervisor)
Department of Biosciences & Bioengineering
Indian Institute of Technology Guwahati
Guwahati, 781 039, India

ACKNOWLEDGEMENTS

It is a pleasant task for me to express my gratitude to completion with the support and encouragement of all those who contributed in many ways and had profound impact on this study. It would not have been possible without the support and encouragement of many people including my supervisor, doctoral committee members, my family, my friends and colleagues. I would like to thank all those people who made this thesis possible and an unforgettable experience for me. At the end of my thesis, it is a pleasant task to express my thanks to all those who contributed in many ways and had profound impact in the success of this study deserves special acknowledgment.

I would like to express my sincere gratitude to God and my family for the blessings strength, encouragement and support upon me to complete this work.

Firstly, from the depth of my heart I express my deep sincere gratitude to the Almighty for the blessings and strength bestowed upon me to complete this work.

At this moment of accomplishment, I am extremely indebted to my thesis supervisor, Professor Arun Goyal, Carbohydrate Enzyme Biotechnology Laboratory, Department of Biosciences and Bioengineering, IIT Guwahati. This work would not have been possible without his guidance, support, encouragement, providing me with the necessary instructions and research facilities. Under his guidance, I successfully overcame many difficulties and learned a lot. I can't forget his how patiently he listened to my problems and provided the necessary instructions in systematic way.

He always used to review my thesis progress, give me valuable suggestions and made corrections numerous times. His unflinching convictions will always inspire me and I hope to continue to work with his noble thoughts. I earnestly thank him for inculcating in me scientific temperament and appreciable work ethics, which helped me to achieve this goal. I thank him for reviewing my thesis progress and making corrections numerous times.

I would also like to express my sincere gratitude to all my doctoral committee members Dr. Ajai B Kunnumakkara, Dr. Senthil Kumar, Prof. S. Kanagarajan and Dr. Sachin Kumar for their valuable suggestions and constructive criticism that has led to the successful completion of my thesis.

I am thankful to Department of Biosciences & Bioengineering and Central Instrumentation Facility (CIF), IITG for providing me instruments for my research work.

I would also like to express my sincere gratitude to Prof. Punyamurthy, Department of Chemistry, IIT Guwahati and his PhD student for Circular Dichroism (CD) analysis. I sincerely thank Prof. Ashish, IMTECH, Chandigarh, for providing SAXS facility. I would also like to express my sincere thanks to Prof. Vimal Katiyar, center for sustainable polymer, Department of Chemical Engineering and his PhD student Mr. Kiran kumar Gali for Contact angle and Universal testing Machine (UTM) analysis.

I would also like to thank the present and previous heads of the Department of Biosciences & Bioengineering, IIT Guwahati, Prof. Latha Rangan, Prof. K. Pakshirajan, and Prof. Venkata V. Dasu for providing me with the necessary facilities.

I am also thankful to my seniors Dr. Shadab Ahamed, Dr. Rishikesh Shukla, Dr. Shraddha Shukla, Dr. T.J.M. Rao, Dr. Saprativ P. Das, Dr. Deeplina Das, Dr. Arabinda Ghosh, Dr. A.K. Verma, Dr. Damini Kothari, Dr. Soumyadeep Chakraborty, Dr. Suchi Singh, Dr. Rwivoo Baruah, Dr. Aruna Rani and Dr. Arun Dhillon for their help and suggestions. I am immensely thankful to my research group members Ashutosh Gupta, Sumitha Banu, Kedar Sharma, Krishan Kumar, Shweta Singh, Priyanka Nath, Abhijeet Thakur, Kaustubh, Parmeshwar, Jabin, Robin and Krishan. I am thanks to my master dissertation group Ines Lobo Antunes, Karthika, Ajit, Priya, Dishant, Akash, Sunetra and Najini. I am grateful to all the people with whom I have worked in the lab at the Department of Biosciences and Bioengineering for their cooperation and support.

I would like to thank my friends Naveen Kumar, Naresh, Amruta, Bethi, Moushamee, Hasna, Alok and Mounika. I would also like to thank my friends Balwant, Dhana, varthika, Philip, Banesh, Yogi, Srikanth, Srinivas anna, Mohan, Payel, Sidharth, Himanshu, Sunanda, Vinay, Bapi, Ajmani, Subbi and Banu for their support.

I wish to acknowledge the support received from other teaching and non-teaching staff of the Department of Biotechnology, IIT Guwahati.

I wish to acknowledge M.H.R.D, Govt. of India for providing me financial assistance of fellowship through Institute, IIT Guwahati.

I wish to acknowledge DST-SERB, Govt. of India for providing financial assistance and also Department of Biotechnology, Govt. of India, New Delhi for providing me for International travel fellowship.

I would like to thank my teachers in my carrier development. I thank to Prof. Santhosh Goyal and Usha Goyal for support. I am sincerely thank to K.K. Singh from CIF, IITGuwahati for his continuous support.

My PhD endeavor would not have been successful without the love, trust, support and blessings of my grandparents, parents, sisters, brother in laws, brothers, niece and nephew. I owe my achievements to my family and friends.

Vikky Rajulapati
September, 2019

SYNOPSIS

Introduction

Carbohydrates are defined structure as polyhydroxy aldehydes (e.g. glucose), polyhydroxy ketones (e.g. fructose), polyhydroxy alcohols (e.g. erythritol), polyhydroxy acids (e.g. lactobionic acid) and their derivative forms. The sugars or saccharides are the typical carbohydrates. The plant cell wall (PCW) is a network of polysaccharides, which is mainly consists of cellulose, hemicellulose and pectin. The chains of cellulose is surrounded by a matrix of pectin. Pectin is a structural complex polysaccharide present in primary cell wall of middle lamella. Pectin is present in walls of all higher plants, gymnosperms, pteridophytes and bryophytes. Approximately, 35% of primary cell walls in dicots and non-graminaceous monocots, 2–10% of grass and up to 5% of walls in woody tissues are composed of pectin. Pectin plays important role in cell–cell adhesion, signaling, cell expansion, leaf abscission and fruit development. There are three primary members of pectin family of polysaccharides, homogalacturonan (HG), rhamnogalacturonan I and rhamnogalacturonan II. HG is a linear homopolymer of α-1,4-linked D-galactopyranosyluronic acid (α-Gal*p*A). The α-Gal*p*A residues of homogalacturonan may be methyl esterified at the C-6 carboxyl position. HG may also be O-acetylated at the C-2 or C-3 position. Homogalacturonan have been isolated from citrus and apple pectin. HG domain is called as the smooth

region of pectin due to the presence of linear chain. The degree of esterification (DE) is defined as the ratio of esterified galacturonic acid groups to total galacturonic acid groups. The pectin classes are based on the DE and are of two types, High methoxyl (HM) pectins and Low methoxyl (LM) pectins.

Carbohydrate active enzymes catalyse the breakdown, biosynthesis or modification of carbohydrates and glycoconjugates (www.cazy.org). Carbohydrate active enzymes have been classified into different families based on protein sequence similarity. They have been classified in the CAZy database as: Glycosyl Transferases (GTs), Glycoside Hydrolases (GHs), Polysaccharide Lyases (PLs), Auxiliary Activities (AA) and Carbohydrate Esterases (CEs). Polysaccharide lyases (PLs) cleave glycosidic bonds in uronic-acid containing polysaccharides. They use a β-elimination reaction mechanism to generate an unsaturated hexenuronic acid residue and a new reducing end at the cleavage site. Carbohydrate esterases (CE) catalyze the de-O-acylation or de-N-acylation of substituted polysaccharides. They remove the ester based modifications present in mono-, oligo- and polysaccharides. Carbohydrate esterases use the esters as a substrate and release carboxylic acid and alcohol.

In the CAZy database the family 8 carbohydrate esterase (CE8) contains a total of 4534 protein sequences as of May 2019 (http://www.cazy.org/CE8.html). Out of 4534 sequences 5 belong to archaea, 3330 belong to bacteria, 1172 belong to eukaryote and 27 belongs to unclassified sequences. The only member representing the class of enzymes is pectin methylesterase (PME, E.C 3.1.1.11). PME hydrolyses the ester decorations from pectin (D-GalA). The crystal structures of these 8 PMEs are available in PDB.

Clostridium thermocellum is an anaerobic, Gram-positive, rod shaped, thermophillic bacterium. *C. thermocellum* displays on its cell surface a muti-enzyme complex called as cellulosome. The family 8 carbohydrate esterase (CE8) from *Clostridium thermocellum* under present study on pectin methylesterase (Fig. 1).

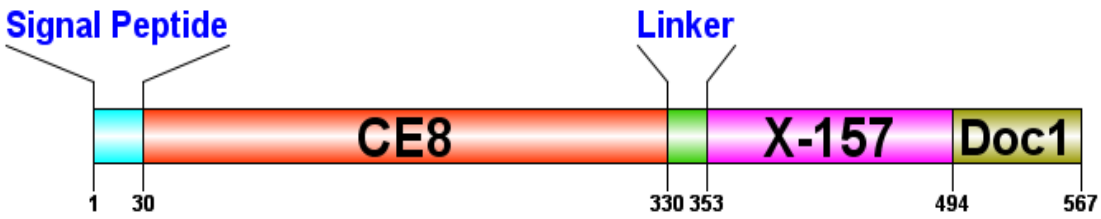

Fig. 1 Molecular architecture of modular protein ABN54147.1 from *C. thermocellum* consisting of a 30 aa signal peptide, N-terminal 300 aa family 8 carbohydrate esterase (CE8), catalytic (*Ct*PME) and C-terminal 141 aa unknown module and followed by 73 aa type 1 dockerin (DOC) modules.

Present work

The present work entitled as "Cloning, expression, purification, biochemical, functional and structure characterization of pectin methylesterase (*Ct*PME) from family 8 Carbohydrate Esterase (CE8) from *Clostridium thermocellum* ATCC 27405 and its applications in textile and food industry" has been divided into 6 chapters.

Chapter 1 is the General Introduction, which describes the brief review of literature dedicated to the importance of different carbohydrates majorly present in the plant cell wall. It presents an elaborate description of pectin and its components. This chapter describes different types of carbohydrate active enzymes and their sequence based classification. It presents a detailed description of Degree of methylation and types. It includes a description of family 8 carbohydrate esterase. Significance of the work has been elaborated in this chapter. Pectinases have wide and immense applications in various industrial processes. Therefore, exploration of any improved microbial strain or

robust enzyme has always been an important approach. Different types of pectin degrading enzymes and their applications have also been discussed in this chapter. A description of *Clostridium thermocellum* and its cellulosome has also been included in this chapter.

Chapter 2 describes amplification and cloning of the full length gene encoding family 8 carbohydrate esterase, Pectin methylesterase (E.C. 3.1.1.11), *Ct*PME*f* and its truncated derivatives, *Ct*PME and *Ct*X157 from the genomic DNA of *Clostridium thermocellum* ATCC 27405 (GenBank Accession No: ABN54147.1, Uniprot ID A3DJL8). The molecular architecture revealed signal peptide towards N-terminal followed by a family 8 carbohydrate esterase catalytic module (*Ct*PME, 35.5 kDa) and Unknown functional module (*Ct*X157, 17.7 kDa) along with 1 dockerin type at end of C-terminal. The PCR amplified fragment of full length gene encoding *Ct*PME*f* showed a band of ~1.3 kb, whereas, the gene encoding catalytic module (*Ct*PME) and binding module (*Ct*X157), displayed the sizes of ~ 0.9 kb and ~ 0.4 kb, respectively. The restriction enzyme digested fragments of genes encoding *Ct*PME*f*, *Ct*PME and *Ct*X157were ligated with linearized pET-28a(+) vector. The ligated mixture was transformed into *E. coli* TOP10 competent cells. The positive clones containing recombinant plasmid DNA were screened by restriction enzyme digestion using enzymes, *NheI* and *XhoI*. The restriction enzyme digested products were electrophoresed and the band of ~ 5.4 kb was produced for pET-28a(+) vector and corresponding bands of ~1.3 kb, ~ 0.9 kb and ~ 0.4 kb were produced from the insert fragments for genes encoding *Ct*PME*f*, *Ct*PME and *Ct*X157, respectively. The recombinant plasmids containing genes encoding *Ct*PME*f*, *Ct*PME and *Ct*X157 were transformed into *E. coli* BL-21 (DE3) cells. The recombinant proteins were expressed

and purified. The purified recombinant proteins displayed a band of approximately, 54.1 kDa for *Ct*PME*f*, 35.5 kDa for *Ct*PME and a band of approximately, 17.6 kDa for *Ct*X157 on SDS-PAGE gels. The intact molecular masses of the proteins were confirmed by the MALDI-TOF MS. The amount of recombinant proteins *viz. Ct*PME, *Ct*PME*f* and *Ct*X157 obtained from 100 ml *E. coli* cultures after purification by IMAC were 2.4±0.15 mg, 1.9±0.18 mg and 1.7±0.21 mg, respectively.

Chapter 3 describes the biochemical and functional characterisation of *Ct*PME and *Ct*PME*f*. The enzyme assay was carried out by alcohol oxidase method, as the product, which exhibits a maximum absorbance at 432 nm (A_{432}). *Ct*PME and *Ct*PME*f* showed maximum enzyme activity at pH 8.5. *Ct*PME and *Ct*PME*f* was active at pH range 7.5-9.0. The optimal temperature of *Ct*PME and *Ct*PME*f* was 50ºC. *Ct*PME and *Ct*PME*f* retained 90% of its activity after incubation at 50°C-60ºC for 30 min. *Ct*PME and *Ct*PME*f* was stable at the temperatures 40°C to 70°C and retained 80% activity. *Ct*PME and *Ct*PME*f* also showed better activity towards apple pectin, 70%, 55% and 25% methyl-esterified citrus pectin and lower activity against with non-methylated PGA. Both *Ct*PME and *Ct*PME*f* showed high activity towards high methylated pectin polysaccharide, citrus pectin containing with 85% esterified. Maximum activity of both, *Ct*PME and *Ct*PME*f* was against citrus pectin with 85% esterified at 18.8 U/mg and 20.1 U/mg, respectively. *Ct*PME and *Ct*PME*f* had similar values of K_m, 3.1 mg/ml and 3.4 mg/ml, respectively, with CP (85% esterified). The presence of 5 mM Ca^{2+} increased the activity of *Ct*PME and *Ct*PME*f* by 50% and 42%, respectively. The presence of 5 mM EDTA decreased the activity of *Ct*PME and *Ct*PME*f* by 40% and 38%, respectively. In case of *Ct*X157 protein, no esterase activity was observed. The melting study of *Ct*PME revealed that it starts unfolding at 68ºC and the protein was completely

distorted at 90ºC. The protein-melting peak of *Ct*PME shifted to higher temperature in the presence of Ca^{2+} ions. This further corroborated the fact that Ca^{2+} ions, not only enhances the activity, but also imparts the thermal stability to the protein structure. The recombinant *Ct*PME enzyme was expressed and produced using different culture media. Maximum concentration of *Ct*PME and *Ct*PME*f* obtained with AIM-LB medium was 150 mg/L and 160 mg/L, respectively.

Chapter 4 focuses on the structural aspects of *Ct*PME. The structure of *Ct*PME of family 8 carbohydrate esterase was characterized. The homology modeled structure of *Ct*PME showed the right handed parallel β helices. Multiple sequence alignment of *Ct*PME with previously (Uniprot Id: 2ntb and 1qjv) known pectin methylesterase revealed the conserved and semi-conserved amino acid residues (Asp, Asp and Arg). Multiple sequence alignment revealed that *Ct*PME has conserved residue active site. *Ct*PME showed maximum sequence identity (38%) with PME of *Erwinia chrysanthemi* (*Ec*PME). The secondary structure prediction by PsiPred and Circular Dichroism analysis showed the presence of approximately, 3% α-helix, 40% β-sheet and 57% random coils. The structure of *Ct*PME based on homology modelling showed a right-handed parallel β-helical structure. The structure validation by Ramachandran plot revealed 98.9% amino acid residues in the allowed region and only 1.1% amino acid residues were present in the disallowed region. Comparison of *Ct*PME structure with that of PME protein from *Erwinia chrysanthemi* showed conserved catalytic cleft. The substrate-binding pocket of *Ct*PME was found at the same location as previously recognized in *Ec*PME. The superposed 3D-structures showed that the key residues, Asp165, Asp186 and Arg242 of *Ct*PME perfectly aligned with the key residues Asp178, Asp199 & Arg267 of *Ec*PME. Docking analysis of *Ct*PME established key residues of

the active site cleft. The analysis showed that *Ct*PME had higher affinity towards the methylated D-galacturonic acid (mD-GalA) than D-galacturonic acid. Molecular dynamics simulation of modelled *Ct*PME was performed, the structural stability and compactness of the structure over a 20 ns duration. SAXS showed the *Ct*PME structure in solution form. Guinier plot showed the *Ct*PME structure was a globular form. Kratky plot gave indication that protein is fully folded in solution. The *ab initio* derived dummy atom model of *Ct*PME superposed well with its modeled structure. This study on *Ct*PME provided an insight into the structural determinants, stability, substrate recognition and the structure in solution form.

Chapter 5 describes the application of recombinant pectin methylesterase (*Ct*PME) and pectate lyase (*Ct*PL1B, E.C.4.2.2.2) from *Clostridium thermocellum* for enzymatic degumming of jute fiber or bioscouring of cotton fabric. The degumming of jute fibers and bioscouring of cotton fabric using alkaline pectinases, *Ct*PME, *Ct*PL1B and their mixture was studied and compared with NaOH treatment. The mixture of both enzymes displayed effective degumming of jute fiber and bioscouring of cotton fabric as compared with the individual enzymes. The optimum concentration of enzymes for degumming of jute fiber and bioscouring of cotton fabric was 10 mg/ml (4.2 U/ml) of crude *Ct*PME or 10 mg/ml (6.0 U/ml) of crude *Ct*PL1B under optimum conditions of time 60 min, 100 rpm and 50°C. In case of mixed enzymes, 5 mg/ml (2.1 U/ml) of crude *Ct*PME and 5 mg/ml (3.0 U/ml) of crude *Ct*PL1B were optimized. FESEM images showed that the mixture of enzymes more effectively removed the pectin and associated waxy compounds from the surface of jute fiber at 60 min of treatment. The mixture of enzymes was more efficient as compared with individual enzymes, nevertheless similar to that of NaOH treated. The weight loss of enzyme treated jute fiber and cotton fabric

was measured. Degumming of jute fiber and bioscouring of cotton fabric mixed enzymes treatment showed significant weight loss as compared with the respective of individual enzyme treatment and similar to that of NaOH treatment. The alkaline pectinase bioscoured of cotton fabric, wettability and contact angle were determined. The wettability analysis showed that the cotton fabric treated with *Ct*PME, *Ct*PL1B, mixture of enzymes and NaOH absorbed a drop of water in 21 s, 18 s, 10 s and 8 s, respectively. The contact angle was showed less than 20° with respective of wettability time. The FESEM analysis of the enzyme treated cotton fabric showed a smooth surface as compared with the control. ATR-FTIR analysis of enzyme treated jute fiber or cotton fabric showed difference in the surface exposed functional groups as compared with the controls. The mechanical properties such as Young Modulus and ultimate tensile strength of degummed jute fiber and bioscoured cotton fabric were investigated by UTM analysis. The mixed enzymes degumming of jute fiber or bioscouring of cotton fabric gave Young's Modulus and UTS values similar to those of chemical treatment. The UTM analysis showed that jute fibers treated with the enzyme mixture had higher tensile strength than the control. All these results showed that the use of mixture of *Ct*PME and *Ct*PL1B enzymes could be potentially useful enzymes for textile industry replacing the chemical process by Green process. To the best of our knowledge, this is the first study on the use of a recombinant pectin methylesterase, *Ct*PME with pectate lyase, *Ct*PL1B for degumming of jute fiber and bioscouring of cotton fabric. This indicated that the treatment of jute fibers with a mixture of *Ct*PME and *Ct*PL1B could be an alternative to the chemical treatment and sustainable eco-friendly process in textile industry.

Chapter 6 describes the isolation of natural pectin, characterization and effect of mixture of pectic oligosaccharides on normal cells (HEK293) and colon cancer cells (HT29). Natural pectin was isolated from waste citrus peels of *Citrus reticulate* (Sweet orange, mandarin) by ultrasound-assisted extraction (UAE), The yield of extracted orange pectin (EOP) obtained was 23.3%. FESEM analysis of UAE treated orange peel powder (OPP) showed more structural destabilization and porosity as compared with untreated OPP, which was also confirmed by BET analysis. FTIR spectrum showed the increased intensities of O-H, C=C and HC=O in UAE treated OPP as compared to untreated OPP displaying the disruption. These results showed that the UAE treatment is efficient and suitable for EOP extraction. The surface topology of EOP was globular particle like and wrinkled as shown by FESEM. The AFM depicted its fibrous and net-like structure. HPSEC analysis of EOP exhibited the molecular mass of 92.3 kDa. DLS analysis showed the average hydrodynamic diameter of 329.3 nm of EOP. FTIR and NMR spectra showed that EOP contains esterified D-galacturonic acid units. The degree of esterification of EOP was 68% as confirmed by FTIR. TGA-DTG showed the thermal degradation temperature of EOP to be 225°C and XRD analysis showed its semi-crystalline nature. *Ct*PL1B displayed 40% enhanced activity against EOP in the presence of *Ct*PME. The TLC analysis of lysed products of EOP released by *Ct*PL1B were majorly DP2 & DP3, which are methylated pectic oligosaccharides (mPOS) and by mixture of *Ct*PME and *Ct*PL1B, were non methylated pectic oligosaccharides (POS), which were confirmed by HPLC and ESI-MS. *Ct*PME hydrolysed the EOP and gave only the pectic polysaccharide (PP) and not POS. The effects of PP, POS and mPOS on proliferation of HEK293 and HT29 were studied. The proliferation of HEK293 cells was not affected even after 48 h in all the three case and the microscopic observation

also showed no change in the cell morphology as compared with the untreated cells. All of them showed reduced proliferation of HT29 cells, however, mPOS displayed maximum (51%) reduction of proliferation of HT29 cells as compared to POS or PP. The microscopic observation of mPOS treated HT29 cells revealed the reduced connection between the cells and change in cell morphology from undifferentiated to shrunk globular shape. The results displayed that mPOS, POS and PP are biocompatible and display anticancer properties. Pectin being large polymeric compound is difficult to get absorbed by the alimentary canal hence enzymatic degradation facilitates the production of smaller oligosaccharides which can get easily absorbed by the alimentary canal, hence, the pectic oligosaccharides can be produced from orange peels by using the recombinant *Ct*PME and *Ct*PL1B from *Clostridium thermocellum* on a large scale. Therefore, EOP and pectic oligosaccharides can be used for functional food applications enriching the nutritional values. The orange peel, which is generally considered as waste can serve as source for a potent healthcare commodity. Future challenges include its utilization in nano-medicine or chip based to develop an efficient delivery vehicle for therapeutic agents, to further enhance its specificity and finally to have controlled drug release.

CONTENTS

Chapter 1

General Introduction

1. Carbohydrates

Plants are unarguably the most essential form of life on the surface of earth which top the eukaryotic kingdom of organisms. Through photosynthesis, plants convert solar energy into organic carbon that can be further utilized by heterotrophic organisms. The synthesis of organic carbon in the form of carbohydrates is a major biological process. Plants cells are consisting of four major classes of organic molecules, which are proteins, lipids, nucleic acids and carbohydrates. Carbohydrates are the most abundant organic molecules found in nature and are metabolized by nearly all organisms (Wade, 1999). Carbohydrates are biomolecules consisting of carbon (C), hydrogen (H) and oxygen (O) atoms. A typical carbohydrate structure formula is $C_nH_{2n}O_n$ (where n =3 suggesting that carbon atoms are combined with water), commonly the combination of hydrogen-oxygen atom ratio of 2:1. Carbohydrate is the primary source of energy for life. Carbohydrates are defined structure as polyhydroxy aldehydes (e.g. glucose), polyhydroxy ketones (e.g. fructose), polyalcohols (e.g. erythritol), polyhydroxy acids (e.g. lactobionic acid) and their derivative forms (Nelson *et al.*, 2008). The sugars or saccharides (another term for sugar, sweet crystalline soluble

carbohydrate) are the typical carbohydrates. Carbohydrate saccharides are categorized into monosaccharides, disaccharides, oligosaccharides and polysaccharides. Saccharide structure forms a single polyhydroxy aldehyde or polyhydroxy ketone molecule is known as monosaccharide (Wade, 1999). Monosaccharide consists with four or more carbon atoms exist in unit cyclic form (Nelson *et al*., 2008). D-Glucose is the most important monosaccharide in nature and act as an energy precursor for all cellular functions such as protein synthesis, movement and transport. Disaccharides are made up of two monosaccharide units. Sucrose is a common example of a disaccharide consisting of D-Glucose and D-Fructose. Oligosaccharides consist of 2-10 monosaccharide molecules. Polysaccharides consist of more than 10 monosaccharide molecules and can be quite large e.g. Cellulose (Nelson *et al*., 2008). Cellulose contains several thousand D-Glucose units (O'sullivan, 1997). These molecules usually form a cyclic structure, which could be pyran or furan, are present as isomers, α or β. Carbohydrates carry out important cellular functions. They are used as an energy source across all life forms, serve structural and protective role and act as signaling molecule among several other functions (Nelson *et al*., 2008).

1.1 Plant cell wall polysaccharides

Plant cells have rigid cell wall, which is made up of complex polysaccharides such as cellulose, hemicellulose and pectin (Mohnen *et al*., 2008). Polysaccharides are complex macromolecular carbohydrates consisting of chain of monosaccharides linked together by glycosidic bonds (Berg, 2007). The plant cell wall also contains lesser amount of structural glycoproteins hydroxyproline-rich extensions) and phenolic esters (ferulic and coumaric acids) (Matsunaga *et al*., 2004). The cellulose chains are inter linked with hemicellulose by rigid matrix pectin (Taiz *et al*., 2010). The cell wall is both

structurally and functionally important for plant cells. The interconnected network of polysaccharide provides strength to plant cells (Alberts *et al*., 1997). The cell wall carbohydrate polymers are linked by covalent and non-covalent interactions.

Cellulose is a linear homo-polysaccharide of glucose molecules linkage of β-(1,4) glycosidic bonds (Wade, 1999). Cellulose chains are connected to each other through extensive non-covalent bonds. Cellulose module of plant cell wall is organized into amorphous and crystalline domains (O'Sullivan, 1997). There are other types of cellulosic polysaccharides such as laminarin (β-1,3-linked glucose) and lichenan (mixed 1,3-1,4-β-D-glucan) are other type of structural glucan, which are available in the market (Scheller *et al*., 2010).

Hemicelluloses are hetero-polysaccharides that are present in plant cell wall. They are named according to their main chain. The most common hemicellulose polysaccharides are xylans and mannans (Schadel *et al*., 2009). The other hemicellulose polymers commonly present in the nature as xyloglucans, glucuronoxylan, arabinoxylans, arabinogalactans, glucomannans and galactomannans (Schadel *et al*., 2009). Xylan is made of β-1,4-linked xylose residues (Scheller *et al*., 2010). Xylan may also conatin α-L arabinofuranosyl (arabinoxylans), β-D-glucucopyranosyl uronic acid (β-D-Glc*p*A) or 4-*O*-methyl-D-glucucopyranosyluronicacid (glucuroxylans) residues as side chains (Scheller *et al*., 2010; Urbanowicz *et al*., 2012; Cosgrove, 1999). Xyloglucan consisting of β-(1,4) linked d-glucans substituted with xylose (Bhamidi *et al*., 2008).

Mannans are homo-polymers, containing β-(1,4)-D-mannopyranose backbone that is substituted with galactose in galactomanan or glucose in glucomanan (Cui *et al*., 2009). Mannans may be further classified into three subfamilies: (1) glucomannan, (2)

galactomannan and (3) galactoglucomanan (Petkowicz *et al*., 2001). The glucomannan backbone of β-1,4-linked D-mannopyranosyl residues contains randomly distributed β-D-glucose residues in a 3:1 ratio (mannose: glucose). The backbone of galactomannan consists of β-1,4-linked D-mannopyranosyl residues that is substituted with side chains of single α-1,6-linked D-galactopyranosyl residues. Galactoglucomannan backbone is made of β-1,4-linked D-mannopyranosyl residues and randomly distributed β-D-glucose residues linked to mannose residue by β-1,4-linkage and the D-glucose residues are substituted with α-1,6-linked D-galactose residues (Moreira, 2008).

Apart from the carbohydrates, lignin is a large group of aromatic polymers derived from oxidative combination of 4-hydroxyphenylpropanoids (Vanholme *et al*., 2010). Lignin also contains the hydroxycinnamyl alcohols (or monolignols), coniferyl alcohol and sinapyl alcohol, with minor amounts of *p*-coumaryl alcohol (Boerjan *et al*., 2003). Lignin provides strength to cell wall and imparts resistance to microbial attack (Ralph *et al*., 2004).

1.2 Pectin and its components

Pectin refers to a family of structurally complex polysaccharides present in the middle lamella, primary cell wall of plants. It is deposited in the early stages of plant cell growth (O'Neill *et al*., 1990; Ridley *et al*., 2001). Pectin is a heteropolysaccharide composed of a α-(1,4)-D-galacturonic acid backbone with rhamnose, galactose and arabinose as side chain substituents (Bayer *et al*., 1998). Pectic acid is composed of polymers of galacturonic acid (Fig. 1.1) which is hydrophilic and soluble in nature. Pectic acid carboxyl group (COO^-) can also make salt bridges with Mg^{2+} and Ca^{2+} ions to form insoluble gels (Kohn, 1975; Garnier *et al*., 1994). Pectin is present in walls of all higher plants, gymnosperms, pteridophytes and bryophytes (Mohnen *et al*., 2008).

Approximately, 35% of primary cell walls in dicots and non-graminaceous monocots, 2–10% of grass and up to 5% of walls in woody tissues are composed of pectin (O'Neill *et al*., 1990; Ridley *et al*., 2001).

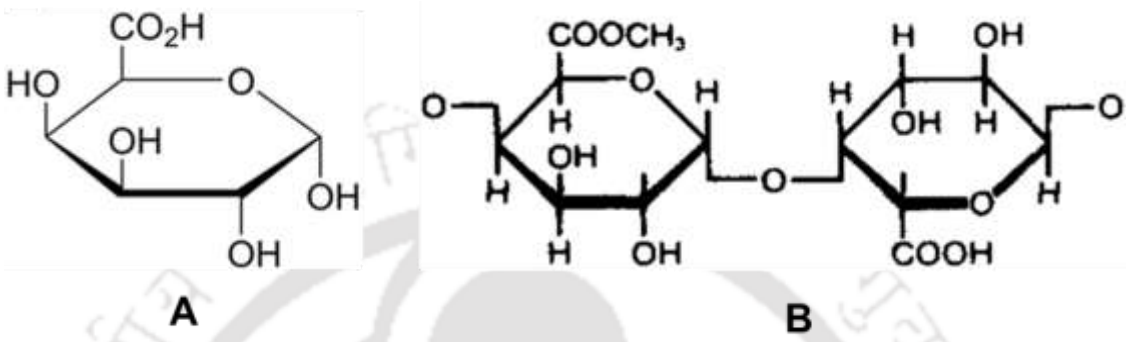

Fig. 1.1 (A) Galacturonic acid the monomeric unit of pectin, (B) Galacturonic acid of methylated monomeric unit α-1,4-linked with non-methylated monomeric unit of pectin.

1.2.1 Types of Pectin

There are three major members of pectin family of polysaccharides, classified based on their structures *viz.*, Homogalacturonan (HG), rhamnogalacturonan I (RG-I) and rhamnogalacturonan II (RG-II).

1.2.1.1 Homogalacturonan

Homogalacturonan (HG) is a linear homopolymer of α-1,4-linked D-galactopyranosyluronic acid (α-Gal*p*A) (Mohnen *et al*., 2008). The α-Gal*p*A residues of homogalacturonan may be methyl esterified at the C-6 carboxyl position. HG may also be O-acetylated at the C-2 or C-3 position (O'Neill *et al*., 1990). Homogalacturonan have been isolated from citrus and apple pectin and these are commercially available pectins in the market. Based on source and extraction of treatment HG may have a side chains with covalent bonds, so it may form a heterogeneous pectin polysaccharide (Ridley *et al.*, 2001) (Fig. 1.2). HG domain is

called as the smooth region of pectin due to the presence of linear chain (Schols *et al*., 1996; Libermans *et al*., 1999).

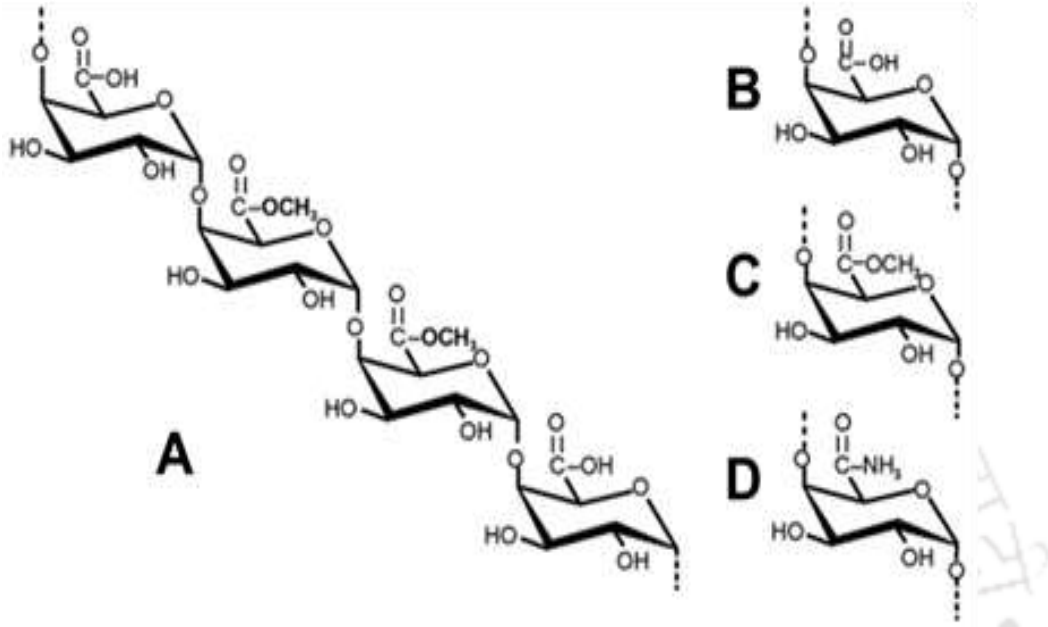

Fig. 1.2 (A) Homogalacturonan of pectin molecule and functional groups (B) carboxyl, (C) Ester and (D) Amide in pectin chain (adopted: Ridley *et al*., 2001).

1.2.1.2 Rhamnogalacturonan I

Rhamnogalacturonan I (RG I) is large and highly variable family of polysaccharides (Albersheim *et al*., 1996). RG-I main chain contains alternating α-Gal*p*A and α-L-rhamnopyranosyl (α-L-Rha*p*) residues (Mohnen *et al*., 2008) (Fig. 1.3). The monomeric unit of RG I main chain is a disaccharide, [→4)-α-D-Gal*p*A-(1→2)-α-L-Rha*p*-(1→]. The sugar composition of RG-I is highly heterogeneous because the rhamnosyl residues (20-80%) are substituted at C-4 with neutral and acidic side chains. The α-L-Rha*p* residues in the RG-I backbone are decorated with side chains of individual, linear or branched α-L-Arabinofuranose (α-L-Ara*f*) and β-D-Galactopyranose (β-D-Gal*p*) residues. The side chains include α-1,5-linked L-arabinan,

β-1,4-linked D-galactans and β-1,3-linked D-galactan (Nakamura *et al*., 2002). The α-1,5-linked L-arabinan may be substituted with α-1,2- and α-1,3-linked arabinose or arabinan branching. The β-1,4-linked D-galactans may be substituted with *O 3*-linked L-arabinose or arabinan branching. The β-1,3-linked D-galactan may be substituted with β-6-linked galactan or arabinogalactan branching. α-L-fucopyranose and β-D-Glc*p*A may also be present in the side chains. RG-I is referred to as the hairy region of pectin due to the presence of side chains (O'Neill *et al*., 2003).

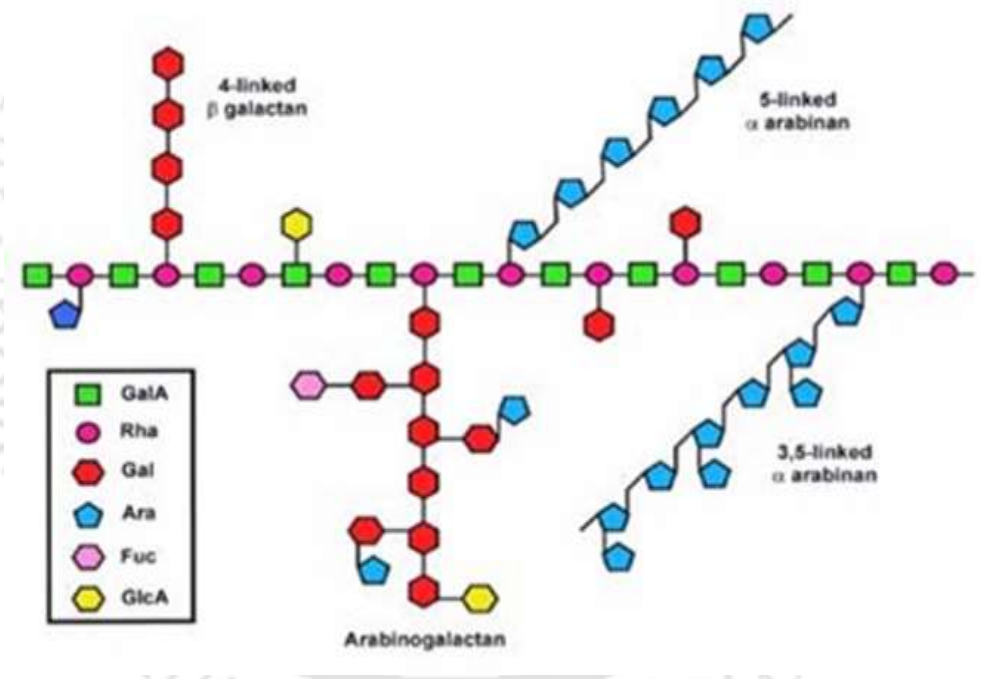

Fig. 1.3 Schematic representation of Rhamnogalacturonan I (adopted from, O'Neill *et al*., 2003).

1.2.1.3 Rhamnogalacturonan II

Rhamnogalacturonan II (RG II) also consists of 1,4-linked α-D-Gal*p*A residues which are decorated with side chains containing upto 12 different monosaccharides (Fig. 1.4) (O'Neill *et al*., 2004). These monosaccharides are linked by using more than 20 different types of linkages. RG-II in the plant cell wall exists in a dimeric form

comprising two separate RG-II monomers cross linked with each other (O'Neill *et al*., 2004). The β-D-apiosyl residues present in the side chains are involved in RG-II dimerization. Interactions of RG-II with HG and RG-I leads to an intricate macromolecular pectin network (Matsunaga *et al*., 2004). The other less abundant members of pectin family are xylogalacturonan (XGA) and apiogalacturonan (AP). XGA is a homogalacturonan that contains substitution of β-D-xylopyranose residues O-3 position. In apiogalacturonans the homogalacturonan main chain is substituted at O-2 or O-3 with D-apiofuranose residues (Zandleven *et al*., 2006).

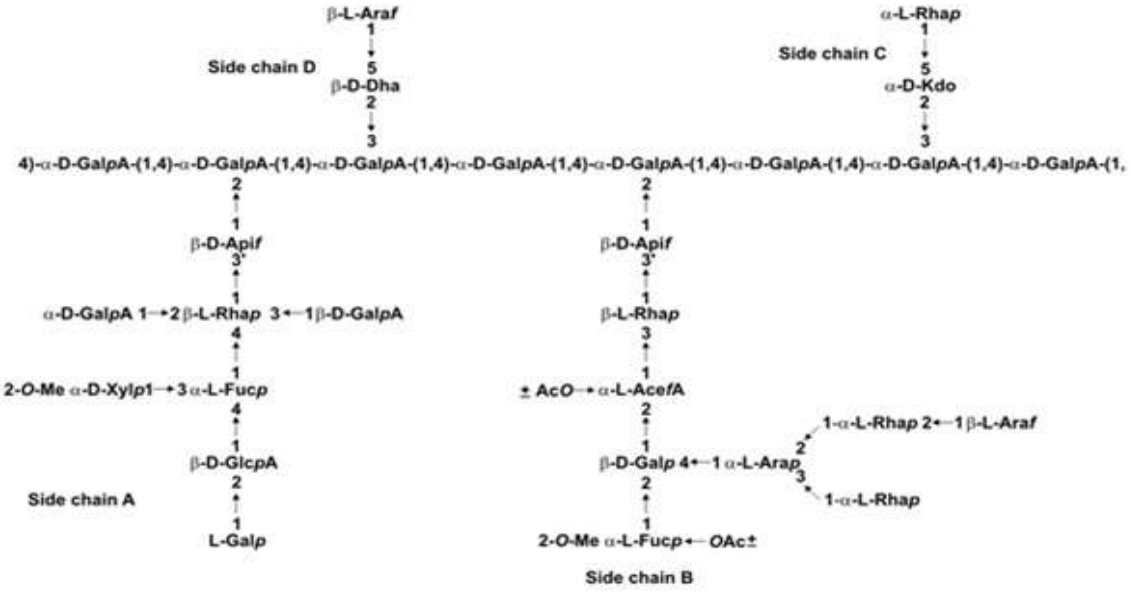

Fig. 1.4 Schematic representation of Rhamnogalacturonan II (adopted from, O'Neill *et al*., 2003).

1.3 Pectin biosynthesis

Pectin is a complex polysaccharide present in primary cell wall of plants. Pectin biosynthesis has been studied for many years, HG biosynthesis *in vitro* was demonstrated in 1965 (Villemez *et al*., 1965). Later, arabinan and galactan biosynthesis was demonstrated (Mc Nab *et al*., 1968; Odzuck and Kauss, 1972). The formation of complex pectin structure required 53-67 different enzyme activities, including glycosyl

transferases, methyl transferases and acetyltransferases (Mohnen, 1999; Mohnen, 2008). The results of investigation supported a model for pectin structure, which suggests that HG, RG-I and RG-II are linked via their backbones (Nakamura *et al*., 2002). Evidence is also available that points towards strong interactions between pectin and other cell wall polysaccharides such as xylan and xyloglucan (Nakamura *et al*., 2002, Popper *et al*., 2007). Studies involving pectin biosynthetic enzyme subcellular fractionation have shown that pectin is synthesized in the Golgi vesicles by membrane bound or associated glycosyltransferases. Pectic biosynthetic activities have been shown to fractionate with Golgi markers (Powell and Brew, 1974; Goubet and Mohnen, 1999; Sterling et al., 2001; Nunan and Scheller, 2003; Geshi et al., 2004) and pectic epitopes can be found in the Golgi vesicles but not in endoplasmic reticulum (Andeme-Onzighi et al., 2000).

1.4 Degree of Esterification (DE)

The structure of pectin is very difficult to determine as it vary and depend on the type of source. Pectin is complex polysaccharides consisting mainly of esterified D-galacturonates linked by α-1,4-glycosidic bond. Pectins also carry non sugar substituents, essentially methanol, acetic acid, phenolic acids and occasionally amide groups. The esterification of galacturonic acid residues with methanol or acetic acid is a very important structural characteristic of pectic substances (Devries et al., 1986). The degree of esterification (DE) is defined as the ratio of esterified galacturonic acid groups to total galacturonic acid groups. The pectin classes are based on the DE and are of two types,

1. **High methoxyl (HM) pectins:** If more than 50% of the carboxyl groups are methylated the pectins are called high-methyl ester pectins.
2. **Low methoxyl (LM) pectins:** If less than 50% of the carboxyl groups are methylated pectins are called low methyl ester (LM) pectins.

This same principal applies to acetylation and called the degree of acetylation (DAc). Acetyl groups are generally present in the 'hairy' rhamnogalacturonan regions and only present in low amount in homogalacturonan from apple and citrus fruits. They can be present in much higher amounts in homogalacturonan from sugarbeet and potato.

Pectin is the polymer of methylated galacturonic acid, where the units are linked by α-1,4-glycosidic bonds (Gibbons et al., 2002). The structure shown Fig. 1.5 has an alternative methyl ester (-$COOCH_3$) and carboxyl groups (-COOH). Here, it has 60% degree of esterification, normally called a DE-60 pectin (Liberman *et al*., 1999). DE affects the gelling properties of pectin due to this unique property. It is less soluble than pectic acid. Pectin is an important ingredient of fruit preservatives, jellies and jams (May, 1988).

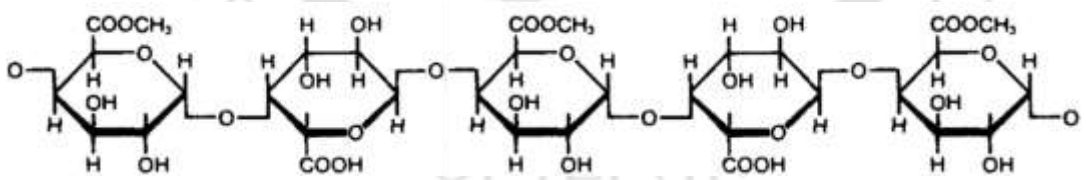

Fig. 1.5 Pectin as a polymer of α-Galacturonic acid with a variable number of methyl ester groups.

Gel formation by pectin molecule is caused by hydrogen bonding between free carboxyl groups on the pectin molecules and between the hydroxyl groups of neighboring molecules of the solvent at equilibrium condition (Sriamornsak, 2003; Fishman *et al*., 2007). The HM pectin forms a gel in the presence of sugar and acid,

which is called as low water-activity gels or sugar-acid pectin gels (Voragen *et al.*, 1995). The high sugar concentration creates low solubility environment for HM pectin, which leads to formation of gel by polymer chain interactions (May, 1988). Several factors such as are strength, degree of methylation (DM), rate of gelation, gelling temperature and texture of gel influence the formation of gel. HM-pectin is used in the confectionary industry for making fruit jellies and as a stabilizer in fruit juices and fermented dairy drinks (Ralet *et al*., 2002).

LM pectin forms a gel in presence of divalent cations, such as Ca^{2+} ions by binding the ionized carboxyl groups and hydroxyl group on the pectin chains. This structure is similar to the egg-box proposed for alginate (Fig. 1.6). The Ca^{2+} ions occupy the electronegative cavities in a two-fold buckled ribbon structure of the GalA residues (Rao and Lopes da Silva, 2006). The gel forming ability of pectin increases with decreasing DM (May, 1988). The DM and Ca^{2+} ions play a key role in the formation of gel with LM pectin. The lower concentration of Ca^{2+} ions leads to formation of gel with less elasticity and strength (Nesseri *et al*., 2008). The overdose of Ca^{2+} ions leads to pectin precipitation. The heat reversibility of LM-pectin gels may be utilized in bakery jams and jellies industries for glazing purpose. LM-pectin also finds application as a stabilizer for preparations of yogurt and fruit/milk desserts products (Ralet *et al*. 2001).

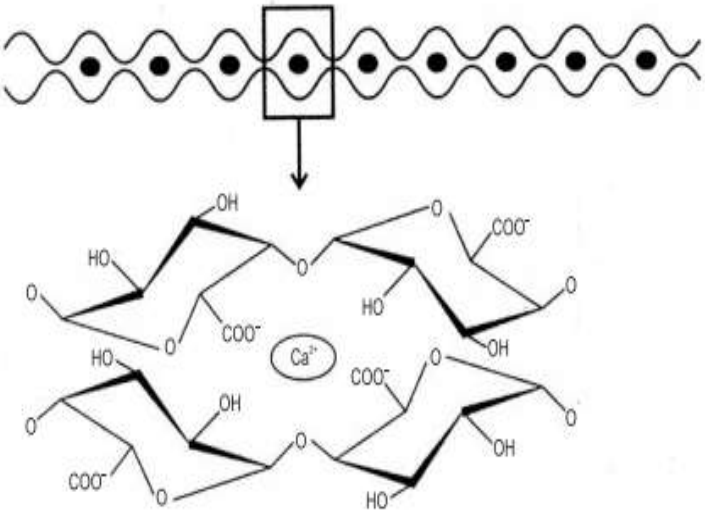

Fig. 1.6 Gel formation of LM pectin in presence of Calcium ions (adopted from: Ralet *et al*. 2002).

1.5 Carbohydrate enzymes

Carbohydrate active enzymes catalyse the breakdown, biosynthesis or modification of carbohydrates and glycoconjugates (www.cazy.org). Carbohydrate active enzymes have been classified into different families based on protein sequence similarity (Cantarel *et al*., 2009). They have been classified in the CAZy database as: Glycosyl Transferases (GTs), Glycoside Hydrolases (GHs), Polysaccharide Lyases (PLs), Auxiliary Activities (AA) and Carbohydrate Esterases (CEs). The enzymes of family glycosyl transferases catalyse the formation of glycosidic bond. Glycoside hydrolases catalyze the hydrolytic cleavage of the glycosidic bond whereas polysaccharide lyase enzymes catalyse non-hydrolytic cleavage of glycosidic bonds using a β-elimination mechanism. The carbohydrate esterase enzymes catalyze the de-O-acylation or de-N-acylation of substituted saccharides. The auxiliary activities enzymes are grouped in to ligninolytic enzymes, which degrade lignin and the lytic polysaccharide mono-oxygenase that cleaves the mono-oxygen bond from the

polysaccharide. As of January 2020, there are 110 families of GTs, 166 families of GHs, 40 families of PLs, 16 families of AA and 17 families of CEs. Carbohydrate active enzymes often display a modular architecture. Their catalytic domains may be associated with one or more specialized substrate binding modules referred to as Carbohydrate Binding Modules (CBMs). CBMs are non-catalytic modules and associated with cazy enzymes, there are 86 families. The information available at CAZy database provide a pool of gene sequences (many yet to be characterized) to study the structure and function of carbohydrate-active enzymes (Cantarel *et al*., 2009).

1.6 Types of Pectinase

Pectinases are class of enzymes, which break down complex pectin polysaccharide of plant tissues into simple form D-galacturonic acids. Pectinases, member of the glycoside hydrolases (GH), polysaccharide lyases (PL) and carbohydrate esterases family of enzymes (Table 1.1). GH and PL family enzymes are categorized as endo or exo based on enzyme mode of action, i.e., random or terminal, respectively. Pectinases are the growing enzymes of biotechnological sector, showing gradual increase importance in their market.

1.6.1 Polygalacturonases

Polygalacturonases (PG, E.C.3.2.1) belong to family 28 of glycoside-hydrolases (GH28) (http://www.cazy.org/GH28.html). Endo-polygalacturonase (E.C.3.2.1.15) hydrolyses the α-(1,4)-glycosidic linkages of polygalacturonic acid randomly and resulting in oligogalacturonides. Exo-polygalacturonase (E.C. 3.2.1.67) cleaves the polygalacturonic acid substrate from one end (reducing and non-reducing) to produce mono-galacturonate (Rombouts and Pilnik, 1980).

1.6.2 Polymethylgalacturonases

Polymethylgalacturonases (PMG, E.C. 3.2.1.15) facilitates the hydrolytic cleavage of α-(1,4)-glycosidic bonds in highly esterified pectin, producing 6-methyl-D-galacturonate (Jayani *et al*., 2005). They show either endolytic or exolytic mode of cleavage mechanism towards their substrates (Blanco *et al.*, 1999).

1.6.3 Pectin methyl esterases

Pectin methyl esterases (PME, E.C 3.1.1.11) catalyse the de-esterification of the methoxyl (methyl) group substitution of galacturonic acid moiety in pectin. Removal of the methoxyl group by PME facilitates polygalacturonases and pectate lyases to cleave the non-esterified polygalacturonan chain (Yadav *et al*., 2009). PME have been classified under family 8 carbohydrate esterase (CE8) in the CAZy database (http://www.cazy.org/CE8. html).

1.6.4 Pectin acetyl esterases

Pectin acetyl esterases (PAE, E.C 3.1.1.6) cleave the acetyl group present at the C-6 carbon of the galacturonic acid moiety of pectin producing pectic acid and acetate (Shevchik *et al*., 1997). They have been classified under family 12 and 13 carbohydrate esterase (CE12 and CE13) in the CAZy database (http://www.cazy.org/html).

1.6.5 Acetyl xylan esterase

Acetyl xylan esterase (AXE, E.C 3.1.1.72) catalyses the hydrolysis of acetyl groups from polymeric xylan, acetylated xylose, acetylated glucose, alpha-napthyl acetate, p-nitrophenyl acetate but not from triacetylglycerol. It does not act on acetylated mannan or pectin. They have been classified under family 1 to 7 carbohydrate esterase (CE1 to CE7) in the CAZy database (http://www.cazy.org/html).

1.6.6 Pectate lyases

Endo-pectate lyases (PL, E.C 4.2.2.2) randomly cleave polygalacturonic acid, while exo-pectate lyases (E.C 4.2.2.9) catalyze the cleavage of polygalacturonic acid from non-reducing end (Jayani *et al*., 2005). As a result of their action α-Δ-4,5-unsaturated-Gal*p*A is produced at the non-reducing end (http://www.cazy.org/PL1.html). Pectate lyases have been classified under family 1, 2, 3, 9 and 10 polysaccharide lyase in the CAZy database (http://www.cazy.org/html).

1.6.7 Pectin lyases

Pectin lyases (PNL, E.C 4.2.2.10) catalyse the breakdown of the α-1,4-glycosidic bond in highly esterified polygalacturonic acid. They possess an endo mode of action (Yadav *et al*., 2009). They have been classified under family 1 polysaccharide lyase (http://www.cazy.org/PL1. html).

1.6.8 Rhamnogalacturonan I rhamnohydrolases

Rhamnogalacturonan I rhamnohydrolases (E.C 3.2.1.174) cause the hydrolytic cleavage of the α-1,4-glycosidic bonds between L-Rha*p* and D-Gal*p*A at the non-reducing end releasing single L-Rha*p* residue (Silva *et al*., 2016). They have been classified glycoside hydrolase family 78 (GH78) (http://www.cazy.org/GH78.html).

1.6.9 Rhamnogalcturonan I galacturonohydrolases

Rhamnogalcturonan galacturonohydrolases (E.C 3.2.1.173) catalyse the removal of terminal non-reducing galacturonosyl residue by breaking of α-1,2-glycosidic bond between D-Gal*p*A and L-Rha*p* at the non-reducing end releasing single D-Gal*p*A residue (Silva *et al*., 2016). They have been classified into glycoside hydrolase family 28 (GH28) (http://www.cazy.org/GH28.html).

1.6.10 Rhamnogalacturonan I endo-hydrolases

Rhamnogalacturonan I endo-hydrolases (E.C 3.2.1.171) catalyse the cleavage of α-1,2-glycosidic bonds between D-Gal*p*A and L-Rha*p* in a random fashion releasing oligogalacturonates (Silva *et al*., 2016). They have been classified into glycoside hydrolase family 28 (GH28) (http://www.cazy.org/GH28.html).

1.6.11 Rhamnogalacturonan lyases

Rhamnogalacturonan lyases catalyze the cleavage of α-1,4-glycosidic bond between Rha*p* and Gal*p*A residues of rhamnogalacturonan I main chain through β-elimination reactin mechanism (Silva *et al*., 2016). The oligosaccharides products formed have α-Δ-4,5-unsaturated-Gal*p*A residue at their non-reducing end. Endo-rhamnogalacturonan (E.C 4.2.2.23) lyases cleave the main chain randomly while exo-rhamnogalacturonan lyases (E.C 4.2.2.24) specifically cleave at the terminal glycosidic bond. Rhamnogalacturonan lyases are grouped in families 4 and 11 of polysaccharide lyases (PL4 and PL11) (http://www.cazy.org/PL4.html, http://www.cazy.org/PL11.html).

1.6.12 Unsaturated rhamnogalacturonyl hydrolases

Unsaturated rhamnogalacturonyl hydrolases (E.C 3.2.1.172) are active only on RG I oligomer with Δ-4,5-unsaturated-Gal*p*A residue at the non-reducing end (Silva *et al*., 2016). They catalyse the cleavage of the α-1,2 glycosidic bond between the Δ-4,5-unsaturated-Gal*p*A and L-Rha*p* releasing single unsaturated D-Gal*p*A. They have been classified into glycoside hydrolase family 105 (GH105) (http://www.cazy.org/GH105.html).

1.6.13 Rhamnogalacturonan acetylesterases

Rhamnogalacturonan acetylesterases (E.C 3.1.1.86) hydrolyze acetyl groups from the rhamnogalacturonan I chain (Searle *et al*., 1992). They have been classified into carbohydrate esterase family 12 (http://www.cazy.org/CE12. html).

1.6.14 Xylogalacturonan hydrolase

Xylogalacturonan hydrolase or xylogalacturonase (E.C 3.2.1.-) hydrolytically cleaves the α-(1,4)-glycosidic linkages between two galacturonate residues in xylose containing rhamnogalacturonan chain, hence producing xylose-galacturonate dimers (Vlugt-Bergmans *et al*., 2000). These enzymes are classified into glycoside hydrolase family 28 (http://www.cazy.org/GH28.html).

1.6.15 Arabinases

Endo-arabinases (E.C 3.2.1.99) catalyse the hydrolysis of α-1,5-linked arabinan side chains of rhamnogalacturonan I (Silva *et al*., 2016). Terminal non-reducing arabinose residues are removed by a-L-arabinofuranosidases (EC 3.2.1.55). They have been classified into glycoside hydrolase family 43 (GH43) (http://www.cazy.org/ GH43.html).

1.6.16 Galactanases

Endo-galactanases (E.C 3.2.1.89) cleave the β-1,3-, β -1,4-, or β-1,6 linked galactose residues in the side chains They have been classified into glycoside hydrolase family 53. β-D-galactosidases (EC 3.2.1.23) remove the β-D-galactose residues from the terminal non-reducing end of galactan side chains (Silva *et al*., 2016). β-D-galactosidases have been classified into glycoside hydrolase family 1, 2 and 42 (GH1 and GH42) (http://www.cazy.org).

Table 1.1 Types of pectin degrading enzymes in CAZy database.

Enzyme Name	Enzyme family	Known enzyme activity	Reference
Polygalacturonase	GH28	Endo-polygalacturonase (E.C.3.2.1.15) & Exo-polygalacturonase (E.C. 3.2.1.67)	Rombouts and Pilnik, 1980
Polymethyl Galacturonase	GH28	Polymethylgalacturonases (E.C. 3.2.1.15)	Blanco *et al.*, 1999
Pectin methyl esterases	CE8	Pectin methyl esterases (E.C. 3.1.1.11)	Yadav *et al.*, 2009
Pectin acetyl esterase	CE12, CE13	Pectin acetyl esterases (E.C. 3.1.1.6)	Shevchik *et al.*, 1997
Pectate lyase	PL1 to 3, PL9,PL10	Endo-pectate lyases (E.C 4.2.2.2) and Exo-pectate lyases (E.C. 4.2.2.9)	Jayani *et al.*, 2005
Pectin lyase	PL1	Pectin lyases (E.C. 4.2.2.10)	Yadav *et al.*, 2009
Rhamnogalacturonan I rhamnohydrolase	GH78	Rhamnogalacturonan I rhamnohydrolase (E.C. 3.2.1.174)	Silva *et al.*, 2016
Rhamnogalcturonan I galacturonohydrolases	GH28	Rhamnogalcturonan galacturonohydrolase (E.C. 3.2.1.173)	Silva *et al.*, 2016
Rhamnogalacturonan I endo-hydrolases	GH28	Rhamnogalacturonan I endo-hydrolases (E.C 3.2.1.171)	Silva *et al.*, 2016
Rhamnogalacturonan lyase	PL4, PL11	Endo-rhamnogalacturonan lyases (E.C 4.2.2.23) and Exo-rhamnogalacturonan lyases (E.C. 4.2.2.24)	Silva *et al.*, 2016
Unsaturated rhamnogalacturonyl hydrolases	GH105	Unsaturated rhamnogalacturonyl hydrolases (E.C. 3.2.1.172)	Silva *et al.*, 2016
Rhamnogalacturonan acetylesterase	CE12	Rhamnogalacturonan acetylesterase (E.C. 3.1.1.86)	Searle *et al.*, 1992
Xylogalacturonan hydrolase	GH28	Xylogalacturonan hydrolase or xylogalacturonase (E.C. 3.2.1.-)	Vlugt-Bergmans *et al.*, 2000
Arabinase	GH43	Endo-arabinases (E.C. 3.2.1.99)	Silva *et al.*, 2016
Galactanase	GH53	Endo-galactanases (E.C. 3.2.1.89)	Silva *et al.*, 2016

1.7 Carbohydrate Esterases family

Carbohydrate esterases (CE) catalyze the de-O-acylation or de-N-acylation of substituted polysaccharides. They remove the ester based modifications present in mono-, oligo- and polysaccharides. Carbohydrate esterases use the esters as a substrate and release carboxylic acid and alcohol. It includes two types of substitution, one in which sugar plays the role of the "acid", such as pectin methyl esters for 4-O-methyl-glucuronoyl methylesterase from *Schizophyllum commune* (Li *et al*., 2007). Secondly, in which the sugar behaves as the alcohol, such as acetylated xylan for acetyl xylan esterase (family 1 and 2 CEs) from *Clostridium thermocellum* ATCC 27405 (Montanier *et al*., 2009). Carbohydrate esterases are classified into 16 families based on their sequence similarities and the known enzymes are reported in CAZY database (Lombard *et al*., 2010).

1.8 Family 8 Carbohydrate Esterase

The family 8 carbohydrate esterase (CE8) contains a total of 4534 protein sequences in the CAZy database as of May 2019 (http://www.cazy.org/CE8.html). Out of 4534 sequences 5 belong to archaea, 3330 belong to bacteria, 1172 belong to eukaryote and 27 belongs to unclassified sequences. The only member representing the class of enzymes is pectin methylesterase (PME, E.C 3.1.1.11). PME hydrolyses the ester decorations from pectin (D-GalA). Till date, 48 PMEs from various organisms have been biochemically characterized. Out of these, 8 PMEs have been structurally characterized; 4 of which belong to bacteria and 4 to eukaryotes (http://www.cazy.org/CE8.html). The crystal structures of these 8 PMEs are available in PDB.

The structurally characterized CE8 enzymes are the bacterial proteins including PmeA from *Erwinia chrysanthemi* B374 (PDB Id: 1QJV), PmeA from *Erwinia chrysanthemi* 3937 (PDB Id: 2NTB), YbhC from *E. coli* (PDB Id: 3GRH) and YeCE8 from *Yersinia enterocolitica* (PDB Id: 3UW0), (Jenkins *et al*., 2001; Fries et al., 2007; Eklof *et al*., 2009; Boraston & Abbott, 2012). The PMEs from the eukaryotic plants sources such as, carrot (*Daucus carota*, PDB Id: 1GQ8), tomato (*Solanum lycopersicum*; PDB Id: 1XG2), rice (*Sitophilus oryzae*, PDB Id: 4PMH) and *Aspergillus niger* (PDB Id: 5C1C) have also been characterized (Johansson *et al*., 2002; Di *et al*., 2005; Teller et al., 2014; Kent et al., 2016). All these structures have a right-handed β-helix fold, which is a common fold for different pectin-related enzymes such as polygalacturonases and rhamnogalacturonases (members of GH28), pectin and pectate lyases (from PL1, PL3 and PL9) including CE8 PMEs (Jenkins & Pickersgill, 2001). The enzymes typically have an open active site cleft, capable of accommodating the long pectin chains and an Asp-Asp-Arg catalytic triad. The Arg residue is substituted for Gln in some cases (Boraston and Abbott, 2012, Teller et al., 2014).

1.8.1 Mechanism of action of PME

Pectin methylesterase (PME) (EC 3.1.1.11) catalyses the removal of decorated methyl groups from pectin to form de-methylated pectate and methanol (Fig. 1.7) (Ralet et al., 2005).

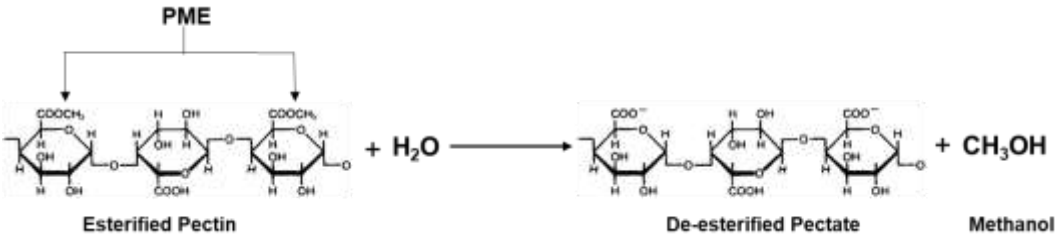

Fig. 1.7 Pectin methylesterase action on pectin polysaccharide.

1.8.2 Applications of PME

Pectin methylesterases find applications mainly in food, textile industries and processes involving retting of fibers such as flax. In plants, pectin methylesterase plays an important role in cell wall metabolism during fruit ripening (Pressey and Avants, 1982; Kashyap *et al*., 2001). PME helps cell wall extension during pollen germination and pollen tube growth, stem elongation, tuber yield and root development (Seymour et al., 1987). PME has also been shown to play a role in a plants response to pathogen attack (Koch and Nevins, 1989).

Production of enzymes that degrade pectin component of plant cell wall occupies around 10% of the overall manufacturing of enzyme preparations. These enzymes are widely used in the food industry in the production of juices, fruit drinks and wines (Semenova, et al., 2006).

1.9 Applications of Pectin polysaccharide

Pectin has a role in plant growth and development, defense mechanism, cell-cell adhesion, providing structural stability to cell wall, regulation of cell permeability and fruit development (Ridley *et al*., 2001; Willats *et al*., 2001). Pectin is used as a gelling, thickening and stabilizing agent in food and cosmetic industry, pectic polysaccharides have displayed health benefits *viz.* lowering cholesterol, blood glucose level, inhibiting cancer and enhances immunity (Jackson *et al*., 2007; Inngjerdingen *et al*., 2007).

1.10 Applications of microbial pectinases

Microbial pectinases have found widespread applications in various industrial processes such as food and textile industry, paper making, wastewater treatment, tea and coffee fermentation, citrus oil extraction, plant fiber degumming etc.

1.10.1 Food processing

Pectinases are used in extraction and clarification of fruit juice by degradation of pectin and thus decreasing the filtration time (Blanco *et al*., 1999). Pectinases when used in conjunction with enzymes like cellulase, arabinase and xylanase increase the volume of juice during extraction (Gailing *et al*., 2000). Softening of the peel in citrus fruits by pectinases during vaccum infusion process reduces labour and help in recovery of the intact pulp. Pectinases are widely used in pickle processing, preparation of vegetable puree and maceration of soybean for tofu making (Baker *et al*., 1996). During wine manufacturing process addition of pectinases to macerated fruits improves its colour and stability (Revilla *et al*., 2003). Tea fermentation is accelerated in presence of pectinase, whereas coffee fermentation is facilitated by removal of the mucilaginous coat on coffee beans (Carr, 1985).

1.10.2 Textile processing

Bioscouring of cotton fabric by pectinase to remove the non-cellulosic material facilitates proper dyeing of the fabric. This environmental friendly process is an alternative to chemical scouring by caustic soda (Hoondal *et al*., 2000).

1.10.3 Paper and Pulp making

Pectinases facilitate depolymerization of pectin during paper and pulp making which reduces the cationic demand and pitch deposit on whitewater (Reid *et al*., 2004).

1.10.4 Plant fiber degumming

Pectinase in association with xylanase facilitates the degumming of plant fiber which easily releases the intact fibers which is also an economic and eco-friendly process (Kapoor *et al*., 2001).

1.10.5 Wastewater treatment

Wastewater released from food processing industries contains pectin. Depolymerization of pectin by pectinases helps in removal of pectinaceous material and further accelerates the activated sludge process (Hoondal *et al*., 2000).

1.10.6 Citrus oil extraction

Oil extraction from citrus peels by the action of pectinases reduces the emulsifying properties of pectin, thus facilitating efficient extraction and collection of oil (Scott, 1975).

1.11 The microorganism, *Clostridium thermocellum*

The microorganism, *Clostridium thermocellum* belongs to the bacterial kingdom and phylum firmicutes. *Clostridium thermocellum* is considered a class of *clostridia*, the order is *clostridiales* and the family is *clostridiaceae*. *C. thermocellum* is an anaerobic, gram-positive, rod shape, thermophilic, cellulolytic and ethanologenic bacterium. It was isolated in 1926 by Viljoen et al. while identifying novel organisms capable of degrading cellulose. It is capable of directly converting cellobiose and cellulose into ethanol (Bayer *et al*., 2000a). The common cellular structure of *C. thermocellum* is rod-shaped bacteria as shown in Scanning Electron Microscopic image (Fig. 1.8A) (Lamed *et al*., 1987) and Transmission Electron Microscopic image (Fig. 1.8B) (Fontes and Gilbert, 2010). Ethanol is one of the main product of fermentation by *C. thermocellum* due to which it has attracted scientific attention for development into a potential organism for Consolidated Bioprocessing (Akinosho *et al*., 2014). However, there are some draw back using this organism to practical approach due to its low ethanol yield and along with production of other products such as acetate, formate and lactate. The cellulose degrading bacteria produces a large complex cellulase system

known as the cellulosome, which consists approx. 20 catalytic protein modules these are involved in the cellulose degradation and the transport of sugar monomers (Bayer *et al*., 2000b; Fontes *et al*., 2010). *C. thermocellum* displays on its cell surface a muti-enzyme complex called as cellulosome model organism (Fontes *et al*., 2010).

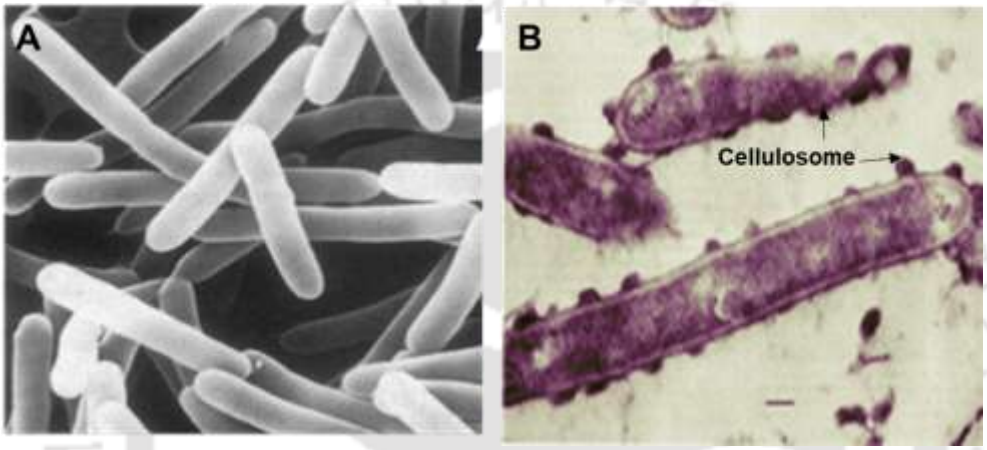

Fig. 1.8 (A) Scanning electron microscope (SEM) images of *Clostridium thermocellum*, showing normal rod shaped cells (adapted from Lamed *et al*., 1987); (B) Transmission electron microscope (TEM) image of cationized ferritin (CF) stained *Clostridium thermocellum* grown on cellobiose (adapted from Fontes and Gilbert, 2010).

1.12 Significance and objectives of the present study

1.12.1 Significance of the study

Pectin degrading enzymes find application in various industrial processes like bioscouring, juice extraction, vegetable puree production, fiber retting, degumming and waste water treatment and many others. Therefore, the search of better enzymes that degrade various components of pectin, is important. Several enzymes from the cellulosomal complex of *Clostridium thermocellum* have been studied but never an enzyme from CE8 family. *Clostridium thermocellum* genome contains a gene encoding a putative pectin methylesterase, which has been classified under family 8 carbohydrate esterase. Till date, this enzyme has not been reported from *Clostridium thermocellum.* Cloning and purification of this enzyme would enable to characterize its biochemical and structural aspects. This will enable to make desirable changes at the DNA level, to obtain an enzyme, which can easily fulfill the need of modern day food, beverage, textile and oil industries. Determination of the *in-silico* structure will help in understanding the key residues involved in catalysis and the mode of enzyme action. The proposed study involves the cloning, expression and purification of a modular family 8 carbohydrate esterase, *Ct*PME*f* (GenBank Acession number ABN54147.1, Uniprot ID A3DJL8) its associated unknown functional module (*Ct*X157) and the catalytic module (*Ct*PME) from *Clostridium thermocellum* ATCC 27405 genome. BLAST analysis showed that *Ct*PME is a putative pectin methylesterase. Biochemical and functional characterization of the full length *Ct*PME*f* and its truncated derivative *Ct*PME will be carried out to determine their activity against different pectin polysaccharides and to understand their cleavage hydrolysis with various esterified pectins. Binding and activity assays of the unknown functional module, *Ct*X157 will be

carried out to determine its affinity towards various plant cell wall carbohydrates. Structural study of *Ct*PME, will be undertaken to determine the active site catalytic amino acid residues. Its application along with other pectate lyase (*Ct*PL1B) in degumming of jute fiber and bioscouring of cotton fabric will be studied. Employing *Ct*PME and other pectate lyase on pectin, pectic oligosaccharides will be produced and their effect on normal and colon cancer cells will be studied. The reasons for selecting pectin methylesterase (PME) of the family 8 carbohydrate esterase (CE8) from *Clostridium thermocellum* are summarized below:

1. *Ct*PME*f* from *Clostridium thermocellum* is a putative pectin methylesterase, which shall be thermostable, efficient and robust in hydrolyzing the polysaccharides.
2. Pectin methylesterase belonging to family 8 carbohydrate esterase (CE8) hydrolyzes pectin to give de-esterified pectic polysaccharide. The de-esterified pectic polysaccharide can be more efficiently degraded by polygalacturonase or pectate lyase.
3. Study of biochemical properties of *Ct*PME will elucidate the essential parameters, which would be beneficial for industrial downstream applications.
4. The structural insights of *Ct*PME will reveal the molecular determinants of substrate specificity.

1.12.2 Specific objectives

1. Cloning, expression and purification of full-length module, *Ct*PME*f* of family 8 carbohydrate esterase and its truncated derivative, *Ct*PME from *Clostridium thermocellum* genomic DNA.
2. Biochemical characterization of catalytic, *Ct*PME and full length, *Ct*PME*f* modules.
3. Structure modeling, ligand docking study and SAXS analysis of catalytic (*Ct*PME) module.
4. Application of *Ct*PME in degumming of jute fiber and bioscouring of cotton fabric.
5. Extraction of pectin from orange peels and production of pectic oligosaccharides, and study their effect on colon cancer cell lines.

1.13 References

Akinosho, H., Yee, K., Close, D., Ragauskas, A. (2014) The emergence of *Clostridium thermocellum* as a high utility candidate for consolidated bioprocessing applications. Frontiers in Chemistry, 2: 66.

Albersheim, P., Darvill, A.G., O'Neill, M.A., Schols, H.A., Voragen, A.G.J. (1996) An hypothesis: the same six polysaccharides are components of the primary cell walls of all higher plants. Proceedings of International Symposium on Progress in Biotechnology, Pectins and pectinases, Vol. 14 (eds. Visser, J., Voragen, A.G.J.), Elsevier Sciences, Amsterdam, NL, p. 47–53.

Alberts, B., Johnson, A., Lewis, J., Raff, M., Roberts, K.,Walter, P. (1997) Molecular Biology of the Cell Garland Science, New York, 2002.

Andème-Onzighi, C., Lhuissier, F., Vicré, M., Yamada, H., Driouich, A. (2000) A (1→ 3, 6)-β-d-galactosyl epitope containing uronic acids associated with bioactive pectins occurs in discrete cell wall domains in hypocotyl and root tissues of flax seedlings. Histochemistry and Cell Biology, 113(1): 61-70.

Baker, R.A., Wicker, L. (1996) Current and potential application of enzyme infusion in the food industry. Trends in Food Science and Technology, 7: 279–284.

Bayer, E.A., Chanzy, H., Lamed, R., Shoham, Y. (1998) Cellulose, cellulases and cellulosomes. Current Opinion Structural Biology, 8: 548–557.

Bayer, E.A., Shoham, Y., Lamed, R. (2000a) Cellulose-decomposing prokaryotes and their enzyme systems. (3rd ed.) Dworkin, M., Falkow, S., Rosenberg, E., Schleifer, K.H., and Stackebrandt, E. (ed.), In The Prokaryotes: An Evolving Electronic Resource for the Microbiological Community, 2: 578–617.

Bayer, E.A., Shoham, Y., Lamed R. (2000b) The cellulosome-an exocellular organelle for degrading plant cell wall polysaccharides. In Doyle, R.J. (ed.). Glycomicrobiology. Kluwer Academic/Plenum Publishers, New York. 387–439.

Berg, J.M. (2007) In Biochemistry, (6th ed), pp. 310–323. New York: W.H. Freeman.

Bhamidi, S., Scherman, M. S., Rithner, C. D., Prenni, J. E., Chatterjee, D., Khoo, K.-H., McNeil, M. R. (2008) The identification and location of succinyl residues and the characterization of the interior arabinan region allow for a model of the complete primary structure of *Mycobacterium tuberculosis* mycolyl arabinogalactan. Journal of Biological Chemistry, 283(19): 12992–13000.

Blanco, P., Sieiro, C., Villa, T.G. (1999) Production of pectic enzymes in yeasts. FEMS Microbiology Letters, 175: 1–9.

Boerjan, W., Ralph, J., Baucher, M. (2003) Lignin biosynthesis. Annual Review of Plant Biology, 54: 519–546.

Boraston, A. B., Abbott, D. (2012) Structure of a pectin methylesterase from *Yersinia enterocolitica*. Acta Crystallographica Section F: Structural Biology and Crystallization Communications, 68(2): 129-133.

Cantarel, B.L., Coutinho, P.M., Rancurel, C., Bernard, T., Lombard, V., Henrissat, B. (2009) The Carbohydrate-Active EnZymes database (CAZy): an expert resource for Glycogenomics. Nucleic Acids Research, 37: 233–238.

Carr, J.G. (1985) Tea, coffee and cocoa. In: Wood BJB, editor. Microbiology of fermented foods, vol. 2. London: Elsevier Science Ltd., p. 133–154.

Cosgrove, D.J. (1999) Enzymes and other agents that enhance cell wall extensibility. Annual Review of Plant Physiology and Plant Molecular Biology, 50: 391–417.

Cui, S.W., Wang, Q. (2009) Cell wall polysaccharides in cereals: chemical structures and functional properties. Structural Chemistry, 20: 291–297.

De Vries, J. A., Hansen, M., Søderberg, J., Glahn, P. E., Pedersen, J. K. (1986) Distribution of methoxyl groups in pectins. Carbohydrate Polymers, 6(3): 165-176.

Di Matteo, A., Giovane, A., Raiola, A., Camardella, L., Bonivento, D., De Lorenzo, G., Cervone, F., Bellincampi, D., Tsernoglou, D. (2005) Structural basis for the interaction between pectin methylesterase and a specific inhibitor protein. The Plant Cell, 17(3): 849-858.

Nasseri, A. T., Thibault, J. F., Ralet, M. C. (2008) Citrus Pectin: Structure and Application in Acid Dairy Drinks. Tree Science Biotechnology, 2: 60-70.

Eklöf, J. M., Tan, T. C., Divne, C., Brumer, H. (2009) The crystal structure of the outer membrane lipoprotein YbhC from *Escherichia coli* sheds new light on the phylogeny of carbohydrate esterase family 8. Proteins: Structure, Function, and Bioinformatics, 76(4): 1029-1036.

Fishman, M. L., Cooke, P. H., Chau, H. K., Coffin, D. R., Hotchkiss, A. T. (2007) Global structures of high methoxyl pectin from solution and in gels. Biomacromolecules, 8(2): 573-578.

Fontes, C. M. G. A., Gilbert, H. J. (2010) Cellulosomes: highly efficient nanomachines designed to deconstruct plant cell wall complex carbohydrates. Annual Review of Biochemistry, 79: 655–681.

Fries, M., Ihrig, J., Brocklehurst, K., Shevchik, V. E., Pickersgill, R. W. (2007) Molecular basis of the activity of the phytopathogen pectin methylesterase. The EMBO Journal, 26(17): 3879-3887.

Gailing, M.F., Guibert, A., Combes, D. (2000) Fractional factorial designs applied to enzymatic sugar beet pulps pressing improvement. Bioprocess Engineering, 22: 69–74.

Garnier, C., Axelos, M. A., Thibault, J. F. (1994) Selectivity and cooperativity in the binding of calcium ions by pectins. Carbohydrate Research, 256(1): 71-81.

Geshi, N., Jørgensen, B., Ulvskov, P. (2004) Subcellular localization and topology of β- (1→4) galactosyltransferase that elongates β-(1→4) galactan side chains in rhamnogalacturonan I in potato. Planta, 218(5): 862-868.

Gibbons, B. J., Roach, P. J., Hurley, T. D. (2002) Crystal structure of the autocatalytic initiator of glycogen biosynthesis, glycogenin. Journal of Molecular Biology, 319(2): 463-477.

Hoondal, G.S., Tiwari, R.P., Tiwari, R., Dahiya, N., Beg, Q.K. (2000) Microbial alkaline pectinases and their applications: a review. Applied Microbiology and Biotechnology 59: 409–418.

Inngjerdingen, K.T., Patel, T.R., Chen, X., Kenne, L., Allen, S., Morris, G.A., Harding, S.E., Matsumoto, T., Diallo, D., Yamada, H., Michaelsen, T.E., Inngjerdingen. M., Paulsen, B.S. (2007) Immunological and structural properties of a pectic polymer from *Glinus oppositifolius*. Glycobiology, 17: 1299–1310.

Jackson, C.L., Dreaden, T.M., Theobald, L.K., Tran, N.M., Beal. T.L., Eid, M., Gao M.Y., Shirley, R.B., Stoffel, M.T., Kumar, M.V., Mohnen, D. (2007) Pectin induces apoptosis in human prostate cancer cells: correlation of apoptotic function with pectin structure. Glycobiology, 17: 805–819.

Jayani, R.S., Saxena, S., Gupta, R. (2005) Microbial pectinolytic enzymes: A review. Process Biochemistry, 40: 2931–44.

Jenkins, J., Mayans, O., Smith, D., Worboys, K., Pickersgill, R. W. (2001) Three-dimensional structure of *Erwinia chrysanthemi* pectin methylesterase reveals a novel esterase active site1. Journal of Molecular Biology, 305(4): 951-960.

Jenkins, J., Pickersgill, R. (2001) The architecture of parallel β-helices and related folds. Progress in Biophysics and Molecular Biology, 77(2): 111-175.

Johansson, K., El-Ahmad, M., Friemann, R., Jörnvall, H., Markovič, O., Eklund, H. (2002) Crystal structure of plant pectin methylesterase. FEBS letters, 514(2-3): 243-249.

Kapoor, M., Beg, Q.K., Bhushan, B., Singh, K., Dadich, K.S., Hoondal, G.S. (2001) Application of alkaline and thermostable polygalacturonase from Bacillus sp. MG-cp-2 in degumming of ramie (*Boehmeria nivea*) and sunn hemp (*Crotolaria juncia*) bast fibers. Process Biochemistry, 36: 803–807.

Kashyap, D.R., Vohra, P.K., Tewari, R. (2001) Application of pectinases in the commercial sector: a review. Bioresource Technology, 77: 215–27.

Kent, L. M., Loo, T. S., Melton, L. D., Mercadante, D., Williams, M. A., Jameson, G. B. (2016) Structure and properties of a non-processive, salt requiring, and acidophilic pectin methylesterase from *Aspergillus niger* provide insights into the key determinants of processivity control. Journal of Biological Chemistry, 291(3), 1289-1306.

Koch, J. L., Nevins, D. J. (1989) Tomato fruit cell wall: I. Use of purified tomato polygalacturonase and pectin methylesterase to identify developmental changes in pectins. Plant Physiology, 91: 816-822.

Kohn, R. (1975) Ion binding on polyuronates-alginate and pectin. Pure and Applied Chemistry, 42(3), 371-397.

Lamed, R., Naimark, J., Morgenstern, E., Bayer, E. A. (1987) Specialized cell surface structures in cellulolytic bacteria. Journal of Bacteriology, 169: 3792–3800.

Li, X. L., Spániková, S., de Vries, R. P., Biely, P. (2007) Identification of genes encoding microbial glucuronoyl esterases. FEBS Letters, 581: 4029-4035.

Libermans, M., Mutaftschiev, S., Jauneau, A., Vian, B., Catesson, A., Goldberg, R. (1999) Mung bean hypocotyl homogalacturonan: localization, organization and origin. Annals of Botany, London 84: 225–233.

Lombard, V., Bernard, T., Rancurel, C., Brumer, H., Coutinho, P. M., Henrissat, B. (2010) A hierarchical classification of polysaccharide lyases for glycogenomics. Biochemical Journal, 432(3): 437-444.

Matsunaga, T., Ishii, T., Matsumoto, S., Higuchi, M., Darvill, A., Albersheim, P., O'Neill, M.A. (2004) Occurrence of the primary cell wall polysaccharide rhamnogalacturonan II in pteridophytes, lycophytes, and bryophytes. Implication for the evolution of vascular plants. Plant Physiology, 134: 339–351.

May, C. D. (1990) Industrial pectins: sources, production and applications. Carbohydrate Polymers, 12(1): 79-99.

McNAB, J. M., Villemez, C. L., Albersheim, P. (1968) Biosynthesis of galactan by a particulate enzyme preparation from Phaseolus aureus seedlings. Biochemical Journal, 106(2): 355-360.

Mohnen, D. (1999) Biosynthesis of pectins and galactomannans. In: Pinto, B.M. (Ed.), Comprehensive Natural Products Chemistry, Vol. 3, Carbohydrates and their Derivatives Including Tannins, Cellulose, and Related Lignins. Elsevier, Oxford: 497–527.

Mohnen, D. (2008) Pectin structure and biosynthesis. Current opinion in Plant Biology, 11(3): 266-277.

Mohnen, D., Bar-Peled, M., Somerville, C. (2008) Biosynthesis of Plant Cell Walls. Biomass Recalcitrance, Chapter 5 (eds. Himmel, M.), pp. 94–187. Blackwell Publishing, Oxford.

Montanier, C., Money, V.A., Pires, V.M., Flint, J.E., Pinheiro, B.A., Goyal, A., Prates, J.A., Izumi, A., Stalbrand, H., Morland, C., Cartmell, A., Kolenova, K., Topakas, E., Dodson, E.J., Bolam, D.N., Davies, G.J., Fontes, C.M., Gilbert, H.J. (2009) The active site of a carbohydrate esterase displays divergent catalytic and noncatalytic binding functions. PLoS Biology, 7, e71.

Moreira, L. R. S. (2008) An overview of mannan structure and mannan-degrading enzyme systems. Applied Microbiology and Biotechnology, 79(2): 165.

Nakamura, A., Furuta, H., Maeda, H., Takao, T., Nagamatsu, Y. (2002) Analysis of the molecular construction of xylogalacturonan isolated from soluble soybean polysaccharides. Bioscience, Biotechnology and Biochemistry, 66(5): 1155-1158.

Nakamura, A., Furuta, H., Maeda, H., Takao, T., Nagamatsu, Y. (2002) Structural studies by stepwise enzymatic degradation of the main backbone of soybean soluble polysaccharides consisting of galacturonan and rhamnogalacturonan. Bioscience, Biotechnology and Biochemistry, 66(6): 1301-1313.

Nelson, D. L., Lehninger, A. L., Cox, M. M. (2008) Lehninger Principles of Biochemistry. Macmillan.

Nunan, K. J., Scheller, H. V. (2003) Solubilization of an arabinan arabinosyltransferase activity from mung bean hypocotyls. Plant Physiology, 132(1), 331-342.

O'Neill, M., Albersheim, P., Darvill, A. (1990) The pectic polysaccharides of primary cell walls. In: Methods in Plant Biochemistry, Vol. 2. (eds. Dey D.M.), pp: 415–441. Academic Press, London.

O'Neill, M. A., York , W. S (2003) The composition and structure of plant primary cell walls. In The Plant Cell Wall. Edited by Rose JKC. Ithaca, New York: Blackwell Publishing/CRC Press; 2003:1-54.

O'Neill, M.A., Ishii, T., Albersheim, P., Darvill, A.G. (2004) Rhamnogalacturonan II: structure and function of a borate cross-linked cell wall pectic polysaccharide. Annual Review of Plant Biology, 55: 109–139.

Odzuck, W., Kauss, H. (1972) Biosynthesis of pure araban and xylan. Phytochemistry, 11(8): 2489-2494.

O'sullivan, A. C. (1997) Cellulose: the structure slowly unravels. Cellulose, 4(3): 173-207.

Petkowicz, C. D. O., Reicher, F., Chanzy, H., Taravel, F. R., Vuong, R. (2001) Linear mannan in the endosperm of *Schizolobium amazonicum*. Carbohydrate Polymers, 44(2): 107-112.

Popper, Z. A., Fry, S. C. (2008) Xyloglucan-pectin linkages are formed intra-protoplasmically, contribute to wall-assembly and remain stable in the cell wall. Planta, 227(4), 781-794.

Powell, J. T., Brew, K. (1974) Glycosyltransferases in the Golgi membranes of onion stem. Biochemical Journal, 142(2): 203-209.

Pressey, R., Avants, J. K. (1982) Solubilization of cell walls by tomato polygalacturonases: effects of pectinesterases. Journal of Food Biochemistry, 6(1), 57-74.

Ralet, M, C., Bonnin, E., Thibault, J. F. (2002) Pectins polysaccharides from Eukaryotes. Biopolymers (Vol 6), In: De Baets S, Van-damme EJ, Steinbüchel A (Eds) Polysaccharides II- Wiley-VCH Verlag, Weinheim, Germany, p 345-380.

Ralet, M. C., Cabrera, J. C., Bonnin, E., Quéméner, B., Hellìn, P., Thibault, J. F. (2005) Mapping sugar beet pectin acetylation pattern. Phytochemistry, 66(15): 1832-1843.

Ralet, M. C., Dronnet, V., Buchholt, H. C., Thibault, J. F. (2001) Enzymatically and chemically de-esterified lime pectins: characterisation, polyelectrolyte behaviour and calcium binding properties. Carbohydrate Research, 336(2): 117-125.

Ralph, J.,Lapierre, C., Marita, J. M., Kim, H., Lu, F., Hatfield, R. D., Ralph, S., Chapple, C., Franke, R., Hemm, M.R., Van Doorsselaere, J., Sederoff, R. R., O'Malley, D. M., Scott, J. T., MacKay, J. J., Yahiaoui, N., Boudet, A., Pean, M., Pilate, G., Jouanin, L., Boerjan, W. (2004) Elucidation of new structures in lignins of CAD- and COMT-deficient plants by NMR. Phytochemistry, 57: 993–1003.

Rao, M. A., Lopes da Silva, J. A. (2006) Pectins: structure, functionality, and uses. In: Food Polysaccharides and their Applications (2nd Edn.), Stephen AM, Phillips GO, Williams PA (Eds) CRC Press/Taylor & Francis, Boca Raton, FL, USA, p 353-411.

Reid, I., Richard, M. (2004) Purified pectinase lowers cationic demand in peroxide-bleached mechanical pulp. Enzyme Microbial Technology 34: 499–504.

Revilla, I., Ganzalez-san jose, M. L. (2003) Addition of pectolytic enzymes: an enological practice which improves the chromaticity and stability of red wines. International Journal of Food Science and Technology, 38: 29–36.

Ridley, B. L., O'Neill, M. A., Mohnen, D. (2001) Pectins: structure, biosynthesis, and oligogalacturonide-related signaling. Phytochemistry, 57: 929–967.

Rombouts, F. M., Pilnik, W. (1980) Pectic enzymes. In: Rose AH, Ed. Microbial Enzymes and Bioconversions. Academic Press London, 5: 227–72.

Schadel, C., Blochl, A., Richter, A., Hoch, G. (2009) Short-term dynamics of nonstructural carbohydrates and hemicelluloses in young branches of temperate forest trees during bud break. Tree Physiology, 29: 901–911.

Scheller, H. V., Jensen, J. K., Sørensen, S. O., Harholt, J., Geshi, N. (2007) Biosynthesis of pectin. Physiologia Plantarum, 129(2): 283-295.

Scheller, H. V., Ulvskov, P. (2010) Hemicellulose. Annual Review Plant Biology, 61: 263–289.

Schols, H. A., and Voragen, A. G. J. (1996) Complex pectins: Structure elucidation using enzymes. In: J. Visser and A.J. Voragen (editors) Pectins and Pectinases, Elsevier Science, Amsterdam, p. 3–19.

Scott, D. (1975) Enzymes, industrial. In: Grayson M, Ekarth D, Othmer K, editors. Encyclopedia of chemical technology. New York: Wiley, p. 173–224.

Searle-Van Leeuwen, M. J. F., Van Den Broek, L. A. M., Schols H. A., Beldman, G., Voragen, A. G. J. (1992) Rhamnogalacturonan acetylesterase: a novel enzyme from *Aspergillus aculeatus*, specific for the deacetylation of hairy (ramified) regions of pectins. Applied Microbiology Biotechnology, 38: 347-9.

Semenova, M. V., Sinitsyna, O. A., Morozova, V. V., Fedorova, E. A., Gusakov, A. V., Okunev, O. N., Sokolova, L. M., Koshelev, A. V., Bubnova, T. V., Vinetskii, Y. P., Sinitsyn, A. P. (2006) Use of a preparation from fungal pectin lyase in the food industry. Applied Biochemistry and Microbiology, 42(6): 598-602.

Seymour, G. B., Lasslett, Y., Tucker, G. A. (1987) Differential effects of pectolytic enzymes on tomato polyuronides in vivo and invitro. Phytochemistry, 26: 3137-3139.

Shevchik, V. E., Hugouvieux-Cotte-Pattat, N. (1997) Identification of a bacterial pectin acetyl esterase in *Erwinia chysanthemi* 3937. Molecular Microbiology, 24(6): 1285–1301.

Silva, I. R., Jers, C., Meyer, A. S., Mikkelsen, J. D. (2016) Rhamnogalacturonan I modifying enzymes: an update. New Biotechnology, 33(1), 41-54.

Sriamornsak, P. (2003) Chemistry of pectin and its pharmaceutical uses: a review. Silpakorn University International Journal, 3(1-2): 206-228.

Sterling, J. D., Quigley, H. F., Orellana, A., Mohnen, D. (2001) The catalytic site of the pectin biosynthetic enzyme α-1,4-galacturonosyltransferase is located in the lumen of the Golgi. Plant Physiology, 127(1), 360-371.

Taiz, L., Zeiger, E. (2010) Cell walls: structure, biogenesis, and expansion. Plant Physiology. Sinauer Associates, Sunderland, 327.

Teller, D. C., Behnke, C. A., Pappan, K., Shen, Z., Reese, J. C., Reeck, G. R., & Stenkamp, R. E. (2014) The structure of rice weevil pectin methylesterase. Acta Crystallographica Section F: Structural Biology Communications, 70(11): 1480-1484.

Urbanowicz, B. R., Peña, M. J., Ratnaparkhe, S., Avci, U., Backe, J., Steet, H. F., Foston, M., Li, H., O'Neill, M. A., Ragauskas, A. J., Darvill, A. G., Wyman, C., Gilbert, H. J., York, W. S. (2012) 4-O-methylation of glucuronic acid in Arabidopsis glucuronoxylan is catalyzed by a domain of unknown function family 579 protein. Proceedings of National Academy Science, USA, 109: 14253–14258.

Vanholme, R., Demedts, B., Morreel, K., Ralph, J., Boerjan, W. (2010) Lignin biosynthesis and structure. Plant Physiology, 153(3): 895-905.

Viljoen, J. A., Fred, E. B., Peterson, W. H. (1926) The fermentation of cellulose by thermophilic bacteria. The Journal of Agricultural Science, 16(1): 1-17.

Villemez, C. L., Lin, T. Y., Hassid, W. Z. (1965) Biosynthesis of the polygalacturonic acid chain of pectin by a particulate enzyme preparation from Phaseolus aureus seedlings. Proceedings of the National Academy of Sciences of the United States of America, 54(6): 1626-1632.

Vlugt-Bergmans, C. J. B., Meeuwsen, P. J. A., Voragen, A. G. J., Van Ooyen, A. J. J. (2000) Endo-xylogalacturonan hydrolase, a novel pectinolytic enzyme. Applied Environmental Microbiology, 66(1): 36–41.

Voragen, A. G. J., Pilnik, W., Thibault, J. F., Axelos, M. A. V., Renard, C. M. G. C. (1995) Pectins, Food Polysaccharides and their Applications, A.M. Stephen (Ed), Marcel Dekker, Inc., New-York, USA, p. 287-339. Goubet, F., Mohnen, D. (1999) Solubilization and partial characterization of homogalacturonan-methyltransferase from microsomal membranes of suspension-cultured tobacco cells. Plant Physiology, 121(1): 281-290.

Voragen, A. G., Coenen, G. J., Verhoef, R. P., Schols, H. A. (2009) Pectin, a versatile polysaccharide present in plant cell walls. Structural Chemistry, 20(2): 263-275.

Wade Jr, L. G. (1999) Organic chemistry. Prentice-Hall Inc.

Willats, W. G. T, McCartney, L., Mackie, W., Knox, J. P. (2001) Pectin: cell biology and prospects for functional analysis. Plant Molecular Biology, 47: 9–27.

Yadav, S., Yadav, P. K., Yadav, D., Yadav, K. D. S. (2009) Pectin lyase: a review. Process Biochemistry, 44(1): 1-10.

Zandleven, J., Beldman, G., Bosveld, M., Schols, H. A., Voragen, A. G. J. (2006) Enzymatic degradation studies of xylogalacturonans from apple and potato, using xylogalacturonan hydrolase. Carbohydrate Polymers, 65(4): 495-503.

Chapter 2

Cloning, expression and purification of family 8 Carbohydrate esterase (CE8), Pectin methylesterase (*Ct*PME) and derivatives from *Clostridium thermocellum* ATCC 27405

2.1 Introduction

The major constituents of plant cell wall (PCW) are the polysaccharides that accumulate to form a network. These polysaccharides are cellulose, hemicellulose and pectin (Fontes & Gilbert, 2010). The PCW is able to fulfil its structural role by providing strength and protection to the cell owing to the presence of cellulose, hemicellulose and lignin (Vincken *et al*., 2003). PCW has several functional roles such as cell-cell adhesion, cell signalling, wall porosity, pollen tube growth, leaf abscission. The pectin component of the cell wall has been credited to play these roles (Ridley *et al*., 2001). Structural role of pectin in promoting upright growth of plants has also been reported (Matsunaga *et al*., 2004). Pectin is a naturally occurring flexible and complex polysaccharide present in the middle lamella of plant cell wall and plant-derived food products. Pectin is present throughout the plant kingdom. More than 80% of the total pectin consists of D-galactopyranosyluronic acid (DGal*p* A), and the rest is rhamnose (Rha*p*), galactose (Gal*p*), xylose (Xyl*p*) and arabinose (Ara*f*) (Ridley *et al*., 2001).

Citrus and apple are a major source of commercial production of pectin for industrial applications. Pectin is used in food industry for its stabilizing and gelling properties. Traditionally, it is used as gelling agents in jellies, jams and marmalades. Pectin is also used in confectionery, acidified milk products and bakery fillings (May, 1990; Rolin, 2002). Pectin is categorized into three different kinds of polymers based on the covalent bonding of galacturonic acid. The primary structural elements of pectin are homogalacturonan (HG), rhamnogalacturonan I (RG-I) and rhamnogalacturonan II (RG-II), which are discussed in chapter 1, section 1.2.

Degradation of plant cell wall makes a reservoir of nutrients available for recycling. Nature has bestowed a diverse group of microorganisms with enzymes to breakdown the plant cell wall polysaccharides (Ochiai *et al*., 2007**,** Pages *et al*., 2003 and McKie *et al*., 2001). When pectin comes under microbial attack both glycoside hydrolases, polysaccharide lyases and pectin esterases are recruited. Glycoside hydrolases cleave the glycosidic bonds via an acid-base catalytic mechanism (Koshland *et al*., 1953). Polysaccharide lyases cleave their substrates *via* a β-elimination mechanism, generating a double bond between C-4 and C-5 in the residue at the non-reducing end (Moran *et al*., 1968). Glycoside hydrolases and polysaccharide lyases have been classified into different families based on sequence similarity (Lombard *et al*., 2014). Many of the plant cell wall polysaccharide degrading enzymes are modular in nature and have one or more specialized substrate binding module(s) referred to as Carbohydrate Binding Module(s) (CBM) in addition to a catalytic module (Duan *et al*., 2016).

Pectin methylesterases (PMEs; EC: 3.1.1.11) are a group of enzymes, belonging to family 8 carbohydrate esterase (CE8) categorized under pectin esterase

superfamily (CAZy database, www.cazy.org). PME hydrolyses methyl esters at the C-6 position of D-Galp A residues in HG and releases pectate and the methanol (Fraeye *et al.,* 2010). The de-esterified pectate is further degraded by polygalacturonase, pectate lyase and rhamnogalacturonan lyase (Kashyap *et al*., 2001), which are produced by different organisms such as bacteria, fungi and plants, as well as insects (Jiang *et al*., 2013). In plants, pectin methylesterase used for ripening by destabilization in cell wall metabolism (Frenkel *et al*., 1998). Plant-derived PMEs work under alkaline conditions (pH 7.0–9.0) (Michelis, 2001; Duvetter *et al*., 2006), whereas fungal, e.g. *Aspergillus niger*, PMEs work under acidic conditions (Limberg *et al*., 2000; Kim *et al*., 2013; Kent *et al*., 2016). Phytopathogenic micro-organisms can degrade plant cell walls through its PME during the plant invasion; therefore, this enzyme is known to be a virulence factor of phytopathogens (Michelis, 2001).

The modular protein, Cthe_2949 (GenBank accession number ABN54147.1 and Uniprot ID A3DJL8) of *Clostridium thermocellum* ATCC 27405 (renamed as *Ruminiclostridium thermocellum*) is a modular carbohydrate-active enzyme. Its nucleotide and protein sequences were retrieved from the CAZy database and analyzed by different computational approaches including the BLAST tool. The protein sequence, Cthe_2949 contained 567 amino acids. BLAST analysis revealed that the protein, Cthe_2949 contained a N-terminal putative pectin methylesterase (PME) module (*Ct*PME) belonging to carbohydrate esterase family 8 (CE8), linker and X-157 (Unknown function module) and followed by a Dockerin at C-terminal.

The molecular architecture of CE8 protein sequence was drawn by using the DOG2.0 software and presented in Fig. 2.1. The Conserved Domains Database was referred for determining the regions of conserved domains (http://www.ncbi.nlm.nih.

gov/cdd/). The CE8 protein sequence was analysed by InterProScan (http://www.ebi.ac.uk/Tools/pfa/iprscan/) to identify various domains. The N-terminal contains the signal peptide was predicted between 1 to 30 amino acids by SignalP 3.0 server (http://www.cbs.dtu.dk/services/SignalP-3.0/). Towards the N-terminal, downstream of the signal peptide, a stretch of 300 amino acids, the catalytic module *Ct*PME showed similarity to the super family of pectin methyl esterases (Fig. 2.1). A short stretch of 22 amino acids (331-353) linker region connects another module spanning from amino acids, from 354 to 494, an un known module named *Ct*X157. This is followed a type I dockerin from 503 to 567 amino acids and a Ca^{2+} ion binding site from 509 to 551 amino acid residues at the C-terminal. The interaction between enzymes borne Dockerin modules and the Cohesin modules of a scaffold protein gives rise to the celluosomal complex (Fontes *et al*., 2010). The presence of a putative Dockerin I at C-terminal and the subcellular localisation score predicted by PSORT server indicated that the protein encoded by sequence Cthe_2429 is an extracellular enzyme and probably integrates as a component of the *C. thermocellum* cellulosome.

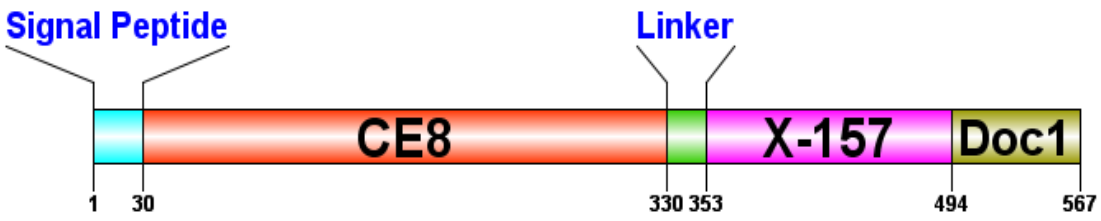

Fig. 2.1 Molecular architecture of protein Cthe_2949 showing CE8 and derivative domains.

In the present study the genes encoding CE8 and its truncated derivatives *Ct*PME-catalytic, *Ct*X157 (Unknown) and *Ct*PME-X157 (*Ct*PME*f*) were cloned. All the proteins were expressed in *Escherichia coli* and purified by immobilized metal ion affinity chromatography (IMAC) for further biochemical, functional and structural characterization.

2.2 Materials and Methods

2.2.1 Chemicals, reagents and kits

The oligonucleotide primers for PCR amplification of genes encoding *Ct*PME*f*, *Ct*PME and *Ct*X157 were procured from Eurofins, India. BIOTAQ DNA polymerase was supplied by Bioline, UK. dNTPs and $MgCl_2$ were obtained from GeNei, India. PCR tubes (0.2 ml) were from Axygen, Germany. Restriction enzymes *Nhe*I, and *Xho*I were purchased from Promega, USA. The expression vector, pET28a(+) was purchased from Novagen, Germany. T_4 DNA ligase and 10x ligase buffers were purchased from Promega, USA. RNAse solution (20 mg/ml), glacial acetic acid (99.9% pure), Trizma base (Tris free base), ethidium bromide, Bradford reagent, nuclease free water (pH 8.0) and components of polyacrylamide gel electrophoresis were obtained from Sigma-Aldrich, USA. The GenElute miniprep, plasmid isolation kit and GenElute gel-extraction kit was from Sigma-Aldrich, USA. DNA was electrophoresed on agarose gels prepared by using Agarose, with low EEO (Electroendosmosis) purchased from Sigma-Aldrich, USA. DNA marker, Hyperladder I was purchased from Bioline, UK. Protein markers were procured from Fermentas, Canada and GeNei, Bangalore India. Disodium ethylenediamine tetra acetate salt (EDTA), glucose, sodium hydroxide, sodium dodecyl sulphate (SDS), LB medium and SOC medium components were supplied by Himedia Pvt. Ltd., India. The antibiotic, kanamycin was procured from Sigma-Aldrich, USA. Lysozyme purchased from Himedia Pvt. Ltd., India. Mini-PROTEAN Tetra Cell purchased from Bio-Rad Laboratories (India) Private Limited. The protein staining dye Coomassie Brilliant Blue R250 was procured from Himedia Pvt. Ltd., India and methanol from Merck, India. The genomic DNA of *Clostridium thermocellum* ATCC 27405 (Renamed as

Ruminiclostridium thermocellum ATCC 27405) was purchased from Leibniz Institute DSMZ - German Collection of Microorganisms and Cell Cultures. The collection no. ATCC 27405, JCM 9322, NCIMB 10682 for DSM NO. 1237 for same organism genomic DNA.

2.2.2 Microorganisms

Commercially available *E. coli* TOP10 and *E. coli* BL-21 (DE3) cells were obtained from Novagen, Germany.

2.2.3 PCR amplification of genes encoding *Ct*PME, *Ct*X157 and *Ct*PME*f*

The genes encoding *Ct*PME, *Ct*X157 *and Ct*PME*f* were amplified with designed oligonucleotide primers using the *Clostridium thermocellum* ATCC 27405 genomic DNA as template. The primers contained the restriction enzyme sites of *Nhe*I and *Xho*I as mentioned in Table 2.1. Amplification of each module was done following the scheme presented in Fig. 2.2. Components of 50 µl PCR reaction mixture and the PCR cycles for amplification are given in Tables 2.2 and 2.3, respectively. PCR amplification was performed in a thermal cycler (Takara, GeneAmp PCR System 9700). The PCR amplicons were electrophoresed on a 0.8 % (w/v) agarose gel along with a DNA marker (Hyper ladder I) as mentioned in Section 2.2.4.

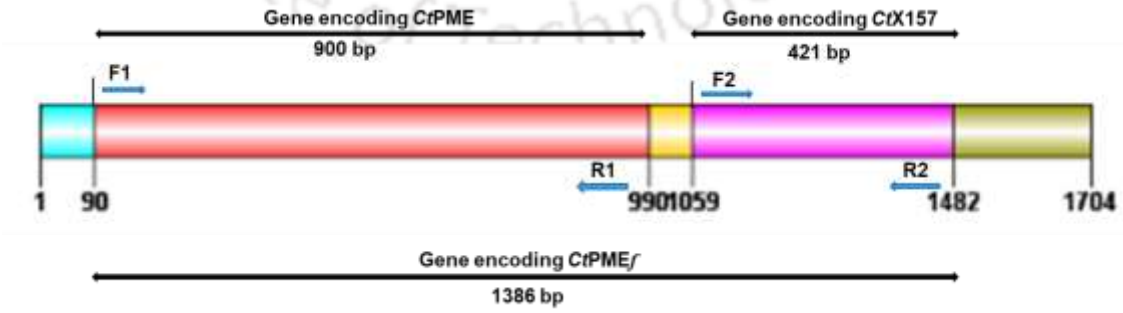

Fig. 2.2 Schematic presentation showing primers used for PCR amplification of genes encoding *Ct*PME, *Ct*X157 and *Ct*PME*f* from 2460 bp gene sequence of protein ABN54147.1 of *Clostridium thermocellum*.

Table 2.1 Oligonucleotide primers used for PCR amplification of genes encoding *Ct*PME, *Ct*X157 and *Ct*PME*f* from *Clostridium thermocellum*, nucleotides shown in bold represent the restriction enzyme sites.

Module	Primer name	Primer sequence
*Ct*PME	F1	5'- cg**ggctagc**gcagcggtcaatgcggat-3'
	R2	5'- cc**ctcgag**ttagagcgcaaccggattcca-3'
*Ct*X157	F2	5'- cg**ggctagc**ggccaattgataaaatcattaacg-3'
	R2	5'- cc**ctcgag**ttatatgacaatataattcacagccc-3'
*Ct*PME*f*	F1	5'- cg**ggctagc**gcagcggtcaatgcggat -3'
	R1	5'- cc**ctcgag**ttatatgacaatataattcacagccc -3'

Table 2.2 PCR reaction setup for amplification of genes encoding *Ct*PME, *Ct*X157 and *Ct*PME*f* from *Clostridium thermocellum.*

PCR components	Volume (µl)	Final concentration
10x reaction buffer	5.0	1x
dNTP mix (100 mM)	1.0	2 mM
Forward primer (15 µM)	1.5	0.45 µM
Reverse primer (15 µM)	1.5	0.45 µM
Sigma water, pH 8.0	38.0	--
Genomic DNA (15 µg/ml)	0.5	7.5 ng
Taq DNA polymerase (2.5 U/µl)	2.5	6.25 U
Total	**50.0**	--

Table 2.3 Conditions for PCR thermal cycles for amplification of genes encoding *Ct*PME, *Ct*X157 and *Ct*PME*f* from *Clostridium thermocellum.*

Step	***Ct*PME**	***Ct*X157**	***Ct*PME*f***	CYCLES
Initial Denaturation	94°C for 4 min	94°C for 4 min	94°C for 4 min	1
Denaturation	94°C for 30 s	94°C for 30 s	94°C for 0.5 min	30
Annealing	65°C for 1 min	60°C for 30 s	60.8°C for 1 min	
Extension	68°C for 1 min	68°C for 1 min	68°C for 1 min	
Final Extension	68°C for 10 min	68°C for 10 min	68°C for 10 min	1

2.2.4 Agarose gel electrophoresis of PCR amplified products

The PCR amplified products were electrophoresed on 0.8% (w/v) agarose gel prepared in 1x TAE buffer. A stock solution of TAE buffer was prepared according to Sambrook and Russell (2001) keeping the concentrations of components to 10x (400 mM Tris-acetate, 10 mM EDTA, pH 8.0). A gel was prepared by dissolving agarose (400 mg for 0.8% (w/v) and 500 mg for 1.0% (w/v) gel) in 50 ml of 1x TAE buffer by heating in a microwave oven to get a clear solution. Then 5.0 µl of ethidium bromide (5.0 mg/ml) was added when the solution temperature was around 50°C. The solution was mixed well and poured on the casting apparatus, comb was placed and the gel was allowed to solidify. 1x TAE (Tris-acetate-EDTA) buffer was used for preparation of agarose gels and also as an electrophoresis buffer (Sambrook and Russel, 2001). The DNA sample and DNA loading dye were mixed in 4:1 ratio and the gel was run at constant 50 Volt till the dye migrated over 70% of the gel length. The DNA bands were then visualized under UV illumination in a gel documentation system (BioRad XR).

2.2.4.1 DNA loading buffer

The DNA or sample loading buffer was prepared by mixing the components mentioned below in Table 2.4. A 5x stock solution of DNA loading buffer was prepared and mixed with 4 volumes of DNA to make it to 1x before loading on to agarose gels. The final pH of the DNA loading dye adjusted to pH 8.0.

Table 2.4 Composition of 5x DNA loading buffer.

Components	Final concentration (5x)
Tris-HCl (pH 8.0)	50 mM
Glycerol	25% (w/v)
EDTA	5.0 mM
Bromophenol blue	0.2% (w/v)
Xylene cyanol	0.2% (w/v)

2.2.5 Extraction of DNA from agarose gel

The PCR amplified DNA or other plasmids were extracted and purified from agarose gel using a kit (GenElute, Sigma-Aldrich, USA), following the protocol provided by the manufacturer as discussed in Section 2.2.5.1. The extracted DNA was eluted in 30 µl elution buffer supplied with the kit.

2.2.5.1 Protocol for extraction of DNA from agarose gel

1. 1.5 ml sterile microcentrifuge tube was weighed and the weight was noted.
2. The PCR amplified DNA or plasmid was excised from gel using sharp sterile scalpel and transferred to the micro-centrifuge tube. The tube was weighed again and the weight of excised gel was determined by subtracting the weight of the empty tube.
3. Now, 3 volumes of Gel solubilisation solution were added to every 1 volume of gel (100 mg ~ 100 µl).
4. The micro-centrifuge tube containing excised gel was incubated at 50°C for 10 min (or until the gel slice dissolved completely)
5. 1 gel volume of isopropanol was added to this solution.
6. GenElute binding column G was placed in a 2 ml collection tube provided with the kit. 500 µl of column preparation solution was added over column

membrane and centrifuged at 16,000***g*** for 1 min. The flow through was discarded.

7. The solution containing PCR-amplified DNA or plasmid (~700 µl) were added to DNA binding columns and centrifuged at 16,000***g*** for 1 min at room temperature discarding the flow through. If the volume was more than 700 µl, the remaining solution was centrifuged similarly and again the flow through was discarded.
8. 700 µl of Wash solution was added to each the DNA bound spin column and the mixture centrifuged at 16000g for 1 min at room temperature, discarding the flow through. The column was given an additional spin of 1 min at 16000***g*** to completely remove the residual ethanol.
9. Now the column containing bound DNA was placed on a fresh 1.5 ml sterile microcentrifuge tube. 30 µl of DNAse free water (Sigma-Aldrich, USA) or eluent solution (10 mM Tris-HCl, pH 8.5) was added at the centre of the column. The column was incubated for 2 min at room temperature and then centrifuged at 16000***g*** for 1 min. For efficient recovery of DNA, the elution solution was preheated to 65°C prior to adding it to the membrane. Eluting at 65°C improves the DNA recovery by 2 to 3-fold.
10. The PCR-amplified DNA or plasmid were eluted from GenElute spin columns and collected in 1.5 ml sterile microcentrifuge tube and stored at -20°C for further use.

2.2.6 Preparation of culture medium

The most commonly used LB medium for growing the *E. coli* cells containing recombinant plasmid was prepared by dissolving the ingredients (Table 2.5) in 800 ml of deionized water. The pH was adjusted to 7.2 and final volume was made up to 1 litre. 100 ml of LB medium was then transferred to 250 ml conical flask and autoclaved at 121°C at 15 psi for 20 min. The filter sterilized antibiotic (Kanamycin; 50 µg/ml) was added to autoclave and cooled LB medium prior to inoculation.

Table 2.5 Composition of Luria-Bertani medium (Sambrook *et al*., 1989)

Components	Final concentration (%, w/v)
Tryptone	1.0
Yeast extract powder	0.5
Sodium chloride	1.0

2.2.6.1 Preparation of LB-agar medium

LB agar medium was prepared by boiling 1.8% (w/v) Agar Agar type I in broth medium (Table 2.6). The medium was autoclaved as described in Section 2.2.6 cooled to around 40-45°C and appropriate amount of antibiotics (kanamycin; 50 µg/ml) was added under laminar air flow. 25 ml of medium supplemented with antibiotics were poured in sterile petri plates and allowed for 15- 20 min to solidify. After solidification, petri plates were stored at 4°C.

Table 2.6 Composition of Luria-Bertani Agar medium (Sambrook *et al*., 1989)

Components	Final concentration (%, w/v)
Tryptone	1.0
Yeast extract powder	0.5
Sodium chloride	1.0
Agar-Agar	1.8

2.2.7 Preparation of SOC medium

The SOC (super optimal medium with catabolic repression) was prepared using ingredients mentioned in Table 2.7. It is a modified SOB (super optimal broth) with addition of glucose (Hanahan, 1983). Bactotryptone, yeast extract powder and NaCl was autoclaved. 1 M stock solutions of KCl, $MgCl_2$, $MgSO_4$ and glucose were filter-sterilized and required quantities added to above solution in the laminar hood to finally make the SOC medium.

Table 2.7 Composition of SOC medium (Sambrook *et al*., 1989).

Component	Final concentration
Bactotryptone	2.0 (%, w/v)
Yeast extract powder	0.5 (%, w/v)
NaCl	10 mM
KCl	2.5 mM
$MgCl_2$	10 mM
$MgSO_4$	10 mM
Glucose	20 mM

2.2.8 Preparation of *E. coli* TOP10 competent cells

Day 1

1. 50 µl of culture of *E. coli* TOP10 cells from glycerol stock was inoculated into 5.0 ml LB medium (Sambrook *et al*., 1989) contained in a test tube and grown overnight at 37ºC and 180 rpm.
2. 0.1 M $CaCl_2$ solution was filter-sterilized by passing through 0.22 µm filter in laminar air flow and kept in refrigerator.

Day 2

3. 1.0 ml culture from day 1 was inoculated into 100 ml LB medium kept in 250 ml conical flask and incubated at 37ºC with 180 rpm till cell Optical Density reached 0.4-0.6 at 550 nm.
4. Micro-centrifuge tubes, 50 ml centrifuge tubes (round bottom) and micro tips were autoclaved and kept on ice and placed in a laminar air flow hood.
5. 40 ml culture was transferred aseptically to round bottom centrifuge tubes.
6. The tubes were centrifuged at 4ºC with 4000***g*** for 10 min.
7. The step was repeated to centrifuge the entire 100 ml culture.
8. The cell pellet was re-suspended in 3-4 ml sterile, ice-chilled 0.1 M $CaCl_2$ solution followed by making up the final volume to 20 ml. The cell suspension in centrifuge tubes was kept on ice for 10 min.
9. The tube was centrifuged again at 4000***g*** at 4ºC for 10 min.
10. The supernatant was carefully removed and the pellet re-suspended in 3.0 ml of sterile ice chilled 0.1 M $CaCl_2$ solution.
11. 200 µl of competent cells were aliquoted into each 1.5 ml microcentrifuge tube containing 10% (v/v) glycerol (final concentration) and kept at -80ºC for further use.

2.2.9 Cloning of genes encoding *Ct*PME, *Ct*X157 and *Ct*PME*f* into pET28a(+) vector

The pET-28a(+) is a modified form of pBR322 plasmid. It is a frequently used vector for cloning and expression of recombinant proteins in *E. coli*. pET-28a(+) vector has a strong T7 promoter system originally developed by Studier and colleagues (Studier and Moffatt, 1986; Studier *et al.*, 1990). The expression of genes cloned in pET plasmids is under the control of T7 bacteriophage promoter. The cloned genes are transcribed by T7 RNA polymerase of the host cell. The genes cloned in pET vectors remain transcriptionally silent in the uninduced state. The proteins encoded by the cloned genes are transcribed and contain a His_6-Tag, which single step purification using affinity chromatography. The pET-28a(+) vector allows for incorporation of expressed protein with an N-terminal His_6-Tag/thrombin/T7-Tag in addition to an optional C-terminal His_6-Tag sequence (Fig. 2.3). The location of sequence encoding His-Tag, T7 promoter, T7 terminator, kanamycin resistance and f1 origin are indicated in the Fig. 2.3.

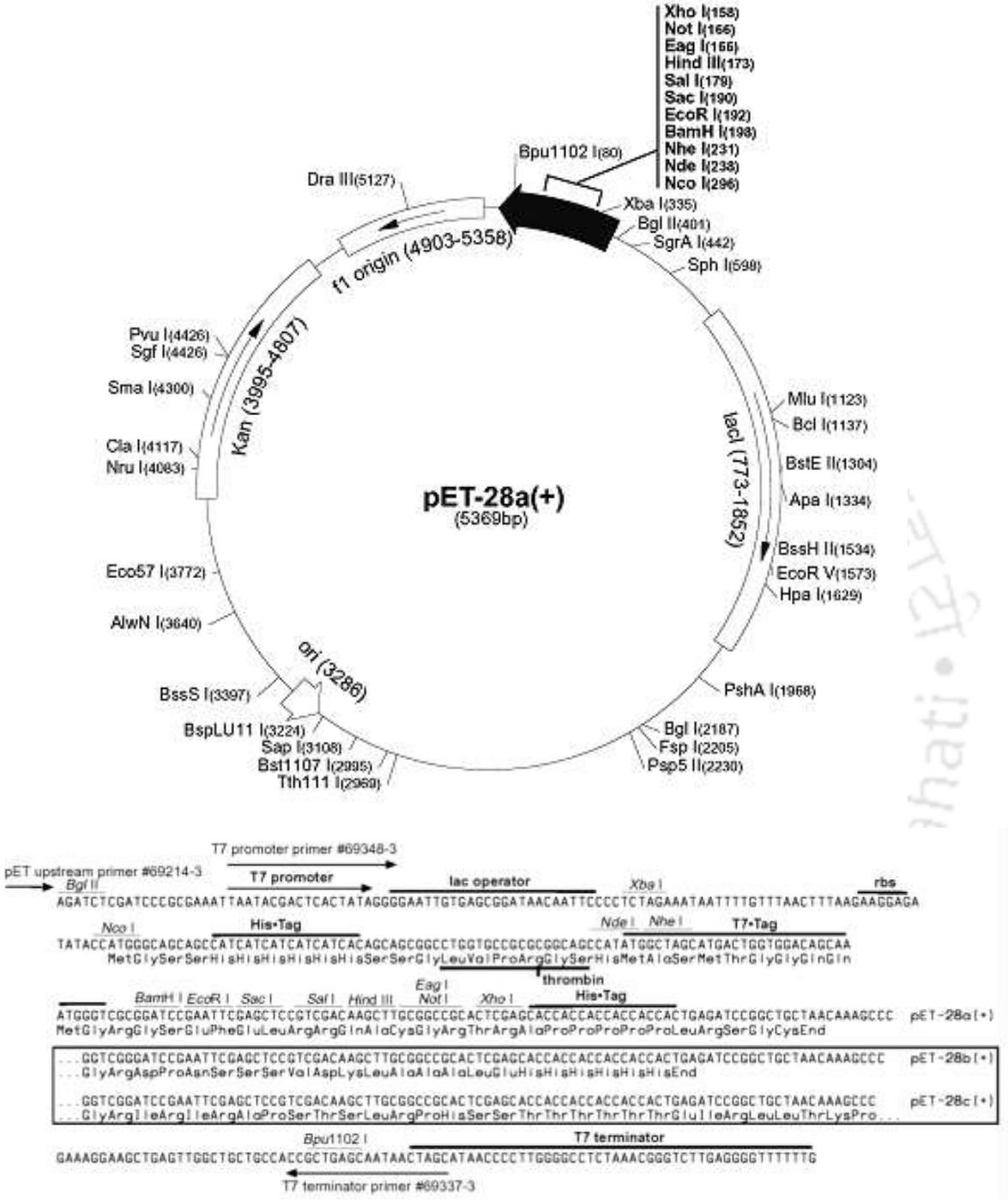

Fig. 2.3 Restriction map of the pET-28a(+) expression vector showing multiple cloning site (158-203 bp), restriction enzyme sites, N-terminal His_6-Tag coding sequence (270-287 bp), C-terminal His_6-Tag coding sequence (140-157 bp), T7 promoter (370-386), T7 terminator (26-72 bp), pBR322 origin (3286 bp), kanamycin marker (3995-4807 bp) and a f1 origin (4903-5358). *Nhe*I cuts at 231 and *Xho*I at 158.

2.2.9.1 Restriction digestion of PCR amplified genes encoding *Ct*PME, *Ct*X157 and *Ct*PME*f* and pET-28a(+) plasmid DNA

The pET-28a(+) vector was digested with *Nhe*I-*Xho*I restriction enzymes (Table 2.8). PCR amplified genes encoding *Ct*PME, *Ct*X157 and *Ct*PME*f* were also digested with *Nhe*I-*Xho*I to prepare them for ligation with restriction digested pET-28a(+) vector (Table 2.9). The digestion reactions were incubated in a water bath at 37°C for 90 min. The *Nhe*I-*Xho*I digested pET vector and PCR amplified genes were purified from agarose gel as described in Section 2.2.5.

Table 2.8 Restriction enzyme digestion of pET-28a (+) plasmid DNA.

Reaction components	**Volume (µl)**
10x buffer	3.0
Nuclease free water	4.5
Bovine serum albumin (10 mg/ml)	0.5
Plasmid DNA (approx. 13 ng/ µl)	20.0
*Nhe*I (10 U/µl)	1.0
*Xho*I (10 U/µl)	1.0
Total	30.0

Table 2.9 Restriction enzyme digestion of PCR amplified genes encoding *Ct*PME, *Ct*X157 and *Ct*PME*f*.

Reaction component	Gene encoding *Ct*PME (µl)	Gene encoding *Ct*X157 (µl)	Gene encoding *Ct*PME*f* (µl)
10x buffer	3.0	4.0	4.0
Nuclease-free water	4.5	13.5	6.5
Bovine serum albumin (10 mg/ml)	0.5	0.5	0.5
PCR amplified product	20 (~125 ng)	20 (~100 ng)	20(~100 ng)
*Nhe*I (10 U/µl)	1 (118 ng)	1 (68.7 ng)	1 (15 ng)
*Xho*I (10 U/µl)	1	1	13.5
Total	30	40	30

2.2.9.2 Ligation of restriction digested genes encoding *Ct*PME, *Ct*X157 and *Ct*PME*f* into pET-28a(+) vector

The *Nhe*I-*Xho*I digested genes encoding *Ct*PME, *Ct*X157 and *Ct*PME*f* were ligated into pET-28a(+) vector, which was also digested with same restriction enzymes as described in Section 2.2.9.1. Three ligation reactions were setup using the reaction components mentioned in Table 2.10 and incubated at 16°C overnight to get maximum number of transformants. The reactions were setup at an insert: vector molar ratio of 3:1, where the amount of insert is calculated as mentioned below:

$$\frac{\text{amount of vector (ng)} \times \text{size of insert (kb)}}{\text{Size of vector (kb)}} \times \text{insert :vector molar ratio} = \text{amount of insert (ng)}$$

$$\frac{50 \text{ (ng)} \times 0.9 \text{ (kb)}}{5.369 \text{ (kb)}} \times \frac{3}{1} = 25.1 \text{ ng (}Ct\text{PME)}$$

$$\frac{50 \text{ (ng)} \times 0.42 \text{ (kb)}}{5.369 \text{ (kb)}} \times \frac{3}{1} = 11.7 \text{ ng (}Ct\text{X157)}$$

$$\frac{50 \text{ (ng)} \times 1.453 \text{ (kb)}}{5.369 \text{ (kb)}} \times \frac{3}{1} = 40.6 \text{ ng (}Ct\text{PME}f\text{)}$$

Table 2.10 Components of reaction for ligating genes encoding *Ct*PME, *Ct*X157 and *Ct*PME*f* into pET-28a(+) expression vector.

Reaction component	Gene encoding *Ct*PME (µl)	Gene encoding *Ct*X157 (µl)	Gene encoding *Ct*PME*f* (µl)
10x Rapid Ligation Buffer	1	1.5	2.5
pET-28a(+) Vector	5 (50 ng)	6.2 (50 ng)	5 (50 ng)
Restriction digested product	2.15 (60 ng)	6 (10 ng)	13.5 (15 ng)
T4 DNA Ligase (3 Units/µl)	1	1	1
Nuclease-free water	0.85	0.3	3
Total	10	15	25

2.2.9.3 Transformation of ligated recombinant DNA into *E. coli* TOP10 cells

The *E. coli* TOP10 competent cells were transformed with ligation reactions, after overnight ligation. Preparation of *E. coli* competent cell preparation has been described in Section 2.2.8. The step-wise transformation protocol is described below:

1. The micro-centrifuge tube containing competent cell (200 µl) was taken out from -80°C and kept on ice for 5 min.
2. 10 µl of ligation mixture was added to cells and the tube was gently tapped 4-5 times and kept on ice for 30 min. The cells were occasionally tapped gently during 30 min incubation.
3. The cells were given a heat shock at 42°C for 40s.
4. The cells were immediately transferred back to the ice and kept for 5 min.
5. 800 µl of super optimal medium with catabolite repression (SOC) (Hanahan, 1983; Sambrook *et al*., 1989; given in Section 2.2.7) (previously incubated at 37°C) was added to the transformed cells.
6. The transformed cells were incubated at 37°C in a shaking incubator at 220 rpm for 1h.
7. The cells were centrifuged at 2000***g***, 25°C for 5 min.
8. 800 µl supernatant was discarded and the cell pellet was re-suspended in remaining 200 µl supernatant.
9. The 200 µl cells were spread plated on LB agar plates as described in Section 2.2.6.1 supplemented with antibiotics. The LB agar plates were incubated overnight at 37°C.

10. The transformation efficiency was calculated using the following formula,

$$\text{Transformation efficiency} = \frac{\text{No. of colonies on LB plate}}{\text{Amount of insert (µg)}} = \text{cfu/µg}$$

The 15-20 µl of ligation mixture was added to 200 µl *E. coli* TOP10 competent cells, following the above transformation protocol. The transformed TOP10 cells were plated on LB plates supplemented with kanamycin (50 µg/ml) and grown overnight at 37°C, 180 rpm.

2.2.9.4 Isolation of plasmid DNA from transformed colonies by miniprep kit

Overnight incubated plates were observed for colonies. Colonies preferably from the centre of the plate were randomly picked in a laminar air flow and grown overnight in 5 ml LB medium supplemented with kanamycin (50 µg/ml). The plasmid DNA from this 5 ml culture was isolated by miniprep kit (Sigma-Aldrich, USA) following the protocol mentioned in Section 2.2.9.4.1.

2.2.9.4.1 Plasmid isolation protocol by miniprep kit

1. 10 ml from each of the grown culture containing recombinant plasmid were pelleted in 1.5 ml microcentrifuge tube aseptically.
2. The cells were then centrifuged at 14000***g*** for 1 min and the process was repeated six times with 1.5 ml culture (Total 9ml culture).
3. The resulting cell pellet of each recombinant derivative was re-suspended in 200 µl resuspension solution and vortexed. RNAse at final concentration of 0.3 mg/ml was added to the re-suspension solution prior to use.
4. 200 µl of lysis solution was added to each tube and the tubes were inverted gently 5-6 times to ensure mixing and allowed to stand for 2-5 min.

5. 350 µl of neutralization solution was added to the mixture and the tubes were inverted again for 4–6 times to mix properly.
6. The mixture was centrifuged at 16,000***g*** for 10 min.
7. The DNA binding columns were prepared and activated by adding 500 µl of column preparation solution to binding column and centrifuging at 14,000***g*** for 1 min. The flow through accumulated in collection tube was discarded.
8. The clear lysate was then transferred to activated DNA binding column, centrifuged at 14,000***g*** for 1 min and the flow through in the collection tube was discarded again.
9. The plasmid DNA bound to the column was washed with wash solution and spun at 14,000***g*** for 1 min. The flow through was discarded and the column was given another 1 min spin at 14,000***g*** for removing the wash solution completely.
10. The DNA binding column was transferred to a fresh sterile microcentrifuge tube and 30 µl of TE buffer solution or DNAse free water was added at the centre of binding column. The microcentrifuge tube was allowed to stand for 10 min at room temperature and then plasmid DNA was eluted by centrifugation at 14,000***g*** for 1 min.
11. The eluted plasmid DNA in sterile microcentrifuge tube was stored at -20°C.

2.2.9.5 Screening of recombinant plasmid DNAs for positive clones by restriction digestion

15 µl of recombinant plasmids from pET-28a(+) clones of *Ct*PME, *Ct*X157 and *Ct*PME*f* that were isolated in the last step, were taken in separate fresh sterile micro-centrifuge tubes for restriction enzyme digestion analysis. The recombinant plasmid DNA of each of the above mentioned derivatives was digested with restriction enzymes, *Nhe*I and *Xho*I, to check for positive clones following a 30 µl reaction mixture set up as mentioned in Table 2.8.

2.2.10 Preparation of competent *E. coli* BL-21 (DE3) cells

The competent *E.coli* BL-21 (DE3) cells were prepared by calcium chloride method following the protocol as discussed in Section 2.2.8. Finally, 10% (v/v) glycerol (final concentration) was added to competent cells and 200 µl aliquots were made in sterile microcentrifuge tubes and stored at -80°C for further use.

2.2.11 Transformation of recombinant plasmids containing genes encoding *Ct*PME, *Ct*X157 and *Ct*PME*f* into *E. coli* BL21 (DE3)

2 µl of from each of the recombinant plasmid of positive pET-28a(+) clone isolated in Section 2.2.9.5 was used for transformation of 200 µl *E. coli* BL-21 cells for protein expression following the transformation protocol described in Section 2.2.9.3. Recombinant plasmids containing genes encoding *Ct*PME, *Ct*X157 and *Ct*PME*f* were transformed into *E. coli* BL-21 cells and plated on LB agar plates supplemented with kanamycin (50 µg/ml) and grown overnight at 37°C.

2.2.12 Expression of recombinant *Ct*PME, *Ct*X157 and *Ct*PME*f* proteins

The *E. coli* BL21(DE3) cells used as host for expression of proteins, *Ct*PME, *Ct*X157 and *Ct*PME*f* were cultured in 100 ml of LB medium supplemented with kanamycin (50 µg/ml) incubated at 37°C, 180 rpm. After the cell growth reached mid

exponential phase (A_{600} = 0.6). The cells expressing *Ct*PME, *Ct*X157 and *Ct*PME*f* were cooled to 24°C and after cooling the cultures were induced with isopropyl-β-D-thiogalactopyranoside (IPTG) at a final concentration of 1 mM and further incubated at 180 rpm for 12-16 h.

2.2.13 Sodium dodecyl sulphate-Polyacrylamide gel electrophoresis (SDS-PAGE) analysis of recombinant proteins

The recombinant proteins were separated on SDS-PAGE gel on the basis of their respective molecular size. PAGE was used to separate components of a protein mixture based on their size (Laemmli, 1970; Sambrook *et al*., 1989). The expression and purification of *Ct*PME, *Ct*X157 and *Ct*PME*f* were analysed by running on 12% (w/v) SDS-PAGE gel using ingredients as mentioned in Tables 2.11 and 2.12.

Table 2.11 Composition of SDS-PAGE components for preparation of resolving gel.

Component	**12% gel volume (ml)**
Acrylamide solution *(30%,w/v)	4.0
Deionized water	0.7
SDS (10%,w/v)	1.0
Glycerol (50%,v/v)	1.0
1.5 M Tris-HCl (pH 8.8)	3.3
APS (10%,w/v)	0.1
TEMED	0.01
Total	**10 ml**

**mixture of 29.2% (w/v) acrylamide and 0.8% (w/v) N,N'-Methylenebis(acrylamide).*

Table 2.12 Composition of SDS-PAGE components for preparation of stacking gel.

Components	**4% gel volume (ml)**
Acrylamide solution* (30%, w/v)	0.7
Deionized water	2.8
SDS (10%, w/v)	0.5
0.5 M Tris-HCl (pH 6.8)	1.0
APS (10%, w/v)	0.05
TEMED	0.005
Total	**5 ml**

**mixture of 29.2% (w/v) acrylamide and 0.8% (w/v) N,N'-Methylenebis(acrylamide).*

SDS-PAGE was run using 1 x Tris-Glycine (pH 8.3-8.5) running buffer at constant 40 mA current. The expressed and purified protein samples were visualised after staining the gel with staining soultion containing (0.25%, w/v) Coomassie Brilliant Blue (CBB) R-250 dye 100 ml solution of deionized water, methanol and glacial acetic acid in 5:4:1 ratio. The gels were de-stained by immersing the gel in de-staining solution containing deionized water, methanol and glacial acetic acid in 5:4:1 ratio. The gels were subjected to gentle rocking with periodic change of de-staining solution was done, until the protein bands were clearly visible.

2.2.14 Purification of recombinant *Ct*PME, *Ct*X157 and *Ct*PME*f* proteins

The recombinant *Ct*PME, *Ct*X157 and *Ct*PME*f* proteins containing a His_6-tag at the N-terminal were purified through a single step purification method based on immobilized metal-ion affinity chromatography (IMAC) as described in Section 2.2.14.1. The purification of these recombinant proteins was carried out by using 1.0 ml sepharose columns (HiTrap chelating HP, GE Healthcare). The composition of binding as well as elution buffers used for affinity column purification is mentioned in Table 2.13.

Table 2.13 Composition of buffers required for purification of recombinant proteins by affinity purification (IMAC).

Buffers	Composition
Equilibration buffer	50 mM Tris-HCl, pH 8.5 500 mM NaCl, 50 mM Imidazole
Elution buffer	50 mM Tris-HCl, pH 8.5 500 mM NaCl, 350 mM Imidazole
Cleaning buffer	50 mM Tris-HCl, pH 8.0 500 mM NaCl, 50 mM EDTA

2.2.14.1 IMAC purification protocol for recombinant *Ct*PME, *Ct*X157 and *Ct*PME*f* proteins

1. The bacterial cells (100 ml culture) were harvested by centrifugation at 9,000***g*** at 4°C for 10 min. The cell pellet was re-suspended in 7 ml of 50 mM Tris-HCl buffer, pH 8.5.
2. 1 mM phenyl methane sulfonyl fluoride (PMSF) and 0.2 mg/ml lysozyme were added to re-suspended solution and incubated at 4ºC for 20 min.
3. The cells were sonicated on ice for 30 min (7s on and 15s off pulse; with 33% amplitude) and centrifuged at 12,000***g*** at 4ºC for 30 min to get the crude cell free extract.
4. The cell free extract was passed through a 0.45 µm filter membrane before loading onto 1 ml HiTrap chelating HP column. The column was pre-washed with 5 volumes of filtered and degassed water to remove the alcohol.
5. Column was charged using 2.0 ml of 0.1 M $NiSO_4$ solution and the unbound Ni^{2+} ions were washed away with 2-5 volumes of water.
6. Then the column was equilibrated with 10 volumes of equilibration buffer (Table 2.13).
7. The filtered cell free extract of recombinant protein was loaded on to the column at a flow rate of 0.5 ml/min.
8. The column was then washed with 50 column volumes of equilibration buffer to remove the unbound proteins.
9. The retained protein of interest was then eluted with elution buffer under a gradient of 0-100% imidazole concentration and 1 ml fractions were collected (Carvalho *et al.*, 2004).

10. The column was cleaned using cleaning buffer as mentioned in Table 2.13, washed with 5 volumes of water and incubated in 1N NaOH at 4°C for 2h. The column was then washed with 50 volumes of water to remove NaOH, and finally stored in 20% (v/v) ethanol at 4°C.

The purified recombinant proteins *Ct*PME, *Ct*X157 and *Ct*PME*f* were dialyzed (Cut off 3-5 kDa) against 50 mM Tris-HCl buffer, pH 8.5 containing 200 mM NaCl. The purity and molecular mass of recombinant proteins were verified by SDS-PAGE as described in Section 2.2.13.

2.2.15 Protein concentration determination of purified recombinant proteins

The concentration of purified protein was determined from their corresponding absorbance at 280 nm using the equation below (Layne, 1957; Stoscheck, 1990). The absorbance was measured after appropriate dilution of the protein using a spectrophotometer (Gene Quant, GE Health care) having a path length of 1 cm. The molar extinction co-efficient 43570 $M^{-1}cm^{-1}$ for *Ct*PME, 30940 $M^{-1}cm^{-1}$ for *Ct*X157 and 76125 $M^{-1}cm^{-1}$ for *Ct*PME*f*, respectively were used.

$$\text{Concentration of protein (mg/ml)} = \frac{\text{Absorbance at 280 nm x Mol. weight (Da)}}{\text{Extinction coefficient } (M^{-1}cm^{-1}) \text{ x Path length (1 cm)}}$$

2.2.16 MALDI-TOF MS analysis of *Ct*PME, *Ct*X157 and *Ct*PME*f*

The Matrix-Assisted Laser Desorption/Ionization-Time of Flight Mass Spectrometry (MALDI-TOF MS) analysis of *Ct*PME, *Ct*X157 and *Ct*PME*f* were carried out to know its intact molecular mass. MALDI-TOF MS analysis of *Ct*PME, *Ct*X157 and *Ct*PME*f* were performed using an Ultraflex workstation (Bruker Daltonics, Bremen, Germany) equipped with a nitrogen laser of 337 nm, operated in linear positive mode with a laser power intensity of 60%. After a delayed extraction time of 350 ns, the ions were accelerated to a kinetic energy of 22 kV before detection. The mass spectrometer was calibrated with a mixture of maltodextrins (Avebe, Foxhol, Netherlands; MD20; mass range m/z 7,000 -50,000). The data were processed using the Bruker Daltonics flex Analysis software (Savary et al. 2013). The matrix was prepared using two solutions. Solution A contained 4 mg/ml Sinapinic acid (trans-3, 5-dimethoxy-4-hydroxycinnamic acid) dissolved in 100% ethanol. Solution B contained 4 mg/ml Sinapinic acid dissolved in TA30 solvent, which contained 0.1% trifluoroacetic acid (TFA) and acetonitrile in 30:70 (v/v) ratios. All solutions were stored at -20°C. The sample was prepared by initially mixing 0.5 µl of solution B with 0.5 µl of *Ct*PME, *Ct*X157 and *Ct*PME*f*, respective protein sample and adding then equal volume of solution A and was properly mixed. The sample 2 µl was drop spotted onto the stainless steel MALDI-TOF sample analysis target plate and allowed to dry for 1-2 h. The samples were prepared freshly (using freshly purified enzyme) 2 h before analysis (Shevchenko et al. 2009).

2.3 Results and Discussion

2.3.1 PCR amplification of genes encoding *Ct*PME, *Ct*X157 and *Ct*PME*f*

The genes encoding *Ct*PME, *Ct*X157 and *Ct*PME*f* were amplified from genomic DNA of *Clostridium thermocellum* ATCC 27405 using the conditions mentioned in Section 2.2.3, and detected on 0.8% (w/v) agarose gel and are displayed in Fig. 2.4 below. The PCR products were purified from gel using gel extraction kit as mentioned in Section 2.2.5 and stored at -20°C.

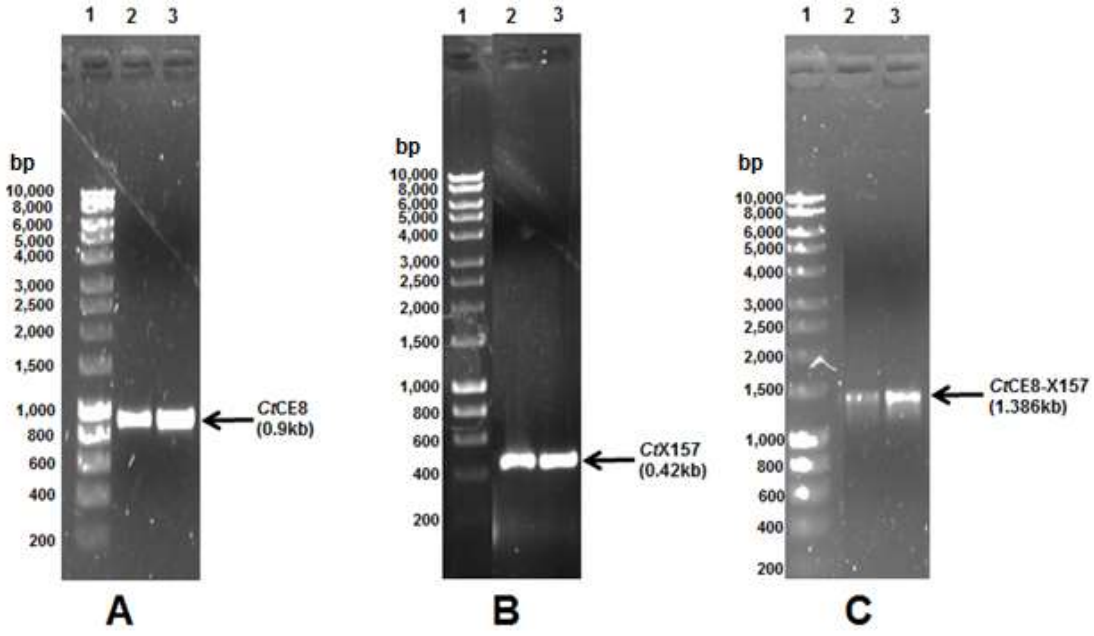

Fig. 2.4 Agarose gels (0.8%, w/v) showing PCR amplified genes encoding: (A) *Ct*PME (lane 2 & 3), (B) *Ct*X157 (lane 2 & 3) and (C) *Ct*PME*f* (lane 2 & 3) around 0.9 kb, 0.42 kb and 1.3 kb, respectively. Lane 1- DNA marker (Hyperladder I, Bioline).

2.3.2 Cloning of genes encoding *Ct*PME, *Ct*X157 and *Ct*PME*f* into pET-28a (+) vector

The restriction enzyme digested genes encoding *Ct*PME, *Ct*X157 and *Ct*PME*f* were ligated with the linearized fragments of pET-28a(+) vector following the protocol mentioned in Section 2.2.10.1. The ligated product was transformed into *E. coli* TOP10 competent cells and grown overnight on LB agar plates grown at 37°C under stationary condition. The transformation efficiency of *E. coli* TOP10 competent cells was 1.5 x10^6 cfu/µg.

2.3.2.1 Isolation of recombinant plasmid DNA

Plasmid DNA from grown colonies after cloning into pET-28a(+) was isolated using Plasmid miniprep kit following the protocol mentioned in Section 2.2.13.3.1. The isolated plasmids were visualized after electrophoresis on 0.8% (w/v) agarose gel. Positive clones were confirmed by restriction digestion of this isolated plasmid DNA.

2.3.2.2 Restriction digestion of isolated plasmid DNA for confirmation of positive clone

The isolated plasmids were digested with *Nhe*I and *Xho*I restriction enzymes for confirming the positive clones. The plasmids after restriction digestion were electrophoresed on 0.8% (w/v) agarose gels. *NheI* and *XhoI* digested fragments of gene encoding *Ct*PME, (Fig. 2.5A; Lane 2-4), *Ct*X157 (Fig. 2.5B; Lane 2) and *Ct*PME*f* (Fig. 2.5 C; Lane 2) were visualized on agarose gels around 0.9 kb, 0.42 kb and 1.3 kb respectively. Linearized pET-28a (+) vector was visualized at around 5.3 kb after restriction digestion. The positives clones were sequenced (Scigenom Labs Pvt. Ltd, India) and no undesired mutations were detected (Fig. 2.6, 2.7, 2.8, 2.9, 2.10 & 2.11).

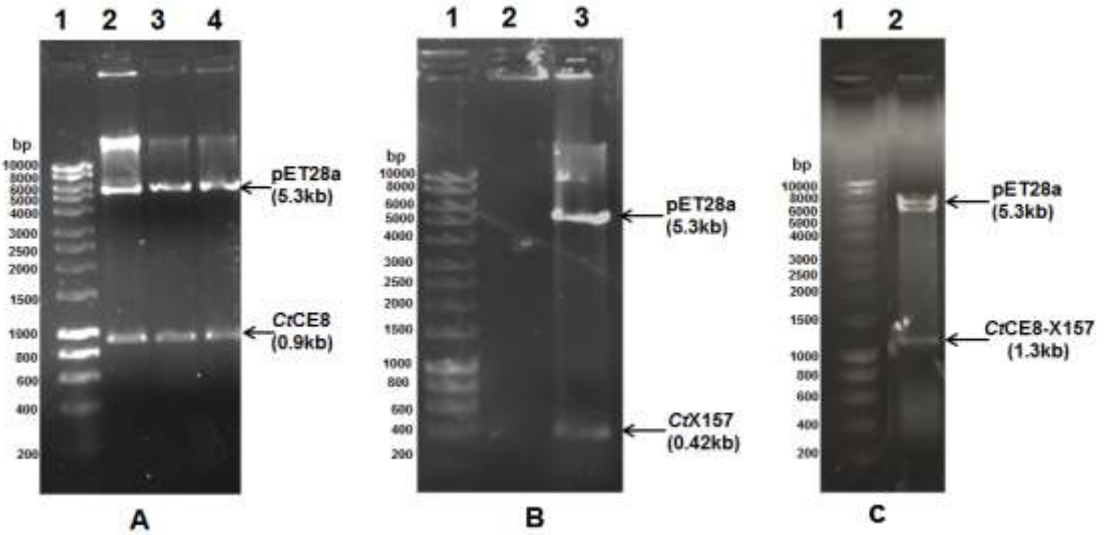

Fig. 2.5 Agarose gel (0.8%, w/v) showing *Nhe*I-*Xho*I digested recombinant plasmid containing genes encoding (A) *Ct*PME, (Lane 1, 2 & 3: 0.9 kb), (B) *Ct*X57, (Lane 3: 0.42 kb) and (C) *Ct*PME*f* (Lane 2: 1.3 kb). In all cases Lane 1: DNA marker (Hyper ladder I, Bioline).

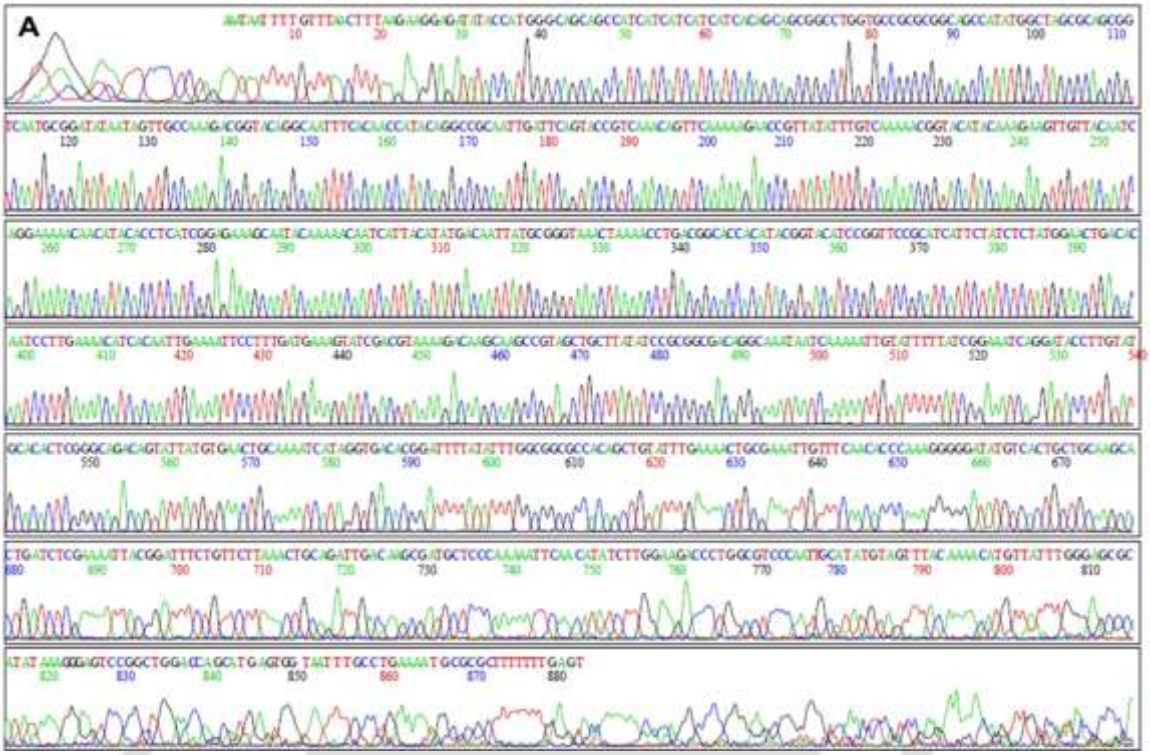

B

AAATAATTTTGTTTAACTTTAAGAAGGAGATATACCATGGGCAGCAGCCATCATCATCATCAT
CACAGCAGCGGCCTGGTGCCGCGCGGCAGCCATATGGCTAGCGCAGCGGTCAATGCGGATATA
ATAGTTGCCAAAGACGGTACAGGCAATTTCACAACCATACAGGCCGCAATTGATTCAGTACCG
TCAAACAGTTCAAAAAGAACCGTTATATTTGTCAAAAACGGTACATACAAAGAAGTTGTTACA
ATCAGGAAAAACAACATACACCTCATCGGAGAAAGCAATACAAAAACAATCATTACATATGAC
AATTATGCGGGTAAACTAAAACCTGACGGCACCACATACGGTACATCCGGTTCCGCATCATTC
TATCTCTATGGAACTGACACAATCCTTGAAAACATCACAATTGAAAATTCCTTTGATGAAAGT
ATCGACGTAAAAGACAAGCAAGCCGTAGCTGCTTATATCCGCGGCGACAGGCAAATAATCAAA
AATTGTATTTTTATCGGAAATCAGGATACCTTGTATGCACACTCGGGCAGACAGTATTATGTG
AACTGCAAAATCATAGGTGACACGGATTTTATATTTGGCGGCGCCACAGCTGTATTTGAAAAC
TGCGAAATTGTTTCAACACCCAAAGGGGGATATGTCACTGCTGCAAGCACTGATCTCGAAAAT
TACGGATTTCTGTTCTTAAACTGCAGATTGACAAGCGATGCTCCCAAAAATTCAACATATCTT
GGAAGACCCTGGCGTCCCAATTGCATATGTAGTTTACAAAACATGTTATTTGGGAGCGCATAT
AAAGGGAGTCCGGCTGGACCAGCATGAGTGGTAATTTGCCTGAAAATGCGCGCTTTTTTTGAG
T

Fig. 2.6 DNA Sequencing of *Ct*PME. (A**)** Electropherogram showing the DNA sequencing result for cloned gene encoding *Ct*PME. Sequencing was done using T7 forward primer and (B) The deduced sequence (trimmed).

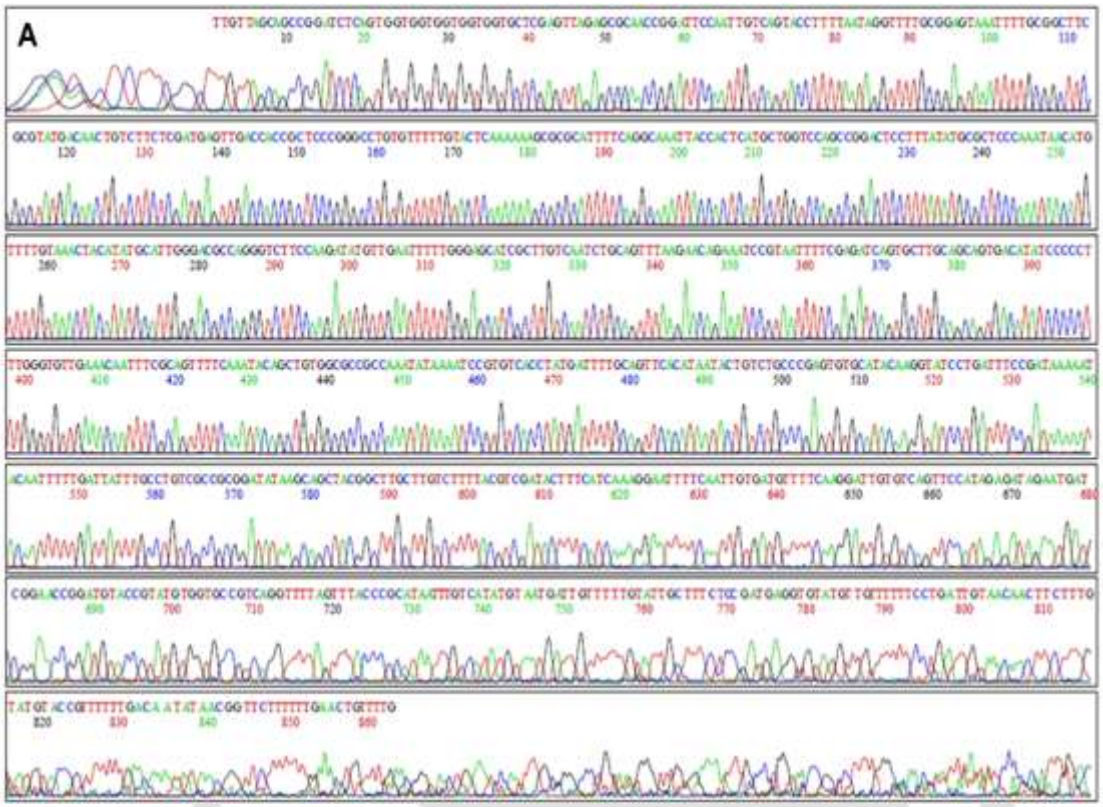

B

TTGTTAGCAGCCGGATCTCAGTGGTGGTGGTGGTGGTGCTCGAGTTAGAGCGCAACCGGATTC
CAATTGTCAGTACCTTTTAATAGGTTTTGCGGAGTAAATTTTGCGGCTTCGGCGTATGACAAC
TGTCTTCTCGATGAGTTGACCACCGCTCCCGGGCCTGTGTTTTTGTACTCAAAAAAGCGCGCA
TTTTCAGGCAAATTACCACTCATGCTGGTCCAGCCGGACTCCTTTATATGCGCTCCCAAATAA
CATGTTTTGTAAACTACATATGCATTGGGACGCCAGGGTCTTCCAAGATATGTTGAATTTTTG
GGAGCATCGCTTGTCAATCTGCAGTTTAAGAACAGAAATCCGTAATTTTCGAGATCAGTGCTT
GCAGCAGTGACATATCCCCCTTTGGGTGTTGAAACAATTTCGCAGTTTTCAAATACAGCTGTG
GCGCCGCCAAATATAAAATCCGTGTCACCTATGATTTTGCAGTTCACATAATACTGTCTGCCC
GAGTGTGCATACAAGGTATCCTGATTTCCGATAAAAATACAATTTTTGATTATTTGCCTGTCG
CCGCGGATATAAGCAGCTACGGCTTGCTTGTCTTTTACGTCGATACTTTCATCAAAGGAATTT
TCAATTGTGATGTTTTCAAGGATTGTGTCAGTTCCATAGAGATAGAATGATGCGGAACCGGAT
GTACCGTATGTGGTGCCGTCAGGTTTTAGTTTACCCGCATAATTTGTCATATGTAATGATTGT
TTTTGTATTGCTTTCTCCGATGAGGTGTATGTTGTTTTTTCCTGATTGTAACAACTTCTTTGT
ATGTACCGTTTTTTGACAATATAACGGTTCTTTTTTGAACTGTTTTG

Fig. 2.7 DNA Sequencing of *Ct*PME, (A**)** Electropherogram showing the DNA sequencing result for cloned gene encoding *Ct*PME, Sequencing was done using T7 reverse primer and (B) The deduced sequence (Trimmed).

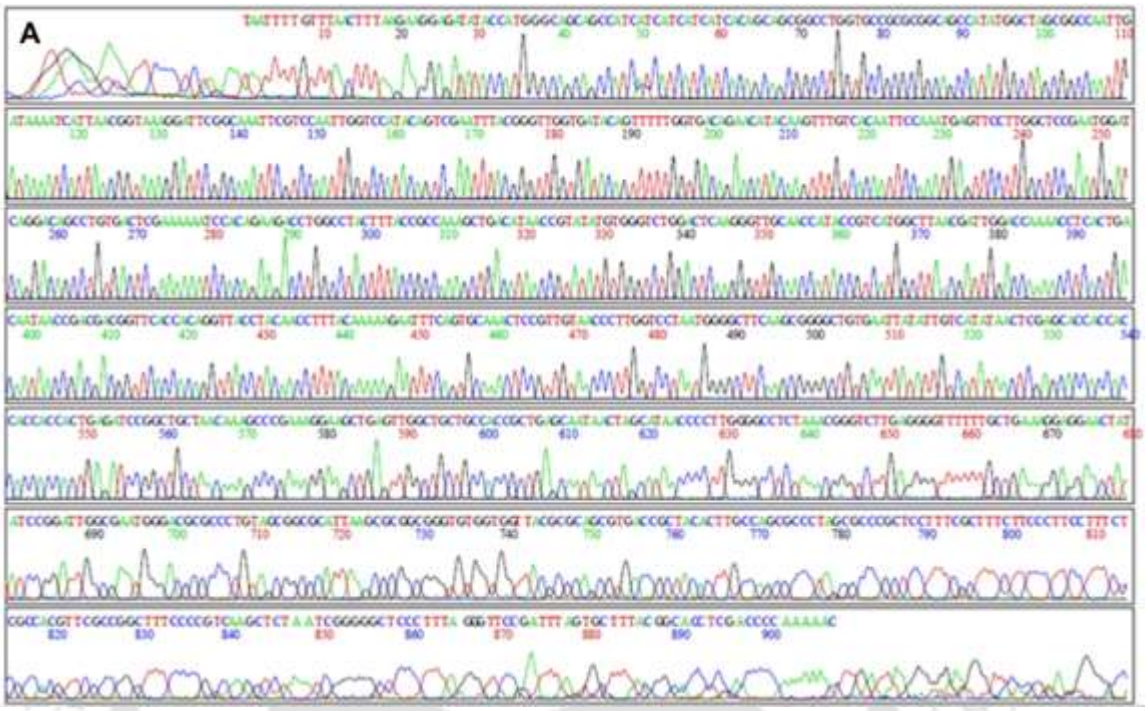

B

TAATTTTGTTTAACTTTAAGAAGGAGATATACCATGGGCAGCAGCCATCATCATCATCATCAC
AGCAGCGGCCTGGTGCCGCGCGGCAGCCATATGGCTAGCGGCCAATTGATAAAATCATTAACG
GTAAAGGATTCGGCAAATTCGTCCAATTGGTCCATACAGTCGAATTTACGGGTTGGTGATACA
GTTTTTGGTGACAGAACATACAAGTTTGTCACAATTCCAAATGAGTTCCTTGGCTCCGAATGG
ATCAGGACAGCCTGTGACTCGAAAAAATCCACAGAAGACCTGGCCTACTTTACCGCCAAAGCT
GACATAACCGTATATGTGGGTCTGGACTCAAGGGTTGCAACCATACCGTCATGGCTTAACGAT
TGGACCAAAACCTCACTGACAATAACCGACGACGGTTCACCACAGGTTACCTACAACCTTTAC
AAAAAGAATTTCAGTGCAAACTCCGTTGTAACCCTTGGTCCTAATGGGGCTTCAAGCGGGGCT
GTGAATTATATTGTCATATAACTCGAGCACCACCACCACCACCACTGAGATCCGGCTGCTAAC
AAAGCCCGAAAGGAAGCTGAGTTGGCTGCTGCCACCGCTGAGCAATAACTAGCATAACCCCTT
GGGGCCTCTAAACGGGTCTTGAGGGGTTTTTTGCTGAAAGGAGGAACTATATCCGGATTGGCG
AATGGGACGCGCCCTGTAGCGGCGCATTAAGCGCGGCGGGTGTGGTGGTTACGCGCAGCGTGA
CCGCTACACTTGCCAGCGCCCTAGCGCCCGCTCCTTTCGCTTTCTTCCCTTCCTTTCTCGCCA
CGTTCGCCGGCTTTCCCCGTCAAGCTCTAATCGGGGGCTCCCTTTAGGGTTCCGATTTAGTGC
TTTACGGCACCTCGACCCCAAAAAC

Fig. 2.8 DNA Sequencing of *Ct*X157 (A**)** Electropherogram showing the DNA sequencing result for cloned gene encoding *Ct*X157. Sequencing was done using T7 forward primer and (B) The deduced sequence (Trimmed).

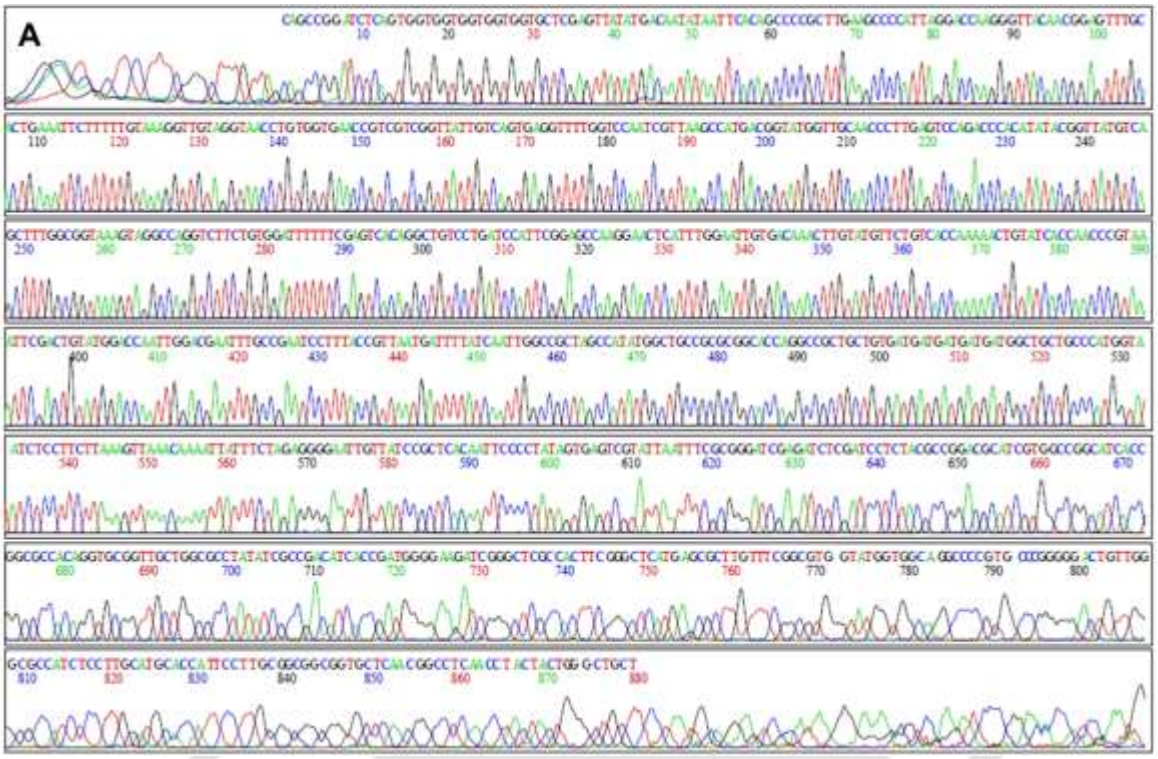

B

CAGCCGGATCTCAGTGGTGGTGGTGGTGGTGCTCGAGTTATATGACAATATAATTCACAGC
CCCGCTTGAAGCCCCATTAGGACCAAGGGTTACAACGGAGTTTGCACTGAAATTCTTTTTG
TAAAGGTTGTAGGTAACCTGTGGTGAACCGTCGTCGGTTATTGTCAGTGAGGTTTTGGTCC
AATCGTTAAGCCATGACGGTATGGTTGCAACCCTTGAGTCCAGACCCACATATACGGTTAT
GTCAGCTTTGGCGGTAAAGTAGGCCAGGTCTTCTGTGGATTTTTTCGAGTCACAGGCTGTC
CTGATCCATTCGGAGCCAAGGAACTCATTTGGAATTGTGACAAACTTGTATGTTCTGTCAC
CAAAAACTGTATCACCAACCCGTAAATTCGACTGTATGGACCAATTGGACGAATTTGCCGA
ATCCTTTACCGTTAATGATTTTATCAATTGGCCGCTAGCCATATGGCTGCCGCGCGGCACC
AGGCCGCTGCTGTGATGATGATGATGATGGCTGCTGCCCATGGTATATCTCCTTCTTAAAG
TTAAACAAAATTATTTCTAGAGGGGAATTGTTATCCGCTCACAATTCCCCTATAGTGAGTC
GTATTAATTTCGCGGGATCGAGATCTCGATCCTCTACGCCGGACGCATCGTGGCCGGCATC
ACCGGCGCCACAGGTGCGGTTGCTGGCGCCTATATCGCCGACATCACCGATGGGGAAGATC
GGGCTCGCCACTTCGGGCTCATGAGCGCTTGTTTCGGCGTGGTATGGTGGCAGGCCCCGTG
CCCGGGGGGACTGTTGGGCGCCATCTCCTTGCATGCACCATTCCTTGCGGCGGCGGTGCTCA
ACGGCCTCAACCTACTACTGGGCTGCT

Fig. 2.9 DNA Sequencing of *Ct*X157 (A**)** Electropherogram showing the DNA sequencing result for cloned gene encoding *Ct*X157. Sequencing was done using T7 reverse primer and (B) The deduced sequence (Trimmed).

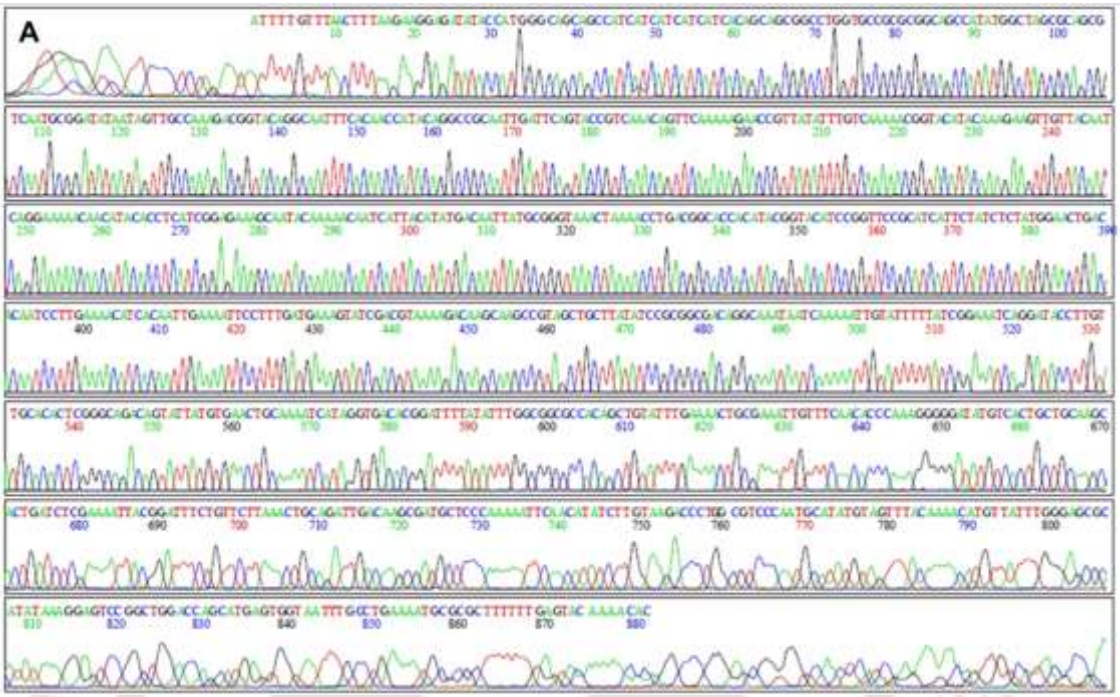

B

ATTTTGTTTAACTTTAAGAAGGAGATATACCATGGGCAGCAGCCATCATCATCATCACAG
CAGCGGCCTGGTGCCGCGCGGCAGCCATATGGCTAGCGCAGCGGTCAATGCGGATATAATAGT
TGCCAAAGACGGTACAGGCAATTTCACAACCATACAGGCCGCAATTGATTCAGTACCGTCAAA
CAGTTCAAAAAGAACCGTTATATTTGTCAAAAACGGTACATACAAAGAAGTTGTTACAATCAG
GAAAAACAACATACACCTCATCGGAGAAAGCAATACAAAAACAATCATTACATATGACAATTA
TGCGGGTAAACTAAAACCTGACGGCACCACATACGGTACATCCGGTTCCGCATCATTCTATCT
CTATGGAACTGACACAATCCTTGAAAACATCACAATTGAAAATTCCTTTGATGAAAGTATCGA
CGTAAAAGACAAGCAAGCCGTAGCTGCTTATATCCGCGGCGACAGGCAAATAATCAAAAATTG
TATTTTTATCGGAAATCAGGATACCTTGTATGCACACTCGGGCAGACAGTATTATGTGAACTG
CAAAATCATAGGTGACACGGATTTTATATTTGGCGGCGCCACAGCTGTATTTGAAAACTGCGA
AATTGTTTCAACACCCAAAGGGGGATATGTCACTGCTGCAAGCACTGATCTCGAAAATTACGG
ATTTCTGTTCTTAAACTGCAGATTGACAAGCGATGCTCCCAAAAATTCAACATATCTTGTAAG
ACCCTGGCGTCCCAATGCATATGTAGTTTACAAAACATGTTATTTGGGAGCGCATATAAAGGA
GTCCGGCTGGACCAGCATGAGTGGTAATTTGCCTGAAAATGCGCGCTTTTTTGAGTACAAAAC
AC

Fig. 2.10 DNA Sequencing of *Ct*PME*f* (A**)** Electropherogram showing the DNA sequencing result for cloned gene encoding *Ct*PME*f*. Sequencing was done using T7 forward primer and (B) The deduced sequence (Trimmed).

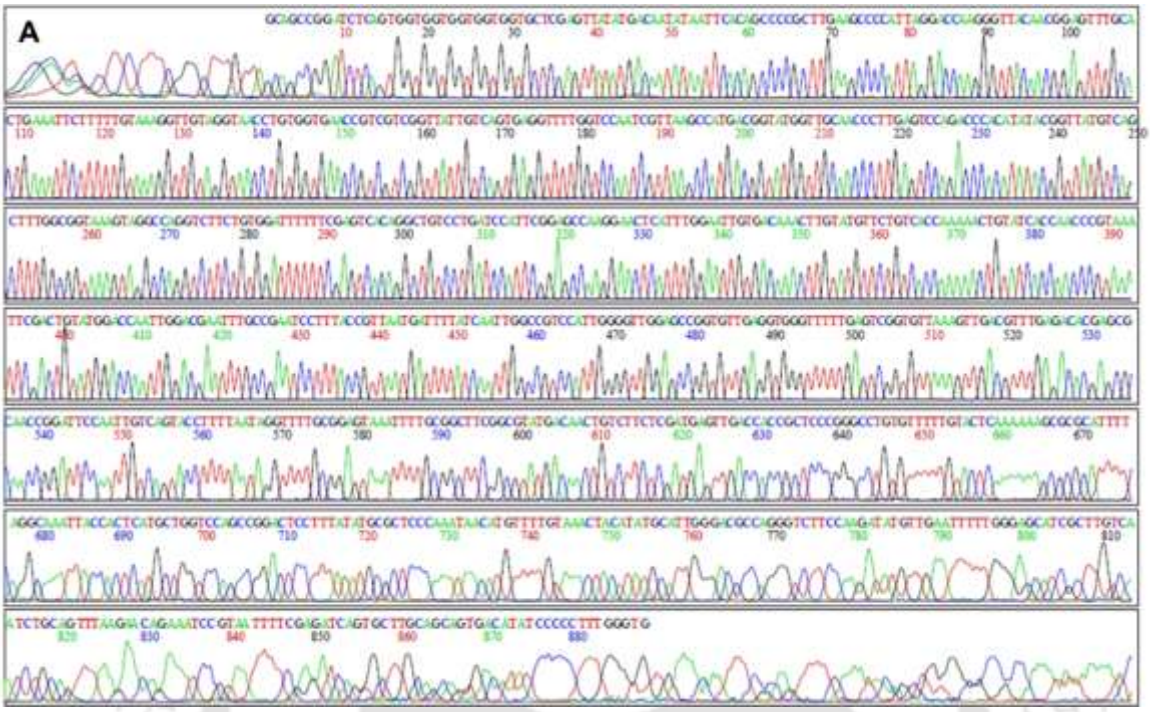

B

GCAGCCGGATCTCAGTGGTGGTGGTGGTGGTGCTCGAGTTATATGACAATATAATTCACAGCC
CCGCTTGAAGCCCCATTAGGACCAAGGGTTACAACGGAGTTTGCACTGAAATTCTTTTTGTAA
AGGTTGTAGGTAACCTGTGGTGAACCGTCGTCGGTTATTGTCAGTGAGGTTTTGGTCCAATCG
TTAAGCCATGACGGTATGGTTGCAACCCTTGAGTCCAGACCCACATATACGGTTATGTCAGCT
TTGGCGGTAAAGTAGGCCAGGTCTTCTGTGGATTTTTTCGAGTCACAGGCTGTCCTGATCCAT
TCGGAGCCAAGGAACTCATTTGGAATTGTGACAAACTTGTATGTTCTGTCACCAAAAACTGTA
TCACCAACCCGTAAATTCGACTGTATGGACCAATTGGACGAATTTGCCGAATCCTTTACCGTT
AATGATTTTATCAATTGGCCGTCCATTGGGGTTGGAGCCGGTGTTGAGGTGGGTTTTTGAGTC
GGTGTTAAAGTTGACGTTTGAGACACGAGCGCAACCGGATTCCAATTGTCAGTACCTTTTAAT
AGGTTTTGCGGAGTAAATTTTGCGGCTTCGGCGTATGACAACTGTCTTCTCGATGAGTTGACC
ACCGCTCCCGGGCCTGTGTTTTTGTACTCAAAAAAGCGCGCATTTTCAGGCAAATTACCACTC
ATGCTGGTCCAGCCGGACTCCTTTATATGCGCTCCCAAATAACATGTTTTGTAAACTACATAT
GCATTGGGACGCCAGGGTCTTCCAAGATATGTTGAATTTTTGGGAGCATCGCTTGTCAATCTG
CAGTTTAAGAACAGAAATCCGTAATTTTCGAGATCAGTGCTTGCAGCAGTGACATATCCCCCT
TTGGGTG

Fig. 2.11 DNA Sequencing of *Ct*PME*f* (A**)** Electropherogram showing the DNA sequencing result for cloned gene encoding *Ct*PME*f*. Sequencing was done using T7 reverse primer and (B) The deduced sequence (Trimmed).

2.3.3 Expression and purification of recombinant proteins

The *E. coli* BL21 (DE3) competent cells were transformed with recombinant pET-28a (+) plasmids containing genes encoding *Ct*PME, *Ct*X157 and *Ct*PME*f*. The transformation efficiencies of *E. coli* BL21 (DE3) and *E. coli* BL21 (DE3) pLysS cells were 1.8×10^6 and 5×10^5. The colonies were picked randomly and grown in 5 ml LB medium supplemented with kanamycin (50 µg/ml) as described in Section 2.2.12. The cells were induced for expression of protein at mid exponential stage as described in Section 2.2.12. Protein expression was analysed using SDS-PAGE gels by loading uninduced as well as the induced cells in adjacent wells, as depicted in Fig. 2.12, 2.13 and 2.14.

The recombinant proteins were purified by immobilized metal ion affinity chromatography as described in Section 2.2.14 and then dialysed for removal of imidazole and sodium chloride. The recombinant *Ct*PME, *Ct*X157 and *Ct*PME*f* expressed as soluble proteins and after purification displayed homogeneous single bands on SDS-PAGE gels (Fig. 2.12, 2.13 and 2.14). The molecular masses of the recombinant *Ct*PME, *Ct*X157 and *Ct*PME*f* including the N-terminal histidine tag were calculated to be 35.5 kDa, 17.6 kDa and 54.1 kDa respectively, which are in close agreement with those observed on SDS-PAGE gels.

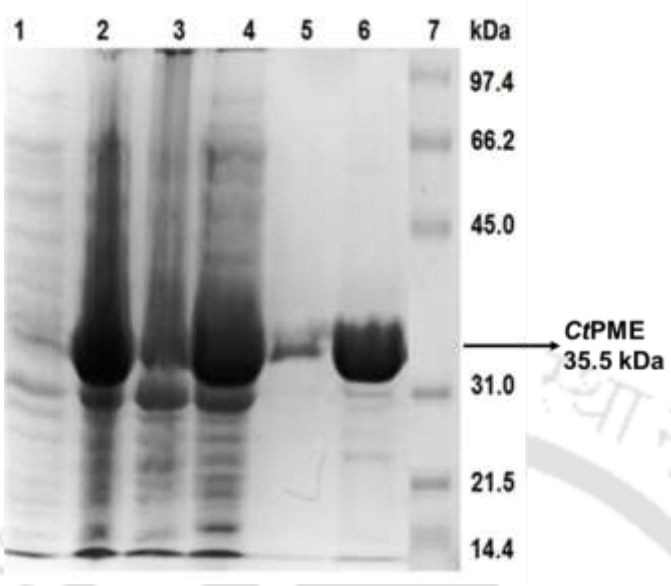

Fig.2.12 SDS-PAGE (12%) gel showing expression and purification of recombinant *Ct*PME in *E. coli* BL-21 cells, Lane 1: Uninduced cells, Lane 2: Induced cells, Lane 3: Cell pellet (cell debris after sonication), Lane 4: Cell free extract, Lane 5: Last column fraction, Lane 6: Purified and dialyzed *Ct*PME (35.5 kDa approx.), Lane 7: Protein marker (Bangalore GeNei, India).

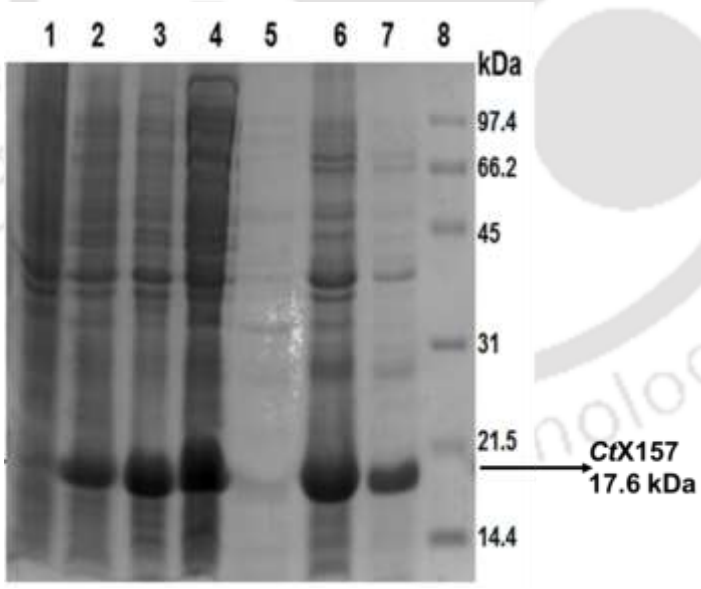

Fig. 2.13 SDS-PAGE (12%) gel showing expression and purification of recombinant *Ct*PME in *E. coli* BL-21 cells, Lane 1: Uninduced cells, Lane 2: Induced cells, Lane 3: Cell pellet (cell debris after sonication), Lane 4: Cell free extract, Lane 5: Last column fraction, Lane 6&7: Purified and dialyzed *Ct*X157 (17.6 kDa approx.), Lane 8: Protein marker (Bangalore GeNei, India).

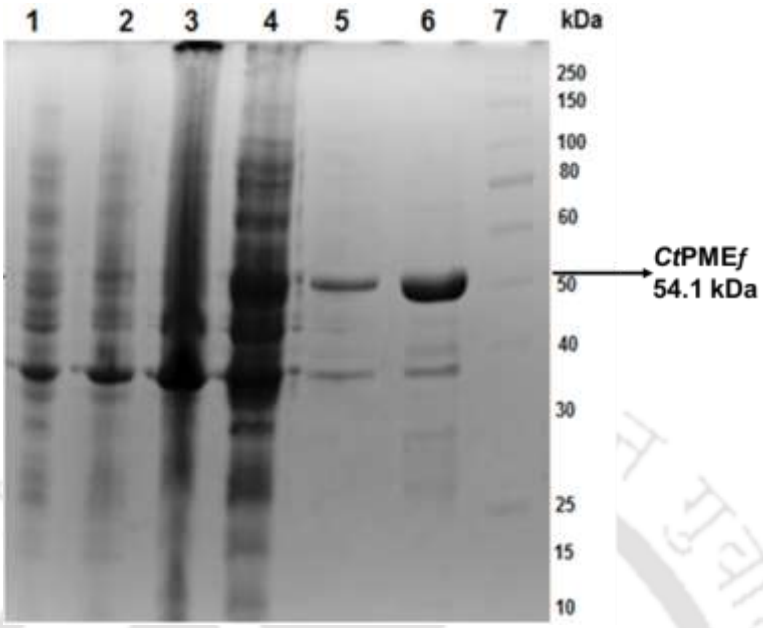

Fig. 2.14 SDS-PAGE (12%) gel showing expression and purification of recombinant *Ct*PME in *E. coli* BL-21 cells, Lane 1: Uninduced cells, Lane 2: Induced cells, Lane 3: Cell pellet (cell debris after sonication), Lane 4: Cell free extract, Lane 5: Last column fraction, Lane 6: Purified and dialyzed *Ct*PME*f* (54.1 kDa approx.), Lane 7: Protein marker (Fermentas, India).

2.3.4 Protein estimation of expressed and purified recombinant derivatives

The amount of purified recombinant proteins obtained from 100 ml of grown cultures was calculated using the formula mentioned in Section 2.2.15 and listed in Table 2.14. The total amount of recombinant enzymes present in eluted 2 ml of was 2.4±0.15 mg (*Ct*PME), 1.7±0.21 mg (*Ct*X157), and 1.9±0.18 mg (*Ct*PME*f*) as displayed in Table 2.14.

Table 2.14 Purified recombinant proteins obtained from 100 ml cultures.

Recombinant Protein	Protein concentration (mg/ml)	Volume of purified protein (ml)	Total amount of purified protein (mg)
*Ct*PME	1.20±0.15	2.0	2.4±0.15
*Ct*X157	0.85±0.21	2.0	1.7±0.21
*Ct*PME*f*	0.93±0.18	2.0	1.9±0.18

2.3.5 MALDI-TOF MS analysis of *Ct*PME, *Ct*X157 and *Ct*PME*f*

The MALDI-TOF MS analysis of purified *Ct*PME, *Ct*X157 and *Ct*PME*f* were showed the intact molecular mass, 35558.1 Da, 17645.1 Da and 53483.9 Da, respectively, in linear positive mode (Fig. 2.15) similar to the apparent molecular mass observed by SDS-PAGE.

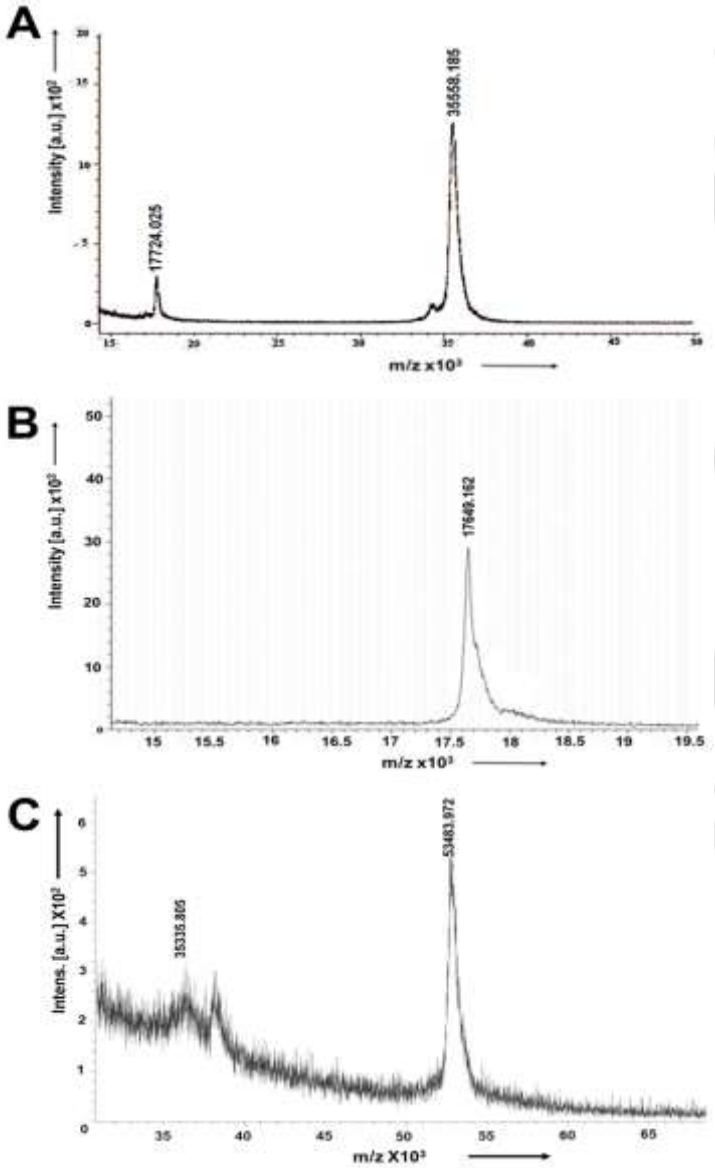

Fig. 2.15 MALDI-TOF MS analysis (A) Intact mass of *Ct*PME (35558.18 Da), (B) Intact mass of *Ct*X157 (17649.16 Da) and (C) Intact mass of *Ct*PME*f* (53483.97).

2.4 Conclusions

Family 8 carbohydrate esterase (CE8) *Ct*PME and its truncated derivative, *Ct*X157 and full length, *Ct*PME*f* were cloned from the genomic DNA of *Clostridium thermocellum* ATCC 27405 (GenBank Accession No: ABN54147.1). The molecular architecture showed signal peptide towards N-terminal followed by a family 8 carbohydrate esterase, pectin methylesterase catalytic module (*Ct*PME), X-157 unknown function module (*Ct*X157) and full length module *Ct*PME*f*. The PCR amplified fragment of full length gene encoding *Ct*PME*f* showed a band of ~1.5 kb, whereas, the gene encoding catalytic module (*Ct*PME) and unknown function module (*Ct*X157), displayed the sizes of ~ 0.9 kb and ~ 0.4 kb, respectively. The restriction enzyme digested fragments of genes encoding *Ct*PME*f*, *Ct*X157 and *Ct*PME*f* were ligated with linearized pET-28a(+) vector. The ligated mixture was transformed into *E. coli* TOP10 competent cells. The positive clones containing recombinant plasmid DNA were screened by restriction enzyme digestion using enzymes, *NheI* and *XhoI*. The restriction enzyme digested products were electrophoresed and the band of ~ 5.4 kb was produced for pET-28a(+) vector and corresponding bands of ~0.9 kb, ~ 0.4 kb and ~ 1.5 kb were produced from the insert fragments for genes encoding *Ct*PME, *Ct*X157 and *Ct*PME*f*, respectively. The recombinant plasmids containing genes encoding *Ct*PME, *Ct*X157 and *Ct*PME*f* were transformed into *E. coli* BL-21 (DE3) cells. The recombinant proteins were expressed and purified. The purified recombinant proteins displayed a band of approximately, 35.5 kDa for *Ct*PME, 17.6 kDa for *Ct*X157 and 54.4 kDa for *Ct*PME*f* on SDS-PAGE gels. The amount of recombinant *Ct*PME, *Ct*X157 and *Ct*PME*f* proteins obtained from 100 ml *E. coli* cultures after purification by Immobilized Metal Ion Affinity Chromatography (IMAC) were

2.4±0.15 mg, 1.7±0.21 mg and 1.9±0.18 mg, respectively. The purified recombinant proteins molecular mass confirmed by MALDI-TOF MS, which were displayed 35558.1 Da, 17645.1 Da and 53483.9 Da, *Ct*PME, *Ct*X157 and *Ct*PME*f* were showed the intact molecular mass, respectively,

2.5 References

Duan, C. J., Feng, Y. L., Cao, Q. L., Huang, M. Y., Feng, J. X. (2016) Identification of a novel family of carbohydrate-binding modules with broad ligand specificity. Scientific Reports, 6: 9392.

Duvetter, T., Fraeye, I., Sila, D. N., Verlent, I., Smout, C., Hendrickx, M., et al. (2006) Mode of de-esterification of alkaline and acidic pectin methyl esterases at different pH conditions. Journal of Agricultural and Food Chemistry, 54: 7825–7831.

Fontes, C. M., Gilbert, H. J. (2010) Cellulosomes: highly efficient nanomachines designed to deconstruct plant cell wall complex carbohydrates. Annual Reviews of Biochemistry, 79: 655-681.

Fraeye, I., Duvetter, T., Doungla, E., Van Loey, A., Hendricks, M. (2010) Fine-tuning the properties of pectin–calcium gels by control of pectin fine structure, gel composition and environmental conditions. Trends in Food Science & Technology, 21: 219–228.

Frenkel, C., Peters, J. S., Tieman, D. M., Tiznado, M. E., Handa, A. K. (1998) Pectin methylesterase regulates methanol and ethanol accumulation in ripening tomato (*Lycopersicon esculentum*) fruit. Journal of Biological Chemistry, 273: 4293-4295.

Hanahan, D. (1983). Studies on transformation of *Escherichia coli* with plasmids. Journal of Molecular Biology, 166(4): 557-580.

Jiang, X., Chen, P., Yin, M., Yang, Q. (2013) Constitutive expression, purification and characterisation of pectin methylesterase from *Aspergillus niger* in Pichia

pastoris for potential application in the fruit juice industry. Journal of the Science of Food and Agriculture, 93: 375–381.

Kashyap, D. R., Vohra, P. K., Chopra, S., Tewari, R. (2001) Applications of pectinases in the commercial sector: A review. Bioresource Technology, 77: 215–227.

Kent, L. M., Loo, T. S., Melton, L. D., Mercadante, D., Williams, M. A., Jameson, G. B. (2016) Structure and properties of a non-processive, salt requiring and acidophilic pectin methylesterase from *Aspergillus niger* provide insights into the key determinants of processivity control. Journal of Biological Chemistry, 291: 1289–1306.

Kim, Y., Williams, M. A., Galant, A. L., Luzio, G. A., Savary, B. J., Vasu, P., et al. (2013) Nanostructural modification of a model homogalacturonan with a novel pectin methylesterase: Effects of pH on nanostructure, enzyme mode of action and substrate functionality. Food Hydrocolloids, 33: 132–141.

Koshland, D. E. (1953) Stereochemistry and the mechanism of enzymatic reactions. Biological Reviews, 28: 416-436.

Laemmli, U. K. (1970). SDS-page Laemmli method. Nature, 227: 680-685.

Limberg, G., Korner, R., Buchholt, H. C., Christensen, T. M., Roepstorff, P., Mikkelsen, J. D. (2000) Analysis of different de-esterification mechanisms for pectin by enzymatic fingerprinting using endopectin lyase and endopolygalacturonase II from *Aspergillus niger*. Carbohydrate Research, 327: 293–307.

Lombard, V., Golaconda, R. H., Drula, E. (2014) The Carbohydrate-active enzymes database (CAZy) in 2013. Nucleic Acids Research, 42: D490-D495.

Matsunaga, T., Ishii, T., Matsumoto, S. (2004) Occurrence of the primary cell wall polysaccharide rhamnogalacturonan II in pteridophytes, lycophytes and bryophytes: Implications for the evolution of vascular plants. Plant Physiology, 134: 339-351.

May, C. D. (1990) Industrial pectins: Sources, production and applications. Carbohydrate Polymers, 12: 79–99.

McKie, V. A., Vincken, J. P., Voragen, A. G. (2001) A new family of rhamnogalacturonan lyases contains an enzyme that binds to cellulose. Biochemical Journal, 355: 167–177.

Micheli, F. (2001) Pectin methylesterases: Cell wall enzymes with important roles in plant physiology. Trends in Plant Science, 6: 414–419.

Moran, F. S, Nasuno, S., Starr, M. P. (1968) Extracellular and intracellular polygalacturonic acid trans-eliminase of *Erwinia carotovora*. Archives of Biochemistry and Biophysics, 123: 298–306.

Ochiai, A., Itoh, T., Kawamata, A. (2007) Plant cell wall degradation by saprophytic *Bacillus subtilis* strains: gene clusters responsible for rhamnogalacturonande polymerization. Applied and Environmental Microbiology, 73: 3803-3813.

Pages, S., Valette, O., Abdou, L. (2003) A rhamnogalacturonan lyase in the *Clostridium cellulolyticum* cellulosome. Journal of Bacteriology, 185: 4727-4733.

Pressey, R., Avants, J. K. (1982) Solubilization of cell walls by tomato polygalacturonases: Effects of pectinesterases. Journal of Food Biochemistry, 6: 57–74.

Ridley, B. L., O'Neill, M. A., Mohnen, D. (2001) Pectins: Structure, biosynthesis, and oligogalacturonide-related signaling. Phytochemistry, 57: 929–967.

Rolin, C. (2002) 8 Commercial pectin preparations. Pectins and Their Manipulation, 15, 222.

Sambrook, J., Fritsch, E. F., Maniatis, T. (1989). Molecular cloning: a laboratory manual (No. Ed. 2). Cold spring harbor laboratory press.

Savary, B. J., Vasu, P., Cameron, R. G., McCollum, T. G., Nunez, A. (2013) Structural characterization of the thermally tolerant pectin methylesterase purified from *Citrus sinensis* fruit and its gene sequence. Journal of Agricultural and Food Chemistry, 61: 12711–12719.

Shevchenko, A., Tomas, H., Havli, J., Olsen, J. V., Mann, M. (2006) In-gel digestion for mass spectrometric characterization of proteins and proteomes. Nature Protocols, 1: 2856–2860.

Vincken, J. P., Schols, H. A., Oomen, R. J. (2003) If homogalacturonan were a side chain of rhamnogalacturonan I. Implications for cell wall architecture. Plant Physiology, 132: 1781-1789.

Chapter 3

Biochemical characterization of *Ct*PME and *Ct*PME*f*

3.1 Introduction

Pectin methylesterases (PMEs) are majorly found in plants, fungi, bacteria and also insects (Jiang et al., 2013; Kent et al., 2015). In plants, they are localized as cell wall-associated enzymes existing in isoforms, helping in modifications during the plant growth (Micheli, 2001). PMEs play a key role in the cell wall changes in various vegetative (root, shoot and stem elongation) and reproductive (pollen and seed germination) processes in *Arabidopsis sp.* and other dicotyledons plants (Wolf et al., 2009). PMEs have been also shown to be produced as a response to pathogen attack in plants (Kars et al., 2005). PMEs have a molar mass in the range of 24-54 kDa and are active as monomers (Pelloux et al., 2007). Plant and bacterial PMEs have been shown to be active in alkaline and neutral pH range, whereas fungal PMEs are active in acidic pH (Benen et al., 2003; Fraeye et al., 2010). Plant and bacterial PMEs de-esterify the pectin in a random or block-wise fashion (Mercadante et al., 2014). Most of the fungal PMEs follow random de-esterification except those from *Aspergillus nidulans* and *Trichoderma reesei* (Kent et al., 2015). PMEs produced from various sources have

different molecular weight, pI, pH optima, temperature optima, stability, substrate specificity, metal ion and salt dependency (Kohli and Gupta, 2015).

Bacteria are good sources for obtaining PMEs because of low economic input, resource consumption and easy handling required for their production (Kohli and Gupta, 2015). Alkaline and acidic PMEs from different bacterial sources have been characterized, such as *Erwinia carotovora* (McMillan *et al.*, 1992; Heikinheimo *et al*., 1995), *Pseudomonas solanacearum* (Schell *et al*., 1994), *Xanthomonas campestris* (Liao *et al*., 1996), *Bacillus* sp. MG-cp-2 (Kapoor *et al.*, 2001), *Bacillus sp.* DT-7 (Kashyap *et al*., 2001), *Bacillus sp*. MBRL 576 (Bhardwaj and Garg, 2001), *Erwinia* and *Xanthomonas* (Ladjama et al., 2007), *Bacillus subtilis* PEL168 (Zhang *et al*., 2013), *Paenibacillus xylanolyticus* (Giacobbe *et al*., 2014) and *Bacillus licheniformis* (Remoroza *et al*., 2015).

PME activity assays were performed earlier by the titrimetric method by using methyl red as a pH indicator (Kertesz, 1955). The PME activity determination by methanol analysis is more accurate and reproducible as well as faster as it can be performed in small volumes (Salas *et al*., 2017). Several methods have been developed to measure PME activity based on methanol quantification, by direct quantification of methanol by gas chromatography (McFeeters and Armstrong, 1984) or analysis after its subsequent oxidation to formaldehyde by $KMnO_4$ or alcohol oxidase (Bartolome and Hoff, 1972). Later, methanol oxidation by $KMnO_4$ (Wood and Siddiqui, 1971) or alcohol oxidase (Klavons and Bennett, 1986) slightly modified PME assay. However, to overcome the disadvantages, Anthon and Barrett (2004) performed three independent assays (Acetyl acetone, MBTH-3-methyl-2-benzothiazolinone hydrazone

and Purpald) with the addition of alcohol oxidase and found acetyl acetone to be more suitable for the PME assay.

Carbohydrate esterases catalyze the de-O or de-N-acylation of substituted saccharides, which is an ester to form as acid and alcohol. The two classes of substrates for carbohydrate esterases are: those in which the sugar plays the role of the "acid", such as pectin methyl esters and those in which the sugar behaves as the alcohol, such as in acetylated esters (Lombard et al., 2010). Glycoside hydrolases, polysaccharide lyases and carbohydrate esterases have been classified into different families based on sequence similarity (Lombard *et al*., 2014).

Enzymes that can break down the cell wall polysaccharides are of key importance in conversion of lignocellulosic biomass into bio-ethanol and production of prebiotics (Koukiekolo *et al*., 2005; Aachary *et al*., 2011). The pectinases are one such class of industrial enzymes that are used in paper and textile industries, coffee and tea fermentation, treatment of feedstock for biofuel production and recovery of valuable products of plant origin like essential oils (Kashyap *et al*., 2001). Some anaerobic bacteria are better equipped at cleaving the recalcitrant structural polysaccharides, an attribute probably acquired along the evolutionary ladder. (Fontes *et al*., 2010). *C. thermocellum* is an anaerobic, thermophilic bacterium possessing cellulosome, a multi-enzyme complex which afforded a new meaning of enzyme modularity and concerted enzyme action (Lamed *et al*., 1983). The cellulosomal complex has also been reported from other microorganisms (Bayer *et al*., 1994). Several studies involving cellulases and hemicellulases from this bacterium in bio-ethanol production found them to be better than those of fungal origin. (Das *et al*., 2012; Anbar *et al*., 2012). However, studies on pectin degrading enzymes from *C. thermocellum* have been sporadic. The

members of family 8 Carbohydrate Esterase (CE8) characterised earlier are pectin methylesterases (PMEs) from *Erwinia chrysanthemi, Solanum lycopersicum, Yersinia enterocolitica, Daucus carota, , Sitophilus oryzae* and *Bacillus licheniformis* DSM13 (Laurent *et al*., 2000; D'Avino *et al*., 2003; Boraston & Abbott, 2012; Johansson *et al*., 2002; Teller *et al*., 2014; Remoroza *et al*., 2015). In the present study, biochemical characterisation of the full length *Ct*PME*f* and *Ct*PME was carried out.

Biochemical and functional characterization of *Ct*PME*f* and *Ct*PME is essential to know the reaction mechanism of catalysis and to determine their substrate specificity. In the present study, the full length module *Ct*PME*f* and truncated catalytic module *Ct*PME were biochemically and functionally characterized. The enzyme activities of *Ct*PME*f* and *Ct*PME against various pectic polysaccharides and other carbohydrates were determined. The specific activity and kinetic parameters of both these enzymes were compared to explore the influence of unknown function protein on the enzyme activity. The influence of various metal ions, reagents and chaotropic agents on enzyme activity of catalytic module *Ct*PME and full length module *Ct*PME*f* was studied. Structural stability of catalytic module *Ct*PME and full length module *Ct*PME*f* under the influence of varying temperatures and metal ion was studied. Different commercial media were also used to investigate the production of *Ct*PME and *Ct*PME*f*.

3.2 Materials and Methods

3.2.1 Substrates and reagents

Pectins from citrus fruits (Citrus pectin, CP-with varying degree of methyl esterification) and polygalacturonic acid (PGA) were purchased from Sigma Aldrich Chemical Co., USA. Potato galactan (PG), pectic galactan from potato (PPG) and pectic galactan from lupin (PGL), rhamnogalacturonan from soyabean (RGS) and potato (RGP) were purchased from Megazyme International, Ireland. Citrus pectin from CP Kelco and apple pectin (AP) was gifted by Prof. Carlos Fontes, Faculty of Veterinary Medicine, Lisbon, Portugal. Trizma (Tris base), glycine, sodium hydroxide, Alcohol oxidase (AO from *Pichia pastoris*) and glacial acetic acid were procured from Sigma-Aldrich Chemical Co., USA. Disodium 2-[2-carboxylatomethyl-(carboxymethyl)-amino]-ethyl-(carboxymethyl)-amino] acetate (disodium EDTA), Ammonium acetate and acetyl acetone, ethylene glycol-bis(2-aminoethylether)-N,N,N′,N′-tetraacetic acid (EGTA) and salts of metal ions *viz.* Na^{+} (NaCl), K^{+} (KCl), Li^{+} (LiCl), Ca^{2+} ($CaCl_2.2H_2O$), Mg^{2+} ($MgCl_2.7H_2O$), Mn^{2+} ($MnCl_2 \cdot 4H_2O$), Zn^{2+} ($ZnSO_4 \cdot 7H_2O$), Cu^{2+} ($CuSO_4 \cdot 5H_2O$), Co^{2+} ($CoCl_2 \cdot 6H_2O$), Ba^{2+} ($BaCl_2$), Al^{3+} ($AlCl_3 \cdot 6H_2O$) and Fe^{3+} ($FeCl_3 \cdot 6H_2O$) were procured from Himedia Laboratories Pvt. Ltd., India. The chaotropic agents (urea and guanidine hydrochloride) and surfactants (SDS, Tween 20, Tween 80 and Triton X100) were procured from Himedia Laboratories Pvt. Ltd., India. Luria-Bertani, Terrific Broth, Tryptone Yeast extract and Auto Induction medium-LB (AIM-LB) were procured from Himedia Laboratories Pvt. Ltd., India.

3.2.2 Biochemical characterization of *Ct*PME*f* and *Ct*PME

3.2.2.1 Enzyme activity assay

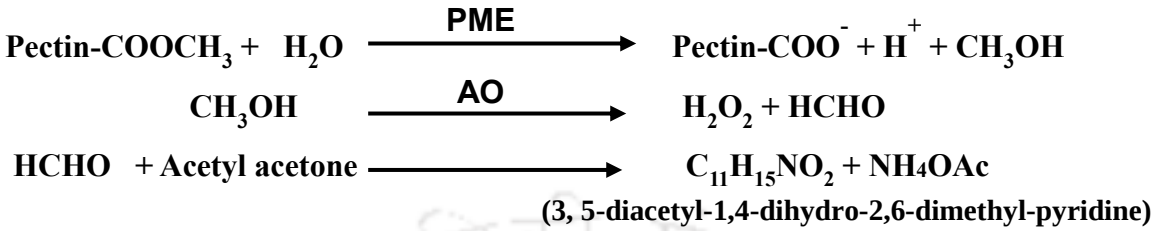

The enzyme assay reaction mixture (100 µl) contained 1% (w/v) substrate CP (>85% methyl esterified) dissolved in 90 µl Tris-HCl buffer (pH 8.5) and 10 µl of *Ct*PME or *Ct*PME*f* enzyme (0.08 mg/ml). The reaction mixture was incubated at 50°C for 15 min followed by 5 min incubation on ice to stop the reaction. Then 10 µ1 of alcohol oxidase (AO-0.01 U/µl) and 90 µl of Tris-HCl buffer (pH 8.5) were added and incubated at 37°C for 10 min to convert methanol to formaldehyde. 200 µl Nash reagent was added to the reaction mixture and same was transferred to the water bath at 60°C and incubated for 15 min. After the removal from water bath, 600 µl of the water was added to make a final volume of 1 ml and centrifuged at 13,000g for 2 min. The absorbance of the supernatant was measured at 412 nm (A_{412}) using UV-Visible spectrophotometer (Gene Quant, GE Healthcare, USA). The molar extinction coefficient 7,100 $M^{-1}cm^{-1}$ for the product, diacetyl-dihydro-dimethylpyridine was used (Anthon & Barrett, 2004). One unit of enzyme activity was defined as the amount of enzyme that releases 1 µmole of product per minute, under the described assay conditions. Nash reagent was used and prepared fresh for enzyme assay. 3.08 g of ammonium acetate was dissolved in 6 ml of Milli-Q water, followed by addition of 41 µl acetyl acetone and 59 µl of glacial acetic acid, Milli-Q water was added to make the final volume to 20 ml (Anthon and Barrett. 2004).

3.2.2.2 Calculation of enzyme activity

The activity of the enzyme was expressed as U/ml and the specific activity as U/mg of protein. One Unit of enzyme activity was defined as the amount of enzyme that forms 1 µmole of product (Diacetyl dihydro dimethyl pyridine) per minute. The enzyme activities of *Ct*PME*f* and *Ct*PME were calculated as described below,

$$\text{Enzyme activity (U/ml)} = \frac{\Delta A_{412} \times 1000}{\varepsilon \times t \times v}$$

Where,

ΔA_{412} = Absorbance of Diacetyl dihydro dimethyl pyridine

ε = Molar extinction of Diacetyl dihydro dimethyl pyridine at A_{412}, 7100 $M^{-1}cm^{-1}$

t = Time of reaction in min

v = Volume of enzyme at reaction in ml

$$\text{Specific activity (U/mg)} = \frac{\text{Enzyme activity (U/ml)}}{\text{Concentration of protein used (mg/ml)}}$$

3.2.3 Substrate specificity of *Ct*PME*f* and *Ct*PME

The substrate specificity of *Ct*PME was analyzed against various pectin substrates (1%, w/v) *viz.* Citrus pectin of varying degrees of methyl esterification (85%, 75-50% & 25%), apple pectin, poly galacturonic acid (PGA), pectic galactan from potato and lupin, rhamnogalacturonan from soybean (RGS) and potato (RGP). *Ct*PME*f* or *Ct*PME (10 µL of 0.08 mg/ml) was taken in the reaction mixture (100 µl) containing the respective substrate in Tris-HCl buffer (pH 8.5) and incubated at 50°C for 15 min. The absorbance at 412 nm (A_{412}) was measured. The substrate specificity was

determined after optimizing the conditions of pH and temperature for the reaction. The enzyme activity and specific activity was calculated by using the formula mentioned in the previous Section 3.2.2.2.

3.2.4 Determination of optimum pH of *Ct*PME*f* and *Ct*PME

The optimum pH of *Ct*PME*f* and *Ct*PME was determined by using citrus pectin (CP) (>85% methyl esterified) as substrate. The enzyme assay was performed under a wide range of pH using for different buffers. The enzyme activity of *Ct*PME*f* and *Ct*PME (10 µl of 0.08 mg/ml) was determined by incubating with 1% (w/v) CP (85% esterified) in 100 µl reaction mixture at 50°C for 15 min using different buffers: 50 mM sodium-citrate (pH 3.0-5.5), 50 mM sodium phosphate (pH 6.0-7.5), 50 mM Tris-HCl (pH 8.0-9.5) and Glycine-NaOH (pH 9.5-12.0). The absorbance at 412 nm was measured and the enzyme specific activity was calculated as mentioned earlier in Section 3.2.2.2. The reaction was performed in triplicate sets and reported as mean±SD.

3.2.5 Determination of optimum temperature of *Ct*PME*f* and *Ct*PME

The optimized pH was used for determination of optimum temperature. The optimum temperature of *Ct*PME*f* and *Ct*PME was studied by taking the enzyme (10 µl of 0.08 mg/ml) in a 100 µl reaction mixture with 1% (w/v) CP (85% methyl esterified) dissolved in 50 mM Tris-HCl (pH 8.5) and incubating at temperatures ranging between 10°C – 100°C. The A_{412} was measured and the enzyme activity was calculated as described earlier as Section 3.2.2.2. Each reaction was performed in triplicates and reported as mean±SD.

3.2.6 Determination of pH stability of *Ct*PME*f* and *Ct*PME

The pH stability of both enzymes was studied by individually incubating the enzyme (10 µl of 0.08 mg/mL) at 25°C for 30 min in a wide pH range, 3-12 of different buffers: 50 mM sodium-citrate (pH 3.0-5.5), 50 mM sodium phosphate (pH 6.0-7.5), 50 mM Tris-HCl (pH 8.0-9.5) and Glycine-NaOH (pH 9.5-12.0). The enzyme activity was assayed by taking 10 µl of 0.08 mg/mL enzyme with 1% (w/v) CP (85% esterified) dissolved in respective buffer and performed standard assay. After the incubation the enzyme activity was determined by measuring A_{412} as mentioned earlier in Section 3.2.2.2. The specific activity for both the enzymes was calculated as mentioned earlier in Section 3.2.2.2. Residual activity was determined. All the reaction was performed in triplicate sets and reported as mean±SD.

3.2.7 Determination of temperature stability of *Ct*PME*f* and *Ct*PME

The effect of temperature on stability of *Ct*PME*f* and *Ct*PME was determined by incubating the enzymes (100 µl of 0.08 mg/mL) in Tris-HCl buffer (pH 8.5) at different temperatures ranging from 10°C to 100°C for 30 min. The residual activity of this incubated *Ct*PME*f* and *Ct*PME (10 µl of 0.08 mg/mL) was determined after performing assay in 100 µl reaction volume with 1% (w/v) CP (85% esterified) dissolved in 50 mM Tris-HCl buffer of 8.5 for *Ct*PME*f* and *Ct*PME. The specific activity for both the enzymes was calculated as mentioned earlier in Section 3.2.2.2. All the reactions were performed in triplicates and reported as mean±SD.

3.2.8 Determination of kinetic parameters of *Ct*PME*f* and *Ct*PME

Kinetic parameters of *Ct*PME*f* and *Ct*PME were determined by assaying their activity against different concentrations of substrates under optimized conditions of temperature and pH. The kinetic parameters of *Ct*PME were determined by using citrus

pectin (degree of methyl esterification 85%, 75-50% and 25%) and apple pectin. The enzyme (10 µl of 0.08 mg/ml) was taken in 100 µl reaction mixture containing respective substrate in 50 mM Tris HCl (pH 8.5) and incubated at 50ºC for 15 min. The substrate concentration was varied from 0.01% (w/v) to 3.0% (w/v). After the incubation the enzyme activity was determined by measuring A_{412} as mentioned earlier. The specific activity was calculated as mentioned in Section 3.2.2.2 and k_{cat} and K_m were determined by using the Michaelis-Menten plot and Lineweaver-Burk plot. All the reactions were performed in triplicates and reported as mean±SD.

3.2.9 Effect of metal ions on activity of *Ct*PME*f* and *Ct*PME

The effect of different metal ions, detergents and chaotropic agents on *Ct*PME activity was determined. The effect of metal ions on the activity of *Ct*PME was studied by taking respective metal ion *viz.* Na^+ (NaCl), K^+ (KCl), Li^+ (LiCl), Ca^{2+} ($CaCl_2.2H_2O$), Mg^{2+} ($MgCl_2$), Mn^{2+} ($MnCl_2{\cdot}4H_2O$), Zn^{2+} ($ZnSO_4{\cdot}7H_2O$), Cu^{2+} ($CuSO_4{\cdot}5H_2O$), Co^{2+} ($CoCl_2{\cdot}6H_2O$), Ba^{2+} ($BaCl_2$), Al^{3+} ($AlCl_3{\cdot}6H_2O$) and Fe^{3+} ($FeCl_3{\cdot}6H_2O$) in the reaction mixture. The reaction was carried out in 100 µl mixture, containing enzyme (10 µl of 0.08 mg/mL) and 1% (w/v) CP (85% esterified) in 50 mM Tris HCl (pH 8.5) by incubating at 50ºC for 15 min. The concentration of metal ions was varied between 0 and 20 mM. Similarly, the effect of chelating agents, disodium EDTA and EGTA, and also detergents (SDS, Tween 20, Tween 80 and Triton X100) were studied by varying their concentration from 0 to 20 mM in the reaction mixture. The chaotropic agents (urea and guanidine hydrochloride) were varied from 1 to 8 M in the reaction mixture. The blank with the substrate having the respective additive was also run and assayed in parallel. The enzyme activity was calculated by measuring A_{412}

and following the method as described earlier in Section 3.2.2.2. All the reactions were performed in triplicates and reported as mean ± SD.

3.2.10 Protein-melting study of *Ct*PME*f* and *Ct*PME

Protein melting curves was generated by subjecting 1 ml recombinant *Ct*PME*f* *Ct*PME (0.05 mg/ml) to varying temperatures from 25°C to 100°C and measuring the change in the absorbance at 280 nm by a UV-Visible spectrophotometer (Varian, Cary 100-Bio, USA) equipped with a peltier temperature controller system as explained by Dvortsov et al. (2009). The purified *Ct*PME*f* and *Ct*PME both dialyzed against 50 mM Tris-HCl buffer (pH 8.5) containing 300 mM NaCl was used. The effect of Ca^{2+} ions on the protein melting curve of *Ct*PME was studied by adding 5 mM $CaCl_2$. The blank contained the buffer and 5 mM $CaCl_2$. The protein melting experiment was also performed by adding 5 mM $CaCl_2$ and 5 mM EDTA to 1 ml enzyme solution (0.05 mg/ml) and the change in absorbance at 280 nm was measured. The change in absorbance with the varying temperature was plotted. Similarly, the experiment was performed for *Ct*PME*f* to know the influence of unknown function module on the catalytic module *Ct*PME. The reactions were performed in triplicates and reported as mean ± SD.

3.2.11 Effect of different media on *Ct*PME*f* and *Ct*PME production

In order to obtain higher production of *Ct*PME*f* and *Ct*PME, the cells expressing *Ct*PME*f* and *Ct*PME were grown in five different media (100 ml). The five media *viz.* LB, 5x LB, Terrific Broth (TB), Tryptone Yeast extract (TY) were prepared, as described earlier (Tripati et al., 2009) and also the Auto Induction medium-LB (AIM-LB) medium (Studier, 2005). *Ct*PME was expressed in LB, 5x LB, Terrific Broth (TB), Tryptone Yeast extract (TY) shown in Table 3.1 by following the procedure mentioned

in previous section by the induction by IPTG, whereas in case of AIM-LB, after the culture reached mid exponential phase ($A_{600} \approx 0.6$) it was further incubated at 24°C, 180 rpm for 48 h without adding IPTG (Studier, 2005). *Ct*PME*f* and *Ct*PME expressed using these media was purified as mentioned in the previous Chapter 2 section 2.2.14. The recombinant proteins yield were calculated by following formula

$$\text{Yield (g/g)} = \frac{\text{Total purified protein (g/l)}}{\text{Biomass (g/l)}}$$

Table 3.1 Preparation of 100 ml LB, 5xLB, TB, TY and AIM-LB medium for production of *Ct*PME*f* and *Ct*PME.

Medium	Component	Final concentration (%, w/v)
LB	Tryptone	1.0
	Yeast Extract	0.5
	NaCl	1.0
5xLB	Tryptone	5.0
	Yeast Extract	2.5
	NaCl	2.5
	Glycerol	1.0
TB	Pancreatic digest of casein	1.2
	Yeast extract	2.4
	Di-potassium phosphate	0.94
	Mono-potassium phosphate	0.22
	Glycerol	0.4
TY	Tryptone	2.68
	Yeast extract	2.14
	Di-ammonium hydrogen phosphate	0.16
	Mono-potassium phosphate	0.54
	Magnesium sulphate	0.12
	NaCl	0.85
	Glycerol	0.1
AIM-LB	Tryptone	1.0
	Yeast extract	0.5
	Ammonium sulphate	0.33
	Potassium di hydrogen phosphate	0.68
	Disodium hydrogen phosphate	0.71
	Glucose	0.05
	Lactose	0.2
	Magnesium sulphate	0.015
	100x trace elements	0.00044

3.3 Results and Discussion

3.3.1 Substrate specificity of *Ct*PME*f* and *Ct*PME

The hydrolysis of substrate CP (85% esterified) by *Ct*PME*f* and *Ct*PME was confirmed by increase in the absorbance at 412 nm. Increase in absorbance was caused by the formation of hydrolysis of methyl group in the D-Gal*p*A residue at poly Gal*p*A. Both *Ct*PME*f* and *Ct*PME displayed high activity against CP (85% esterified) and moderate activity against other lower esterified pectins. Both the enzymes showed low activity against polygalacturonic acid (PGA) and other pectins (RGS and RGP) (Table 3.2). *Ct*PME*f* and *Ct*PME were primarily active against esterified component of pectins. It may be easy to comprehend that the low activity of *Ct*PME*f* and *Ct*PME against PGL, RGS and RGP may be due to the low content of esterified D-Gal*p*A residues in this substrate as compared to CP esterified. PGL and PGP contain around 74% and 87% D-Gal*p* respectively, while RGP and RGS contain only 20% D-Gal*p*. Very recently, another PME belonging to CE family 8, *Bli*PME from *Bacillus licheniformis* has been reported which is observed highly methyl-esterified and acetylated pectins (Remoroza *et al*., 2015).

Table 3.2 Activity of *Ct*PME*f* and *Ct*PME towards different polysaccharides.

Substrate (1%, w/v)	*Ct*PME*f* Specific Activity (U/mg)	*Ct*PME Specific Activity (U/mg)
Citrus pectin (85% methylation)	20.1±0.01	18.1±0.04
Apple pectin (75% methylation)	16.5±0.04	14.8±0.05
Citrus pectin (70% methylation)	15.6±0.09	14.1±0.01
Citrus pectin (50% methylation)	12.5±0.02	12.3±0.01
Citrus pectin (25% methylation)	6.4±0.02	8.5±0.08
Polygalacturonic acid	0.5±0.01	1.0±0.03
Rhamnogalacturonan (Potato)	0.7±0.04	0.9±0.13
Rhamnogalacturonan (Soya)	0.8±0.13	0.9±0.04
Pectic galactan (Potato)	0.3±0.07	0.5±0.07
Pectic galactan (Lupin)	0.2±0.02	0.3±0.02
Carboxymethylcellulose	0.2±0.02	0.3±0.05
Other substrates*	NA	NA

*NA = No activity; *=Carob galactomannan, Konjac galactomanan, β-D-Glucan (Barley), Xylan from Beechwood and Birchwood, Arabinoxylan from Wheat and Rye, Curdlan, Laminarin and Lichenan.*

*The reaction of Ct*PME*f* and *Ct*PME *was carried out at 50°C for15 min using pectin substrates (1%, w/v) dissolved in 50 mM Tris-HCl buffer (pH 8.5).*

3.3.2 Optimum pH for activity of *Ct*PME*f* and *Ct*PME

The activity of *Ct*PME*f* and *Ct*PME were studied in the pH, ranging from 3-12. The optimum pH for the activity of both *Ct*PME*f* and *Ct*PME was 8.5 (Fig. 3.1), in line with other PMEs from *Erwinia chrysanthemi, Solanum lycopersicum, Yersinia enterocolitica, Daucus carota, Sitophilus oryzae* and *Bacillus licheniformis* DSM13 (Laurent *et al*., 2000; D'Avino *et al*., 2003; Boraston & Abbott, 2012; Johansson *et al*., 2002; Teller *et al*., 2014; Remoroza *et al*., 2015). These results were consistent with the pH profiles of a previous report on recombinant protein *Bil*PME from *Bacillus*

licheniformis DSM13 (pH 8.0) and PME from *Erwinia chrysanthemi* (pH 8-9). The results showed that both these enzymes were active under alkaline conditions.

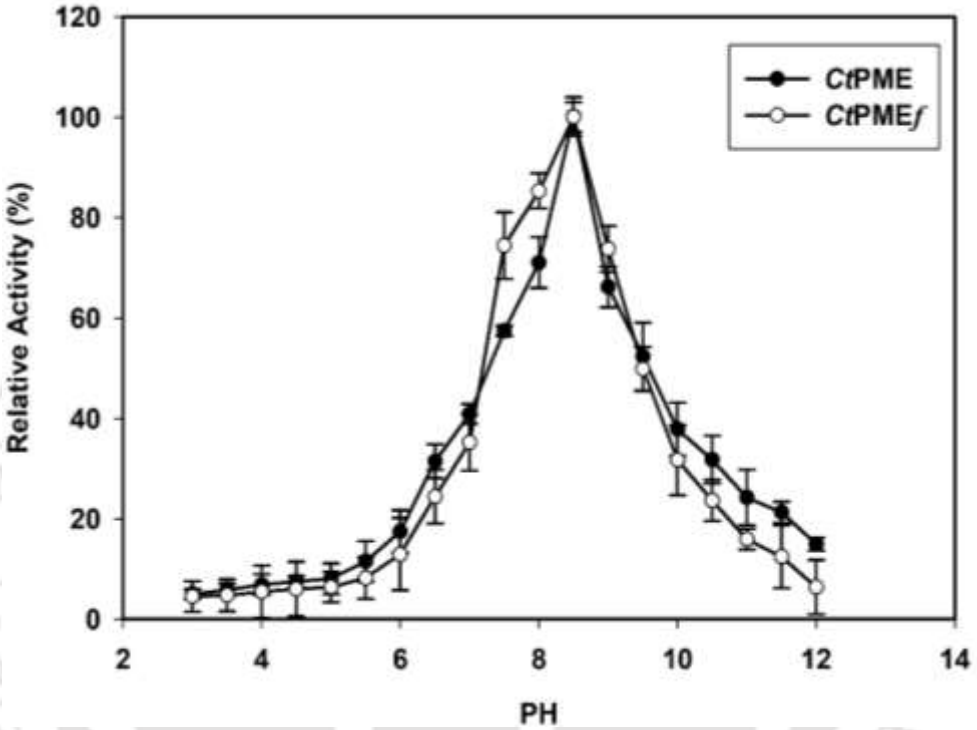

Fig. 3.1 Optimum pH for the activity of *Ct*PME*f* and *Ct*PME.

3.3.3 Optimum temperature for activity of *Ct*PME*f* and *Ct*PME

The activity of *Ct*PME*f* and *Ct*PME were active in temperature ranging from 10°C -100ºC. The optimum temperature of both the recombinant enzymes, *Ct*PME*f* and *Ct*PME was 50ºC (Fig. 3.2). As expected, since these thermophiles enzymes were from a thermophilic bacterium. These results were consistent with the temperature (50°C) profiles of a previous report on recombinant protein *Bil*PME from *Bacillus licheniformis* DSM13 (Remoroza *et al*., 2015) and PME from *Erwinia chrysanthemi* (Laurent *et al*., 2000).

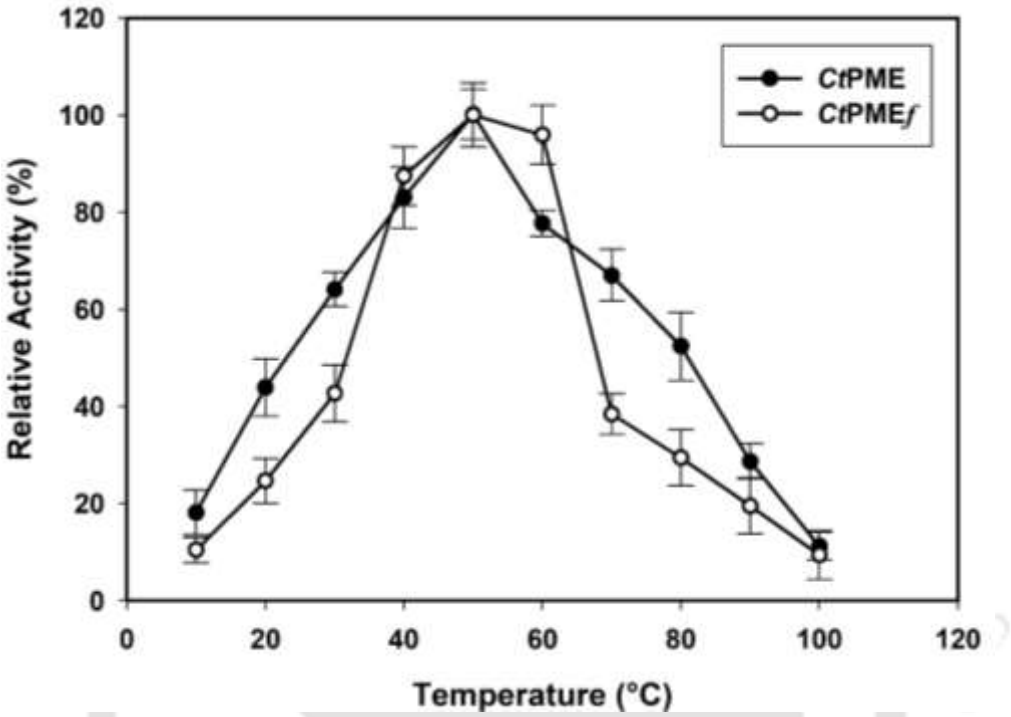

Fig. 3.2 Optimum temperature for activity of *Ct*PME*f* and *Ct*PME.

3.3.4 pH stability of *Ct*PME*f* and *Ct*PME

The pH stability of *Ct*PME*f* and *Ct*PME were investigated in the pH range 3-12. *Ct*PME retained 85% activity in pH range 8.0 to 9.0 and *Ct*PME*f* retained 85% activity in pH range 7.5 to 9.0 (Fig. 3.3).

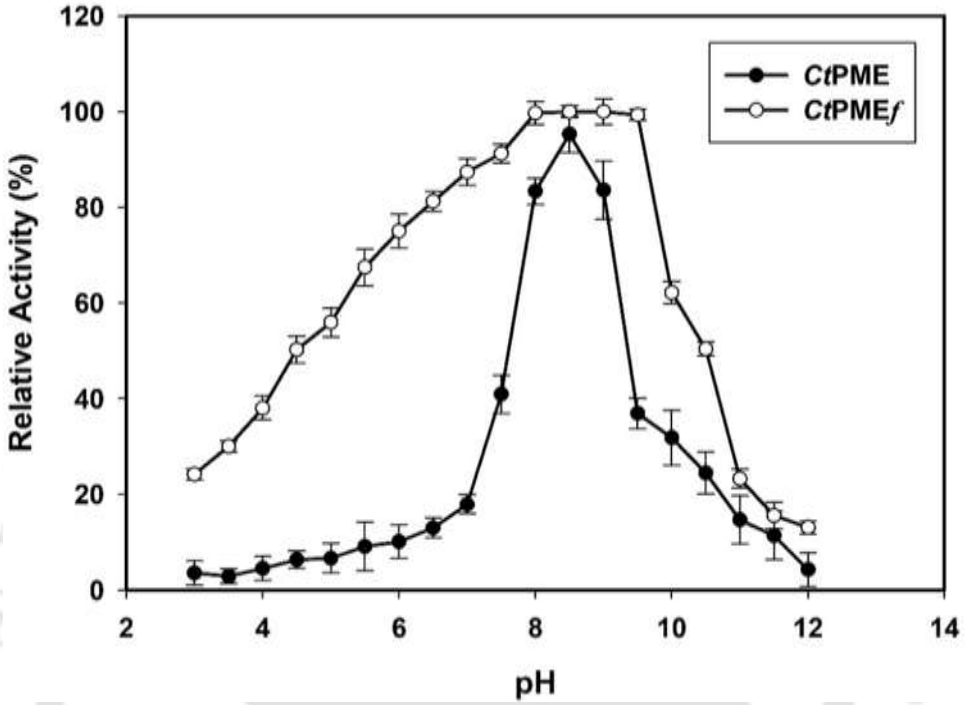

Fig. 3.3 pH stability of *Ct*PME*f* and *Ct*PME.

3.3.5 Temperature stability of *Ct*PME*f* and *Ct*PME

The temperature stability study showed that *Ct*PME*f* and *Ct*PME retained 90% activity after incubation in the temperature range 50ºC to 60°C for 30 min (Fig. 3.4). *Ct*PME*f* and *Ct*PME were stable enzymes the temperatures 40°C to 70°C and retained 80% activity under optimized assay conditions (Fig. 3.4). The loss of enzyme activity after exposure to high temperature disrupts the protein fold causing decreased stability (Branden *et al*., 1991; Creighton, 1992). The activity of the enzyme incubated at 4°C at zero time was taken as 100%.

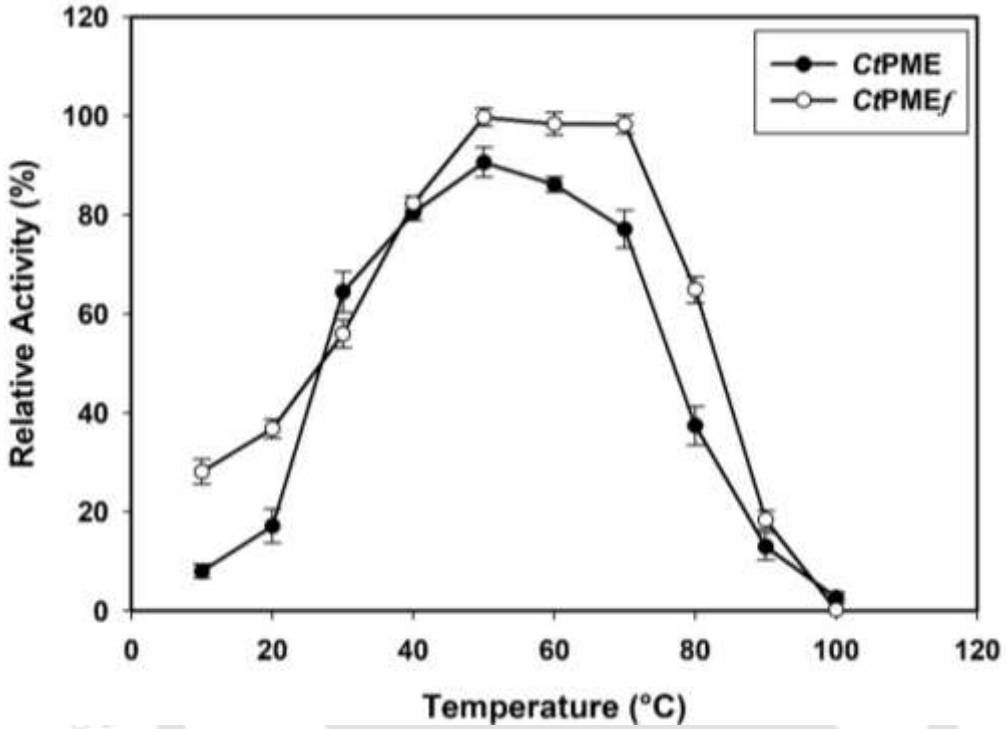

Fig. 3.4 Thermal stability of *Ct*PME*f* and *Ct*PME.

3.3.6 Kinetic parameters of *Ct*PME*f* and *Ct*PME

The kinetic properties of *Ct*PME*f* and *Ct*PME against various substrates were determined (Table 3.3). *Ct*PME*f* and *Ct*PME displayed turnover number (k_{cat}) of 4.1 s^{-1} and 3.77 s^{-1}. *Ct*PME*f* and *Ct*PME displayed catalytic efficiency (k_{cat}/Km) of 1.22 and 1.21 ml/mg s with citrus pectin (85% esterified). *Ct*PME efficiently acted on other substrates viz. apple pectin, citrus pectin (75% esterified), citrus pectin from CP Kelco and citrus pectin (25% esterified); the corresponding turnover number were 3.68 s^{-1}, 3.06 s^{-1}, 2.62 $s^{-1}$and 1.72 s^{-1}, respectively. *Ct*PME, catalytic efficiency were 0.97 ml/mg s, 0.72 ml/mg s, 0.55 ml/mg s and 0.20 ml/mg s, respectively (Table 3.3). *Ct*PME*f* efficiently acted on other substrates viz. apple pectin, citrus pectin (75% esterified), citrus pectin from CP Kelco and citrus pectin (25% esterified); the corresponding

turnover number were 3.44 s^{-1}, 3.2 s^{-1}, 2.6 s^{-1} and 1.3 s^{-1}, respectively. *Ct*PME*f* catalytic efficiency were 0.91 ml/mg s, 0.71 ml/mg s, 0.49 ml/mg s and 0.12 ml/mg s, respectively (Table 3.3). The turnover number and catalytic efficiency of *Ct*PME*f* and *Ct*PME decreased with a decrease in the degree of methyl esterification of citrus pectin from 85% to 25%.

Table 3.3 Kinetic parameters of *Ct*PME*f* and *Ct*PME.

Substrate (1%, w/v)	***Ct*PME*f*¥**			***Ct*PME¥**		
	K_m (mg/ml)	k_{cat} (s^{-1})	k_{cat}/K_m (ml/mg s)	K_m (mg/ml)	k_{cat} (s^{-1})	k_{cat}/K_m (ml/mg s)
Citrus pectin (85% methylation)	3.4	4.1	1.23	3.1	3.7	1.21
Apple pectin (75% methylation)	3.8	3.4	0.91	3.8	3.6	0.97
Citrus pectin (70% methylation)	4.6	3.2	0.71	4.2	3.0	0.72
Citrus pectin (50% methylation)	5.3	2.6	0.49	4.7	2.6	0.55
Citrus pectin (25% methylation)	10.2	1.3	0.12	8.9	1.7	0.20
Polygalacturonic acid	ND	ND	ND	ND	ND	ND

¥*Values are in Mean ± SD (n=3)*
ND = No Activity Detected;
The assays were carried out in 50 mM Tris-HCl buffer (pH 8.5) at 50°C.

3.3.7 Effect of metal ions on the activity of *Ct*PME*f* and *Ct*PME

Multiple Sequence analysis of *Ct*PME*f* revealed the presence of conserved Ca^{2+} ions binding amino acid residues in Dockerin region. Therefore, the effect of mono, divalent and tri valent metal ions on the activity of *Ct*PME*f* and *Ct*PME was analysed. The effect of metal ions (1 mM to 30 mM) on *Ct*PME was studied. The *Ct*PME activity was enhanced by 40% in presence of 5 mM Ca^{2+} or Mg^{2+} ions (Table 3.4). On increasing the concentration of the metal ions beyond 10 mM, the reaction mixture formed a gel. Similar effects of metal ions were also reported by Laurent et al. (2000). *Ct*PME activity

increased by 14% and 17% in the presence of 1 mM Mn^{2+} or Co^{2+} ions, respectively. *Ct*PME was unaffected by 1 mM or 5 mM concentration of Cs^{+}, K^{+} and Li^{+} ions and retained 100% activity. *Ct*PME showed more than 95% activity in presence of 1 mM Ba^{2+}, Fe^{2+} or Al^{3+}. In presence of 1 mM Cu^{2+} or 1 mM Zn^{2+}, the enzyme activity decreased to 50% (Table 3.4). *Ct*PME activity was very low, 4.8% and 2.8%, in the presence of 1 mM and 5 mM Hg^{2+}, respectively. PME from *Aspergillus reptans* was also reported to be inhibited by Hg^{2+} (Arotupin *et al*., 2008). The enzyme activity of *Ct*PME was adversely affected at higher concentrations (> 5 mM) of all metal ions tested (Data not shown). The presence of chelating agents, EDTA (5 mM) and EGTA (5 mM) caused a decrease in enzyme activity of *Ct*PME by more than 45% and 12%, respectively (Table 3.4). Upon increasing the concentration of chelating agent, the activity of *Ct*PME progressively decreased. Similar reduction in activity upon increasing concentration of chelating agent was also observed in case of PME from *Aspergillus reptans* (Arotupin *et al*., 2008) and *Glycine max* (Wu *et al*., 2010). The decrease in activity in presence of EDTA and EGTA indicated that Ca^{2+} may be essential for enzyme activity as EDTA and EGTA specifically binds and chelates calcium ions in 1:1 molar ratio. The residual enzyme activity of *Ct*PME by treatment of 5 mM of detergents *viz.* Triton X100, Tween20, Tween80 and SDS were 100%, 99%, 91% and 71%, respectively. The activity of PME from *E. chrysanthemi* 3937 (Laurent *et al*., 2000) and *Aspergillus flavus* (Jiang *et al*., 2014) was also reduced by 1 mM SDS. *Ct*PME retained more than 82% activity in the presence of low concentration (0.1 M) of GnHCl and Urea. *Ct*PME lost 99% enzyme activity at 6 M concentration of urea. The enzyme activity of *Ct*PME increased by 6%, in presence of 300 mM NaCl. The *Ct*PME retained 90% of its activity in the presence of 0.5 M NaCl and decreased to 50%

by 1 M NaCl. The effect of mono, divalent and tri valent metal ions on the activity of *Ct*PME*f* was analysed. *Ct*PME*f* showed similar effect as catalytic module *Ct*PME. On increasing the concentration up to 15 mM, most of the metal ions caused precipitation of the reaction mixture and formed a gel. A similar observation was reported by Laurent et al. (2000).

Table 3.4 Effect of different additives on the activity of *Ct*PME and *Ct*PME*f*.

Metal ion	*Ct*PME Relative activity (%)[v]		*Ct*PME*f* Relative activity (%)[v]	
	1 mM	**5 mM**	**1 mM**	**5 mM**
Control	100	100	100	100
Ca^{2+}	133.5 ± 0.6	142.0 ± 0.1	134.2 ± 0.1	150.3 ± 0.5
Mg^{2+}	116.0 ± 0.1	140.0 ± 0.5	122.4 ± 0.5	148.2 ± 0.1
Mn^{2+}	114.7 ± 0.8	117.8 ± 0.5	111.5 ± 0.8	107.8 ± 0.5
Co^{2+}	117.7 ± 0.7	109.0 ± 0.6	115.0 ± 0.5	102.0 ± 0.6
Cs^{+}	100.0 ± 0.5	100.0 ± 0.7	100.0 ± 0.1	100.0 ± 0.6
K^{+}	100.0 ± 0.5	100.0 ± 0.7	100.0 ± 0.1	100.3 ± 0.3
Li^{2+}	100.0 ± 0.2	99.6 ± 0.5	100.0 ± 0.3	99.8 ± 0.5
Ba^{2+}	98.7 ± 0.3	97.5 ± 0.4	99.3 ± 0.3	97.7 ± 0.2
Fe^{2+}	99.6 ± 0.1	42.5 ± 0.3	96.8 ± 0.5	32.5 ± 0.1
Al^{3+}	95.4 ± 0.1	39.7 ± 0.2	94.5 ± 0.2	31.0 ± 0.1
Cu^{2+}	48.6 ± 0.7	42.4 ± 0.3	44.0 ± 0.7	22.3 ± 0.3
Zn^{2+}	28.6 ± 0.5	18.0 ± 0.5	28.0 ± 0.5	13.7 ± 0.3
Hg^{2+}	4.8 ± 0.4	2.8 ± 0.7	5.0 ± 0.8	2.9 ± 0.7
Detergent				
SDS	82.1 ± 0.4	71.7 ± 0.4	80.4 ± 0.4	70.0 ± 0.1
Tween 80	97.2 ± 0.5	91.5 ± 0.5	98.3 ± 0.5	92.4 ± 0.8
Tween 20	100.0 ± 0.5	99.8 ± 0.4	100.1 ± 0.5	98.3 ± 0.4
Triton 100	100.0 ± 0.6	100.0 ± 0.7	100.1 ± 0.1	100.0 ± 0.5
Chelating & Chaotropic agent				
EDTA	69.0 ± 0.4	62.6 ± 0.2	69.0 ± 0.2	60.1 ± 0.6
EGTA	85.7 ± 0.1	88.6 ± 0.1	89.4 ± 0.7	88.6 ± 0.1
Urea	97.6 ± 0.2(0.1M)	25.3 ± 0.2(5M)	96.6 ± 0.4(0.1M)	24.8 ± 0.6(5M)
GnHCl	85.1 ± 0.1(0.1M)	16.1 ± 0.1(5M)	84.8 ± 0.7(0.1M)	15.5 ± 0.6(5M)
NaCl	82.3 ± 0.5(0.1M)	106.5 ± 0.3(0.3M)	79.5 ± 0.1(0.1M)	108.2 ± 0.2(0.3M)

[V]=*Values are mean ± SD (n=3) relative to the control without any metal ions or reagent added. The assays were carried out in 50 mM Tris-HCl buffer (pH 8.5) at 50°C.*

3.3.8 Protein melting study of *Ct*PME and *Ct*PME*f*

The melting-curve analysis of *Ct*PME displayed a single melting peak at 80°C in absence of any additive (Fig. 3.5 Solid line). The peak for recombinant *Ct*PME shifted towards higher temperature, 85°C in presence of 5 mM Ca^{2+} ions (Fig. 3.5, Dotted line). When, 5 mM concentration of EDTA sodium salt was added to the enzyme containing 5 mM Ca^{2+} ions, the melting temperature shifted back to the native melting temperature, 80°C (Fig. 3.5, Dash-dot line). The shifting back of melting peak in the presence of EDTA was due to chelation of Ca^{2+} ions making them unavailable to stabilize the enzyme. The melting curve analysis of *Ct*PME showed that Ca^{2+} ions impart structure stability to the enzyme as in the presence of 5 mM Ca^{2+} ions the complete unfolding of *Ct*PME was observed at 5°C higher than in the absence of Ca^{2+} ions. *Ct*PME*f* showed the similar pattern of melting curve as compared to *Ct*PME and no significant change was observed. The enzyme activity of *Ct*PME was significantly enhanced in the presence of Ca^{2+} (Table 3.4). This shows that Ca^{2+} ions are involved in catalysis and to some extent important for structural integrity. This highlighted the role of Ca^{2+} ions in shifting the melting peak to a higher temperature imparting the stability to the protein fold as also reported earlier (Sultan *et al*., 2012).

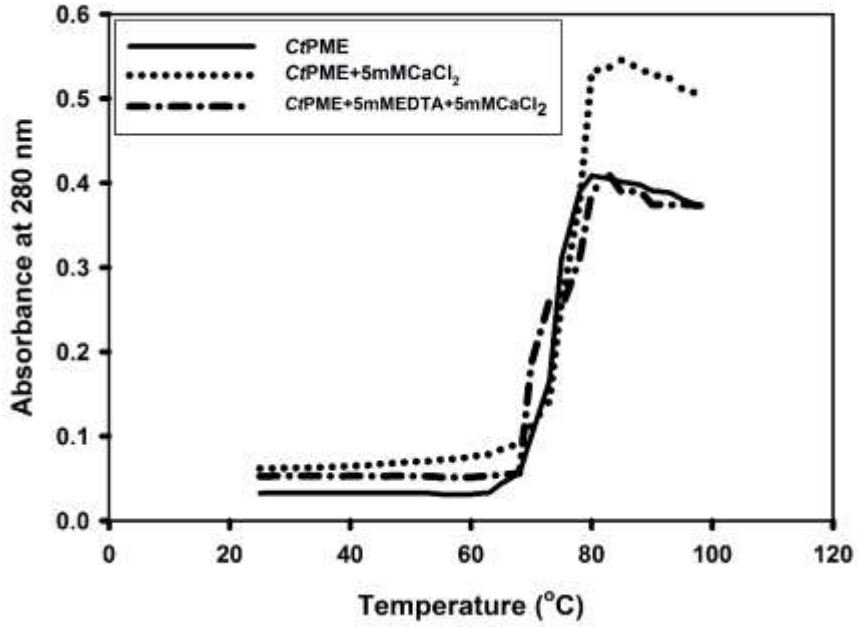

Fig. 3.5 Protein melting analysis of *Ct*PME showing melting curve with and without additives.

3.3.9 Effect of medium on *Ct*PME and *Ct*PME*f* production

The recombinant *Ct*PME enzyme was expressed and produced using different culture media. The dry cell weight (DCW) obtained from the culture grown in AIM medium (25 g/l) was maximum followed by TB (18 g/l), TY (17 g/l), 5x LB (12 g/l) and LB (8 g/l) medium (Fig. 3.6). The maximum concentration of *Ct*PME (114 mg/l) was obtained with AIM-LB medium followed by TB (63 mg/l), TY (58 mg/l), 5xLB (34 mg/l) and LB (15 mg/l) medium (Fig. 3.6). Similarly, the recombinant *Ct*PME*f* enzyme was expressed and produced using different culture media. The dry cell weight (DCW) obtained from the culture grown in AIM LB medium (21 g/l) was maximum followed by TB (19 g/l), TY (16 g/l), 5x LB (12 g/l) and LB (9.5 g/l) medium (Fig. 3.7). The maximum concentration of *Ct*PME*f* (98 mg/l) was obtained with AIM-LB medium followed by TB (71 mg/l), TY (56 mg/l), 5xLB (34 mg/l) and LB (14.8 mg/l) medium

(Fig 3.7). The maximum yields 0.014 g/g and 0.013 g/g of *Ct*PME and *Ct*PME*f* were obtained with AIM LB medium (Table 3.5 & 3.6). The other media TB, TY, 5xLB and LB gave *Ct*PME yields of 0.01 g/g, 0.009 g/g, 0.006 g/g and 0.003, respectively (Table 3.5). *Ct*PME*f* yields obtained with the media TB, TY, 5xLB and LB were 0.01 g/g, 0.008 g/g, 0.005 g/g and 0.002 g/g, respectively (Table 3.6). These results showed that the production of recombinant *Ct*PME*f* and *Ct*PME could be further improved by optimizing the concentration of medium ingredients (Tripathi *et al*., 2009; Studier. 2005). This study is important for obtaining high yields of recombinant protein concentration for industrial applications.

Table 3.5 Effect of different media on production of recombinant *Ct*PME.

Medium	*E. coli* biomass (g/l)	Purified Protein (mg/l)	Protein purified (ml)	Total purified Protein (mg/l)	Yield (g/g)
LB	8.0	15.1	1.8	27.1	0.003
5xLB	12.6	34.2	2.4	82.0	0.006
TY	17.1	58.5	2.8	163.8	0.009
TB	18.3	63.1	3.0	189.3	0.010
AIM-LB	25.2	114.3	3.2	365.7	0.014

Table 3.6 Effect of different media on production of recombinant *Ct*PME*f*

Medium	*E. coli* biomass (g/l)	Purified Protein (mg/l)	Protein purified (ml)	Total purified Protein (mg/l)	Yield (g/g)
LB	9.58	14.8	1.4	20.7	0.002
5xLB	12.0	34.6	2.2	76.1	0.005
TY	16.3	56.1	2.6	145.8	0.008
TB	19.4	71.5	3.1	221.6	0.011
AIM-LB	21.3	98.4	3.0	295.2	0.013

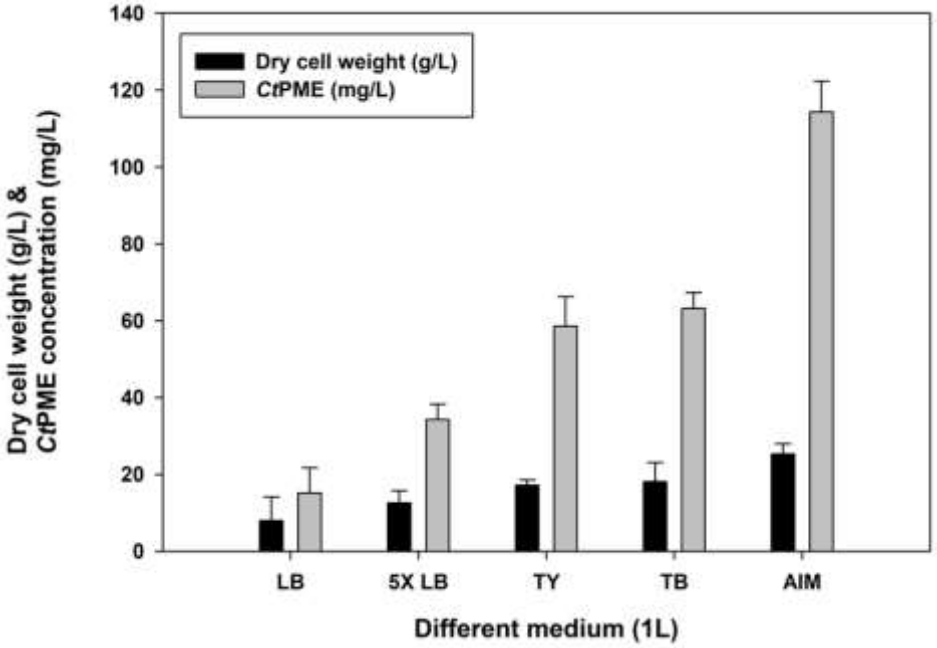

Fig. 3.6 Effect of *Ct*PME under different media and dry cell weight. LB-Luria Bertani; 5x LB-Luria–Bertani; TY-Tryptone yeast extract; TB-Terrific Broth and AIM-LB-Auto-Induction Medium-LB.

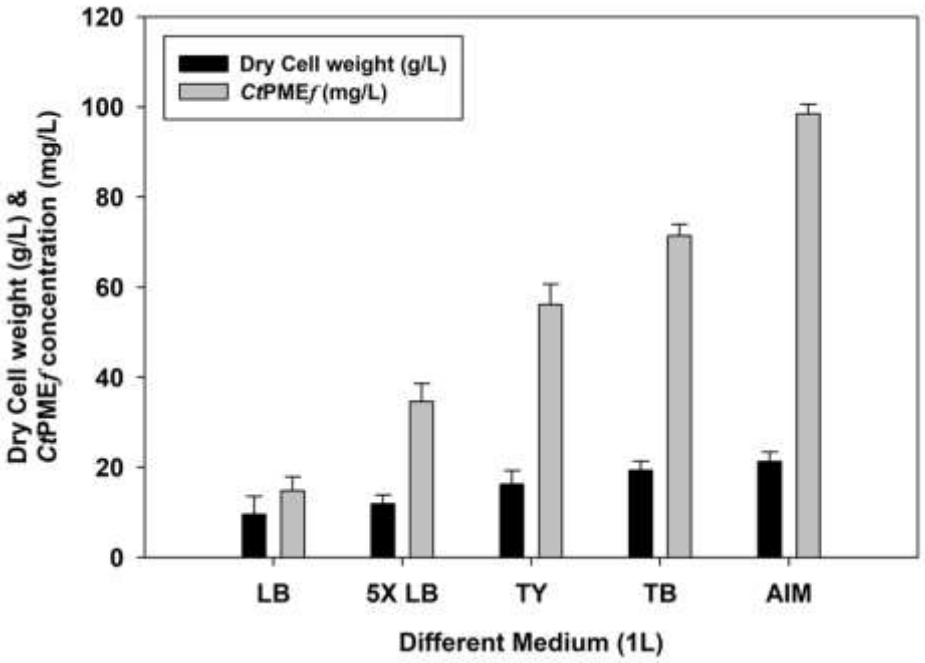

Fig. 3.7 Production of *Ct*PME*f* under different media and dry cell weight. LB-Luria–Bertani; 5x LB-Luria–Bertani; TY-Tryptone yeast extract; TB-Terrific Broth and AIM-LB-Auto-Induction Medium-LB.

3.4 Conclusions

Thermostable enzymes are important resources in various industrial processes that occur at higher temperatures. The recombinant pectin methylesterase (*Ct*PME*f* and *Ct*PME) from *C. thermocellum* de-esterified the methyl esterified pectin polymers, leading to a formation of pectate and methanol. *Ct*PME*f* and *Ct*PME showed maximum enzyme activity at pH 8.5. *Ct*PME*f* was active at pH range 7.0-9.0 while *Ct*PME was active only at pH 8.0-9.0. The optimal temperature of *Ct*PME*f* and *Ct*PME was 50ºC. *Ct*PME*f* and *Ct*PME retained 90% of its activity after incubation at 50ºC for 30 min. *Ct*PME*f* and *Ct*PME retained 80% of its activity after incubation at 40 or 70ºC for 30 min. Both *Ct*PME*f* and *Ct*PME showed high activity towards CP containing 85% esterified pectin polysaccharides. Maximum activity of both, *Ct*PME*f* and *Ct*PME was against CP (85% esterified) 20.1 U/mg and 18.8 U/mg, respectively. *Ct*PME*f* and *Ct*PME had similar values of K_m, 3.4 mg/ml and 3.1 mg/ml respectively, with CP (85% esterified). In case of *Ct*X157 protein, no esterase activity was observed. The enzyme activity of *Ct*PME was significantly enhanced in the presence of Ca^{2+}. The presence of 5 mM Ca^{2+} increased the activity of *Ct*PME*f* and *Ct*PME by 50% and 48%, respectively. Approximately, 10 times the higher yield of *Ct*PME was obtained by AIM medium than by LB resulting in affective production for industrial purpose. This enzyme can be used in combination with other enzymes for efficient and complete degradation of pectic polysaccharides forming produce pectin oligosaccharides, which have applications in healthcare. The enzyme described in this study will be competent enough for industrial processes such as fruit juice extraction, vegetable and fruit maceration and textile industry. This enzyme plays a role in de-methylation of pectin leading to pectin gels, which are useful in confectionary industry.

3.5 References

Aachary, A. A., Prapulla, S. G. (2011) Xylooligosaccharides (XOS) as an emerging prebiotic: microbial synthesis, utilization, structural characterization, bioactive properties, and applications. Comprehensive Reviews in Food Science and Food Safety, 10: 2-16.

Anbar, M., Gul, O., Lamed, R. (2012) Improved thermostability of *Clostridium thermocellum* endoglucanase Cel8A by using consensus-guided mutagenesis. Applied and Environmental Microbiology, 78: 3458-3464.

Anthon, G. E., Barrett, D. M. (2004) Comparison of three colorimetric reagents for the determination of methanol with alcohol oxidase, Application to the assay of pectin methylesterase. Journal of Agricultural and Food Chemistry, 52: 3749-3753.

Arotupin, D. J., Akinyosoye, F. A., Onifade, A. K. (2008) Purification and characterization of pectin methylesterase from *Aspergillus repens* isolated from cultivated soil. African Journal of Biotechnology, 7: 1991–1998.

Bartolome, L. G., Hoff, J. E. (1972) Gas-chromatographic methods for the assay of pectin methylesterase, free methanol, and methoxy groups in plant tissues. Journal of Agricultural and Food Chemistry, 20: 262-266.

Bayer, E. A., Morag, E., Lamed, R. (1994) The cellulosome- a treasure-trove for biotechnology. Trends in Biotechnology, 12: 379-386.

Benen, J. A. E., Van Alebeek, G. J. W. M., Voragen, A. G. J., Visser, J. (2003) Pectic esterases. In Handbook of food enzymology, 849-856. Dekker.

Bhardwaj, V., Garg, N. (2014) Production, purification of pectinase from *Bacillus sp.* MBRL576 isolate and its application in extraction of juice. International Journal of Science and Research, 3: 648-652.

Boraston, A. B., Abbott, D. (2012) Structure of a pectin methylesterase from *Yersinia enterocolitica*. Acta Crystallographica Section F: Structural Biology and Crystallization Communications, 68: 129-133.

Branden, C., Tooze, J. (1991) In Introduction to Protein Structure, (2nd ed.), Garland publishing, Taylor and Francis Group, Ney York, NY.

Creighton, T.E. (1992) In Proteins: Structures and Molecular Properties, (2nd ed.), Freeman, W. H. & Company, Macmillan Higher Education, Ney York, NY.

Das, S. P., Ravindran, R., Ahmed, S. (2012) Bioethanol production involving recombinant *C. thermocellum* hydrolytic hemicellulase and fermentative microbes. Applied Biochemistry and Biotechnology, 167:1475-1488.

D'Avino, R., Camardella, L., Christensen, T. M., Giovane, A., & Servillo, L. (2003) Tomato pectin methylesterase: modeling, fluorescence, and inhibitor interaction studies—comparison with the bacterial (*Erwinia chrysanthemi*) enzyme. Proteins: Structure, Function, and Bioinformatics, 53: 830-839.

Dvortsov, I. A., Lunina, N. A., Chekanovskaya, L. A., Schwarz, W. H., Zverlov, V. V., Velikodvorskaya, G. A. (2009) Carbohydrate-binding properties of a separately folding protein module from β-1, 3-glucanase Lic16A of *Clostridium thermocellum*. Microbiology, 155: 2442-2449.

Fontes, C. M., Gilbert, H. J. (2010) Cellulosomes: highly efficient nanomachines designed to deconstruct plant cell wall complex carbohydrates. Annual Reviews of Biochemistry, 79: 655-681.

Fraeye, I., Duvetter, T., Doungla, E., Van Loey, A., Hendricks, M. (2010) Fine-tuning the properties of pectin–calcium gels by control of pectin fine structure, gel composition and environmental conditions. Trends in Food Science & Technology, 21: 219–228.

Giacobbe, S., Pepe, O., Ventorino, V., Birolo, L., Vinciguerra, R., Faraco, V. (2014) Identification and characterisation of a pectinolytic enzyme from *Paenibacillus xylanolyticus*. BioResources, 9: 4873-4887.

Heikinheimo, R., Flego, D., Pirhonen, M., Karlsson, M. B., Eriksson, A., Mae, A., Tapio Palva, E. (1995) Characterization of a novel pectate lyase from *Erwinia carotovora subsp. carotovora*. MPMI-Molecular Plant Microbe Interactions, 8: 207-217

Jiang, X., Chen, P., Yin, M., Yang, Q. (2013) Constitutive expression, purification and characterisation of pectin methylesterase from *Aspergillus niger* in *Pichia pastoris* for potential application in the fruit juice industry. Journal of the Science of Food and Agriculture, 93: 375–381.

Jiang, X., Jia, Q., Chen, L., Chen, Q., Yang, Q. (2014) Recombinant expression and inhibition mechanism analysis of pectin methylesterase from *Aspergillus flavus*. FEMS Microbiology Letters, 355: 12–19.

Johansson, K., El-Ahmad, M., Friemann, R., Jörnvall, H., Markovič, O., Eklund, H. (2002) Crystal structure of plant pectin methylesterase. FEBS letters, 514: 243-249.

Kapoor, M., Beg, Q. K., Bhushan, B., Singh, K., Dadhich, K. S., Hoondal, G. S. (2001) Application of an alkaline and thermostable polygalacturonase from *Bacillus sp.*

MG-cp-2 in degumming of ramie (*Boehmeria nivea*) and sunn hemp (*Crotalaria juncea*) bast fibres. Process Biochemistry, 36: 803-807.

Kars, I., McCalman, M. E. L. Y. S. I. A., Wagemakers, L., van Kan, J. A. (2005) Functional analysis of *Botrytis cinerea* pectin methylesterase genes by PCR-based targeted mutagenesis: *Bc*pme1 and *Bc*pme2 are dispensable for virulence of strain B05.10. Molecular Plant Pathology, 6: 641-652.

Kashyap, D. R., Vohra, P. K., Chopra, S., Tewari, R. (2001) Applications of pectinases in the commercial sector: A review. Bioresource Technology, 77: 215–227.

Kent, L. M., Loo, T. S., Melton, L. D., Mercadante, D., Williams, M. A., Jameson, G. B. (2016) Structure and properties of a non-processive, salt-requiring, and acidophilic pectin methylesterase from *Aspergillus niger* provide insights into the key determinants of processivity control. Journal of Biological Chemistry, 291: 1289-1306.

Kertesz, Z. I. (1955) [18] Pectic enzymes. In: Colowick SP, Kaplan NO (eds) Methods in Enzymology, Academic Press, New York, 1: 158–166.

Klavons, J. A., Bennett, R. D. (1986) Determination of methanol using alcohol oxidase and its application to methyl ester content of pectins. Journal of Agricultural and Food Chemistry, 34: 597-599.

Kohli, P., Gupta, R. (2015) Alkaline pectinases: a review. Biocatalysis and Agricultural Biotechnology, 4: 279-285.

Koukiekolo, R., Cho, H. Y., Kosugi, A. (2005) Degradation of corn fibre by *Clostridium cellulovorans* cellulases and hemicellulases and contribution of scaffolding protein CbpA. Applied and Environmental Microbiology, 71: 3504-3511.

Ladjama, A., Taibi, Z., Meddour, A. (2007) Production of pectinolytic enzymes using *Streptomyces* strains isolated from palm grove soil in Biskra area (Algeria). In African Crop Science Conference Proceedings, 8: 1155-1158.

Lamed, R., Setter, E., Bayer, E. A. (1983) Characterization of a *cellulose*-binding, cellulase-containing complex in *Clostridium thermocellum*. Journal of Bacteriology, 156: 828-836.

Laurent, F., Kotoujansky, A., & Bertheau, Y. (2000) Overproduction in *Escherichia coli* of the pectin methylesterase A from *Erwinia chrysanthemi* 3937: one-step purification, biochemical characterization, and production of polyclonal antibodies. Canadian Journal of Microbiology, 46: 474-780.

Liao, C. H., Gaffney, T. D., Bradley, S. P., Wong, L. J. C. (1996) Cloning of a pectate lyase gene from *Xanthomonas campestris pv. malvacearum* and comparison of its sequence relationship with pel genes of soft-rot Erwinia and *Pseudomonas*. MPMI-Molecular Plant Microbe Interactions, 9: 14-21.

McFeeters, R. F., Armstrong S. A. (1984) Measurement of pectin methylation in plant cell walls. Analytical Biochemistry, 139: 212-217.

McMillan, G. P., Johnston, D. J., Perombelon, M. C. M. (1992) Purification to homogeneity of extracellular polygalacturonase and isoenzymes of pectate lyase of *Erwinia carotovora subsp. atroseptica* by column chromatography. Journal of Applied Bacteriology, 73: 83-86.

Mercadante, D., Melton, L. D., Jameson, G. B., Williams, M. A. (2014) Processive pectin methylesterases: the role of electrostatic potential, breathing motions and bond cleavage in the rectification of Brownian motions. PLoS One, 9(2).

Micheli, F. (2001) Pectin methylesterases: cell wall enzymes with important roles in plant physiology. Trends in Plant Science, 6: 414-419.

Pelloux, J., Rustérucci, C., Mellerowicz, E. J. (2007) New insights into pectin methylesterase structure and function. Trends in Plant Science, 12: 267-277.

Remoroza, C., Wagenknecht, M., Buchholt, H. C., Moerschbacher, B. M., Gruppen, H., & Schols, H. A. (2015) Mode of action of *Bacillus licheniformis* pectin methylesterase on highly methyl-esterified and acetylated pectins. Carbohydrate Polymers, 115: 540–550.

Salas-Tovar, J. A., Flores-Gallegos, A. C., Contreras-Esquivel, J. C., Escobedo-García, S., Morlett-Chávez, J. A., Rodríguez-Herrera, R. (2017) Analytical methods for pectin methylesterase activity determination: A review. Food Analytical Methods, 10: 3634-3646.

Schell, M. A., Denny, T. P., Huang, J. (1994) Extracellular virulence factors of *Pseudomonas solanacearum*: role in disease and regulation of expression. In Molecular Mechanisms of Bacterial Virulence. Springer, Dordrecht. 311-324.

Studier, F. W. (2005) Protein production by auto-induction in high-density shaking cultures. Protein Expression and Purification, 41: 207-234.

Sultan, A. M., Amid, A., Hamzah, M. (2012) Molecular dynamics study of the effect of calcium ions on the thermostability of *Bacillus amyloliquefaciens* phytase. Australian Journal of Basic and Applied Sciences, 6:109–116.

Teller, D. C., Behnke, C. A., Pappan, K., Shen, Z., Reese, J. C., Reeck, G. R., & Stenkamp, R. E. (2014) The structure of rice weevil pectin methylesterase. Acta

Crystallographica Section F: Structural Biology Communications, 70: 1480-1484.

Tripathi, N. K., Shrivastva, A., Biswal, K. C., & Rao, P. L. (2009) Methods: Optimization of culture medium for production of recombinant dengue protein in Escherichia coli. Industrial Biotechnology, 5: 179-183.

Wolf, S., Mouille, G., Pelloux, J. (2009) Homogalacturonan methyl-esterification and plant development. Molecular Plant. 2: 851-860.

Wood, P., Siddiqui, I. R. (1971) Determination of methanol and its application to measurement of pectin ester content and pectin methyl esterase activity. Analytical Biochemistry, 39: 418-428.

Wu, H. C., Hsu, S. F., Luo, D. L., Chen, S. J., Huang, W. D., Lur, H. S., Jinn, T. L. (2010) Recovery of heat shock-triggered released apoplastic Ca^{2+} accompanied by pectin methylesterase activity is required for thermotolerance in soybean seedlings. Journal of Experimental Botany, 61:2843–2852.

Zhang, C., Yao, J., Zhou, C., Mao, L., Zhang, G., Ma, Y. (2013) The alkaline pectate lyase PEL168 of *Bacillus subtilis* heterologously expressed in *Pichia pastorisis* more stable and efficient for degumming ramie fiber. BMC biotechnology, 13: 26.

Chapter 4

SAXS and homology modelling based structure analysis of pectin methylesterase from *Clostridium thermocellum* ATCC 27405

4.1 Introduction

Plant cell walls are the forefronts of defense system against bacterial and fungal pathogens. They mainly comprise cellulose, hemicellulose and pectin (Lebeda *et al*., 2001). Phytopathogenic and saprophytic microorganisms produce a group of polysaccharide-degrading enzymes to penetrate plant cell wall and obtain access to nutrients (Lebeda *et al*., 2001). The cellulose/hemicellulose network enclosed in a jel-like matrix of pectin. The cellulases and hemicellulases of invading microbes can carry out the hydrolysis of cellulose and hemicellulose only after the pectin-degrading enzymes have disrupted the plant cell wall (Lagaert *et al*., 2009). Pectinases such as pectin methylesterases (PME), polygalacturonases (PG) and pectate lyases (PL) are involved in degradation of pectin polymer. Pectin is a polymer of α-D-galacturonic acid (α-D-Gal*p*A) residues. The α-D- Gal*p*A residues may be methyl esterified, the extent of which varies based on the source (Herron *et al*., 2000). PME (EC 3.1.1.11) catalyses the de-esterification of homogalacturonan chain of pectin, resulting in de-esterified homogalacturonan, which is now susceptible to the depolymerization by PG and PL (Kashyap *et al*., 2001). PME influences the porosity and mechanical properties of the

plant cell wall by the accumulation of polygalacturonan chain into calcium-linked gels through demethylation (Willats *et al*., 2001). PMEs produced by plants are involved in physiological processes, such as microsporogenesis (Tieman and Handa, 1994), seed germination, pollen growth (Wen *et al*., 1999), root development (Micheli *et al*., 2000), polarity of leaf growth (Pilling et al., 2000), stem elongation (Micheli, 2001), loss of tissue integrity and fruit ripening (Pilling *et al*., 2004). PMEs defend the plant from fungal infections (Wiethölter *et al*., 2003). Tobacco Mosaic Virus employ PMEs for its systemic spread in plants (Dorokhov *et al*., 1999; Chen *et al*., 2000; Chen and Citovsky, 2000). Symbiotic (Lievens *et al*., 2002) as well as pathogenic microorganisms also express PMEs at the time of invading plants (De Lorenzo *et al*., 1997; Jiang *et al*., 2014).

The amino acid sequence of PMEs from prokaryotes and eukaryotes share the regions with sequence similarity. Till date, 3-dimensional structure of PMEs of three bacterial i.e. *Erwinia chrysanthemi* (renamed as *Dickeya dadantii*) (PDB ID: 1QJV_A) (Jenkins *et al*., 2001), *Yersinia enterocolitica* (PDB ID: 3UW0_A) (Boraston and Abbott, 2012) and *Dickeya dadantii* (PDB ID: 2NTB_A) (Fries *et al*., 2007) and two of plants, *Daucus carota* (PDB ID: 1GQ8_A) (Johansson *et al*., 2002) and *Solanum lycopersicum* (PDB ID: 1XG2_A) (Di Matteo *et al*., 2005) have been determined. The sequence of PME from *Erwinia chrysanthemi* shows variation from most of the other PME sequences such as PMEs from *Ralstonia solanacearum* (Tans-Kersten *et al*., 1998) and *Aspergillus tubingensis* (Khanh *et al*., 1991) as also reported earlier (Jenkins *et al*., 2001). The crystal structure of PME from *Erwinia chrysanthemi* conveyed a β-helix structure similar to that found in other pectinolytic enzymes such as pectate lyase from *Erwinia chrysanthemi* (Lietzke *et al*., 1996) and *Bacillus subtilis* (Pickersgill *et al*., 1994) and polygalacturonase from *Erwinia carotovora* (Pickersgill *et al*., 1998).

Clostridium thermocellum is an anaerobic, thermophilic and plant carbohydrate degrading bacterium. It produces a unique multi-enzyme complex known as cellulosome that can expedite plant cell wall degradation (Bayer *et al*., 1983). In the cellulosomes with the cohesin-dockerin interaction organizes a variety of enzymes into one complex (Lamed et al., 1983). Often these enzymes are associated with carbohydrate binding modules (CBMs) which help in degradation of crystalline substrates (Bayer *et al*., 2008). In the Carbohydrate-Active Enzymes database (CAZy; http://www.cazy.org) enzymes that synthesize, modify and cleave oligo/polysaccharides have been classified into sequence based families (Lombard *et al*., 2014). In the CAZy database Pectate lyases (PL, EC 4.2.2.2) have been categorized under polysaccharide lyase (PL) family 1 (PL1) and 9 (PL9) (Chakraborty *et al*., 2015) and Pectin methylesterases have been categorized under carbohydrate esterase (CE) family 8 (CE8) (Lombard *et al*., 2014). Recently biochemical characterization of cellulosomal pectate lyase, *Ct*PL1B and pectin methylesterase, *Ct*PME (Uniport ID: A3DJL8; locus tag: Cthe_2949) from *Clostridium thermocellum* was reported (Chakraborty *et al*., 2015; Rajulapati and Goyal, 2017). *Ct*PME is a modular enzyme containing N-terminal signal peptide, followed by a catalytic module belonging to family 8 Carbohydrate Esterase and a Dockerin at C-terminal (Rajulapati and Goyal, 2017). In the present study, the three dimensional (3D) modelled structure of *Ct*PME from *Clostridium thermocellum* was determined by homology modelling. Molecular dynamic simulation and docking of ligand was performed to ascertain the catalytic center and residues involved. The validation of secondary structure was done by CD analysis. The structure of *Ct*PME in aqueous solution was analysed by SAXS (Small Angle X-ray Scattering).

4.2 Materials and Methods

4.2.1 Amino acid sequence analysis of *Ct*PME

The amino acid sequence (300 amino acids) of *Ct*PME belonging to family 8 carbohydrate esterases (CE8), was retrieved from NCBI database, with a GenBank accession number ABN54147.1 and UniProt ID: A3DJL8. Search for putative domains in the *Ct*PME sequence was done using BLASTp against the PDB database (Altschul *et al*., 1997). The query sequence *Ct*PME was aligned with the known sequences and the presence of conserved and semi conserved residues was evaluated (Sievers and Higgins2014). The sequences were aligned by using the Clustal Omega tool (Sievers *et al*., 2011) available on EMBL-EBI services (http://www.ebi.ac.uk/Tools/msa/clustalo/) (Li et al., 2015). The alignment file was analysed for conserved and semi conserved residues by ESPript 3.0 (Robert and Gouet, 2014).

4.2.2 Secondary structure analysis of *Ct*PME

The secondary structure of *Ct*PME was determined by using PsiPred server (http://bioinf.cs.ucl.ac.uk/psipred/) and topology plot was created by using PDBSum (http://www.ebi.ac.uk/thornton-srv/databases/pdbsum/Generate.html) analysis software.

4.2.2.1 Secondary structure determination of *Ct*PME by Circular Dichroism

The recombinant *Ct*PME, cloned, expressed and characterized earlier as described in chapter 2 was used in the present study (Rajulapati and Goyal, 2017). The secondary structure of *Ct*PME was determined by Circular Dichroism (CD) analysis. The protein (25 µM) in 50 mM Tris-HCl buffer, pH 8.0 was used. The far-UV CD spectrum was recorded on spectropolarimeter (JASCO J-1500, Jasco Corporation, Tokyo), equipped with a peltier system for temperature control at 25°C and quartz

cuvette of path length 0.1 cm. The CD spectrum was measured in the far UV region (190-250 nm) at a scanning rate of 50 nm/min and 1 nm bandwidth with an average of six scans. The molar residual ellipticity (mre deg cm^2dmol^{-1}) was quantified from the ellipticity (θ) values for specified range of the wavelength (Kelly *et al*., 2005). The CD spectrum was normalized for buffer contributions and the secondary structure was predicted using K2D3 server (Perez-Iratxeta and Andrade-Navarro, 2008). The mre values were uploaded to the K2D3 server (http://k2d3.ogic.ca/) to estimate the percentage of different secondary structures present in *Ct*PME. CD data was compared with predicted secondary structure data to confirm the result.

4.2.3 Homology modelling of *Ct*PME

The three dimensional structure of *Ct*PME was built by using Modeller 9.18 (http://salilab.org/modeller/). The comparative protein structure modelling was carried out based on closely related protein structures complying the spatial restraints (Sali and Blundell, 1993; Webb and Sali, 2017). Multiple template approach was followed, where the query template of *Ct*PME was modelled based on other closely related PMEs. BLAST analysis showed that amino acid sequence of PMEs from *Erwinia chrysanthemi* (1QJV), *Yersinia enterocolitica* (3UW0), *Aspergillus niger* (5C1C), *Solanum lycopersicum* (1XG2), *Daucus carota* (1GQ8) and *Sitophilus oryzae* (4PMH) are closely related to *Ct*PME. The 3D model of *Ct*PME was generated after 100 GA (Genetic Algorithm) runs. The best modelled structure was chosen by assessing the least global DOPE (discrete optimized protein energy) assessment score of the models (Shen and Sali, 2006). The modelled *Ct*PME was also analyzed secondary structure by using 2Struc server (http://2struc.cryst.bbk.ac.uk/twostruc).

4.2.4 Refinement and quality assessment of modelled *Ct*PME structure

The best modelled structure with least DOPE assessment score was energy minimized on energy minimization server, YASARA (http://www.yasara.org/ minimizationserver.html). On this server, an extensive statistical analysis of protein structure is done based on the common structural feature and 3D coordinates with thousands of known structures present in PDB. Hence, the resulting energy function is known as knowledge based potential and has been incorporated into two new force fields (Krieger *et al*., 2009). The final energy minimized structure of *Ct*PME was assessed by structural analysis and verification server (SAVES) on the MBI-UCLA servers, USA (http://services.mbi.ucla. edu/SAVES/).

4.2.5 Molecular Dynamic simulation of *Ct*PME modelled structure

The molecular dynamic (MD) simulation was performed by using GROMACS v4.6.5 software (Berendsen *et al*., 1995). The *Ct*PME energy-minimized model structure was placed in a specified cubic box of single point charge (SPC) with water molecules. The cubic box of dimension was 9.122x7.527x10.477 nm and volume was 719.36 nm^3. The MD simulation was performed in presence of 22,043 solvent (water) molecules. These molecules occupied 719.364 nm^3 volume and 999.976 g/l density. No counter ions were added during the simulation. MD simulation was performed till 20 ns and the time points were taken at intervals of 0.1 ns. The initial equilibration of whole system in NVT ensemble (constant number of particles, volume and temperature) was carried out for 500 ps by restraining. The system was again equilibrated for 500 ps by NPT ensemble (constant number of particles, pressure and temperature) twice, once with restraints and then without restraints. The production run was performed for 20 ns with NPT ensemble adopting a 2 fs integration time. The linear constraint solver

(LINCS) algorithm (Hess *et al*., 1997) was used to constrain the bonds associated with hydrogen atoms and radius of gyration. The variation in the *Ct*PME backbone (root mean square deviation, RMSD) was estimated by the least square fitting method. During the MD production run, the modelled *Ct*PME structure was shown as a function of time, to ascertain its stability in the solvent system.

4.2.6 Active site analysis of *Ct*PME

The sequence of *Ct*PME was aligned with the sequence of other solved crystal structure PMEs of *Erwinia chrysanthemi* (PDB ID: 1QJV_A) (Jenkins et al., 2001), *Yersinia enterocolitica* (PDB ID: 3UW0_A) (Boraston and Abbott, 2012) and *Dickeya dadantii* (PDB ID: 2NTB_A) (Fries et al., 2007) from PDB. To find the active site of *Ct*PME, the structure of *Ct*PME was superposed with structure of its homologue of *Erwinia chrysanthemi* (PDB ID: 1QJV_A) (Jenkins *et al*., 2001) and the surface view was analysed by PyMol software (Schrodinger, 2016).

4.2.7 Ligand-binding annotation of *Ct*PME structure

The catalytic pocket and active site residues of *Ct*PME were determined by docking the MD simulated modelled structure with different ligands. Docking simulations were accomplished in AutoDock 4.2.1 (Morris *et al*., 2009), along with the viewer MGLTools 1.5.6 (http://mgltools.scripps.edu/). The ligands (D-galacturonic acid (GAL) and methyl D-galacturonic acid) for docking study were dowloaded from PubChem (http://www.ncbi.nlm.nih.gov) in 3D SDF format. The docking analysis was performed following the method as described earlier by Chakraborty *et al*. (2015). The grid box was arranged at the active site, the grid box parameters set to X, Y and Z coordinates were 76.0, 66.0 and 74.0 followed by grid center were fixed to 63.705, 20.816 and 46.245, respectively, with 0.375Å grid point spacing. 30 GA runs were used

to obtain 30 different docked conformations of ligands. The docked conformations were then ranked according to the binding free energy. The docked conformation of ligand with lowest binding energy was chosen to generate the protein-ligand complex. The conformation with minimal binding free energy was considered for further analysis. The resulting protein-ligand complex was visualized by PyMol and UCSF Chimera softwares. Ligplot analysis was done to analyse interactions between protein structure and ligand (Wallace et al., 1995; Laskowski and Swindells, 2011).

4.2.8. Small Angle X-ray Scattering Analysis (SAXS) of *Ct*PME

Scattering data for *Ct*PME were collected using home source small-angle X-ray scattering system (SAXSpace, Anton Paar GmbH, Graz, Austria). The X-ray scattering pattern of *Ct*PME was recorded with a one-dimensional CMOS Mythen detector (Dectris, Baden, Switzerland). The incident radiation wavelength was set to 1.5 Å. The distance between sample and detector was 317 mm. Line collimation system was used for incident X-rays on 40 µl sample containing *Ct*PME at 7.5, 10 and 15 mg/ml respectively, and matched buffer (50 mM Tris-HCl buffer, pH 8.5) filled in a thermos-stated quartz capillary of 1 mm diameter for two independent exposure of 30 min. SAXS datasets for sample and matched buffer were processed using SAXStreat and SAXSquant softwares. The data collected on line collimation system was desmeared to represent scattering arising from point collimation using the beam profile. Intensity of scattering, I(Q) was obtained as a function of Q, where Q was considered as $4\pi \sin\theta/\lambda$. where Q=scattering vector, λ= wavelength and 2θ= scattering angle, respectively. The scattering pattern of *Ct*PME was examined visually in Primus program of ATSAS 2.8 suite (Franke and Svergun, 2009) to confirm the integrity and non-aggregation of *Ct*PME. The radius of gyration (R_g) was estimated using Guinier's equation (Guiner *et*

al., 1955) as well as inverse Fourier transform method as implemented in the Primus package. The distance distribution function P(r), maximum particle diameter (D_{max}) of *Ct*PME were computed using GNOM (Semenyuk and Svergun, 1991). The estimation of molecular weight for *Ct*PME was done by SAXSMoW program (Fischer *et al*., 2010). The *ab initio* method was used for the low-resolution reconstruction shape of *Ct*PME using momentum transfer range from 0.016 nm^{-1} to 0.36 nm^{-1} of the scattering curve by using DAMMIF program (Volkov and Svergun, 2003). The 20 independent Dummy Residue Model (DRM) runs of *Ct*PME reconstructed by DAMMIF. These 20 independent solutions were subsequently averaged, clustered and refined by DAMAVER (Svergun, 1999) and DAMMIN (Louis-Jeune *et al*., 2012) to create the final *abinitio* shape. The resolution of modelled structure was determined by SASRES program (Tuukkanen *et al*., 2016). The fitting of DAMMIF generated model and homology modelled structure of *Ct*PME were evaluated against the experimental SAXS data by the CRYSOL program (Svergun et al., 1995). The homology modelled structure of *Ct*PME was superposed on the DRM using PyMOL.

Results and Discussion

4.3.1 Sequence analysis of *Ct*PME

BLAST result revealed that the *Ct*PME protein with GenBank Accession No. ABN54147.1. The amino acid sequence of *Ct*PME (UniProt ID: A3DJL8), from *Clostridium thermocellum* showed similarity with the bacterial PMEs of *Erwinia chrysanthemi*, *Yersinia enterocolitica*, fungal PME of *Aspergillus niger* and plant PMEs from *Solanum lycopersicum* and *Daucus carota* and insect PME of *Sitophilus oryzae* (Table 4.1). *Ct*PME showed maximum sequence identity (38%) with PME of *Erwinia chrysanthemi* (*Ec*PME). The multiple sequence alignment (MSA) was performed using Clustal Omega and ESPript 3 softwares. The results showed conserved, semi-conserved and dispersive amino acids residues. The conserved residues were showed with red colour background and semi-conserved residues highlighted with red colour (Fig. 4.1). MSA of *Ct*PME showed the 6 α-helix (3α + 3η), 26 β-sheets and 11 turns (TT). The alignment showed that Gln142, Val144, Ala145, Gln164, Asp165, Leu167, Tyr168, Gly183, Asp186, Phe189, Leu240, Gly241, Arg242 and Trp244 are some of conserved amino acids. The conserved residues Asp165, Asp186 and Arg242 are catalytic residues represented by star (Fig. 4.1).

Table 4.1 BLAST analysis of *Ct*PME amino acid sequence showing identity with its homologues.

PDB ID	Organism	Identity (%)	Query Cover (%)	E-value	Total Score	Resolution (A˚)
1QJV_A	*Erwinia chrysanthemi*	38%	93%	3e-60	196	2.37
1XG2_A	*Solanum lycopersicum*	36%	95%	5e-45	155	1.90
3UW0_A	*Yersinia enterocolitica*	36%	89%	2e-53	179	3.50
1GQ8_A	*Daucus carota*	35%	96%	4e-41	145	1.75
5C1C_A	*Aspergillus niger*	34%	95%	2e-32	122	1.80
4PMH_A	*Sitophilus oryzae*	31%	83%	5e-25	103	1.79

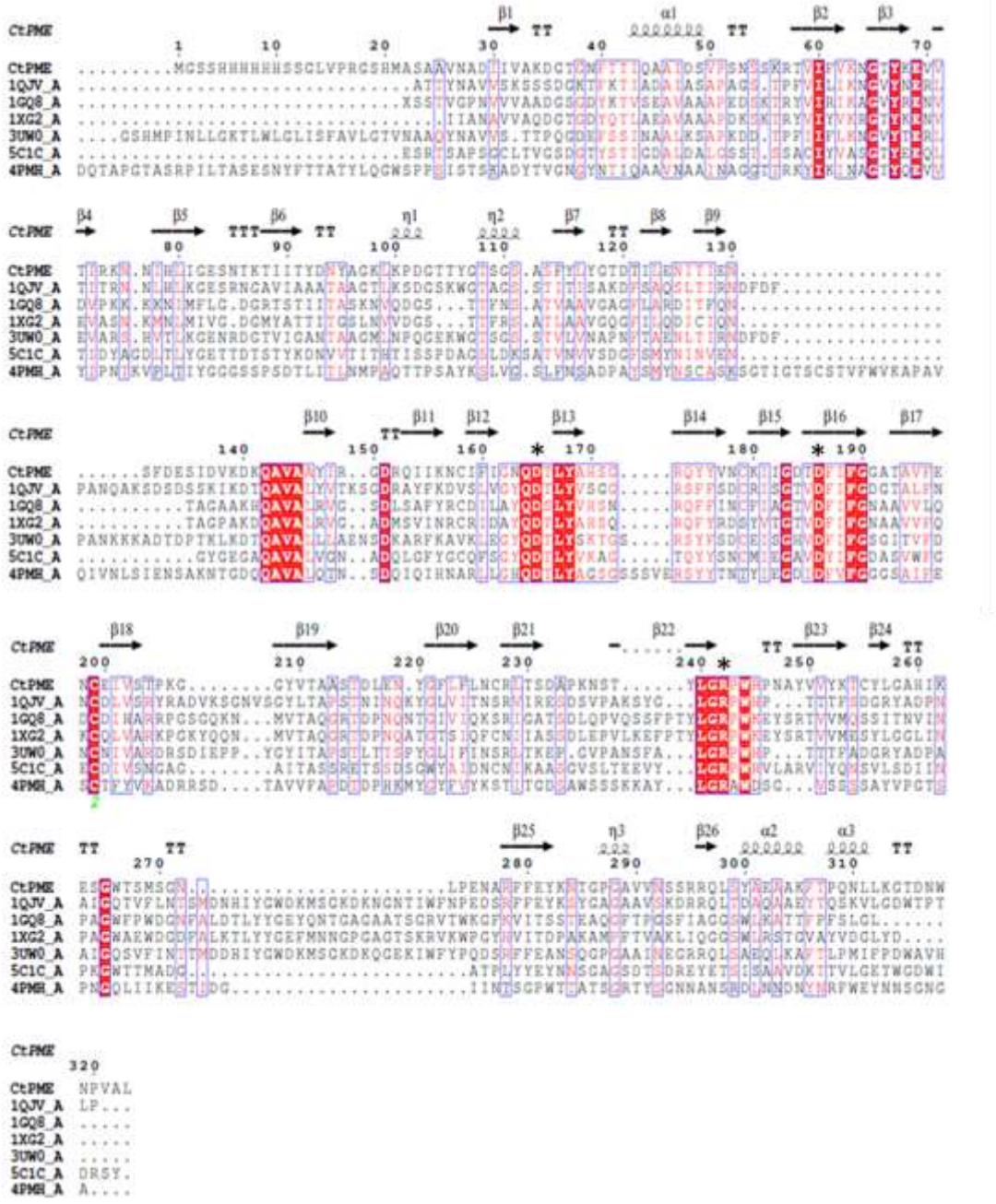

Fig. 4.1 Multiple Sequence Alignment (MSA) of *Ct*PME from *Clostridium thermocellum* showing the conserved (red background), semi-conserved (red colour letters) and dispersive amino acids (black colour letters). The secondary structure elements of *Ct*PME have been shown above the sequences. ('α'- alpha helix, 'β'- beta strand, 'T'-turn and 'η'- 3_{10} helix).

4.3.2 Secondary structure of *Ct*PME

The secondary structure of *Ct*PME predicted by the PsiPred revealed the presence of 5.0% α-helices, 33.3% β-strands and 61.7% random coils (Fig. 4.2A and Table 4.2). The β-strands present throughout the structure form the parallel β-sheets, which are quite common in the structures of PMEs and is evident from previous reports (Jenkins *et al*., 2001; Johansson *et al*., 2009). The 2Struc prediction server revealed that *Ct*PME contained 8.4% α-helices, 31.9% β-strands and 59.7% random coils and *Ec*PME contained 8.8% α-helices, 36.3% β-strands and 55.0% random coils (Table 4.2). The Circular Dichroism (CD) spectrum of *Ct*PME was analyzed by using the K2D3 server, where the data points were compared with the available secondary structures of known protein (Zheng *et al*., 2011). This revealed that *Ct*PME contained 3.1% α-helices, 40.1% β-strands and 56.9% random coils (Fig. 4.2B). All these results were more or less in agreement with each other for the secondary structure elements of *Ct*PME.

Table 4.2 Secondary structure analysis of *Ct*PME by 2Struc, PsiPred and CD.

Secondary structure element	***Ec*PME 2Struc (%)**	***Ct*PME 2Struc (%)**	***Ct*PME PsiPred (%)**	***Ct*PME CD Analysis (%)**
α- Helix	8.8	8.4	5.0	3.1
β- Sheet	36.3	31.9	33.3	40.1
Random Coil	55.0	59.8	61.7	56.9

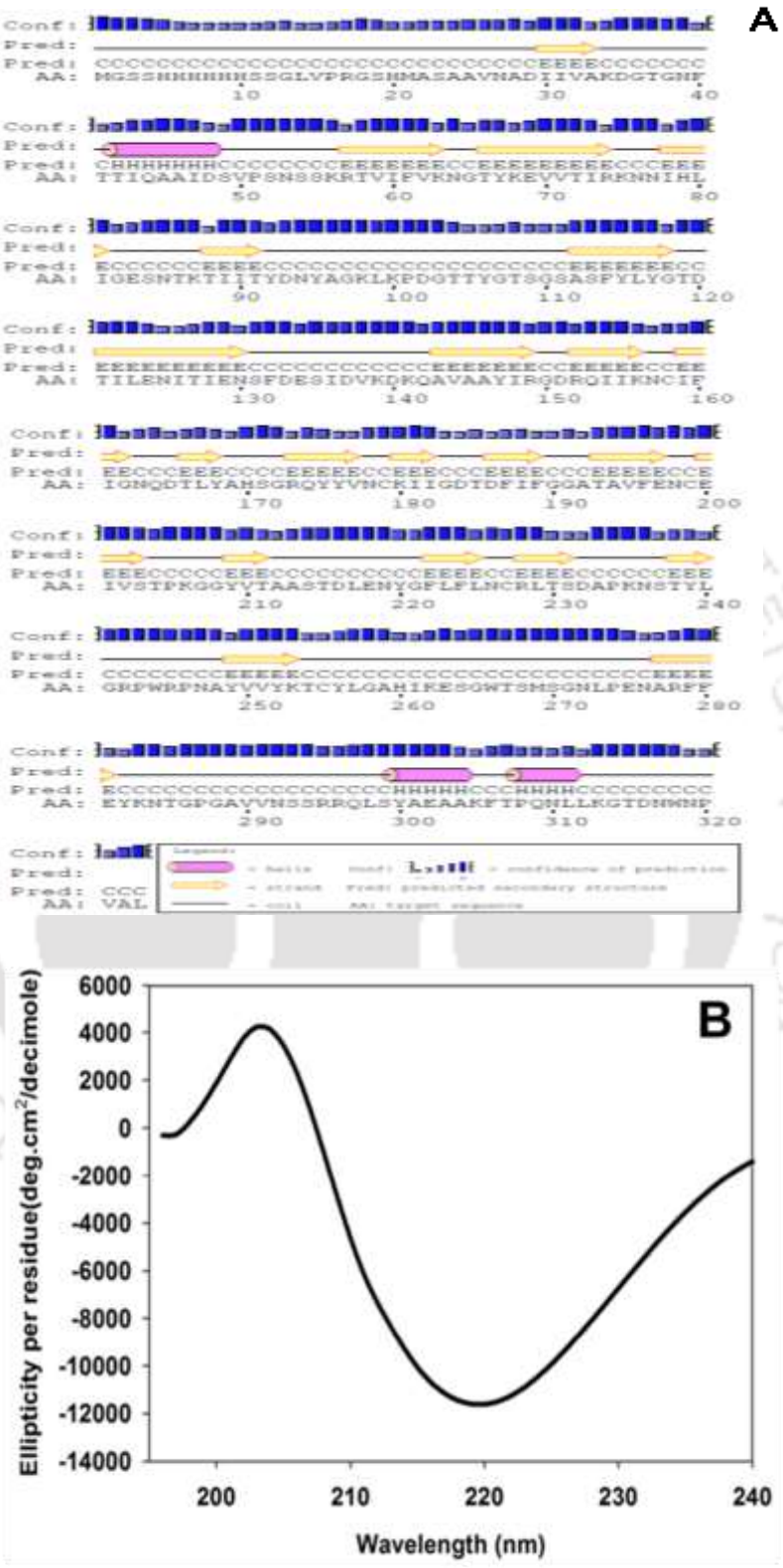

Fig. 4.2 Secondary structure analysis of *Ct*PME. A) PsiPred prediction showing the amino acid residues of α-helix, β-sheet and random coil, B) Far-UV Circular Dichroism (CD) spectrum analyzed by K2D3 software.

4.3.3 Homology modelling or 3D-structure of *Ct*PME

Multiple sequence alignment showed stretches of semi-conserved residues among the aligned sequences (Fig. 4.1). Some stretches of amino acid sequence of *Ct*PME were identical to one sequence while some stretches were identical to other sequence. Therefore, multiple sequences were used for modelling even though they had similar identity and coverage. Therefore, 3D crystal structure model of *Ec*PME structure chosen during modelling was used. The 3D modelled structure of *Ct*PME represented the conventional parallel β-helix structure (Fig. 4.3A). The basic structural domains are having the fold into a right-handed parallel β-sheet, whose sheets were arranged in parallel helical manner. Similar type of structure was found in most of the PMEs (Jenkins *et al*., 2001; Johansson *et al*., 2009). *Ct*PME modelled structure showed 29 amino acid residues long loop at N-terminal region followed by right-handed parallel β-helical structure. Each turn of β-helix consists of three β-sheets, PB1, PB2 and PB3. These β-sheets are connected by the loops i.e. PB1 is linked to PB2 via a loop T1, PB2 connected to PB3 through T2 and PB3 to PB1 by T3 (Fig. 4.3A). The N-terminal long loop continues with Ala24-Ala25-Val26 amino acids initial parallel β-sheet (β1). These parallel β-helices extend into a large loop and an α-helix (α6) towards the C-terminal with Val321-Ala322-Leu323. The modelled CtPME structure showed the right-handed parallel β-sheets were well modelled throughout structure. The modelled *Ct*PME structure is rich in strands and random coils (Fig. 4.3A) as found in other PMEs studied previously (Jenkins *et al*., 2001; Johansson *et al*., 2009).

4.3.4 Refinement and Quality assessment of modelled *Ct*PME

The quality of the modelled *Ct*PME structure after energy minimization was evaluated on the UCLA SAVES server (https://services.mbi.ucla.edu/SAVES/). The Ramachandran plot showed that 83.7% residues (236 amino acids) are in the most favorable region, 13.8% in additional allowed region (39 amino acids), 1.4% in the generously allowed region (4 amino acids) and only 1.1% in the disallowed region (3 amino acids) indicating that *Ct*PME has a stable conformation (Fig. 4.3B). Three amino acid residues, Tyr 95, Asp133 and Leu273 were in the disallowed region. In VERIFY 3D, the 1D-3D plot showed that 86.69% of amino acid present in modelled *Ct*PME have an overall score of more than 0.2 (Fig. 4.3C). PDBsum was used to develop the topology plot of *Ct*PME (Fig. 4.3D). ProSA results confirmed that the modelled *Ct*PME resided in the X-ray zone with Z-score of -6.96 (Fig. 4.3E). The local energy plot showed modelled structure quality as a function of amino acid sequence position. Positive value represented the error prone part of the structure at around 120-150 amino acid residues (Fig. 4.3F). The residues were coloured with blue and red corresponding to low-energy and high-energy, respectively (Fig. 4.3G). The refinement and quality assessment results were acceptable enough to support further studies on *Ct*PME.

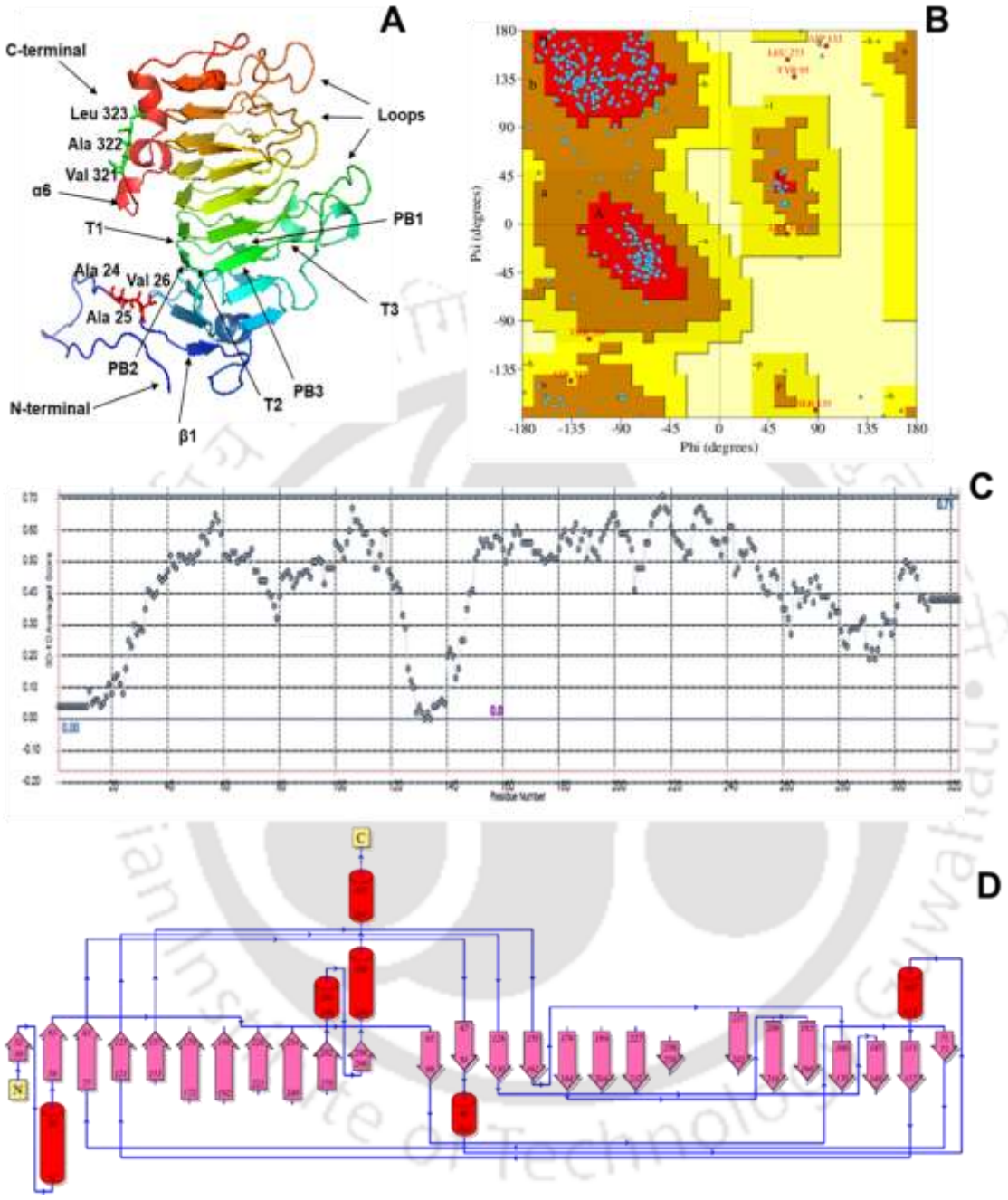

Fig. 4.3 Homology modelled 3D-structure of CtPME and its validation. A) 3D structure (rainbow colours) showing right handed parallel β-helix with N-terminal (blue colour) and C-terminal (red colour). The structure shows long loop start with Ala24, Ala25 and Val26 β1-sheet in N-terminal, α6- helix end with Val321, Ala322 and Val323 in C-terminal and parallel β-sheets (PB1, PB2 & PB3) with Turns (T1, T2 & T3), B) Ramachandran Plot (UCLA SAVES software) showing the most favorable, additional allowed and generously allowed regions of amino acid residues, C) VERIFY 3D showed the score was more than 0.2, D) Topology view of *Ct*PME showing the N and C-terminal region with α-helix, β-sheets and random coil.

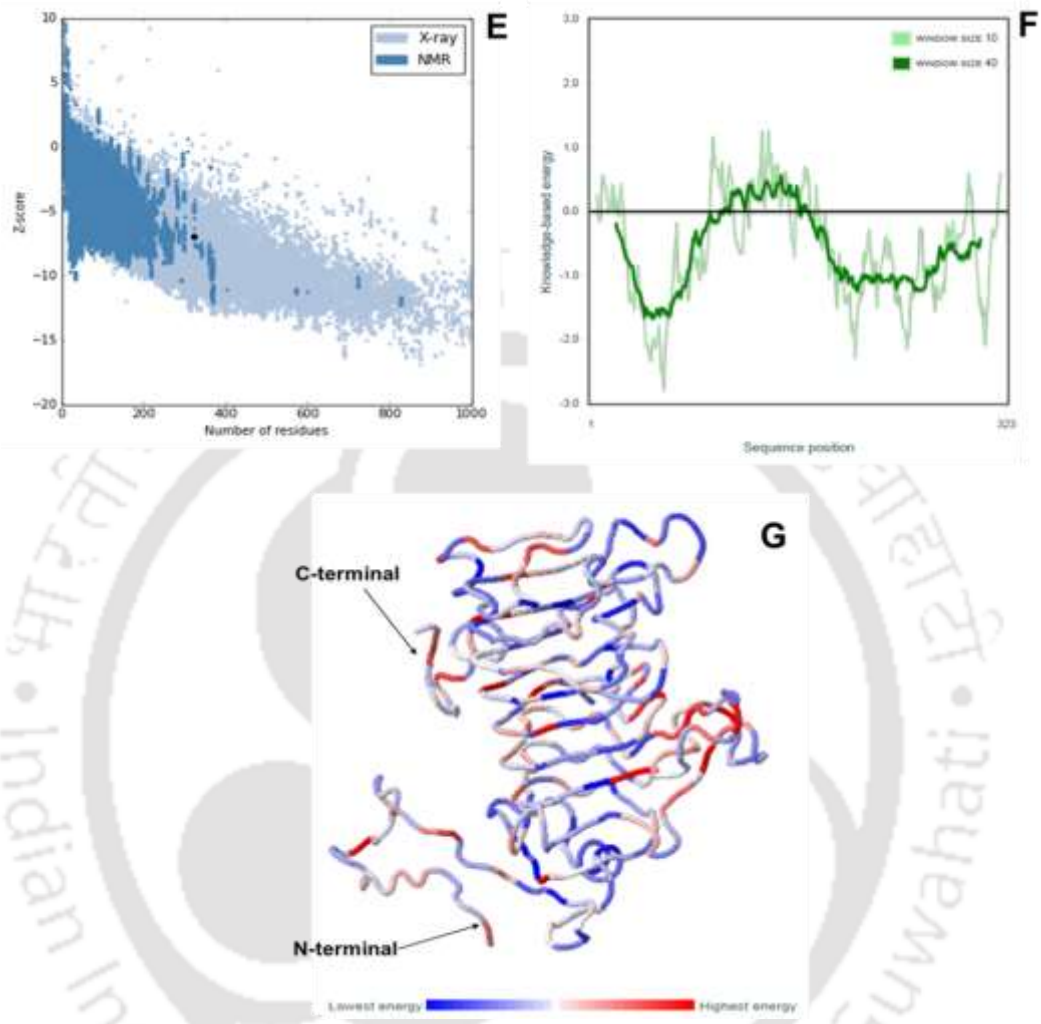

Fig. 4.3 Homology modelled 3D-structure of *Ct*PME and its validation. E) ProSA plot showed Z-score, -6.96 for overall model quality, F) ProSA amino acid residue score plot and G) ProSA local energy 3D structure.

4.3.5 Active site analysis of *Ct*PME

The active site residues of an enzyme play crucial role in the catalysis of substrate. Most of the lipases and esterases contain a catalytic center comprising Ser-His-Asp triad (Heikinheimo *et al*., 1999). The new active site residues, Asp-Asp-Arg triad from *Ec*PME crystal structure were reported (Jenkins *et al*., 2001). The 3D structure of *Ct*PME was superposed with that of *Ec*PME (Fig. 4.4A). The superposition of modelled structure showed that N-terminal β-sheet, α-helix of *Ct*PME aligned well with the N-terminal β-sheet and α-helix of *Ec*PME. Most of the right-handed parallel β-helices region of *Ct*PME superposed well with right-handed parallel β-helices of *Ec*PME. However, some loop regions (132-142 amino acids, 259-276 amino acids and 285-293 amino acids) of the *Ct*PME structure did not align with the *Ec*PME structure (Fig. 4.4A). Superposition of modelled *Ct*PME structure with input PDB structures (1QJV, 3UW0, 1XG2, 5C1C, 4PMH and 1GQ8) showed the RMSD values 0.903 Å, 0.860 Å, 0.774 Å, 0.728 Å, 0.674 Å and 0.600 Å respectively. This confirmed that right-handed parallel β-helix region of *Ct*PME is modelled well. The orientation of conserved active site residues of *Ct*PME were similar to those of *Ec*PME. The catalytic core site of *Ct*PME was analysed by comparing with the structure of *Ec*PME. The substrate-binding pocket of *Ct*PME was found at the same location as previously recognized in *Ec*PME. The superposed 3D-structures showed that the key residues, Asp165, Asp186 and Arg242 (in blue colour) of *Ct*PME (in cyan colour) perfectly aligned with the key residues Asp178, Asp199 & Arg267 (in orange colour) of *Ec*PME (in green colour) (Fig. 4.4B). The surface view of *Ct*PME showing a deep active site pocket (Fig. 4.4C), similar to *Ec*PME that contains the active site residues (Fig. 4.4D). The vacuum electrostatic view of *Ct*PME showed surface (multicolour) potential range from -57.897

to +57.897 J/C (Fig. 4.4E). Similarly, *Ec*PME showed vacuum electrostatic surface (multicolour) potential energy from -54.269 to +54.269 J/C (Fig. 4.4F).

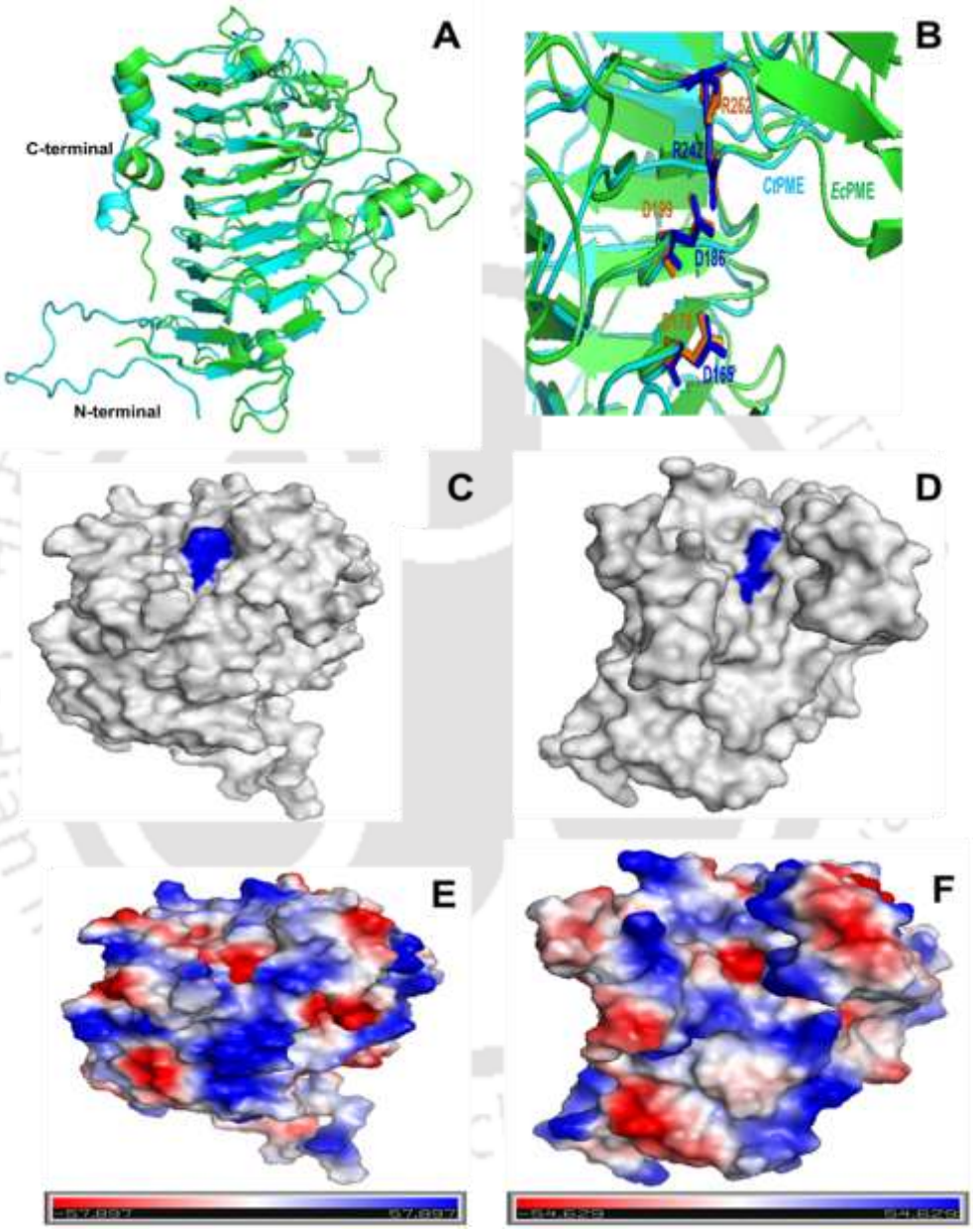

Fig. 4.4 Homology modelled structure of *Ct*PME and its superposition with *Ec*PME of *Erwinia chrysanthemi* (PDB: 1QJV). A) *Ct*PME structure (Cyan colour) superposition with *Ec*PME (Green colour), B) Superposition of active site residues (Indigo colour) of *Ct*PME (Cyan colour) with those (orange) of *Ec*PME (Green colour), C) Surface view of *Ct*PME with active site pocket (in blue) D) Surface view of *Ec*PME with active site pocket (in blue), E) Vacuum electrostatic view of *Ct*PME overall surface structure and F) Vacuum electrostatic view of *Ec*PME overall surface structure.

4.3.6 Molecular Dynamics simulation of *Ct*PME modelled structure

Molecular dynamics simulation of modelled *Ct*PME was performed to analyse the structural stability and compactness of the structure over a 20 ns duration. The MD simulation results showed that after 7 ns the fluctuation in RMSD value of *Ct*PME occurred and continued till 14 ns. After 15 ns the structure was completely stable. The overall deflection was 0.5 nm RMSD (Fig. 4.5A). The simulation showed that during the initial 3 ns, the number of intra molecular hydrogen bonds increased from 170 to 240 and after that the structure was stable. The intramolecular hydrogen bond number remained under 250 until 16 ns. The number of hydrogen bonds remained between 250 to 260 till the end of the run (Fig. 4.5B). The radius of gyration (R*g*) of *Ct*PME structure remained between 2.08 - 2.11 nm during first 13 ns and after that it decreased to 1.94 nm and stayed constant till end of the run (Fig. 4.5C). This suggested that the modelled *Ct*PME structure has a stable conformation. The input modelled structure (Green colour) and final modelled structure (Magenta colour) of *Ct*PME after MD simulation were superposed (Fig. 4.5D). The superposition of input and MD simulated structure showed that the loop regions of these structures slightly vary. These loop regions are the same regions, which did not superpose well over *Ec*PME structure (Fig. 4.4A and 4.5D). The RMSD difference between the energy minimized modelled structure of *Ct*PME and the final developed structure after MD simulation was only 1.202 Å. The MD simulation results showed that the modelled *Ct*PME structure was stable and could be used for further studies.

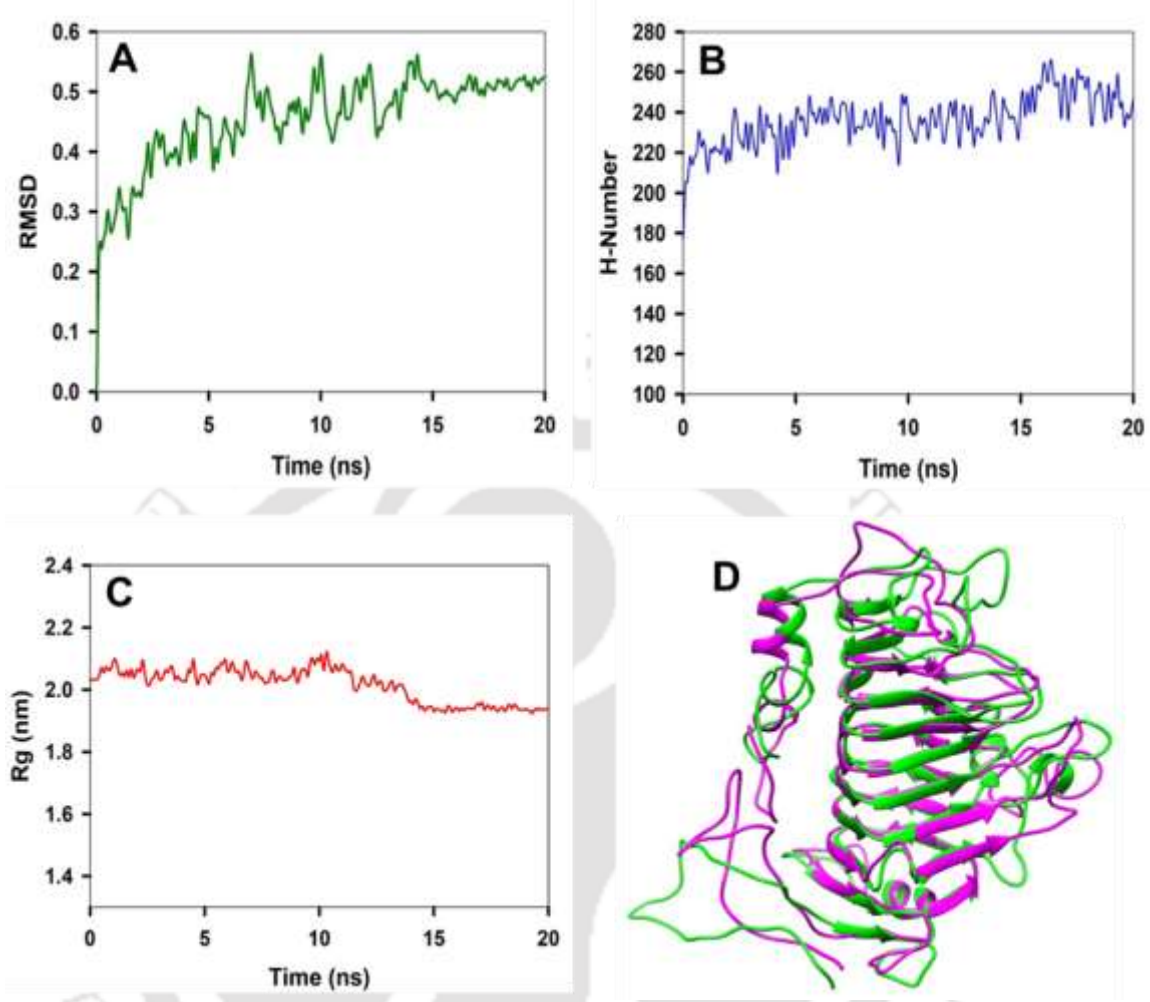

Fig. 4.5 MD simulation of modelled *Ct*PME showing A) RMSD plot, B) Intramolecular hydrogen bond plot, C) Radius of gyration plot and D) *Ct*PME input structure (Green colour) superposition with final MD simulation structure (Magenta colour) and with RMSD of 1.202 Å.

4.3.7 Docking study of *Ct*PME

The docking analysis showed that *Ct*PME had higher affinity (binding energy, -3.93 kcal/mol) for methylated D-galacturonic acid (mD-GalA) than D-galacturonic acid (binding energy, -1.18 kcal/mol) (Table 4.3). In the complex structure, mD-GalA was located within the catalytic cleft, similar binding groove was found in the structure of PME from *Erwinia chrysanthemi* (Jenkins *et al*., 2001). The protein ligand complex was visualized by the UCSF Chimera software. The *Ct*PME and the ligands D-GalA and mD-GalA showed the interaction of active site residues (Fig. 4.6A & 4.6B). The 2D depiction of interaction of ligands (D-GalA, mD-GalA) with protein was generated by LIGPLOT software and is shown in Fig. 4.6C & 4.6D. The docked complex showed that D-GalA made hydrophobic interaction with Ala212 and Trp244 residues of *Ct*PME (Fig. 4.6C). D-GalA made hydrogen bonds with Gln142, Asp165 and Asp186 of *Ct*PME. The residue, Ala212 showed hydrophobic interaction with the ligand mD-GalA (Fig. 4.6D). The residues involved in hydrogen bond interaction with mD-GalA were Gln142, Gln164, Asp165, Asp186 and Trp244 showing interaction with the oxygen atoms in and around methylated galacturonate moiety. These results showed that the affinity of *Ct*PME for mD-GalA is stronger than for D-GalA.

Table 4.3 Active site residues of *Ct*PME showing interaction with ligands.

Ligand	Binding Energy (ΔG) (kcal/mol)	Hydrophobic interaction	Residues present within 3.3Å of active site
D-Galacturonic acid (D-GalA)	-1.18	Ala212, Trp244	Gln142, Asp165, Asp186
methylated D-Galacturonic acid (mD-GalA)	-3.93	Ala212	Gln142, Gln164, Asp165, Asp186, Trp244

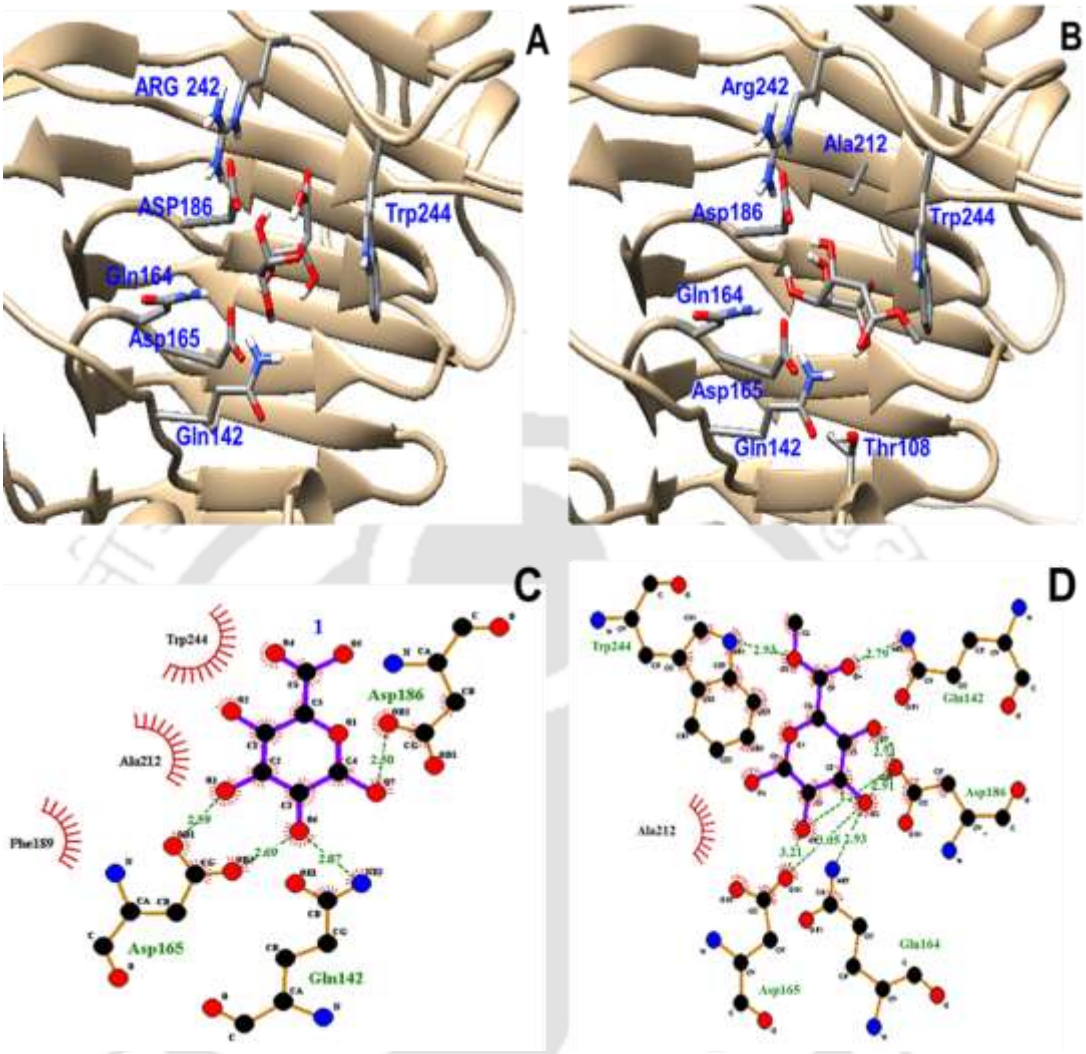

Fig. 4.6 Active site of modelled 3D-structure of *Ct*PME showing the active site cleft with docked ligands. A) Active site showing D-GalA ligand orientation, B) Active site showing mD-GalA ligand orientation, generated by UCSF Chimera, C) 2D schematic presentation of D-GalA interaction with active site residues and D) 2D schematic presentation of mD-GalA orientation at active site residues. Dashed lines show the hydrogen bonds with bond length and the residues displayed in arc with spokes are making hydrophobic interaction. Have been shown as green spheres.

4.3.8 Solution structure of *Ct*PME by Small Angle X-ray Scattering

The solution conformation of *Ct*PME was studied by SAXS data analysis. The initial processing and visual inspection of *Ct*PME scattering pattern at different concentrations confirmed the absence of aggregation and inter particle correlation effect. The scattering pattern of *Ct*PME (Fig. 4.7A) showed a good linear fit at a small q2 region in the Guinier plot and the radius of gyration (R_g) was found to be 2.28±0.11 nm. This indicated the shape of *Ct*PME in the solution to be predominantly globular (Fig. 4.7B). Alternatively, Guinier approximation of rod shaped showed the R_c value of 0.74±0.04 nm. The overall length of *Ct*PME was approximately, 7.47 nm, which shows the low q region of scattering intensity following the Guinier law. The estimation of molecular weight from the Guinier approximation and porod volume for *Ct*PME was calculated, which clearly corroborates with theoretical molecular mass of the monomeric *Ct*PME, 35.2 kDa (Table 4.4). The analysis of Kratky plot of *Ct*PME exhibits the bell shaped peak at low q value and intersect to the high q value, indicates that the *Ct*PME have compact and fully folded conformation in solution (Fig. 4.7C). *Ct*PME showed the maximum diameter of 9.40 nm with an asymmetric bell shaped curve evaluated by using the pair-wise distribution function [*P*(r)] (Fig. 4.7D). The structural parameters obtained by SAXS data processing and analysis are summarized in Table 4.4. The *ab initio* derived Dummy Atom Model (DAM) of *Ct*PME was generated by DAMMIF package without symmetry constraint (Fig. 4.7E). The *Ct*PME model is compact and clearly revealed a single catalytic domain containing hexa-histidine tag at N-terminal with a resolution of 2.6± 0.2 nm. The *ab initio* derived DAM of *Ct*PME showed an excellent fit with the *Ct*PME modelled structure (Fig. 4.7F). The chi^2 values obtained from crysol fitting of the experimental data with the modelled

structure and the *ab initio* constructed structure were 0.021 and 0.071, respectively (Fig. 4.7G). This showed that the homology modelled structure and *ab initio* modelled structure of *Ct*PME matched well with the experimentally collected data. The SAXS based modelling studies of *Ct*PME concluded that the structure has a compact, globular and golf club like model.

Table 4.4 SAXS data collection parameter and derived parameters of *Ct*PME.

Data-collection parameters	***Ct*PME 7.5 mg/ml**	***Ct*PME 10 mg/ml**	***Ct*PME 15 mg/ml**
Instrument	SAXSpace Anton-Paar	SAXSpace Anton-Paar	SAXSpace Anton-Paar
Wavelength (Å)	1.5 Å	1.5 Å	1.5 Å
Q range (nm^{-1})	0.14-0.79	0.14-0.78	0.14-0.79
Exposure time (minutes)	30x2	30x2	30x2
Protein concentration (mg/ml)	7.5	10	15
Temperature (°C)	10	10	10
Structural parameter			
Q range (nm^{-1}) used for analysis	0.17-3.55	0.199-3.56	0.17-3.54
I(0) au from Guinier	110512±3193	113528±3945	114523±2913
Rg nm from Guinier	2.27±0.13	2.25±0.14	2.28±0.11
I(0) au from P(r)	109600±3782	114100±5006	117500
Rg nm from P(r)	2.32±0.18	2.29±.25	2.30±0.17
D_{max} (nm)	9.30	9.35	9.40
Porod volume estimate (nm^3)	55.1	54.8	54.9
Molecular Mass (MM) determination			
I(0) au Lysozyme (14.3 kDa)	43660±924		
MM calculated from I(0) (kDa)	35.4	36.4	36.7
MM calculated from P(r) (kDa) (Porod volume/1.6)	34.4	34.1	34.3
Theoretical mass MM (kDa)	35.2	35.2	35.2
Software employed			
Data processing	Primus	Primus	Primus
P(r) function calculation	GNOM	GNOM	GNOM
Ab initio modelling	DAMMIF	DAMMIF	DAMMIF
Validation and averaging	DAMAVER	DAMAVER	DAMAVER
3-D graphical representation	PyMOL	PyMOL	PyMOL
Modelling parameters			
χ^2	0.012	0.021	0.018
NSD	0.56±0.03	0.58±0.04	0.62±0.03

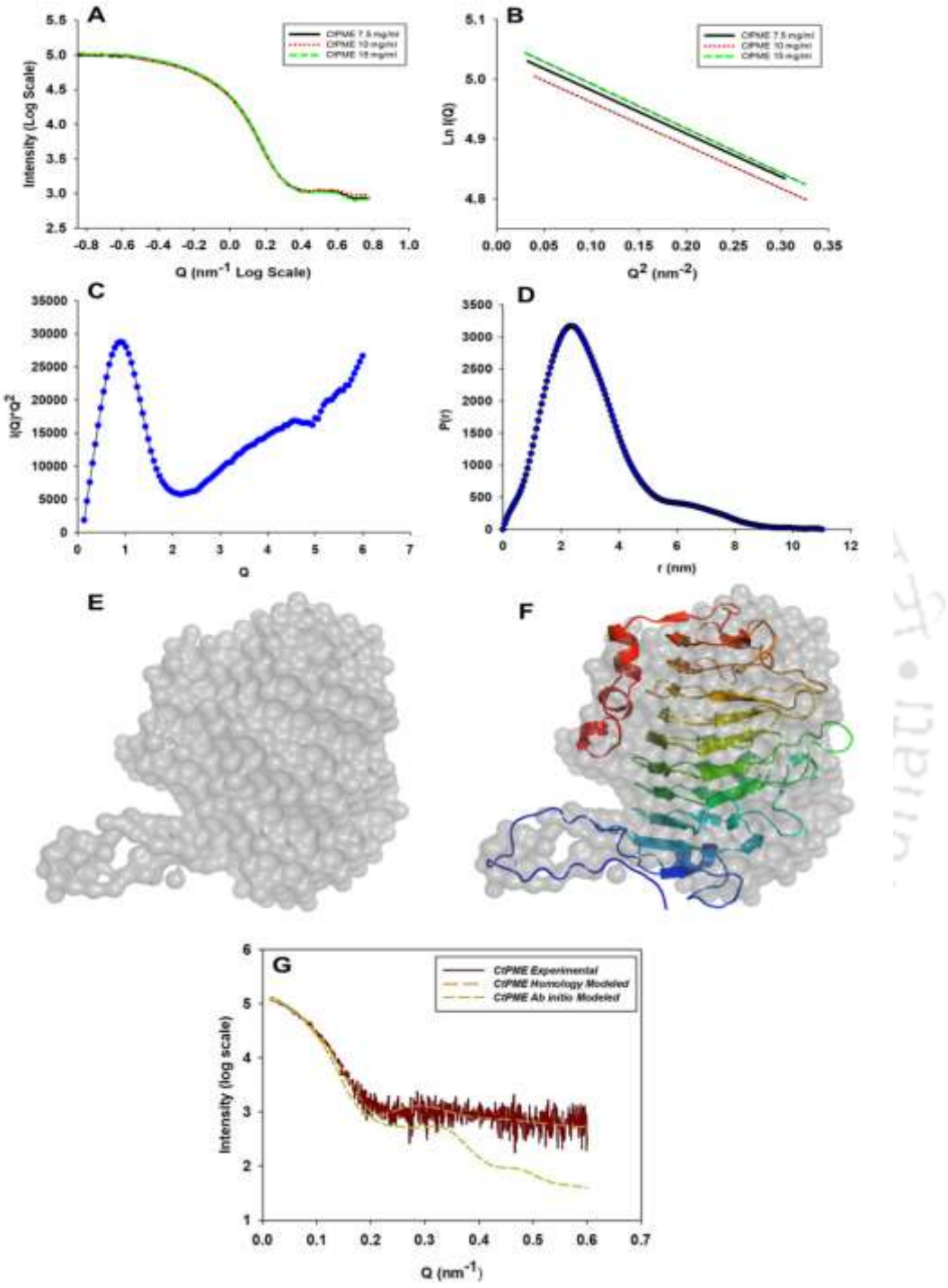

Fig. 4.7 SAXS analysis of *Ct*PME. A) SAXS intensity profile of *Ct*PME, (B) Guinier plot of the SAXS intensities, C) Kratky plot, D) P(r) curve of *Ct*PME as a function of r (E) *ab initio* shape of *Ct*PME and F) Superposition of *ab initio* model with homology modelled *Ct*PME and (G) Crysol fitting of *Ct*PME homology modelled structure and *ab initio* modelled structure with experimental SAXS data.

4.4. Conclusions

The 3D structure of pectin methyl esterase of a family 8, carbohydrate esterase from *Clostridium thermocellum* generated by comparative modelling was stable and compact. The secondary structure CD analysis of *Ct*PME displayed presence of α-helices (3.1%), β-sheets (40.1%) and random coil (56.9%). The 3-D modelled *Ct*PME showed right handed parallel β-helix structure, where three parallel β -sheets were linked by coils. The key residues of *Ct*PME involved in catalysis are Asp165, Asp186 and Arg242. MD simulation showed the stable conformation up to 20 ns. SAXS analysis demonstrated the overall shape and structure of *Ct*PME in solution form. Guinier analysis gave the radius of gyration (Rg) 2.28 nm for globular shape and 0.74 nm for rod shape. Kratky plot gave the indication that protein is fully folded in solution. The *ab initio* derived DAM model of *Ct*PME superposed well with its homology modelled 3D-structure. The most authenticated structure shall be possible by X-ray crystallography. However, the present results provided closer insights of the structure and active site of a cellulosomal pectin methylesterase from *Clostridium thermocellum.*

4.5 References

Altschul, S. F., Madden, T. L., Schäffer, A. A., Zhang, J., Zhang, Z., Miller, W., Lipman, D. J. (1997) Gapped BLAST and PSI-BLAST: a new generation of protein database search programs. Nucleic Acids Research, 25(17): 3389-3402.

Bayer, E. A., Kenig, R., Lamed, R. (1983) Adherence of *Clostridium thermocellum* to cellulose. Journal of Bacteriology, 156(2): 818-827.

Bayer, E. A., Lamed, R., White, B. A., Flint, H. J. (2008) From cellulosomes to cellulosomics. The Chemical Record, 8(6): 364-377.

Berendsen, H. J., van der Spoel, D., van Drunen, R. (1995) GROMACS: a message-passing parallel molecular dynamics implementation. Computer Physics Communications, 91(1-3): 43-56.

Boraston, A. B., Abbott, D. (2012) Structure of a pectin methylesterase from *Yersinia enterocolitica*. Acta Crystallographica Section F: Structural Biology and Crystallization Communications, 68(2): 129-133.

Chakraborty, S., Fernandes, V. O., Dias, F. M., Prates, J. A., Ferreira, L. M., Fontes, C. M., Goyal, A., Centeno, M. S. (2015). Role of pectinolytic enzymes identified in *Clostridium thermocellum* cellulosome. PloS One, 10(2): e0116787.

Chakraborty, S., Sharma, K., Mukherjee, J., N Gupta, M., Goyal, A. (2015) Structural modelling, substrate binding and stability studies of endopectate lyase (PL1B) of family 1 Polysaccharide Lyase from *Clostridium thermocellum*. Protein and Peptide Letters, 22(6): 557-568.

Chen, M. H., Citovsky, V. (2003) Systemic movement of a tobamovirus requires host cell pectin methylesterase. The Plant Journal, 35(3): 386-392.

Chen, M. H., Sheng, J., Hind, G., Handa, A. K., Citovsky, V. (2000) Interaction between the tobacco mosaic virus movement protein and host cell pectin methylesterases is required for viral cell-to-cell movement. The EMBO Journal, 19(5): 913-920.

De Lorenzo, G., Castoria, R., Bellincampi, D., Cervone, F. (1997) Fungal invasion enzymes and their inhibition. In Plant Relationships, Part B, G.C. Carroll and P. Tudzynski, editions. Springer, Berlin, Heidelberg, 61-83.

Di Matteo, A., Giovane, A., Raiola, A., Camardella, L., Bonivento, D., De Lorenzo, G., Cervone, F., Bellincampi, D. Tsernoglou, D. (2005) Structural basis for the interaction between pectin methylesterase and a specific inhibitor protein. The Plant Cell, 17(3): 849-858.

Dorokhov, Y. L., Mäkinen, K., Frolova, O. Y., Merits, A., Saarinen, J., Kalkkinen, N., Atabekov, J.G., Saarma, M. (1999) A novel function for a ubiquitous plant enzyme pectin methylesterase: the host-cell receptor for the tobacco mosaic virus movement protein. FEBS Letters, 461(3): 223-228.

Fischer, H. D. O. N., Oliveira Neto, M. D., Napolitano, H. B., Polikarpov, I., Craievich, A. F. (2010) Determination of the molecular weight of proteins in solution from a single small-angle X-ray scattering measurement on a relative scale. Journal of Applied Crystallography, 43(1): 101-109.

Franke, D., Svergun, D. I. (2009) DAMMIF, a program for rapid ab-initio shape determination in small-angle scattering. Journal of Applied Crystallography, 42(2): 342-346.

Fries, M., Ihrig, J., Brocklehurst, K., Shevchik, V. E., Pickersgill, R. W. (2007) Molecular basis of the activity of the phytopathogen pectin methylesterase. The EMBO Journal, 26(17): 3879-3887.

Guiner, A., Fournet, G., Walker, C. B. (1955) Small angle scattering of X-rays. J. Wiley & Sons, New York.

Heikinheimo, P., Goldman, A., Jeffries, C., Ollis, D. L. (1999) Of barn owls and bankers: a lush variety of α/β hydrolases. Structure, 7(6): R141-R146.

Herron, S. R., Benen, J. A., Scavetta, R. D., Visser, J., Jurnak, F. (2000) Structure and function of pectic enzymes: virulence factors of plant pathogens. Proceedings of the National Academy of Sciences, 97(16): 8762-8769.

Hess, B., Bekker, H., Berendsen, H. J., Fraaije, J. G. (1997) LINCS: a linear constraint solver for molecular simulations. Journal of Computational Chemistry, 18(12): 1463-1472.

Jenkins, J., Mayans, O., Smith, D., Worboys, K., Pickersgill, R. W. (2001) Three-dimensional structure of *Erwinia chrysanthemi* pectin methylesterase reveals a novel esterase active site1. Journal of Molecular Biology, 305(4): 951-960.

Jiang, X., Jia, Q., Chen, L., Chen, Q., Yang, Q. (2014) Recombinant expression and inhibition mechanism analysis of pectin methylesterase from *Aspergillus flavus*. FEMS Microbiology Letters, 355(1): 12-19.

Johansson, K., El-Ahmad, M., Friemann, R., Jörnvall, H., Markovič, O., Eklund, H. (2002) Crystal structure of plant pectin methylesterase. FEBS letters, 514(2-3): 243-249.

Kashyap, D. R., Vohra, P. K., Chopra, S., Tewari, R. (2001) Applications of pectinases in the commercial sector: a review. Bioresource Technology, 77(3): 215-227.

Kelly, S. M., Jess, T. J., Price, N. C. (2005) How to study proteins by circular dichroism. Biochimica et Biophysica Acta (BBA)-Proteins and Proteomics, 1751(2): 119-139.

Khanh, N. Q., Ruttkowski, E., Leidinger, K., Albrecht, H., Gottschalk, M. (1991) Characterization and expression of a genomic pectin methyl esterase-encoding gene in *Aspergillus niger*. Gene, 106(1): 71-77.

Krieger, E., Joo, K., Lee, J., Lee, J., Raman, S., Thompson, J., Tyka, M., Baker, D., Karplus, K. (2009) Improving physical realism, stereochemistry, and side-chain accuracy in homology modeling: four approaches that performed well in CASP8. Proteins: Structure, Function and Bioinformatics, 77(S9): 114-122.

Lagaert, S., Belien, T., & Volckaert, G. (2009) Plant cell walls: Protecting the barrier from degradation by microbial enzymes. In Seminars in cell & developmental biology, Academic Press, 20: 1064-1073.

Lamed, R., Setter, E., Bayer, E. A. (1983) Characterization of a cellulose-binding, cellulase-containing complex in *Clostridium thermocellum*. Journal of Bacteriology, 156(2): 828-836.

Laskowski, R. A., Swindells, M. B. (2011) LigPlot+: multiple ligand–protein interaction diagrams for drug discovery. Journal of Chemical Information and Modeling. 51: 2778-2786.

Lebeda, A., Luhova, L., Sedlarova, M., Jancova, D. (2001) The role of enzymes in plant-fungal pathogens interactions/Die Rolle der Enzyme in den Beziehungen zwischen Pflanzen und pilzlichen Erregern. Zeitschrift für Pflanzenkrankheiten und Pflanzenschutz/Journal of Plant Diseases and Protection, 108: 89-111.

Li, W., Cowley, A., Uludag, M., Gur, T., McWilliam, H., Squizzato, S., S., Park, Y.M., Buso, N., Lopez, R. (2015) The EMBL-EBI bioinformatics web and programmatic tools framework. Nucleic Acids Research, 43(W1): W580-W584.

Lietzke, S. E., Scavetta, R. D., Yoder, M. D., Jurnak, F. (1996) The refined three-dimensional structure of pectate lyase E from *Erwinia chrysanthemi* at 2.2 A resolution. Plant physiology, 111(1): 73-92.

Lievens, S., Goormachtig, S., Herman, S., Holsters, M. (2002) Patterns of pectin methylesterase transcripts in developing stem nodules of *Sesbania rostrata*. Molecular Plant-Microbe Interactions, 15(2): 164-168.

Lombard V., Golaconda, R. H., Drula, E., Coutinho, P. M., Henrissat, B. (2014) The Carbohydrate-active enzymes database (CAZy) in 2013. Nucleic Acids Research, 42: D490–D495.

Louis-Jeune, C., Andrade-Navarro, M. A., Perez-Iratxeta, C. (2012) Prediction of protein secondary structure from circular dichroism using theoretically derived spectra. Proteins: Structure, Function, and Bioinformatics, 80(2): 374-381.

Micheli, F. (2001) Pectin methylesterases: cell wall enzymes with important roles in plant physiology. Trends in Plant Science, 6(9): 414-419.

Micheli, F., Sundberg, B., Goldberg, R., Richard, L. (2000) Radial distribution pattern of pectin methylesterases across the cambial region of hybrid aspen at activity and dormancy. Plant Physiology, 124(1): 191-200.

Morris, G. M., Huey, R., Lindstrom, W., Sanner, M. F., Belew, R. K., Goodsell, D. S., Olson, A. J. (2009) AutoDock4 and AutoDockTools4: Automated docking with selective receptor flexibility. Journal of Computational Chemistry, 30(16): 2785-2791.

Perez-Iratxeta, C., Andrade-Navarro, M. A. (2008) K2D2: estimation of protein secondary structure from circular dichroism spectra. BMC Structural Biology, 8(1): 25.

Pickersgill, R., Jenkins, J., Harris, G., Nasser, W., Robert-Baudouy, J. (1994) The structure of *Bacillus subtilis* pectate lyase in complex with calcium. Nature Structural and Molecular Biology, 1(10): 717-723.

Pickersgill, R., Smith, D., Worboys, K., Jenkins, J. (1998) Crystal structure of polygalacturonase from *Erwinia carotovora ssp. carotovora*. Journal of Biological Chemistry, 273(38): 24660-24664.

Pilling, J., Willmitzer, L., Bücking, H., Fisahn, J. (2004) Inhibition of a ubiquitously expressed pectin methyl esterase in *Solanum tuberosum* L. affects plant growth, leaf growth polarity, and ion partitioning. Planta, 219(1): 32-40.

Pilling, J., Willmitzer, L., Fisahn, J. (2000) Expression of a *Petunia inflata* pectin methyl esterase in *Solanum tuberosum* L. enhances stem elongation and modifies cation distribution. Planta, 210(3): 391-399.

Rajulapati, V., Goyal, A. (2017) Molecular cloning, expression and characterization of pectin methylesterase (*Ct*PME) from *Clostridium thermocellum*. Molecular Biotechnology, 59(4-5): 128-140.

Robert, X., Gouet, P. (2014) Deciphering key features in protein structures with the new ENDscript server. Nucleic Acids Research, 42(W1): W320-W324.

Sali, A., Blundell, T. L. (1993) Comparative protein modelling by satisfaction of spatial restraints. Journal of Molecular Biology, 234(3): 779-815.

Schrodinger, L. (2016) The PyMOL Molecular Graphics System, Version 1.8 Schrödinger, LLC. Cambridge, MA.

Semenyuk, A. V., Svergun, D. I. (1991) GNOM–a program package for small-angle scattering data processing. Journal of Applied Crystallography, 24(5): 537-540.

Shen, M. Y., Sali, A. (2006) Statistical potential for assessment and prediction of protein structures. Protein Science, 15(11): 2507-2524.

Sievers, F., Higgins, D. G. (2014) Clustal Omega, accurate alignment of very large numbers of sequences. Methods in Molecular Biology: Multiple Sequence Alignment Methods, Humana Press, Totowa, NJ, 1079: 105-116.

Sievers, F., Wilm, A., Dineen, D., Gibson, T. J., Karplus, K., Li, W., Lopez, R., McWilliam, H., Remmert, M., Söding, J., Thompson, J. D. (2011) Fast, scalable generation of high-quality protein multiple sequence alignments using Clustal Omega. Molecular Systems Biology, 7(1): 539.

Svergun, D. I. (1999) Restoring low resolution structure of biological macromolecules from solution scattering using simulated annealing. Biophysical Journal, 76(6): 2879-2886.

Svergun, D. I. B. C. K. M. H. J., Barberato, C., Koch, M. H. (1995) CRYSOL–a program to evaluate X-ray solution scattering of biological macromolecules from atomic coordinates. Journal of Applied Crystallography, 28(6): 768-773.

Tans-Kersten, J., Guan, Y., Allen, C. (1998) *Ralstonia solanacearum* pectin methylesterase is required for growth on methylated pectin but not for bacterial wilt virulence. Applied and Environmental Microbiology, 64(12): 4918-4923.

Tieman, D. M., Handa, A. K. (1994) Reduction in pectin methylesterase activity modifies tissue integrity and cation levels in ripening tomato (*Lycopersicon esculentum* Mill.) fruits. Plant Physiology, 106(2): 429-436.

Tuukkanen, A. T., Kleywegt, G. J., Svergun, D. I. (2016) Resolution of ab initio shapes determined from small-angle scattering. IUCrJ, 3(6): 440-447. (Journal from the International Union of Crystallography (IUCr)).

Volkov, V. V., Svergun, D. I. (2003) Uniqueness of ab initio shape determination in small-angle scattering. Journal of Applied Crystallography, 36(3): 860-864.

Wallace, A. C., Laskowski, R. A., Thornton, J. M. (1995) LIGPLOT: a program to generate schematic diagrams of protein-ligand interactions. Protein Engineering, Design and Selection, 8(2): 127-134.

Webb, B., & Sali, A. (2017) Protein Structure Modeling with MODELLER. In Functional Genomics, Humana Press, New York, 39-54.

Wen, F., Zhu, Y., Hawes, M. C. (1999) Effect of pectin methylesterase gene expression on pea root development. The Plant Cell, 11(6): 1129-1140.

Wiethölter, N., Graeßner, B., Mierau, M., Mort, A. J., Moerschbacher, B. M. (2003) Differences in the methyl ester distribution of homogalacturonans from near-isogenic wheat lines resistant and susceptible to the wheat stem rust fungus. Molecular Plant-Microbe Interactions, 16(10): 945-952. (this is right)

Willats, W. G., Orfila, C., Limberg, G., Buchholt, H. C., van Alebeek, G. J. W., Voragen, A. G., Marcus, S.E., Christensen, T.M., Mikkelsen, J.D., Murray, B.S., Knox, J. P. (2001) Modulation of the degree and pattern of methyl-esterification of pectic homogalacturonan in plant cell walls implications for pectin methyl esterase action, matrix properties, and cell adhesion. Journal of Biological Chemistry, 276(22): 19404-19413.

Zheng, X., Guo, J., Xu, L., Li, H., Zhang, D., Zhang, K., Sun, F., Wen, T., Liu, S., Pang, H. (2011) Crystal structure of a novel esterase Rv0045c from *Mycobacterium tuberculosis*. PloS One, 6(5): e20506.

Chapter 5

Green process of degumming of jute fibers and bioscouring of cotton fabric by recombinant pectin methylesterase and pectate lyases from *Clostridium thermocellum*

5.1 Introduction

Pectin is the major constituent of the primary cell walls and middle lamella of plant cells. Pectin is a complex, colloidal, acidic and negatively charged high molecular mass (50-250 kDa) polymer present in the form of calcium and magnesium pectate (Jayani *et al*., 2005; Murad and Azzaz, 2011). Pectin is a polymer of D-galacturonic acid (GalA) residues joined by α-1,4 glycosidic linkages. The GalA residues may be esterified or decorated with the side chains of D-xylose, L-arabinose, D-galactose and L-rhamnose molecules (Gummadi and Kumar, 2006). Pectin is hydrolyzed by pectinolytic enzymes or pectinases, which fall into two main groups, methylesterases and depolymerases. Pectin methylesterases (PME: EC 3.1.1.11), catalyze the removal of the methyl group (de-esterification) from pectin to form pectate. Depolymerases are two types, hydrolases and lyases. Hydrolases act on the backbone of pectin by hydrolytic cleavage and lyases by trans-eliminative cleavage (Wang et al., 2013).

Polygalacturonase (PG: EC 3.2.1.15) catalyses the hydrolytic cleavage of α-1, 4-glycosidic linkages of pectin and produce pectic acid (with carboxyl group), -COOH or $–COOCH_3$ (Boudart *et al*., 1998) or pectate (without carboxyl group) (Norman *et al*., 1999). Pectate lyase (PL: EC 4.2.2.2) catalyses the cleavage of pectin via β-elimination reaction and generates Δ4,5-unsaturated-oligogalacturonate at the non-reducing end (Das *et al*., 2012; Garg *et al*., 2016). PME, PG and PL are found in microorganisms and plants and are the major virulence factors in plant pathogens (Micheli, 2001; De Melo *et al*., 2017). In general, most PL work efficiently under alkaline conditions (pH 8–10) and require additional Ca^{2+} ions for optimal enzymatic activity (Gillespie *et al*., 1990; Chakraborty *et al*., 2017). PME plays a key role in vegetative and reproductive processes in *Arabidopsis* (Wolf *et al*., 2009) and contribute to intercellular adhesion during plant growth (Wu *et al*., 2017).

Alkaline pectinases are most commonly obtained from bacterial sources. Alkaline pectinases have ample applications in textile industry for retting and degumming of plant fibers (Saleem *et al*. 2008). They are also used in many industrial processes including pretreatment of pectic wastewater and degumming of natural fiber crops such as jute, buel, flax, kenaf, ramie, sisal and sunn hemp (Saleem *et al*. 2008; Kandimalla *et al*., 2016). Alkaline pectinases are used in bioscouring of cotton fabrics such as cotton wool, felted cotton, grey-woven cotton, knit cotton and greige cotton (Liu *et al*., 2016; De Melo *et al*., 2017; Khan *et al*., 2018). Retting is a fermentation process, where certain bacteria (e.g., *Bacillus sp.* (Kapoor *et al*., 2001; Cheng *et al*., 2018) or *Pectobacterium sp.* (Duan *et al*., 2016), *Clostridium sp.* (Angelini *et al*., 2015)) and fungi (e.g., *Aspergillus sp.* (Pedrolli *et al*., 2009) or *Penicillium sp.* (Garg *et al*., 2016) release the fiber by decomposing pectin present in the bark. Degumming is a

method, which removes heavily coated, non-cellulosic gummy, especially the pectin content from the cellulose part of the plant fibers. Jute fibers or cotton fabric surface is rough due to the presence of pectin associated non-cellulosic or gummy wax substances. The fibers contain gum (non-cellulosic) that should be removed before it is used in textile manufacturing. The alkaline pH optimum of pectinases from microorganisms is advantageous for degumming of plant fibers because it prevents contamination, reduces the time consumed and improves fiber quality. Additionally, it permits adoption of an open fermentation system (Hoondal *et al*., 2002). Bioscouring is a method in which enzymes remove non-cellulosic gummy substances, especially the pectin content, natural waxes, esters, grease, dirt, oil etc. from the fabric without degradation of its cellulose content to increase the wettability of the fabric (Durden *et al*., 2001).

Traditionally, the degumming and scouring processes are carried out under alkaline and high-temperature conditions (pH 10 and 95°C). This involves high-energy consumption, the fiber damage and requires treatment of alkali containing wastewater after the process, which is challenging. This leads to low quality, poor stability of fabric and the process becomes highly labour intensive and expensive. Chemical treatment produces toxic effluents, which are harmful to the environment and also damages the fabric material (Duan, *et al*., 2018). Degumming and bioscouring processes using microorganisms is a time consuming process, pollution, contamination is also a major problem. To overcome the challenges faced by traditional and chemical degumming and scouring, use of enzymes is desirable in the textile industry to replace harsh conventional chemicals, reduce time, water and energy consumption and to improve the fabric quality.

In this study, the recombinant pectinases, pectin methylesterase, *Ct*PME (a type of pectinase) and pectate lyase, *Ct*PL1B both from *Clostridium thermocellum (renamed as Ruminiclostridium thermocellum)* were used for degumming of jute fiber (bast family member) and bioscouring of cotton fabric (Greige cotton). The production of *Ct*PME (Rajulapati and Goyal, 2017) and *Ct*PL1B (Chakraborty *et al*., 2015) enzymes was reported earlier. The degumming of jute fibers and bioscouring of cotton fabric using alkaline pectinases, *Ct*PME, *Ct*PL1B and their mixture was studied. The removal of pectin from jute fiber by *Ct*PME and *Ct*PL1B was analysed by FESEM (Field Emission Scanning Electron Microscope). Wettability of bioscoured cotton fabric was determined. The weight loss of enzyme treated jute fiber and cotton fabric was also measured. The ATR-FTIR (Attenuated Total Reflectance Fourier Transform Infrared) analysis of jute fiber and cotton fabric showed changes in the surface exposed functional groups after enzyme treatment of jute fiber and cotton fabric. The mechanical properties such as Young Modulus and tensile strength of degummed jute fiber and bioscoured cotton fabric were investigated by UTM (Universal Testing Machine) analysis. These studies provided sufficient support for alkaline *Ct*PME and *Ct*PL1B for their green process applications in the textile industry to replace the chemical approach. To best of our knowledge, this is the first study on the use of a recombinant pectin methylesterase, *Ct*PME with pectate lyase, *Ct*PL1B for degumming of jute fiber and bioscouring of cotton fabric.

5.2 Materials and Methods

5.2.1 Substrates and chemicals

The substrates are polygalacturonic acid (PGA) from citrus fruit and Citrus pectin (CP, >85 methylations) were purchased from Sigma-Aldrich, USA. The other chemicals ($CaCl_2$ and NaCl) and medium components (Tryptone and Yeast extract) were purchased from Himedia Pvt. Ltd., India. Carbon tape (10 mm width) and α-amylase were purchased from Sigma-Aldrich, USA.

5.2.2 Collection of raw jute and cotton fabric material

The raw material of jute fiber (*Corchorus capsularis* L.) was collected from the Kamrup area of Guwahati, Assam, India. The raw cotton fabric (Greige, grey color) was collected from the local market of Guwahati, Assam, India.

5.2.3 Production of pectinases

5.2.3.1 Production of *Ct*PME or *Ct*PL1B

E. coli BL21 (DE3) cells harbouring the recombinant plasmid containing the gene encoding *Ct*PME or *Ct*PL1B were grown in LB medium supplemented with kanamycin (50 µg/ml) for the production of *Ct*PME (Rajulapati and Goyal, 2017) or *Ct*PL1B (Chakraborty *et al*., 2015). 500 ml culture of *E. coli* BL21 (DE3) cells was grown at 37°C and 180 rpm till the mid exponential phase (A_{600} = 0.6). The cells were induced with isopropyl-β-D-thiogalactopyranoside (1 mM) and further incubated at 24°C and 180 rpm for 12 h. After that, the cells were centrifuged at 9000*g*, 4°C for 10 min. The cell pellet was resuspended in 15 ml of 50 mM Tris-HCl buffer (pH 8.5) and then 1 mM phenyl methane sulfonyl fluoride (PMSF) and 0.2 mg/ml lysozyme were added and incubated at 4°C for 20 min. The cells were then sonicated for 30 min (7 s on and 15 s off pulse; 33% amplitude) using an ultra-sonicator (Vibra Cell, Sonics,

USA). The sonicated cells were centrifuged at 19,000*g*, 4°C for 45 min. The cell free supernatant of *Ct*PME or *Ct*PL1B was collected. The protein concentration was assayed by Bradford method using BSA as standard (Bradford, 1976).

5.2.4. Enzyme assay

5.2.4.1 Assay of *Ct*PME

The enzyme activity of crude *Ct*PME was assayed at 50°C for 15 min using citrus pectin (CP) (>85% methyl esterified) as substrate. The reaction mixture (100 µl) contained 1% (w/v) citrus pectin dissolved in 50 mM Tris-HCl buffer (pH 8.5) and 20 µl of crude *Ct*PME. The enzyme activity was determined by the method as reported earlier in Chapter 3 section 3.2.2.1 (Rajulapati and Goyal, 2017).

5.2.4.2 Assay of *Ct*PL1B

The enzyme activity of crude *Ct*PL1B was assayed at 50°C for 15 min using polygalacturonic acid (PGA) as substrate. The reaction mixture (1 ml) contained 0.1% (w/v) PGA dissolved in 50 mM Glycine-NaOH buffer (pH 9.8), 0.6 mM $CaCl_2$ and 20 µl of crude PL1B. The enzyme activity was measured as described earlier (Chakraborty *et al*., 2015).

5.2.5 Enzymatic degumming of jute fiber at small scale

5.2.5.1 Optimization of enzyme concentration

The jute fibers (10 mg) of approximately 10 cm length were weighed and further chopped to 1.3-1.5 cm for degumming experiments following the method as mentioned earlier (Dhillon *et al*., 2017). 10 mg of chopped jute fibers were transferred into 2 ml micro-centrifuge tubes and were treated with different *Ct*PME concentrations (0.42 U/ml; 1 mg/ml, 1.05 U/ml; 2.5 mg/ml, 2.1 U/ml; 5 mg/ml, 4.2 U/ml; 10 mg/ml) or *Ct*PL1B (0.6 U/ml; 1 mg/ml, 1.5 U/ml; 2.5 mg/ml, 3.0 U/ml; 5 mg/ml, 6.0 U/ml; 10

mg/ml) at 50°C and 100 rpm for 60 min . The final reaction volume (1 ml) was made by appropriately diluting the crude enzyme with 50 mM Tris-HCl buffer, pH 8.5. After treatment, the crude *Ct*PME or *Ct*PL1B was removed and jute fibers were washed 3-5 times with water, dried at 60°C for 24 h.

For enzyme mixture degumming experiments, stock solution of *Ct*PME (4.2 U/ml, 10 mg/ml) and *Ct*PL1B (6.0 U/ml, 10 mg/ml) were diluted with 50 mM Tris-HCl buffer, pH 8.5 to make final volume of 1 ml to obtain final concentrations of 0.5 mg/ml, 1 mg/ml, 2.5 mg/ml and 5 mg/ml for each enzyme. For degumming experiments, these concentrations were used at 50°C and 100 rpm for 60 min. In a parallel experiment, jute fibers were incubated without any enzyme in micro-centrifuge tubes (2 ml) containing 1 ml of 50 mM Tris-HCl buffer, pH 8.5 and used as negative control. Jute fiber treated with 1 ml of 5 g/l NaOH was used as a positive control.

5.2.5.2 Optimization of enzyme degumming time

To optimize the degumming time, the jute fibers were treated with 1 ml of *Ct*PME (4.2 U/ml; 10 mg/ml) or 1 ml of *Ct*PL1B (6.0 U/ml; 10 mg/ml) or mixture of 0.5 ml each of *Ct*PME (5 mg/ml; 2.1 U/ml) and *Ct*PL1B (5 mg/ml; 3.0 U/ml was used. The degumming experiments were carried out at 50°C and 100 rpm for different time periods (15 min, 30 min, 45 min, 60 min and 120 min). In a parallel experiment, jute fibers without any enzyme were incubated in micro-centrifuge tubes (2 ml) containing 1 ml of 50 mM Tris-HCl buffer, pH 8.5 and used as negative control. Jute fibers treated with 5 g/l NaOH were used as a positive control. The amount of degumming was analysed by weight loss of jute fibers and imaging the untreated and treated fibers under Field Emission Scanning Electron Microscope (FESEM) (Sigma, Zeiss, Germany). All degumming experiments were performed in triplicates.

5.2.6. Bio-scouring of cotton fabric at small scale

5.2.6.1 Desizing of cotton fabric

The raw plain-woven cotton fabric (Greige, Grey color) was desized before performing any experiments as mentioned by Kalantzi *et al*., (2010). Cotton fabric pieces of approximately, 2.5×6.5 cm (0.1 g) were used for experiment. Cotton fabric was soaked in water and then rinsed with water after 10 min to remove any dust or dirt. 1 mg of α-amylase (58 U/mg, Sigma-Aldrich, USA) dissolved in 100 ml of sodium phosphate buffer, pH 6.8 was used for desizing the cotton fabric pieces (5 x 0.1 g) in a 500 ml beaker at 40°C and 100 rpm for 1 h. After α-amylase treatment, the cotton fabric was washed with water and dried in hot air oven at 50°C for 5h (Kalantzi *et al*., 2010).

5.2.6.2 Optimization of enzyme concentration

The concentrations of crude *Ct*PME and *Ct*PL1B required for bioscouring, were optimized by treating the washed cotton fabric pieces with different concentrations of *Ct*PME or *Ct*PL1B and both combined in individual 25 ml test tube (15 mm x 125 mm). 10 mg/ml stock of *Ct*PME or *Ct*PL1B enzyme was appropriately diluted using 50 mM Tris-HCl buffer, pH 8.5 to make the final volume to 2.5 ml. The cotton fabric was treated with different concentrations of *Ct*PME (0.42 U/ml; 1 mg/ml, 1.05 U/ml; 2.5 mg/ml, 2.1 U/ml; 5 mg/ml, 4.2 U/ml; 10 mg/ml) or different concentrations of *Ct*PL1B (0.6 U/ml; 1 mg/ml, 1.5 U/ml; 2.5 mg/ml, 3.0 U/ml; 5 mg/ml, 6.0 U/ml; 10 mg/ml) and incubated at 50°C, 100 rpm for 60 min. After incubation, the fabric pieces were rinsed with water and then dried at 60°C for 12 h.

Similarly, for bioscouring experiments using the mixture of both enzymes, different concentrations from stocks of *Ct*PME (4.2 U/ml, 10 mg/ml) and *Ct*PL1B (6.0 U/ml, 10 mg/ml) were 0.5 mg/ml (0.156 ml), 1 mg/ml (0.312 ml), 2.5 mg/ml (0.625 ml)

and 5 mg/ml (1.25 ml) of each enzyme. To obtain final volume of 2.5 ml with 50 mM Tris-HCl buffer, pH 8.5 and at 50°C, 100 rpm for 60 min. The cotton fabric immersed in 2.5 ml of 50 mM Tris-HCl buffer (pH 8.5) without any enzyme was used as a negative control. After incubation, the fabric pieces were rinsed with water and then dried at 60°C for 12 h.

5.2.6.3 Optimization of enzyme bioscouring time

The optimization of time period for bioscouring was performed by treating the cotton fabric (2.5×6.5 cm) with 2.5 ml of *Ct*PME (4.2 U/ml, 10 mg/ml), 2.5 ml of *Ct*PL1B (6.0 U/ml, 10 mg/ml) or 2.5 ml mixture of *Ct*PME (2.1 U/ml, 5 mg/ml) and *Ct*PL1B (3.0 U/ml, 5 mg/ml) each of 1.25 ml. The enzyme treatment of cotton fabric was carried out at 50°C and 100 rpm for different time periods *viz.* 15, 30, 45, 60, 90 and 120 min. The water absorption capacity of enzyme treated and the untreated cotton fabric was determined by water drop method as reported earlier (Morozova *et al*., 2006). In a parallel experiment, cotton fabric (same size) incubated in a test tube (25 ml) containing 2.5 ml of 50 mM Tris-HCl buffer (pH 8.5) was used as negative control. The same size cotton fabric treated with 2.5 ml of 5 g/l NaOH was used as a positive control. All bio scouring experiments were performed in triplicate.

5.2.7 Scale up of degumming of jute fibers and bioscouring of cotton fabric at shake flask level

The degumming process of jute fiber was scaled up from 10 mg in 1 ml (with respective treatment) in micro-centrifuge tube (2 ml) to 100 mg in 10 ml (with respective treatment) in a conical flask (100 ml). The size of jute fiber was increased from 10 cm to 20 cm in length. The jute fiber was treated with 10 ml of *Ct*PME (4.2 U/ml; 10 mg/ml) or 10 ml of *Ct*PL1B (6.0 U/ml; 10 mg/ml) or a mixture of enzymes

each 5 ml of *Ct*PME (2.1 U/ml, 5 mg/ml) and 5 ml of *Ct*PL1B (3.0 U/ml, 5 mg/ml), under optimized conditions of 50°C, 100 rpm for 60 min.

Bioscouring of cotton fabric was scaled up from 0.1g (2.5×6.5 cm) in 2.5 ml (with treatment respective) to 1 g (8.5 x 19.5 cm) in 25 ml (with respective treatment) in 100 ml conical flask. The cotton fabric was treated with 25 ml of *Ct*PME (4.2 U/ml, 10 mg/ml) or 25 ml of *Ct*PL1B (6.0 U/ml, 10 mg/ml) or a mixture of enzymes each 12.5 ml of *Ct*PME (2.1 U/ml, 5 mg/ml) and 12.5 ml of *Ct*PL1B (3.0 U/ml, 5 mg/ml) at 50°C, 100 rpm for 60 min.

5.2.7.1 Weight loss analysis of jute fiber and cotton fabric

The weight loss of jute fiber and cotton fabric was measured after the enzymatic or NaOH treatment. The weight loss was expressed as the percentage of weight loss after drying in a hot air oven at 60°C for 12h. The weight loss was calculated with respect to the initial dry weight of the jute fiber and cotton fabric. After the treatment the dried samples were weighed and the weight loss was calculated by using the following formula, weight loss (WL) in percentage, (%) WL = [(W1– W2) / W1] ×100 where, W1 and W2 are the weights of the raw and degummed or bio-scoured samples, respectively (Shanthi & Krishnabai, 2013; Kalantzi *et al*., 2008).

5.2.7.2 FESEM analysis of jute fiber and cotton fabric

The effect of enzyme or chemical treatment on surface topography of jute fiber or cotton fabric (treated and untreated samples) was analysed by FESEM. The samples were dried at 60°C for 12 h prior to the analysis. Jute fiber or cotton fabric samples were cut into approx. size of 1.3 cm length and placed on carbon tape covered by FESEM stub. The samples were coated (double coat) with gold at 30 kV for 20 min by using a

gold coating sputter (HITACHI E-1010 ion sputter) (double coat). The sample stub was analysed by SE2 (Secondary Electron 2 image mode) mode. All FESEM images were collected with scale bar of 20 µm and magnification of 2.0 KX.

5.2.7.3 ATR-FTIR analysis of jute fiber and cotton fabric

The removal of pectin and associated impurities from the surface of jute fiber or cotton fabric was also monitored by using Attenuated Total Reflection-Fourier Transform Infrared Spectrometer (ATR-FIR) equipped with diamond ATR attachment (IRAffinity IS, Shimadzu, Japan). The spectra were analysed for determining the surface exposed functional groups in enzyme treated and un-treated jute fiber or cotton fabric. ATR-FTIR was operated in de-humidified conditions. Scanning spectrum was carried out from 400 to 4000 cm^{-1} with 64 scans per 94 s for the sample and resolution of 4 cm^{-1}. The spectrum was recorded by using a single reflection horizontal ATR accessory with a Diamond crystal fixed at an incident angle of 45°. The spectra were analysed by IR-lab solutions software (Shimadzu, Japan) and plotted.

5.2.7.4 Wetting analysis of cotton fabric by the contact angle measurement

The increase in hydrophilicity of enzyme treated cotton fabric was determined by measuring the Contact Angle made by a drop of water with fabric surface. 2 µl of pre-calibrated water drop was released on to the surface of the cotton fabric by using a syringe. Contact angle apparatus (DSA 25, Kruss, Germany), equipped with a CCD camera was operated at an acquisition speed of 50 frames per second.

5.2.7.5 Mechanical properties of enzyme treated jute fibers or cotton fabric

The enzymatic and chemical treatment after de-moisturized of jute fiber or cotton fabric was analysed by UTM (Universal Testing Machine, Zwick Roell, Z005, Germany) at 25 °C. The UTM analysis was carried out for determining the mechanical

properties such as tensile strength, Young's Modulus, an Ultimate tensile strength of jute fiber and cotton fabric. UTM analysis was performed by using the pneumatic grip with maintained parameters, pressure 5 bar, distance 3 cm and control force load range between the 5N-100N. The jute fiber and cotton fabric approximately, 50 jute fibers and 10 cotton fabrics in a bunch of samples were placed on the sample port (pneumatic grip). The tensile tests were performed in accordance with standard ASTM D638 method setup. The samples were processed by using software Text Xport-III with version V1.2. At least three specimens were tested for each set of samples and the mean values were recorded.

5.3 Results and Discussion

5.3.1 Enzymatic degumming of jute fibers at small scale

5.3.1.1 Optimization of enzyme concentration

The enzymatic and chemically degummed jute fibers appeared light in color and shining as compared with the untreated fibers. The visual analysis showed light brown color of enzyme treated jute fiber as compared with dark brown color of untreated jute fiber. The FESEM images of untreated jute fibers showed the rougher surface owing to the presence of pectin associated non-cellulosic or gummy wax substances as compared with treated. The FESEM images of enzymatic degummed jute fibers showed smooth surface as compared with untreated. The optimum *Ct*PME concentration for degumming of 10 mg jute fiber was 1 ml of 10 mg/ml (4.2 U/ml) at 50°C and 100 rpm in 60 min as the FESEM image showed the most smooth surface as compared with the other concentrations untreated jute fiber (Fig. 5.1). This resulted in a weight loss of 9.6% in the weight of jute fibers, due to the removal of pectin (Table 5.1). The optimum *Ct*PL1B concentration for degumming of jute fibers was 1 ml of 10 mg/ml (6.0 U/ml) at 50°C and 100 rpm in 60 min as the FESEM image showed smoothest surface as compared with the other concentrations untreated jute fiber (Fig. 5.2). This resulted in a 13% weight loss due to the removal of pectin (Table 5.1). The enzymatic treated degummed jute fibers showed much higher weight loss as compared with untreated fibers. The *Ct*PL1B treated jute fiber showed higher weight loss (3.4%) as compared with *Ct*PME treated jute fiber (Table 5.1).

The optimum composition of mixture of both enzymes, for degumming of 10 mg jute fibers was attained, at 0.5 ml of 5 mg/ml (2.1 U/ml) *Ct*PME and 0.5 ml of 5 mg/ml (3.0 U/ml) of *Ct*PL1B treatment at 50°C and 100 rpm in 60 min (Fig. 5.3). The

weight loss of jute fiber was 17.7% (Table 5.1). Thus, the mixture of enzymes was more efficient compared to individual enzymes in removing the pectin from jute fibers.

The FESEM images of the NaOH (5 g/l) treated jute fibers showed smoother surface (Fig. 5.1F, 5.2F & 5.3F) as compared to untreated. The visual analysis showed golden yellow color of NaOH treated jute fiber as compared with dark brown color of untreated ones. The NaOH treatment of 10 mg jute fiber for degumming resulted in 19.7% weight loss (Table 5.1) which was comparable with that of mixture of enzymes. The removal of pectin-associated gum from jute fibers by a mixture of the two enzymes treatment was effective and comparable with that of chemical (NaOH, 5 g/l) treatment. There are very few reports on degumming of jute using any crude or pure enzyme. However, microbial degumming of jute fibers using bacterial isolates was reported but the process involved time periods from 10 h to 15 days (Das *et al*., 2012; Duan *et al*., 2016; Chiliveri *et al*., 2016). The present study reports the degumming time period of 60 min, which is much less as compared with 10 h reported by Chiliveri *et al*., (2016).

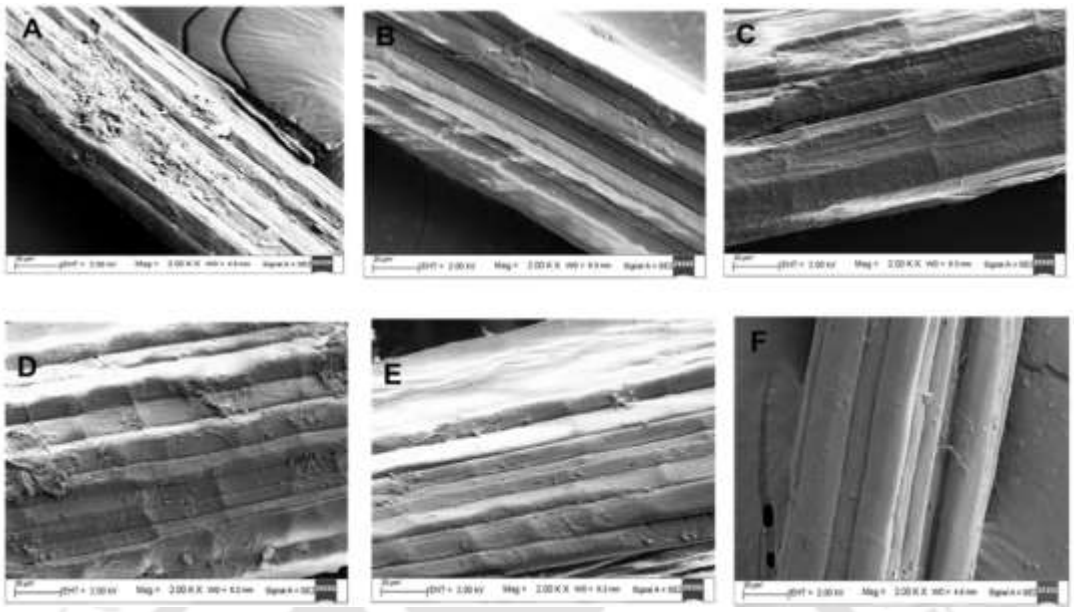

Fig. 5.1 FESEM images of pectin methylesterase (*Ct*PME) degummed jute fibers: (A) Untreated jute fibers (control), (B) *Ct*PME (1 mg/ml, 0.42 U/ml), (C) *Ct*PME (2.5 mg/ml, 1.05 U/ml), (D) *Ct*PME (5 mg/ml, 2.1 U/ml), (E) *Ct*PME (10 mg/ml, 4.2 U/ml) treated jute fibers and (F) Chemically (NaOH, 5 g/l) degummed jute fibers (positive control).

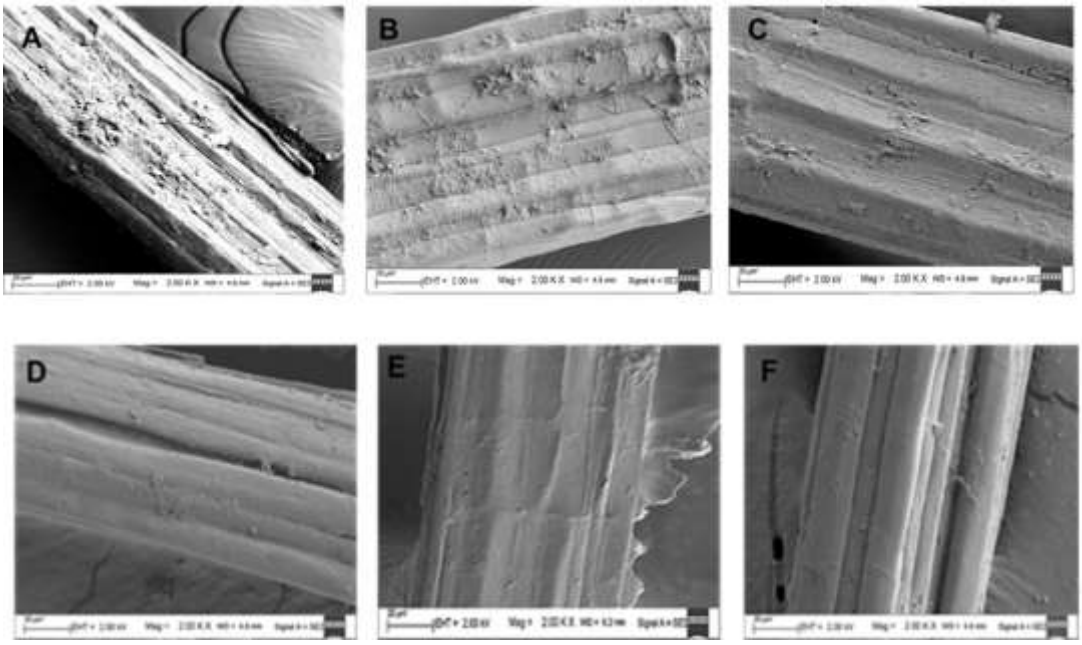

Fig. 5.2 FESEM images of pectate lyase (*Ct*PL1B) degummed jute fibers: (A) Untreated jute fibers (control), (B) *Ct*PL1B (1 mg/ml, 0.6 U/ml), (C) *Ct*PL1B (2.5 mg/ml, 1.5 U/ml), (D) *Ct*PL1B (5 mg/ml, 3.0 U/ml), (E) *Ct*PL1B (10 mg/ml, 6.0 U/ml) treated jute fibers and (F) Chemically (NaOH, 5 g/l) degummed jute fibers (positive control).

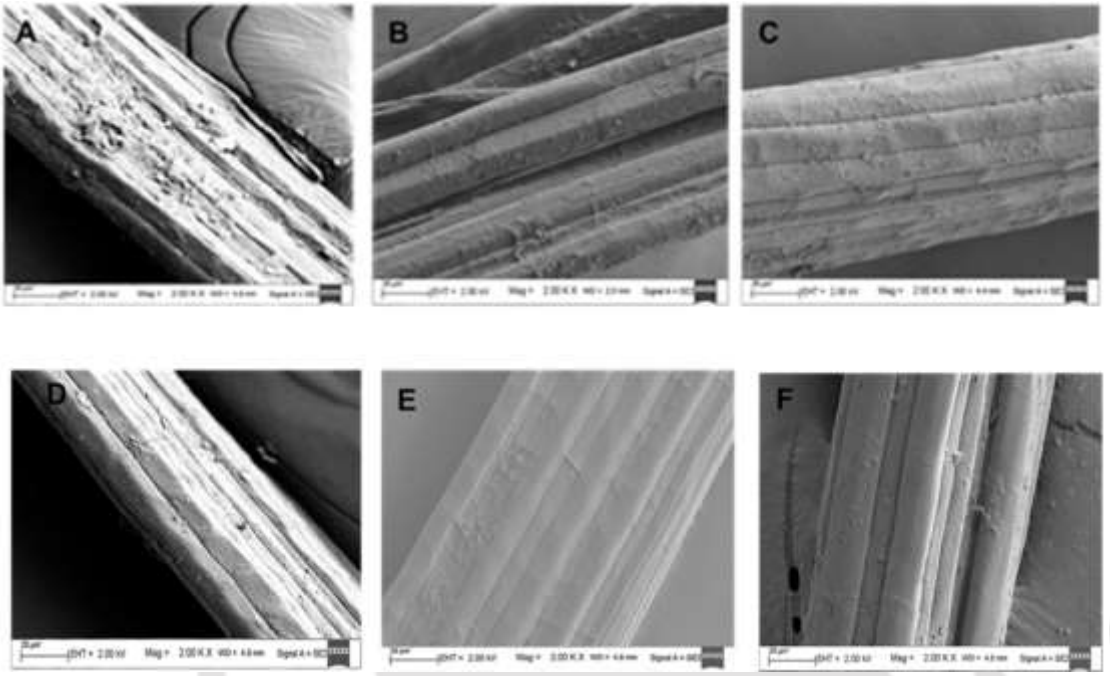

Fig. 5.3 FESEM images of mixed enzymes (*Ct*PME+*Ct*PL1B) degummed jute fibers: (A) Untreated jute fibers (control), (B) *Ct*PME (0.5 mg/ml, 0.21 U/ml) and *Ct*PL1B (0.5 mg/ml, 0.3 U/ml), (C) *Ct*PME (1 mg/ml, 0.42 U/ml) and *Ct*PL1B (1 mg/ml, 0.6 U/ml), (D) *Ct*PME (2.5 mg/ml, 1.05 U/ml) and *Ct*PL1B (2.5 mg/ml, 1.5 U/ml), (E) *Ct*PME (5 mg/ml, 2.1 U/ml) and *Ct*PL1B (5 mg/ml, 3.0 U/ml) treated jute fibers and (F) Chemically (NaOH, 5 g/l) degummed jute fibers (positive control).

5.3.1.2 Optimization of enzyme degumming time

To optimize the degumming time, the jute fibers were treated with 1 ml of *Ct*PME (10 mg/ml; 4.2 U/ml) and 1 ml of *Ct*PL1B (10 mg/ml; 6.0 U/ml) for different time periods at 50°C and 100 rpm. The optimum degumming time period of *Ct*PME, *Ct*PL1B and mixture of the two enzymes was 60 min as the pectin was effectively removed by 60 min as observed through FESEM analysis. The FESEM images of *Ct*PME, *Ct*PL1B and mixed enzyme treated jute fiber revealed that the surface was smoother than that of untreated jute fiber (Fig. 5.4, Fig. 5.5 and Fig. 5.6). The optimum

time for degumming of jute fiber by NaOH (5 g/l) was 60 min at 50°C and 100 rpm (Fig. 5.7). The FESEM image of NaOH (5 g/l) degummed jute fiber showed the smooth surface similar to that of mixed enzymes treated jute fiber. The FESEM images of individual enzyme or their mixture, treated surfaces of jute fiber, after 120 min of enzyme treatment were similar to those treated for 60 min. The degumming time period of 120 min by NaOH treatment, caused damage to the fiber. Pectate lyase and polygalacturonase produced by *Bacillus tequilensis* SV11-UV37 under SSF were used for degumming of kenaf and sunn hemp, took 10-12 h (Chiliveri *et al*., 2016). The degumming of ramie was carried out by using recombinant pectate lyase, where, 4 h of degumming time required (Zhou *et al*., 2017). However, the present study reports the degumming time period of 60 min, which is much less as compared with 4 h reported by Zhou *et al*., (2017).

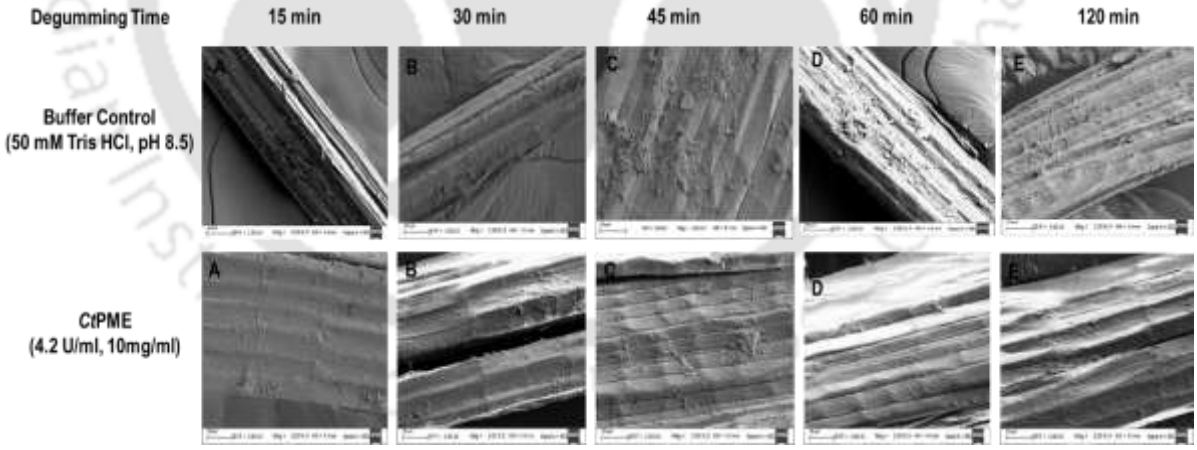

Fig. 5.4 FESEM images of jute fibers degummed using *Ct*PME (10 mg/ml, 4.2 U/ml), (A) 15 min treatment, (B) 30 min treatment, (C) 45 min treatment, (D) 60 min treatment and (E) 120 min treatment.

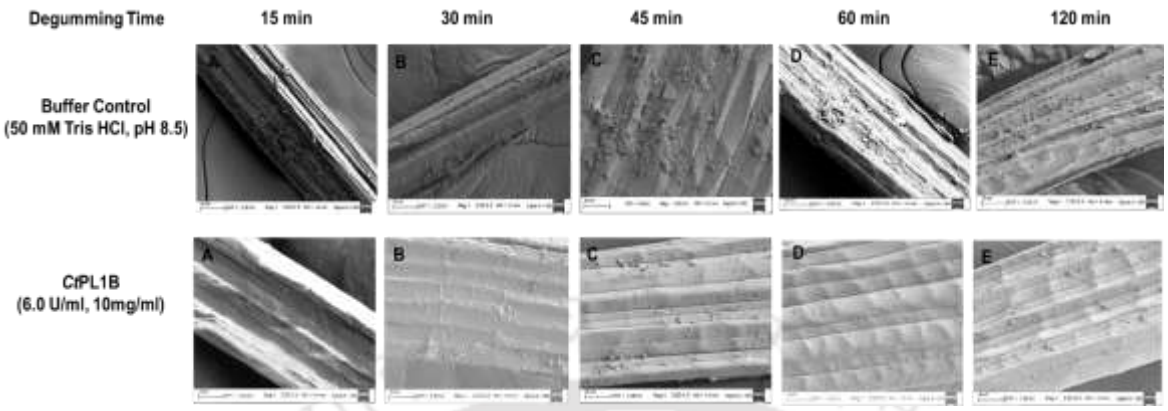

Fig. 5.5 FESEM images of jute fibers degummed using *Ct*PL1B (10 mg/ml, 6.0 U/ml), (A) 15 min treatment, (B) 30 min treatment, (C) 45 min treatment, (D) 60 min treatment and (E) 120 min treatment.

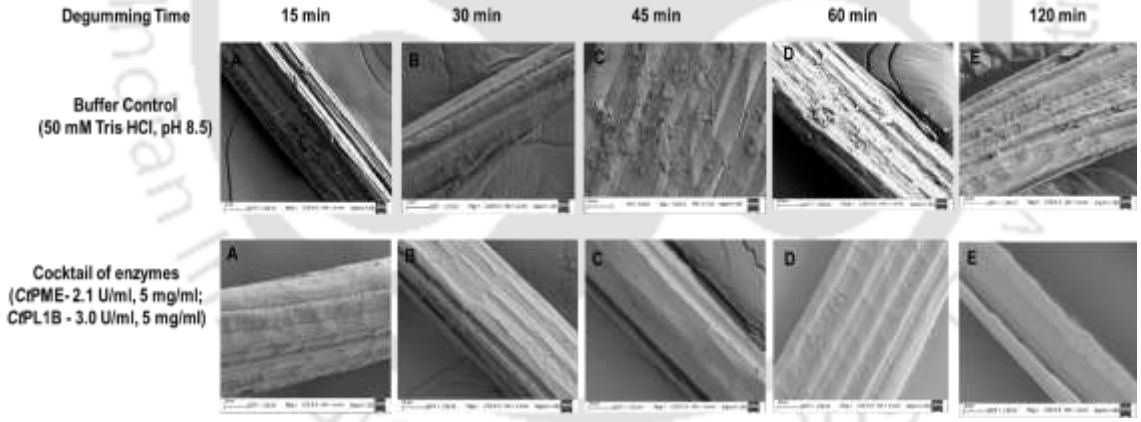

Fig. 5.6 FESEM images of jute fibers degummed using mixture of *Ct*PME (5 mg/ml, 2.1 U/ml) and *Ct*PL1B (5 mg/ml, 3.0 U/ml), (A) 15 min treatment, (B) 30 min treatment, (C) 45 min treatment, (D) 60 min treatment and (E) 120 min treatment.

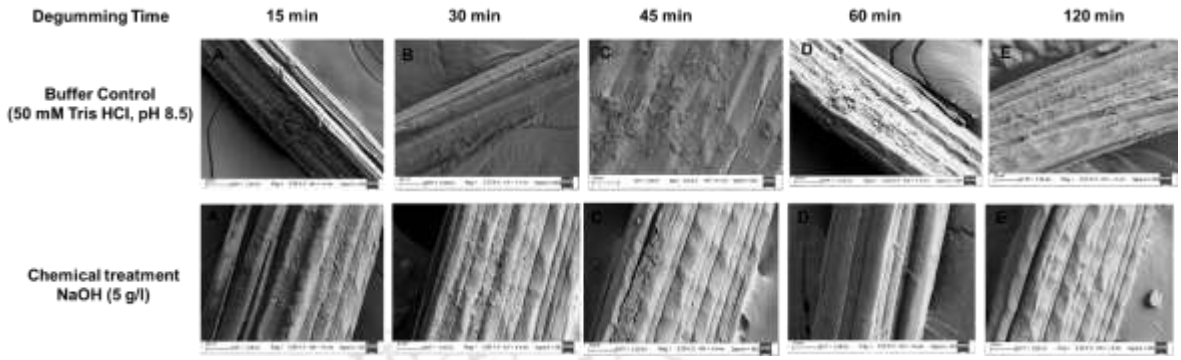

Fig. 5.7 FESEM images of jute fibers degummed using NaOH (5 g/l), (A) 15 min treatment, (B) 30 min treatment, (C) 45 min treatment, (D) 60 min treatment and (E) 120 min treatment.

5.3.2 Bioscouring of cotton fabric at small scale

5.3.2.1 Optimization of enzyme concentration

The cotton fabric (size 2.5×6.5 cm, Weight 0.1 g) was treated with different concentrations of *Ct*PME at 50°C, 100 rpm for 60 min. The optimum concentration of *Ct*PME determined was 2.5 ml of 10 mg/ml (4.2 U/ml) (Fig. 5.8A) as the cotton fabric treated with *Ct*PME showed increased wettability and reduced water absorption time as compared with other concentrations or untreated. The increase in the concentration of crude *Ct*PME from 1 mg/ml (0.42 U/ml) to 10 mg/ml (4.2 U/ml) showed the decrease in absorption time of a drop of water by the cotton fabric from 85 s to 23 s. However, the control, cotton fabric took 30 min to absorb a water drop. The weight loss of *Ct*PME treated cotton fabric was 9.6% under optimized concentration 10 mg/ml (4.2 U/ml) (Table 5.2). The cotton fabric was also treated with different concentrations of *Ct*PL1B at 50°C, 100 rpm for 60 min. The optimum *Ct*PL1B concentration was 2.5 ml of 10 mg/ml (6.0 U/ml) (Fig. 5.8B). The cotton fabric took 55 s and 20s to absorb a water droplet when treated with 1 mg/ml (0.6 U/ml) and 10 mg/ml (6.0 U/ml) of *Ct*PL1B, respectively. The control cotton fabric took 30 min time to absorb a water drop. The

weight loss of cotton fabric was found to be 13.1% under optimized *Ct*PL1B concentration 10 mg/ml (6.0 U/ml) (Table 5.2).

The same size and weight cotton fabric was treated with the mixture of crude enzymes by using different volumes from *Ct*PME (4.2 U/ml, 10 mg/ml) and *Ct*PL1B (6.0 U/ml, 10 mg/ml) stock solutions. The optimum composition of the mixture of enzymes was 1.25 ml of 5 mg/ml of *Ct*PME (2.1 U/ml) and 1.25 ml of 5 mg/ml *Ct*PL1B (3.0 U/ml). After treatment of the cotton fabric with the mixture of enzymes at 50°C, 100 rpm for 60 min, the time taken to absorb a drop of water was reduced to 10 s (Fig. 5.8C). The control fabric took 30 min to absorb a drop of water. The weight loss of cotton fabric treated with the mixture of enzymes was found to be 17.3% (Table 5.2). The same size and weight cotton fabric treated with mixture of the two enzymes showed higher wettability as compared with the individual enzymes. The cotton fabric treated with NaOH (5 g/l) at 50°C, 100 rpm for 60 min showed the water absorption time of 8 s and weight loss of 19.1%. The wettability of mixture of enzyme treated cotton fabric of 10 s was similar to that of 8 s by NaOH. Moreover, the weight losses of the fabric by mixed enzyme and NaOH treatment was also similar. Abdulrachman *et al*., (2017) reported that *Aspergillus aculeatus* endo-polygalacturonase bioscoured cotton fabric showed wettability time of 16.5 s. Aly *et al*., (2010) reported that the cotton fabric treated with a mixture of α-amylase and polygalacturonase enzymes from *Trichoderma harzianum*, supplemented with non-ionic surfactant (Egyptol, 1 g/l), gave wettability time of 13 s. The effectiveness of process reported in this study using mixed enzymes was comparable to chemical treatment therefore is environment friendly.

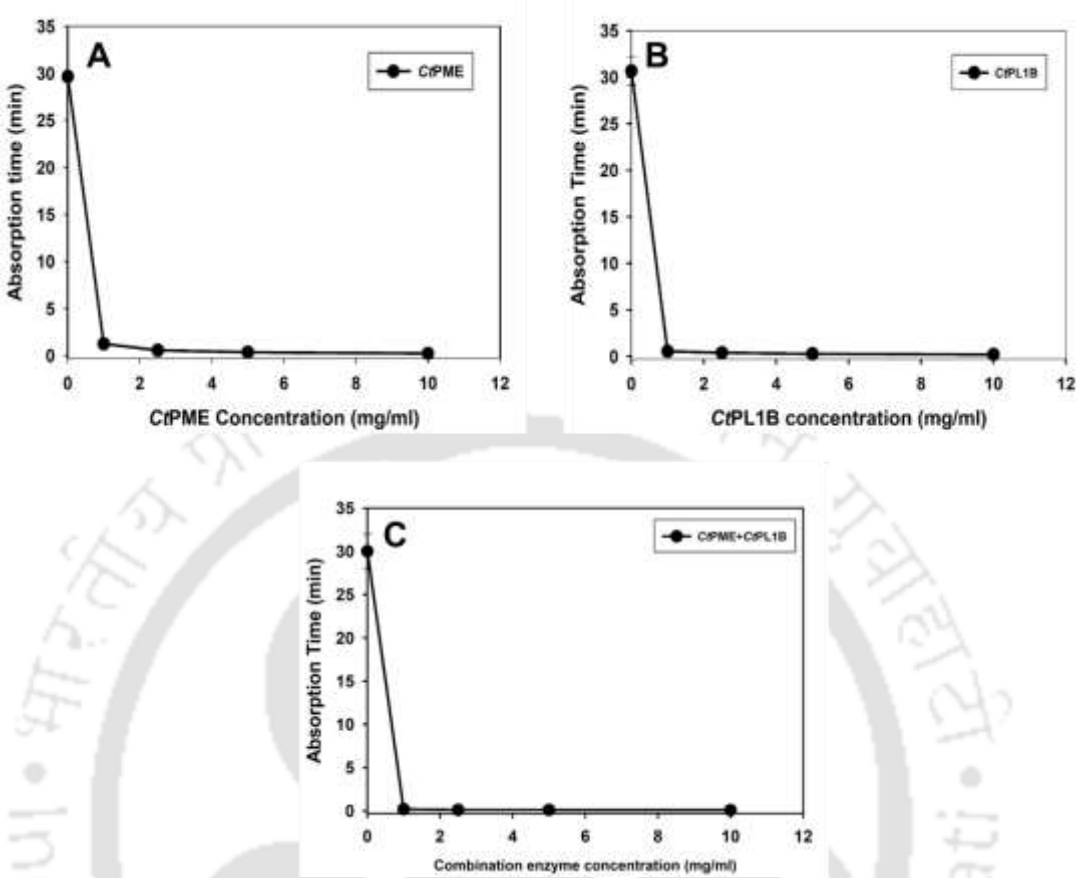

Fig. 5.8 Bioscouring of cotton fabric (A). Effect of crude *Ct*PME enzyme concentration (1 mg/ml, 0.42 U/ml; 2.5 mg/ml, 1.05 U/ml; 5 mg/ml, 2.1 U/ml; 10 mg/ml, 4.2 U/ml) on hydrophilicity of cotton fabric. (B). Effect of crude *Ct*PL1B enzyme concentration (1 mg/ml, 0.6 U/ml; 2.5 mg/ml, 1.5 U/ml; 5 mg/ml, 3.0 U/ml; 10 mg/ml, 6.0 U/ml) on hydrophilicity of cotton fabric. Untreated cotton fabric took 30 min to absorb a drop of water. (C). Effect of mixture of enzymes *Ct*PME and *Ct*PL1B concentrations each 0.5 mg/ml (0.42 U/ml+0.6 U/ml), 1 mg/ml (0.42 U/ml+0.6 U/ml), 2.5 mg/ml (1.05 U/ml+ 1.5 U/ml), 5 mg/ml (2.1 U/ml+3.0 U/ml) on hydrophilicity of cotton fabric. Untreated cotton fabric took 30 min to absorb a drop of water.

5.3.2.2 Optimization of enzyme bioscouring time

The untreated cotton fabric (size 2.5×6.5 cm, weight 0.1 g) took 30 min to absorb a drop of water with treated time was (Fig. 5.9A). The optimum time for bioscouring of cotton fabric was 60 min. The cotton fabric bioscoured with optimized concentration of *Ct*PME, *Ct*PL1B and their mixture took 23 s, 20 s and 10 s, respectively to absorb a drop of water (Fig. 5.9B, Fig. 5.9C and Fig. 5.9D). The cotton fabric treated with NaOH at 50°C, 100 rpm for 60 min showed the water absorption time of 8 s. The enzyme and chemical treatment of cotton fabric for more than 60 min, did not show significant decrease in time taken to absorb a drop of water. Cotton fabrics treated with *Ct*PME, *Ct*PL1B and the mixture of two enzymes showed the weight loss of 9.6%, 13.1% and 17.3%, respectively (Table 5.2). The untreated cotton fabric (control) showed a weight loss of only 0.3% whereas, the positive control, NaOH treated cotton fabric, showed a weight loss of 19.1% (Table 5.2). Mixture of enzymes and NaOH treatment gave similar weight loss percentage.

In a previous study, de Melo *et al*., (2017) reported the use of a combination of commercial pectinase, cellulase and lipase for bioscouring of cotton fabric and achieved a wettability time of 14 s. Dhillon *et al*., (2018) reported the use of a rhmanogalacturonan lyase, *Ct*RGL*f* for bioscouring of cotton and achieved a wettability time of 30 s. In textile industry the acceptable wettability time for cotton fabric is 30 s or less (Abdulrachman *et al*., 2017). Chakraborty *et al*., (2015) reported the use of a nano-particle immobilized pectate lyase for bioscouring and achieved a wettability time of 15 s. Kalantzi *et al*., (2010) reported that the cotton fabric bioscoured with a commercial endo pectate lyase from *Bacillus sp*. (Novozymes, Denmark) showed a wettability time of 5 s. In the present study bioscouring of cotton fabric with a mixture

of *Ct*PME and *Ct*PL1B results in a wettability time of 10 s and similar to NaOH treatment (8 s). This shows that the performance of mixture of *Ct*PME and *Ct*PL1B is better or comparable with previously reported enzymes.

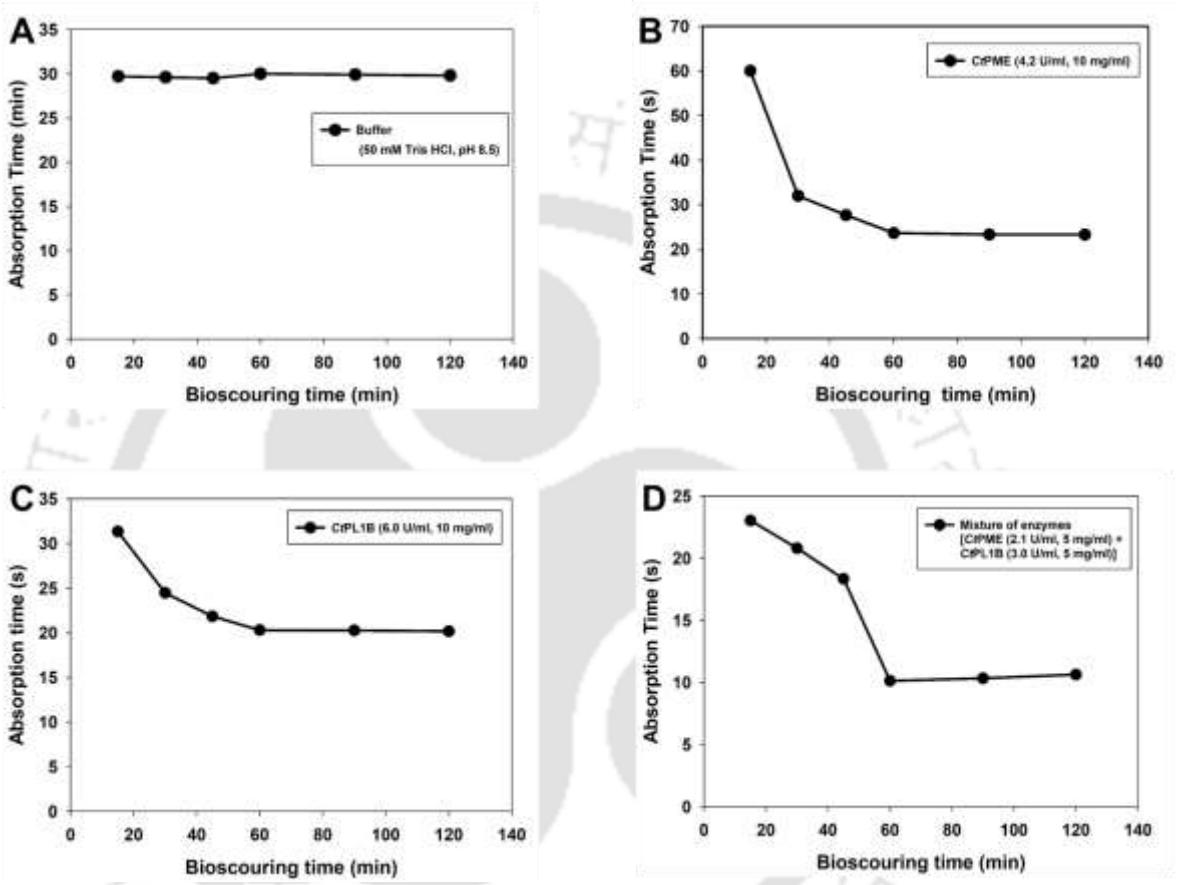

Fig. 5.9 Bioscouring of cotton fabric (A) Control, Buffer as at different time intervals from 15, 30, 45, 60, 90 and 120 min of cotton fabric (B). Effect of crude *Ct*PME enzyme concentration (10 mg/ml, 4.2 U/ml) on hydrophilicity of cotton fabric at different time intervals from 15, 30, 45, 60 90 and 120 min (C). Effect of crude *Ct*PL1B enzyme concentration (10 mg/ml, 6.0 U/ml) on hydrophilicity of cotton fabric at different time intervals from 15, 30, 45, 60, 90 and 120 min and (D). Effect of crude *Ct*PME (5 mg/ml, 2.1 U/ml) and *Ct*PL1B (5 mg/ml, 3.0 U/ml) enzyme concentration and on hydrophilicity of cotton fabric at different time intervals from 15, 30, 45, 60, 90 and 120 min.

5.3.3 Scale up of degumming of jute fibers and bioscouring of cotton fabric at shake flask level

The scale up of degumming of jute fiber and bioscouring of cotton fabric was performed under optimized conditions. The increased size of jute fiber (20 cm, 100 mg) and cotton fabric (8.5 X 19.5 cm, 1 g) was used. The optimum parameters and conditions were *Ct*PME (4.2 U/ml, 10 mg/ml), *Ct*PL1B (6.0 U/ml, 10 mg/ml) and mixture of both enzymes [*Ct*PME (2.1 U/ml, 5 mg/ml) and *Ct*PL1B (3.0 U/ml, 5 mg/ml)], 50 mM Tris HCl, pH 8.5, 50°C, 100 rpm and 60 min.

5.3.3.1 Weight loss analysis of jute fiber and cotton fabric

The jute fiber treated by *Ct*PME, *Ct*PL1B or the mixture of two enzymes showed the weight loss of 9.7%, 12.8% and 17.5%, respectively. The untreated jute fiber (control) showed the weight loss of only 0.3% and whereas the positive control, NaOH treated jute fiber showed 20.1% weight loss (Table 5.1). Jute fibers treated with the mixture of two enzymes gave weight loss similar to that of NaOH treatment.

The cotton fabric treated with *Ct*PME, *Ct*PL1B or the mixture of two enzymes showed the weight loss of 10.0%, 15.1% and 18.3%, respectively. The untreated and chemical treated cotton fabric showed a weight loss of 0.3% and 19.8%, respectively (Table 5.2). The mixed enzymes treated cotton fabric gave similar results weight loss percentage to that obtained by NaOH treatment. The major advantages of bioscouring of enzymatic treatment are (i) saving of time (ii) cost for energy (iii) reduced utilization of water and (iv) reduced environment pollution (Etters, 1999; Tzanoy *et al*., 2001). Abdulrachman *et al*., (2017) reported that bioscouring of Yarn fabric after treatment with endo-polygalacturonase from *A. aculeatus* ATCC16872 caused 5.2% weight loss and wettability 30 s. The present results show that the approach of employing mixture

of enzymes for degumming jute fiber and bioscouring cotton fabric is suitable for replacing the chemical treatment process in textile industry.

Table 5.1 Weight loss of degummed jute fiber by treatment at small scale and scaled up methods.

Treatment method[¥]	10 mg of Jute fiber in 1 ml reaction	100 mg of Jute fiber in 10 ml reaction
	Weight loss (%)	Weight loss (%)
Buffer (50 mM Tris HCl, pH-8.5)	0.3±0.02	0.3±0.05
*Ct*PME (4.2 U/ml, 10 mg/ml)	9.6±0.01	9.7±0.2
*Ct*PL1B (6.0 U/ml, 10 mg/ml)	12.9±0.03	12.8±0.1
Mixture (*Ct*PME+*Ct*PL1B) (each enzyme at 5 mg/ml)	17.7±0.03	17.5±0.2
NaOH (5 g/l)	19.7±0.02	20.1±0.1

[¥] mentioned final treatment under optimized concentrations and degumming time 60 min at 50°C, 100 rpm.

Table 5.2 Weight loss of bioscoured cotton fabric by treatment at small scale and scaled up methods.

Treatment method[¥]	0.1 g of cotton fabric in 2.5 ml reaction	1 g of cotton fabric in 25 ml reaction
	Weight loss (%)	Weight loss (%)
Buffer (50 mM Tris HCl, pH-8.5)	0.3±0.03	0.33±0.2
*Ct*PME (4.2 U/ml, 10 mg/ml)	9.6±0.01	10.0±0.02
*Ct*PL1B (6.0 U/ml 10 mg/ml)	13.1±0.02	15.1±0.2
Mixture (*Ct*PME+*Ct*PL1B) (each enzyme 5 mg/ml)	17.3±0.02	18.3±0.01
NaOH (5 g/l)	19.1±0.01	19.8±0.05

[¥] mentioned final treatment under optimized concentrations and degumming time 60 min at 50°C, 100 rpm.

5.3.3.2 FESEM analysis of Jute fiber and Cotton fabric

The enzyme and NaOH treated scale up jute fibers were analysed by FESEM as mentioned earlier. The FESEM images showed that *Ct*PME, *Ct*PL1B or mixture of enzymes removed wax and pectin and made the surface of jute fiber smooth (Fig. 5.10). The optimal concentration of *Ct*PME or *Ct*PL1B required for efficient jute fiber degumming were 420 U/g or 600 U/g, respectively. The optimum concentration of *Ct*PME and *Ct*PL1B in the mixture of enzymes for degumming of jute fiber was 210 U/g and 300 U/g, respectively. The treatment with mixture of enzymes was better for making the surface smooth than with the individual enzymes and was similar to the results obtained with the chemical treatment (Fig. 5.10). The mixed enzymes degumming of jute fibers made the surface smooth, which is desirable for further processing. This indicated that the treatment of jute fibers with a mixture of *Ct*PME and *Ct*PL1B could be an alternative to the chemical treatment in textile industries making the degumming process ecologically sustainable.

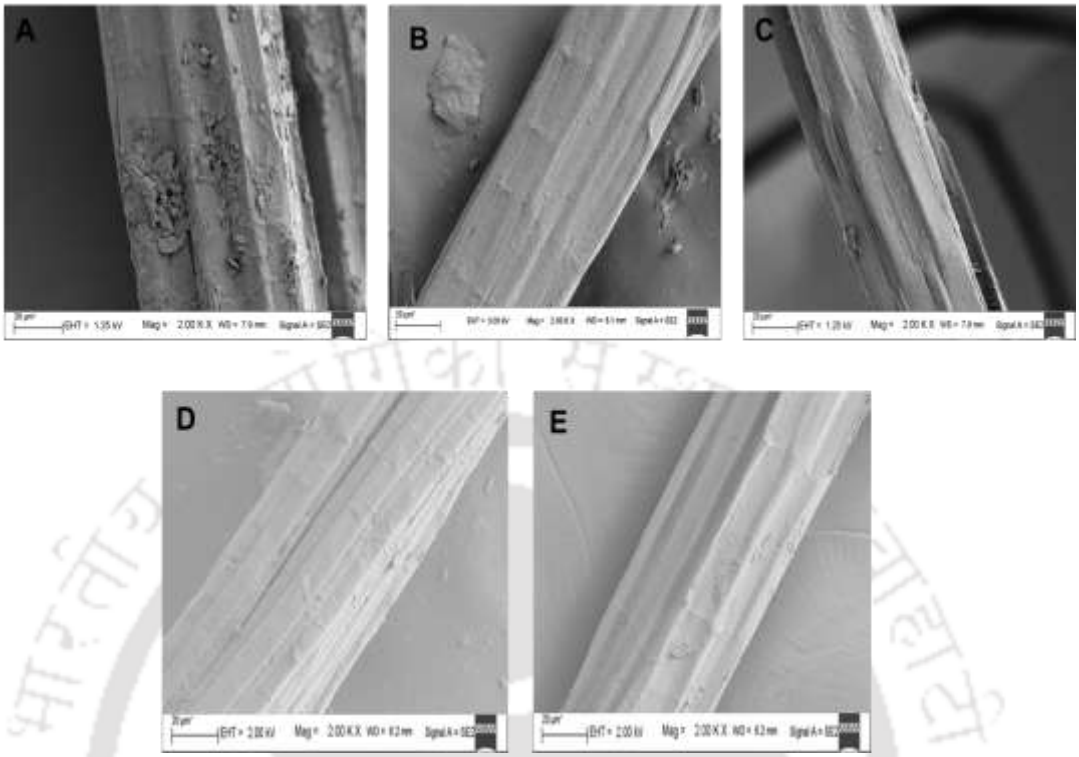

Fig. 5.10 FESEM images of jute fibers degummed under optimized conditions at 50°C and 100 rpm for 60 min, (A) Untreated jute fibers, (B) Degummed jute fibers using *Ct*PME (10 mg/ml, 4.2 U/ml) (C) Degummed jute fibers using *Ct*PL1B (10 mg/ml, 6.0 U/ml) treatment (D) Mixture of *Ct*PME (5 mg/ml, 2.1 U/ml) and *Ct*PL1B (5 mg/ml, 3.0 U/ml) and (E) Chemical (5 g/l NaOH) degumming jute fibers.

The enzyme and NaOH treated scale up cotton fabrics were analysed by FESEM. The FESEM images showed that *Ct*PME, *Ct*PL1B or the mixture of enzymes treated cotton fabric surface is smooth due to the removal of decorated wax and pectin from the samples (Fig. 5.11). Optimum loading of *Ct*PME or *Ct*PL1B enzymes required for effective bioscouring of cotton fabric was 105 U/g and 150 U/g of fabric, respectively. In the case of mixture of enzymes, 52.5 U of *Ct*PME and 75 U of *Ct*PL1B per gram of cotton fabric for bioscouring was found to be optimum. The smoothness of surface of cotton fabric treated by mixture of enzymes was better than the individual enzyme treatments. Wang *et al*., (2006) reported similar observation of parallel ridges

and grooves on the surface enzyme treated cotton fabric. This indicates the removal of pectin and pectin associated waxes by bioscouring (Wang *et al*., 2006; Li and Hardin, 1997). The FESEM images of mixed enzyme treated cotton fabric showed smooth surface, similar to the chemical treatment.

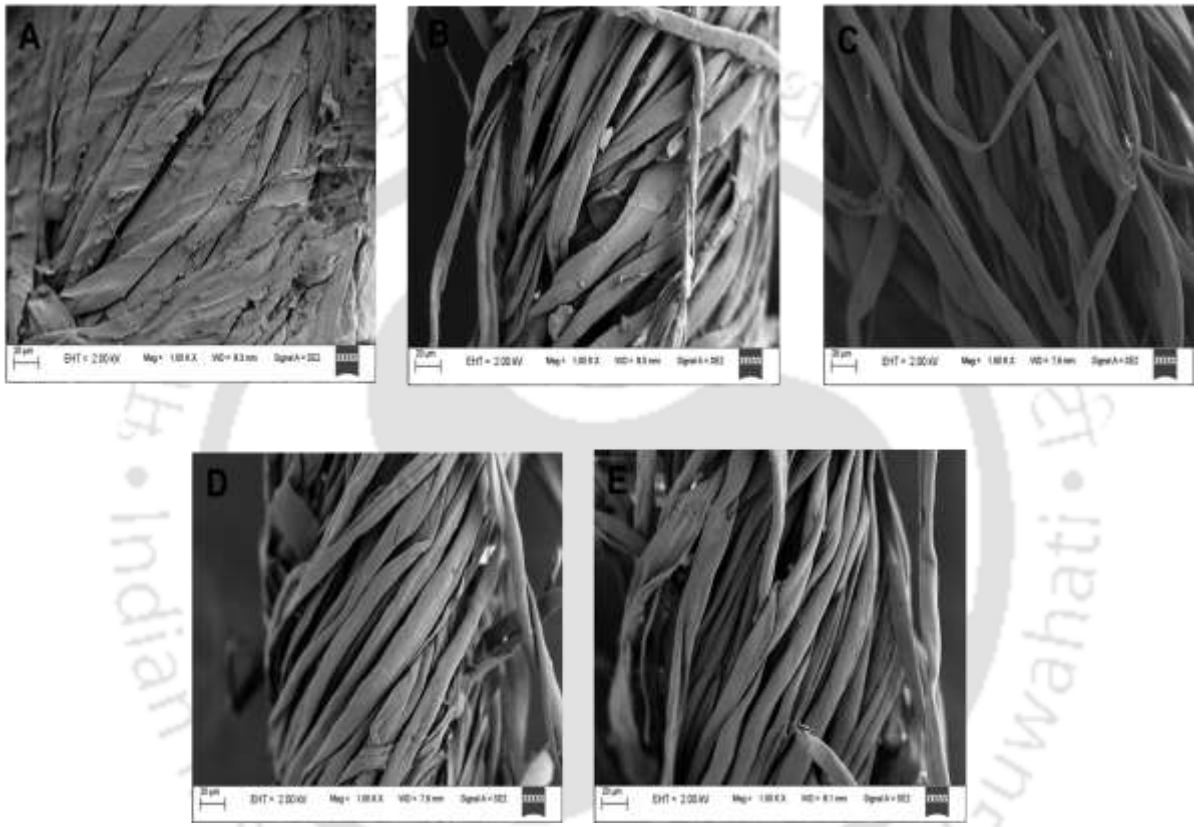

Fig. 5.11 FESEM images of cotton fabric bioscoured under optimized conditions at 50°C and 100 rpm for 60 min. (A) Untreated cotton fabric, (B) Bioscouring cotton fabric using *Ct*PME (10 mg/ml, 4.2 U/ml), (C) Bioscouring cotton fabric using *Ct*PL1B (10 mg/ml, 6.0 U/ml) treatment, (D) Mixture of both enzymes treated cotton fabric using *Ct*PME (5 mg/ml, 2.1 U/ml) and *Ct*PL1B (5 mg/ml, 3.0 U/ml) treatment and (E) Chemical (5 g/l NaOH) scouring cotton fabric.

5.3.3.3 ATR-FTIR analysis of Jute fiber and Cotton fabric

The enzyme and chemical treated jute fibers were analysed by ATR-FTIR. Pectin methylesterase (*Ct*PME) hydrolyzes the C-6 methyl esterified group from α-1,4-galacturonic acid. Pectate lyase (*Ct*PL1B) catalyzes the trans-elimination of α-1,4-glycosidic linkage in pectic acid and forms products with 4,5-unsaturated residues at the non-reducing end. The enzymes and chemical treated jute fiber showed changes in the functional groups observed by ATR-FTIR spectrum (Fig. 12A). ATR-FTIR spectrum of jute fibers showed changes after chemical or enzyme treatment. The intensity of peaks at 3300 cm^{-1} (due to stretching of O–H bonds) and 2918 cm^{-1} (due to stretching of C–H bonds) increased after enzyme and chemical treatment of jute fiber as compared with those of control. This indicated the change in alcohol and alkane groups present in pectin associated gummy material from jute fibers. The enzyme and chemical degummed jute fibers showed significant increase in intensity in peak at 2250 cm^{-1} also, which arose due to stretching of C≡C present in wax associated ester chains. In the ATR-FTIR spectrum of jute fibers treated with NaOH, *Ct*PME or its mixture with *Ct*PL1B the peak at 1731 cm^{-1} (due to stretching of C=O in carboxyl ester) disappeared and the intensity of peak at 1631 cm^{-1} (due stretching of C=O bond of carboxylic group) was reduced. This indicated the loss of methylation present in pectin. These significant changes did not appear in control jute fibers and those treated with *Ct*PL1B spectrum individually. The disappearance of peak at 1731 cm^{-1} indicated the removal of methyl group from pectin, destabilization of waxes and other gummy material (Fig. 5.12A). The peak intensity between 1480-1100 cm^{-1} (due to methyl –C-H bond bending) increased enzyme or chemical treated jute fibers due to removal of methyl group from pectin. Similar observation was reported by Kandimalla *et al.*, (2016). The intensity of

peak at 1025 cm^{-1} due to C-O sharp stretching vibration of alcohol increased in case of chemical or enzyme treated jute fiber which indicates the reduction in glycosidic linkage of the pectin polysaccharide. Similar observation reported by Kandimalla *et al*., (2016) in ramie fiber with NaOH treatment. Similarly, the peaks at 895 cm^{-1} and 550 cm^{-1} due to stretching vibration of C–H and stretching of C–O–C groups, respectively in pyranosyl ring of backbone of pectin indicated the destabilization of pectin polysaccharide backbone. The present enzyme and chemical treatment ATR-FTIR results corroborated with chemical treated jute fiber reported by Wang *et al*., (2019) and Mwaikambo and Ansell, (2002) (chemical treatment of hemp, sisal, jute, and kapok fibers).

The enzyme and chemical treated cotton fabric showed changes in the functional groups as determined by ATR-FTIR spectrum (Fig. 5.12B). ATR-FTIR spectrum showed the increase in intensity of absorption peak at 3403 cm^{-1} (due to stretching of O–H bonds) after enzyme and chemical treatment of cotton fabric as compared with the control, indicating deformation of pectin and pectin associated wax chains. The intensity of peaks between 1749-1631 cm^{-1} (due to C=O ester and carbonyl bonds (1645 cm^{-1}) increased after enzyme and chemical treatment of cotton fabric as compared with the control. This indicated de-esterification of pectin from cotton fabric. The peaks at 2968 cm^{-1} (due to vibration of stretching of C–H bonds) and 1063 cm^{-1} (due to stretching of C–O groups) showed increased intensity for enzyme or chemical treated cotton fabric as compared with the control. Similar observations were reported by Nalankilli *et al*., (2008) (in bunny cotton fabric by chemical and enzyme treatment). This indicated destabilization of pectin polysaccharide present in cotton fabric by enzyme or chemical treatment. The peak at 3742 cm^{-1} (due to stretching of N-H group)

showed decreased intensity after enzyme or chemical treated cotton fabric as compared with the control, which indicated destabilization and removal of amide group of pectin associated with waxes, which was also reported earlier by Rosa *et al*., (2010). The peaks at 896 cm^{-1} and 536 cm^{-1}, representing stretching vibration of C–H and C-O groups respectively, indicated deformation in pectin polysaccharide, as also reported by Liu *et al*., (2016) and Chung *et al*., (2004). The change in pectin structure after enzyme treatment increased the polar functional groups and hence the hydrophilicity on the surface of cotton fabric, which could be the important factor for improved water absorption and dyeing ability as also observed by Brigida *et al*., (2010). The present study, displayed that the mixture enzymes and NaOH treated cotton fabric showed changes in the surface and exposing the functional groups.

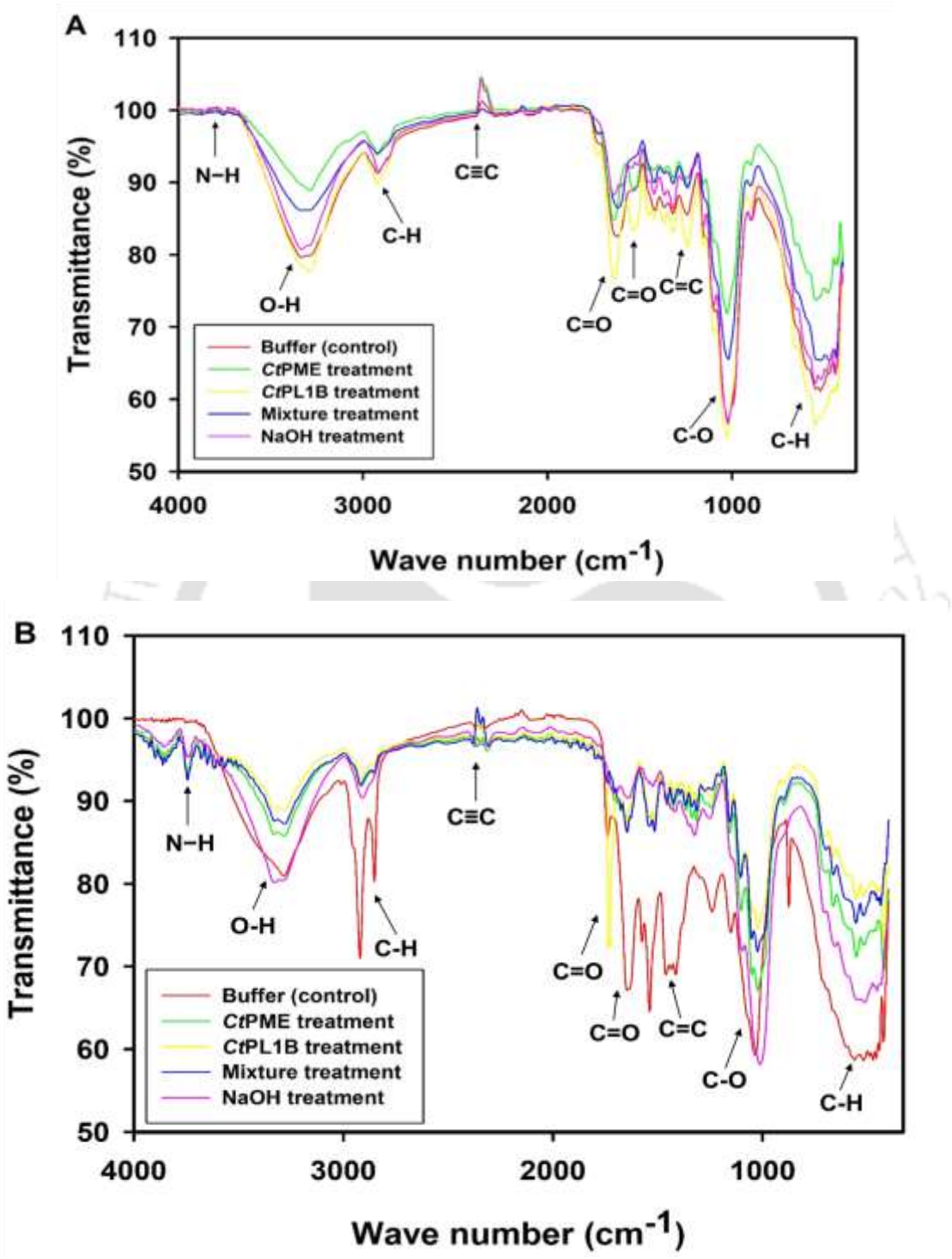

Fig. 5.12 ATR-FTIR analysis of enzyme and chemical treatment A) Degumming of jute fiber and B) Bioscouring of cotton fabric.

5.3.3.4 Contact angle measurement of the cotton fabric

The change in contact angle between the water drop and the surface of cotton fabric with respect to time was measured in case of both enzyme and chemical treated scale up cotton fabric. Reduction in contact angle with time indicates higher wettability and hydrophilic nature of cotton fabric. The digital image frames of water drop are shown in Figure 5.13. The untreated cotton fabric showed a contact angle (θ) of 167˚ at time 0 min and at 30 min the contact angle (θ) was 160˚ (Fig. 5.13A & 13F). The result showed that greige cotton fabric is hydrophobic in nature. *Ct*PME (10 mg/ml, 4.2 U/ml) treated cotton fabric (scale up) showed contact angle (θ) of 167˚ at time 0 s and on increasing the time till 23 s, the contact angle (θ) measured was less than 20˚ (Fig. 5.13B). *Ct*PL1B (10 mg/ml, 6.0 U/ml) treated cotton fabric showed the contact angle (θ) of 165˚ at 0 s, but after 20 s time, the contact angle (θ) was less than 20˚ (Fig. 5.13C). Cotton fabric treated with the mixture of *Ct*PME (5 mg/ml, 2.1 U/ml) and *Ct*PL1B (5 mg/ml, 3.0 U/ml) showed the contact angle (θ) of 165˚ at 0 s and after 10 s, the contact angle (θ) was less than 20˚ (Fig. 5.13D). Similarly, NaOH (5 g/l) treated cotton fabric showed the contact angle (θ) of 165˚ time at 0 s and after 8 s the contact angle (θ) was less than 20˚ (Fig. 5.13E). The cotton fabric treated with NaOH or the mixture of *Ct*PME and *Ct*PL1B showed hydrophilic nature with rapid water absorption capability as compared with the control (Fig. 5.13G). Contact angle θ is inversely proportional to the hydrophilicity of cotton fabric. The results showed that chemically treated cotton fabric was more hydrophilic than control with higher rate of water absorption. In a previous study cotton fabric scoured chemical or pectinase from marine *B. subtilis* showed a contact angle of less than 10° whereas control contact angle was 120° (Joshi *et al.*, 2013). Klug *et al.*, (2006) reported that the contact angle reduced

from 83° to 68° when a plain-woven cotton fabric was treated with endo pectate lyase from *Bacillus pumilus* BK2. Agrawal *et al*., (2007) reported that a contact angle of less than 53° is desirable to achieve sufficient hydrophilicity in the bioscouring process. The present study showed the contact angle of less than 20°, which was much less than the control (167°) and was similar to the values reported earlier (Joshi *et al*., 2013; Agrawal *et al*., 2007; Klug *et al*., 2006).

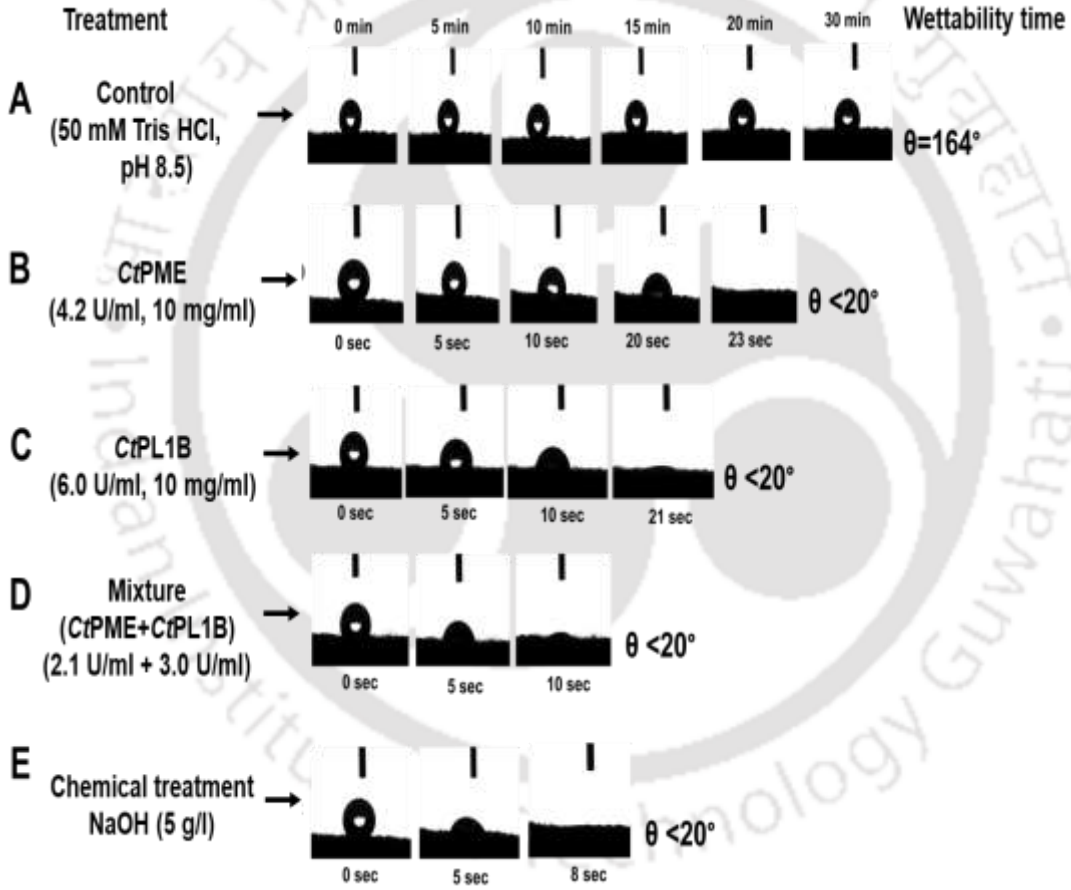

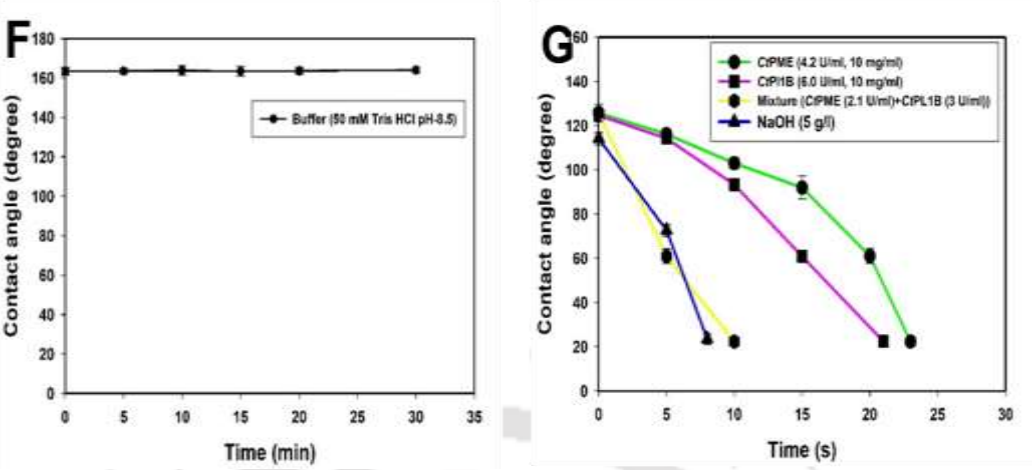

Fig. 5.13 Contact angle measurement of enzymatic and chemically treated cotton fabric. (A) Untreated cotton fabric, (B) *Ct*PME (10 mg/ml, 4.2 U/ml) treated cotton fabric, (C) *Ct*PL1B (10 mg/ml, 6.0 U/ml) treated cotton fabric, (D) Mixture of both enzymes treated cotton fabric using *Ct*PME (5 mg/ml, 2.1 U/ml) and *Ct*PL1B (5 mg/ml, 3.0 U/ml) and (E) Chemically (5 g/l NaOH) treated cotton fabric.

5.3.3.5 Mechanical properties of enzyme treated jute fibers or cotton fabric

The enzyme treated and demoisturized scale up jute fiber and cotton fabric samples were analysed by UTM at 25°C. The jute fiber sample (a bunch approximate 50 fibers) was placed on the sample port. UTM analysis was performed by using the pneumatic pressure control range of 5N-100N. The peaks were analysed and different mechanical properties such as Young's Modulus, Peak Load, Break Load, elongation percentage, Ultimate Tensile Strength (UTS) were determined and are listed in Table 5.3 and Table 5.4. The Young's Modulus of jute fibers degummed by *Ct*PME, *Ct*PL1B, mixture of enzymes and NaOH was 18.06, 25.04, 40.08 and 51.80 [N/mm²], respectively (Table 5.3). The UTS for jute fibers degummed by *Ct*PME, *Ct*PL1B, mixture of enzymes and NaOH was 89.96, 178.43, 245.05 and 262.91 [N/mm²], respectively, (Table 5.3). The Young's Modulus and UTS for untreated jute fibers were 16.08 and 121.69 [N/mm²], respectively (Table 5.3). The enzymes mixture treated jute

fiber Young's Modulus and UTS values were higher than the individual enzyme treated jute fiber neverthless similar to chemical treated jute fiber. Higher values indicated the stronger jute fiber. Saleem *et al*., (2008) reported the tensile strength 171 N/mm^2 for pectinase degummed hemp fiber, which is lower than the value reported in present study.

Table 5.3 UTM analysis of scaled up enzyme and chemical degummed jute fiber.

Treatment method¥	Young Modulus [N/mm²]	Peak Load [N]	Break Load [N]	% Elongation	stress of peak [N/mm²]	Strain %	UTS [N/mm²]
Buffer (50 mM Tris HCl, pH-8.5)	16.08	9.46	0.6	63.6	107.0	0.018	121.7
*Ct*PME (4.2 U/ml, 10 mg/ml)	18.06	10.39	1.4	25.9	89.0	0.074	90.0
*Ct*PL1B (6.0 U/ml, 10 mg/ml)	25.04	16.42	1.6	6.8	5.4	0.026	178.4
Mixture (each 5 mg/ml)	40.08	14.22	0.8	20.8	147.0	0.069	245.0
NaOH (5 g/l)	51.80	10.04	1.6	22.1	86.0	0.024	263.0

¥ mentioned optimized concentration treatment.

The mechanical properties of enzyme and chemically treated cotton fabric were also determined by UTM analysis. The Young's Modulus of cotton fabric bioscoured by *Ct*PME, *Ct*PL1B, a mixture of enzymes and NaOH was 15.7, 18.8, 21.9 and 25.2 [N/mm²], respectively (Table 5.4). The UTS for bioscoured cotton fabric by *Ct*PME, *Ct*PL1B, a mixture of enzymes and NaOH was 68.03, 179.02, 279.48 and 313.26 [N/mm²], respectively (Table 5.4). The Young's Modulus and UTS for untreated cotton fabric were 14.3 and 87.91 [N/mm²], respectively (Table 5.4). The mixture of enzyme was more efficient than individual enzymes in maintaining the strength of the cotton fabric while removing the pectin associated waxy substances.

The mixture of both enzymes treated degumming of jute fiber and bioscouring of cotton fabric showed higher values of Young's Modulus and UTS were observed than individual enzyme treatments (Tables 5.3 & 5.4). The higher values of Young's modulus and UTS indicate that, higher strength will be required to deform the jute fiber and cotton fabric. The values of Young's modulus and UTS was similar in both cases when the mixture of enzymes or NaOH was used for degumming of jute fibers and scouring of cotton fabric (Tables 5.3 & 5.4). Joshi *et al*., (2013) reported a tensile strength of 43.0 N/mm^2 for a pectinase bioscoured cotton fabric, which is much lower as compared with the value of present study.

Table 5.4 UTM analysis of scaled up enzyme and chemical treated cotton fabric

Treatment method¥	Young Modulus [N/mm²]	Peak Load [N]	Break Load [N]	% Elongation	stress of peak [N/mm²]	Strain %	UTS [N/mm²]
Buffer (50 mM Tris HCl, pH-8.5)	14.3	10.90	0.6	20.2	112.7	0.065	87.9
*Ct*PME (4.2 U/ml, 10 mg/ml)	15.7	1.06	0.1	3.1	14.1	0.003	68.0
*Ct*PL1B (6.0 U/ml, 10 mg/ml)	18.8	10.50	2.4	17.0	149.1	0.077	179.0
Mixture (each 5 mg/ml)	21.9	8.50	0.5	13.9	112.4	0.059	279.5
NaOH (5 g/l)	25.2	3.10	0.2	5.9	40.8	0.022	313.3

¥ mentioned final concentration treatment.

5.4 Conclusions

Pectin methylesterase (*Ct*PME) or pectate lyase (*Ct*PL1B) separately and their mixture was used for degumming of jute fiber and bioscouring of cotton fabric. Jute fiber degummed by mixed enzymes showed weight loss similar to NaOH. FESEM analysis showed smooth surface similar to chemically treated jute fibers. Mixed enzyme treatment showed similar wettability of cotton fabric to NaOH. Mixed enzyme degumming of jute fiber or bioscouring of cotton fabric gave Young's Modulus and UTS values similar to NaOH. These results showed that by using the mixture of *Ct*PME and *Ct*PL1B enzymes can replace the chemical treatment process making it green process.

5.5 References

Abdulrachman, D., Thongkred, P., Kocharin, K., Nakpathom, M., Somboon, B., Narumol, N., Chantasingh, D. (2017) Heterologous expression of *Aspergillus aculeatus* endo-polygalacturonase in *Pichia pastoris* by high cell density fermentation and its application in textile scouring. BMC Biotechnology, 17(1): 15.

Agrawal, P. B., Nierstrasz, V. A., Klug-Santner, B. G., Gübitz, G. M., Lenting, H. B., Warmoeskerken, M. M. (2007) Wax removal for accelerated cotton scouring with alkaline pectinase. Biotechnology Journal: Healthcare Nutrition Technology, 2(3): 306-315.

Aly, A. S., Sayed, S. M., Zahran, M. K. (2010) One-step process for enzymatic desizing and bioscouring of cotton fabrics. Journal of Natural Fibers, 7(2): 71-92.

Angelini, L. G., Scalabrelli, M., Tavarini, S., Cinelli, P., Anguillesi, I., Lazzeri, A. (2015) Ramie fibers in a comparison between chemical and microbiological retting proposed for application in biocomposites. Industrial Crops and Products, 75: 178-184.

Anis, P., Eren, H. A. (2002) Comparison of alkaline scouring of cotton vs. alkaline pectinase preparation. AATCC Review, 2(12): 22–26.

Boudart, G., Lafitte, C., Barthe, J. P., Frasez, D., Esquerre-Tugaye, M. T. (1998) Differential elicitation of defense responses by pectic fragments in bean seedlings. Planta, 206(1): 86-94.

Bradford, M. M. (1976) A rapid and sensitive method for the quantitation of microgram quantities of protein utilizing the principle of protein-dye binding. Analytical Biochemistry, 72(1-2): 248-254.

Brigida, A. I. S., Calado, V. M. A., Gonçalves, L. R. B., Coelho, M.A.Z. (2010) Effect of chemical treatments on properties of green coconut fiber. Carbohydrate Polymer, 79: 832–838.

Chakraborty, S., Fernandes, V. O., Dias, F. M., Prates, J. A., Ferreira, L. M., Fontes, C. M., Goyal, A., Centeno, M. S. (2015) Role of pectinolytic enzymes identified in *Clostridium thermocellum* cellulosome. PloS One, 10(2): e0116787.

Chakraborty, S., Rao, J., M., Goyal, A. (2017) Immobilization of recombinant pectate lyase from *Clostridium thermocellum* ATCC27405 on magnetic nanoparticles for bioscouring of cotton fabric. Biotechnology Progress 33(1): 236-244.

Cheng, L., Wang, Q., Feng, X., Duan, S., Yang, Q., Zheng, K., Liu, Z., Peng, Y. (2018) Screening a bacterium and its effect on the biological degumming of ramie and kenaf. Scientia Agricola, 75(5): 375-380.

Chiliveri, S. R., Koti, S., Linga, V. R. (2016) Retting and degumming of natural fibers by pectinolytic enzymes produced from *Bacillus tequilensis* SV11-UV37 using solid state fermentation. Springer Plus, 5(1): 559.

Chung, C., Lee, M., Choe, E. K. (2004) Characterization of cotton fabric scouring by FT-IR ATR spectroscopy. Carbohydrate Polymers, 58(4): 417-420.

Das, B., Chakrabarti, K., Ghosh, S., Majumdar, B., Tripathi, S., Chakraborty, A. (2012) Effect of efficient pectinolytic bacterial isolates on retting and fibre quality of jute. Industrial Crops and Products, 36(1): 415-419.

de Melo da Silva, L. G., de Oliveira, D., Ulson de Souza, A. A., Guelli Ulson de Souza, S. M. (2017) Study and application of an enzymatic pool in bioscouring of cotton knit fabric. The Canadian Journal of Chemical Engineering, 95(7): 1253-1260.

Dhillon, A., Rajulapati, V., Goyal, A. (2018) Bio-scouring of cotton fabric and enzymatic degumming of jute fibres by a thermo-alkaline recombinant rhamnogalacturonan lyase, *Ct*RGL*f* from *Clostridium thermocellum*. The Canadian Journal of Chemical Engineering, 97: 1043–1047.

Duan, S., Cheng, L., Feng, X., Zheng, K., Peng, Y., Liu, Z. (2018) Bio-degumming technology of *Apocynum venetum* bast by *Pectobacterium sp.* DCE-01. Textile Research Journal, 0040517517700198. (this journal follow number only each)

Duan, S., Feng, X., Cheng, L., Peng, Y., Zheng, K., Liu, Z. (2016) Bio-degumming technology of jute bast by *Pectobacterium sp*. DCE-01. AMB Express, 6(1): 86.

Durden, D. K., Etters, J. N., Sarkar, A. K., Henderson, L. A., Hill, J. E. (2001) Applied technology-advances in commercial bio preparation of cotton with alkaline pectinase-bio preparation of cotton is shown to have a positive environmental impact. AATCC review-American Association of Textile Chemists and Colorists, 1(8): 28-31.

Etters, J. N. (1999) Cotton preparation with alkaline pectinase: an environmental advance. Textile Chemist and Colorist and American Dyestuff Reporter, 1(3): 33-36.

Garg, G., Singh, A., Kaur, A., Singh, R., Kaur, J., Mahajan, R. (2016) Microbial pectinases: an ecofriendly tool of nature for industries. 3 Biotech, 6(1): 47.

Gillespie, A. M., Keane, D., Griffin, T. O., Tuohy, M. G., Donaghy, J., Haylock, R. W., Coughlan, M. P. (1990) The application of fungal enzymes in flax retting and the properties of an extracellular polygalacturonase from *Penicillium capsulatum*. In Biotechnology in Pulp and Paper Manufacture, Butterworth-Heinemann, 211-219.

Gummadi, S. N., Kumar, D. S. (2006) Optimization of chemical and physical parameters affecting the activity of pectin lyase and pectate lyase from *Debaryomyces nepalensis*: a statistical approach. Biochemical Engineering Journal, 30(2): 130-137.

Hartzell-Lawson, M. M., Hsieh, Y. L. (2000) Characterizing the noncellulosics in developing cotton fibers. Textile Research Journal, 70(9): 810-819.

Hoondal, G., Tiwari, R., Tewari, R., Dahiya, N. B. Q. K., Beg, Q. (2002) Microbial alkaline pectinases and their industrial applications: a review. Applied Microbiology and Biotechnology, 59(4-5): 409-418.

Imran, M. A., Hussain, T., Memon, M. H., Rehman, M. M. A. (2015) Sustainable and economical one-step desizing, scouring and bleaching method for industrial scale pretreatment of woven fabrics. Journal of Cleaner Production, 108: 494-502.

Jayani, R. S., Saxena, S., Gupta, R. (2005) Microbial pectinolytic enzymes: a review. Process Biochemistry, 40(9): 2931-2944.

Joshi, M., Nerurkar, M., Badhe, P., Adivarekar, R. (2013) Scouring of cotton using marine pectinase. Journal of Molecular Catalysis B: Enzymatic, 98: 106-113.

Kalantzi, S., Mamma, D., Christakopoulos, P., Kekos, D. (2008) Effect of pectate lyase bioscouring on physical, chemical and low-stress mechanical properties of cotton fabrics. Bioresource Technology, 99(17): 8185-8192.

Kalantzi, S., Mamma, D., Kalogeris, E., Kekos, D. (2010) Improved properties of cotton fabrics treated with lipase and its combination with pectinase. Fibres and Textiles in Eastern Europe, 18(5): 86-92.

Kandimalla, R., Kalita, S., Choudhury, B., Devi, D., Kalita, D., Kalita, K., Dash, S., Kotoky, J. (2016) Fiber from ramie plant (*Boehmeria nivea*): a novel suture biomaterial. Materials Science and Engineering: C, 62: 816-822.

Kapoor, M., Beg, Q. K., Bhushan, B., Singh, K., Dadhich, K. S., Hoondal, G. S. (2001) Application of an alkaline and thermostable polygalacturonase from *Bacillus sp*. MG-cp-2 in degumming of ramie (*Boehmeria nivea*) and sunn hemp (*Crotalaria juncea*) bast fibres. Process Biochemistry, 36(8-9): 803-807.

Khan, M. M., Choi, Y. S., Kim, Y. K., Yoo, J. C. (2018) Immobilization of an alkaline endopolygalacturonase purified from *Bacillus paralicheniformis* exhibits bioscouring of cotton fabrics. Bioprocess and Biosystems Engineering, 41(10): 1425-1436.

Klug-Santner, B. G., Schnitzhofer, W., Vrsanska, M., Weber, J., Agrawal, P. B., Nierstrasz, V. A., Guebitz, G. M. (2006) Purification and characterization of a new bioscouring pectate lyase from *Bacillus pumilus* BK2. Journal of Biotechnology, 121(3): 390-401.

Li, Y., Hardin, Z. R. (1997) Enzymatic scouring of cotton: effects on structure and properties. Cellulose, 94(88): 96-100.

Liu, S. Q., Chen, Z. Y., Sun, J. P., Long, J. J. (2016) Ecofriendly pretreatment of grey cotton fabric with enzymes in supercritical carbon dioxide fluid. Journal of Cleaner Production, 120: 85-94.

Micheli, F. (2001) Pectin methylesterases: Cell wall enzymes with important roles in plant physiology. Trends in Plant Science, 6: 414–419.

Morozova, V. V., Semenova, M. V., Salanovich, T. N., Okunev, O. N., Koshelev, A. V., Bubnova, T. V., Sinitsyn, A. P. (2006) Application of neutral-alkaline

pectate lyases to cotton fabric boil off. Applied Biochemistry and Microbiology, 42(6): 603-608.

Murad, H. A., Azzaz, H. H. (2011) Microbial pectinases and ruminant nutrition. Research Journal of Microbiology, 6(3): 246-269.

Mwaikambo, L. Y., Ansell, M. P. (2002) Chemical modification of hemp, sisal, jute, and kapok fibers by alkalization. Journal of Applied Polymer Science, 84(12): 2222-2234.

Nalankilli, G., Saravanan, D., Govindaraj, N., Harish, P. (2008) Efficacy of solvent, alkali and pectinase on removal of non-cellulosics from cotton fibres. Indian Journal of Fibre and Textile Research, 33: 438–442.

Pedrolli, D. B., Monteiro, A. C., Gomes, E., Carmona, E. C. (2009) Pectin and pectinases: production, characterization and industrial application of microbial pectinolytic enzymes. Open Biotechnology Journal, 3: 9-18.

Rajulapati, V., Goyal, A. (2017) Molecular cloning, expression and characterization of pectin methylesterase (*Ct*PME) from *Clostridium thermocellum*. Molecular Biotechnology, 59(4-5): 128-140.

Rosa, I. M., Kenny, J. M., Maniruzzaman, M., Monti, M., Puglia, D. (2010) Effect of chemical treatments on the mechanical and thermal behaviour of okra (*Abelmoschus esculentus*) fibres. Compositional Science Technology, 71: 246–254.

Saleem, Z., Rennebaum, H., Pudel, F., Grimm, E. (2008) Treating bast fibres with pectinase improves mechanical characteristics of reinforced thermoplastic composites. Composites Science and Technology, 68(2): 471-476.

Shanthi, R., Krishnabai, G. (2013) Process optimization for bioscouring of cotton and lycra cotton weft knits by Box and Behnken design. Carbohydrate Polymers, 96(1): 291-295.

Wang, H., Memon, H., AM Hassan, E., Miah, M., Ali, M. (2019) Effect of jute fiber modification on mechanical properties of jute fiber composite. Materials, 12(8): 1226.

Wang, M., Yuan, D., Gao, W., Li, Y., Tan, J., Zhang, X. (2013) A comparative genome analysis of PME and PMEI families reveals the evolution of pectin metabolism in plant cell walls. PLoS One, 8(8): e72082.

Wang, Q., Fan, X., Gao, W., Chen, J. (2006) Characterization of bioscoured cotton fabrics using FT-IR ATR spectroscopy and microscopy techniques. Carbohydrate Research, 341(12): 2170-2175.

Wolf, S., Mouille, G., Pelloux, J. (2009) Homogalacturonan methyl-esterification and plant development. Molecular Plant, 2(5): 851-860.

Wu, H. C., Huang, Y. C., Stracovsky, L., Jinn, T. L. (2017) Pectin methylesterase is required for guard cell function in response to heat. Plant Signaling and Behavior, 12(6): e1338227.

Zhou, C., Xue, Y., Ma, Y. (2017) Cloning, evaluation, and high-level expression of a thermo-alkaline pectate lyase from alkaliphilic *Bacillus clausii* with potential in ramie degumming. Applied Microbiology and Biotechnology, 101(9): 3663-3676.

Chapter 6

Extraction, characterization and anti-cancer activity of pectic oligosaccharides produced from agro-waste of Orange (*Citrus reticulate*) peels

6.1 Introduction

Pectin is a complex natural hetero polysaccharide present in primary plant cell walls. It is an acidic and negatively charged high molecular mass polymer (Murad and Azzaz, 2011). Pectin polysaccharide backbone consists of α (1→4) linked galacturonic acid units (Wang et al., 2015). Pectin polysaccharide may also be methylated ester or acetylated polygalacturonic acid (Sriamornsak, 2003). Pectins are commercially available from natural fruit peels especially citrus, apple, sugar beet and potato. Pectin is a byproduct of fruit juice industry from peel waste (Kratchanova et al., 2004). Citrus peels, apple pomace, sugar beet and potato contains 20-30%, 10-15%, 5-8% and 2-5% of pectin, respectively. Degree of esterification (DE) is an important factor in pectins and their function. Based on DE pectin is categorized into two types, which are high methoxyl pectins (DE>50%) and low methoxyl pectins (DE<50%). Pectin is used in various industry applications such as food, health and pharmaceutical industries (Voragen et al., 2009). Pectin has been used as stabilizer, texturizer, thickener and

emulsifier agent in food and beverage industry (Kermani et al., 2015). Pectin is widely used as a gelling agent in making low calorie products of jellies and jam for diabetics and overweight patients (Gardner et al., 1984). It has also found applications in reducing the blood cholesterol and lowering the low density lipoprotein (Fraser, 1994). Pectin polysaccharide is degraded by pectinases. Major pectinases fall into two main groups, methylesterases and depolymerases. Pectin methylesterases (PME: EC 3.1.1.11), catalyze the removal of the methyl group (de-esterification) from pectin. Depolymerases are classified into two types, hydrolases and lyases. Hydrolases act on the backbone of pectin by hydrolytic cleavage and lyases by trans-eliminative cleavage (Wang et al., 2013). Polygalacturonase (PG: EC 3.2.1.15) catalyses α (1→4) glycosidic linkages of pectin by hydrolytic cleavage (Boudart et al., 1998) while, pectate lyase (PL: EC 4.2.2.2) catalyses the pectin via β-elimination reaction (Chakraborty et al., 2015; Garg et al., 2016).

Colorectal cancer is the 2nd most leading cancer, causing death (Centelles, 2012). Annually, there are 1.8 million colorectal cancer cases and around 50% cases are fatal (World Health Organization, 2018). Several treatments are available to treat colorectal cancer such as surgery, chemotherapy, radiotherapy and immunotherapy (Zhang et al., 2013). However, until now none of them is reliable to cure colorectal cancer. Nowadays, a new way is emerging to treat colorectal cancer by using food additives in diets (Cheong et al., 2010). Pectin and pectic oligosaccharides were reported as an effective inhibitor against proliferation and metastasis, induction of apoptosis in cancer cells thus decreasing the chance of tumor incidence (Jackson et al., 2007). Pectin can block the lipopolysaccharide (LPS) signalling pathway during macrophage activation thus can be an important agent in cancer chemoprevention and

anti-inflammation (Chen *et al*., 2006). Galectin 3 (Gal3) is a conserved evolutionary protein found in all species ranging from lower invertebrates to mammals. Gal3 actively participate in cancer progression and metastasis, it can be activated by glucoconjugates like laminin or fibronectin (Kuwabara and Liu, 1996). Once activated Gal3 mediates self-aggregation of cells, thus allowing detachment of primary tumour cells and progression of secondary tumour (Nangia-Makker et al., 2000). The galacturonic moiety of pectin can successfully bind to carbohydrate recognition domain of Gal3 and hinders its activation, thus inhibiting cell migration and metastatic spread (Inohara and Raz, 1994). Hence pectic oligosaccharides under study when incubated with HT-29 cells might have interacted with the Gal3 and resulted in reduced cell viability (Greco et al., 2004).Pectin and pectic oligosaccharides are dietary food products, which showed significant anti-proliferation activity against cancer cells by inhibiting Gal-3 pathway in metastasis (Cheong et al., 2010).

In this study, pectin was extracted from orange peels using ultrasound assisted extraction method. The physicochemical and structural properties of extracted pectin were characterised. The pectic oligossacharides (POS) were produced by a pectate lyase (*Ct*PL1B) or mixture of *Ct*PME and *Ct*PL1B from *Clostridium thermocellum*. Then *in vitro* study was performed to see the effect of pectic oligosaccharides produced from combinations of enzymes (*Ct*PL1B or *Ct*PME and *Ct*PL1B) on colon cancer (HT29) or normal human embryonic kidney (HEK293) cells.

6.2 Materials and methods

6.2.1a Raw material collection and processing

Sweet oranges (*Citrus reticulate*) were purchased from local market at Guwahati, Assam, India. The peels (~1.6 kg) were washed with water, finely cut with a size of approximately, 3 cm X 3 cm with a knife. The cut fragments were placed on tray and dried in a hot air oven at 70°C for 3-4 days. The dried peels were milled in an electrical grinder (mixture) to obtain powdered sample. The powder was stored in sample bottle with tight cap and kept in a dry environment prior to the experimental analysis.

6.2.1b Chemicals, cell lines and Substrates

Chemical: Oxalic acid, Ammonium oxalate, Sodium nitrate, Sulphuric acid, Hydrochloric acid, ethanol (98.9%) and sodium azide were purchased from Himedia, India. Sulfuric acid, Trifluoroacetic acid, Whatman No. 3, TLC plates (Silica coated aluminium plates) and Deuterium oxide were purchased from Merck Chemical Co. (Darmstadt, Germany). Alcohol oxidase, KBr, cell culture medium RPMI-1640, DMEM low glucose and Thiazolyl Blue Tetrazolium Bromide powder (MTT) were procured from Sigma-Aldrich Pvt. Ltd. Human colon cancer cell line (HT29) and Human embryonic kindney cell line (HEK293) were procured from National Centre for Cell Science-Pune, India.

Substrates: Citrus pectin (>85% esterified, CP) and Polygalacturonic acid (PGA) were purchased from Sigma-Aldrich, USA.

6.2.2 Methods

6.2.2.1 Extraction of pectin from orange peels

Pectin was extracted from agro-waste orange peel powder (OPP) by Ultrasound Assisted Extraction (UAE) method showed flow chart Fig. 6.1 (Johnson et al., 2007). The extraction of pectin from OPP was achieved by using the ammonium oxalate-oxalic acid, as the extracting solvent (Johnson et al., 2007). The solution containing 0.1 M ammonium oxalate and 0.1 M oxalic acid was prepared and adjusted to pH 3.4 (with 1N HCl). The 25 g of OPP was dissolved in 500 ml of 0.1 M ammonium oxalate-oxalic acid solution maintaining solid-liquid ratio of 1:20 (w/v). The extraction was performed in sonicator water bath (Ultrasonic bath, Elmasonic, Germany). UAE was carried out at frequency of 37 kHz, 80°C for 30 min. After sonication, the mixture was allowed to cool down to 25°C and then filtered through muslin cloth followed by filter paper (Whatman filter paper No. 3). The filtrate was collected in flask and three volumes of chilled ethanol (96%) was added to it and kept at 4°C for 12 h for precipitation of pectin polymer. The solid retentate (UAE treated OPP) obtained after UAE treatment was again dissolved in 0.1 M ammonium oxalate-oxalic acid solution and process was repeated. The precipitated orange pectin polymer was separated by filtration using filter paper (Whatman No. 3). The separated orange pectin was washed with 70% (v/v) ethanol and followed by 96% (v/v) ethanol. Finally, extracted orange pectin was washed with 98% (v/v) acetone to remove the monosaccharides and disaccharides (Minkov et al, 1996). The wet extracted orange pectin (EOP) was dried at 40°C in the hot air oven for 12 h (Grassino et al., 2015). The pectin extraction yield was calculated as follows Eq. (1).

$$\text{Pectin Yield (\%)} = \frac{\text{EOP } (W_3)}{\text{OPP}_{\text{Initial}} (W_1) - \text{OPP}_{\text{Residue}} (W2)} \times 100 \qquad \text{Eq 1}$$

Where,

$OPP_{Initial}$ (W_1) = Weight of initial orange peels powder (g),

$OPP_{Residue}$ (W_2) = Weight of filtrate orange peels powder after UAE (g) and

EOP (W_3) = Weight of extracted dried pectin from orange peels (g).

6.2.2.2 FESEM analysis of untreated OPP and UAE treated OPP

The surface morphology of untreated OPP, UAE treated OPP and EOP was analyzed by Field Emission Scanning Electron Microscopy (FESEM). 10 mg of dried untreated OPP or UAE treated OPP was dissolved in 1 ml Milli-Q water. 40 µl each of these samples were placed on glass piece covered with aluminum foil and dried at 80°C for 12 h prior to analysis. The samples were placed on carbon tape covered by FESEM stub and coated with gold ~10 nm thick layer by using a gold coating sputter (HITACHI E-1010 ion sputter) (double coat) at 30 kV for 20 min. The sample stub was analysed by In-Lens SE1 mode. The images were recorded on FESEM (Zeiss, Sigma, Germany) at an accelerating voltage of 2.0 kV at 5000X magnification.

6.2.2.3 FTIR analysis of untreated OPP and UAE treated OPP

Fourier transform infrared spectroscopy **(**FTIR) spectroscopy (Perkin Elmer, Spectrum Two, USA) was used for determining the functional groups present in the raw, UAE treated OPP and EOP. The raw or UAE treated orange peel powder were mixed with KBr in a (sample: KBr) ratio of 1:100 and made a fine powder by using mortar and pestle (Wang et al., 2015). The sample-KBr mixture was pressed to make a pellet by using 15 Ton Hydraulic Press. FTIR spectrophotometer was used to acquire

the spectrum in range of 4000-500 cm^{-1} region in transmission mode. The spectrum was recorded in 32 scans per min and at a resolution of 4 cm^{-1}.

6.2.2.4 Brunauer–Emmett–Teller (BET) analysis of OPP

The surface area, pore size and pore size distribution of raw and UAE treated orange peel powder were measured by sorption analysis (Autosorb-IQ MP, Quantachrome, USA). The samples were dried at 80°C in oven for 12 h prior to the analysis. 100 mg of dried samples were weigh in specialized BET glass tube and degassed at 100°C for 3 h by keeping in a liquid N_2 sorption container (2 L capacity). The degassed samples were further analysed by BET with nitrogen partial pressure (P/P_0) in the range of 3.4×10^{-4} to 0.99.

6.2.2.5 FESEM and FESEM-EDX analysis of EOP

EOP was subjected to surface view and elemental analysis by FESEM and FESEM-Energy-dispersive X-ray spectroscopy **(**FESEM-EDX). The 3 mg sample was dried at 60°C for 12 h and was placed on the FESEM stub using carbon tape and then the gold coating was carried out by sputter (HITACHI E-1010 ion sputter). The sample stubs were analysed by SE2 (Secondary Electron) mode. The image was observed on a FESEM (Zeiss, Sigma, Germany) at an accelerating voltage of 3.0 kV keeping 2000X magnification.

6.2.2.6 AFM analysis of EOP

The Atomic Force Microscope (AFM) was used to determine the surface by using a small probe within the range, 1-10 nm. The EOP sample was analysed by using the MFP-3D-BIO (Cypher, Asylum Research AFM, Oxford Instruments, USA). The stock solution of EOP (1 mg/ml) was prepared in Milli-Q water. 10 µg/ml EOP as working solution was used and 10 µl of sample was dropped on the surface of glass

slide and allowed to dry at 40°C for 12 h. The EOP powder sample was placed on double-sided adhesive tape and then placed on AFM specimen disc. The imaging process was carried out by using Igor Pro 6.37 software. The cantilever tip set point, frequency, amplitude and integral force were 600 mV, 161.3 kHz, 223.3 mV and 30 N/m, respectively. The scan rate of the tip was 0.5–2 Hz and the scan speed of 45.5 m/s with 90° of scan angle. The analysis was performed using tapping imaging mode. The WSxM 5.0 develop 9.1 software was used to further processing of data in offline (Rani et al., 2017).

6.2.2.7 Monosugar composition analysis of EOP

The neutral sugar composition analysis was assessed by using HPLC. The EOP was hydrolyzed by trifluroacetic acid hydrolysis (2 M TFA, 5 h at 80°C) as described in Wikiera et al., (2015). The solutions were filtered through 0.45 µm membrane filters (Axiva, India), before analysis. Individual neutral sugars released from EOP pectin were analysed by an Ion exclusion column [Phenomenex Rezex ROA (H^+) (300 × 7.8 mm)] attached to a guard column [Phenomenex Rezex ROA (H^+) (50 × 7.8 mm)] both connected to HPLC system (Shimadzu, Japan) and column temperature was maintained at 40°C. The method was run in an isocratic mode with mobile phase of 5 mM H_2SO_4 at the flow rate 0.5 ml/min and acquisition time 30 min. Injection volume was kept constant at 10 µl and the data was acquired using RI and UV detectors. The standard monomers D-galacturonic acid, galactose (Gal), rhamnose (Rha), arabinose (Ara), glucose (Glc), mannose (Man) and xylose (Xyl) (Sigma Aldrich, USA) were used as the calibration standard to calculate the individual sugar composition present in EOP.

6.2.2.8 Molecular weight determination and distribution of EOP by HPSEC

The molecular weight distribution of EOP was assessed by High-performance size exclusion chromatography (HPSEC) following the method of Li et al., 2016. The HPSEC system (Shimadzu, Japan) was connected with a size exclusion column [Phenomenex Polysep-GFC-P6000 (300 x 7.8 mm)] attached to a guard column [Phenomenex Polysep-GFC-P (35 x 7.8 mm)] and equipped with RI detector (RID-20A). The mobile phase used was 0.1 M $NaNO_3$ at a flow rate 0.5 ml/min with run time 30 min. The injection volume was 10 µl and column temperature was kept 40°C. The dextran standards of different molecular mass [T10 (10 kDa), T20 (20 kDa), T40 (40 kDa), T70 (70 kDa), T100 (100 kDa), T200 (200 kDa), T270 (270 kDa) and T500 (500 kDa)] each at 1 mg/ml was used for generation of a calibration standard plot to calculate the molecular mass of EOP. First the EOP (1 mg/ml) sample was analysed by HPSEC for Molecular mass determination. Further, 50 mg/ml of EOP was run through HPSEC system to obtain purified EOP for further characterization. The purified EOP was dialyzed against 2 liter Milli-Q water at 4°C with 4 changes for 24 h to remove the salts. The dialyzed solution of EOP was lyophilized and stored at 25°C in 10 ml storage vials.

6.2.2.9 DLS analysis of EOP

The particle size and Zeta potential of EOP was determined by Dynamic Light Scattering (DLS) (Zetasizer nano, Malvern, UK). 1 mg of EOP pectin was dissolved in 1 ml of Milli-Q water, centrifuged at 1000*g* and filtered with 0.45 µm membrane filter. The data were acquired at constant temperature of 25°C as maintained by Joule-Peltier thermostat. The DLS system consisted of a Malvern optics with a 5 mW helium-neon laser and viscosity was set to 0.8 cP. The ZetaSizer worked at a fixed scattering angle of 90° and the wavelength of the laser beam was 632 nm. The dispersions were

measured in 10 mm quartz cuvettes kept in ZetaSizer measuring cell. The integrated control software was used to get the size and charge distribution of result peak with intensity autocorrelation function (Cumulant fit). The samples were run in six scan replicates and each experiment was conducted thrice. The co-efficient of variation for the size measurement was less than 5%, signifying the reproducibility and accuracy of the experiment. All the measurements were well-distinguished from each other.

6.2.2.10 Degree of Esterification of EOP

The degree of esterification (DE) was determined by FTIR spectrum analysis as mentioned by Chaouch et al., (2016b). The sample was prepared as mentioned section 6.2.2.3. It is a ratio between the peak absorbance of methylated carboxyl groups and sum of methylated carboxyl groups and free carboxyl groups present in spectrum. The peak range of methylated carboxyl and free carboxyl groups were 1700-1750 cm^{-1} and 1630-1645 cm^{-1}, respectively. The percentage of DE was determined according to Eq. (2 & 3).

$$\text{Degree of Esterification (\%)} = \frac{A_{1735}}{A_{1735} + A_{1635}} \times 100 \qquad \text{Eq 2}$$

$$\text{Absorbance (A)} = 2 - \log(\%T) \qquad \text{Eq 3}$$

Where,

A_{1635} = Absorbance at 1635 cm^{-1} for non-methyl-esterified carboxyl groups

A_{1735} = Absorbance at 1735 cm^{-1} for methyl-esterified carboxyl groups,

(%) T = Transmittance percentage

6.2.2.11 NMR spectroscopic analysis of EOP

30 mg of lyophilized EOP pectin was dissolved in 1 ml D_2O (99.96%) (Merck, Germany) with addition of NaOD (10 µl) and subjected to Nuclear magnetic resonance (NMR) spectroscopic analysis. The proton NMR spectrum was obtained at 25°C and 16 scans were collected with a relaxation delay of 1 s using 600 MHz NMR spectrometer (Bruker, Avance III-HD, USA). Subsequently, the ^{13}C NMR was performed and in which, 3200 scans were used for collection of spectrum. ^{1}H & ^{13}C NMR spectra was acquired at fitted with a 5-mm probe and equipped with TOPSPIN software (Bruker) for analysis. The chemical shifts of ^{1}H &^{13}C were reported in parts per million (ppm) relative to internal reference as Tetramethylsilane (TMS). All NMR experiment were carried out by using the pulse sequences provided by Bruker.

6.2.2.12 TGA and DSC analysis of EOP

The degradation temperature and phase shift of EOP was analysed by Thermogravimetric Analysis (TGA) and Differential scanning calorimeter (TGA-DSC), the thermal analyzer (NETZSCH STA 449F3A-0232-M, USA). The EOP (8 mg) was placed in a crucible (Al_2O_3) and purge with the nitrogen or argon gas their respective jacket chambers. The empty crucible (without EOP) was used as a blank. The gases (nitrogen or argon) were used to remove the oxygen from respective chambers. The setup gas flow rate was 100 ml/min and a linear heating rate of 10 °C/min was used over a temperature range of 25°C-900°C. The weight loss was determined with respect to the linear increase in temperature. Derivative Thermogravimetric Analysis (DTG) was obtained from TGA graph. Similarly, the DSC analysis of EOP was carried out using thermal analyzer and enthalpy changes were determined.

6.2.2.13 XRD analysis of EOP

The X-ray powder diffraction **(**XRD) pattern of EOP extracted under optimal conditions was recorded using an X-ray diffractometer (Rigaku TTRAX III, USA). The dried 50 mg EOP pectin sample was placed on glass slide and loaded on XRD. The EOP was subjected to X-ray radiation of Cu/Kα with a wavelength of 1.54 Å and maintained 40 kV and 40 mA. The determination of trace phases in powdered samples benefit greatly from its 18 kW rotating anode X-ray source. The sample was scanned with diffraction angle (2θ) between 10° to 70° and the scan speed of 3° per minute. The step size and step time were used 0.05° (2θ) and 1 s/step, respectively. XRD data measurements were made using a high power (18 kW). From Segal *et al.*, (1962) formula, the crystallinity index (CrI) of the sample was determined by Eq. (4).

$$\text{Crystallinity Index (CrI, \%)} = \frac{I_{Crystalline} - I_{Amorphous}}{I_{Crystalline}} \times 100 \qquad \text{Eq 4}$$

Where,

$I_{Crystallinity}$ = Intensity of Crystallinity peak

$I_{Amorphous}$ = Intensity of amorphous peak

6.2.2.14 Enzyme activity against EOP

EOP was used as substrate for measuring the activity of pectin methylesterase (*Ct*PME) and pectate lyase (*Ct*PL1B) from *Clostridium thermocellum*. Pectin methylesterase activity was assayed by the method described by Rajulapati and Goyal, (2017) and pectate lyase activity was measured as explained by Chakraborty et al., (2015) using EOP as substrate. The de-esterification reaction was carried out by taking *Ct*PME (8 µg/ml) in 1 ml reaction mixture containing EOP (1%, w/v) dissolved in 50 mM Tris-HCl buffer, pH 8.5 incubating at 50°C for 15 min (Rajulapati and Goyal,

2017). The digestion of EOP with *Ct*PL1B (7 µg/ml) was carried out in 1 ml reaction mixture containing, 1% (w/v) EOP in 50 mM Glycine-NaOH buffer, pH 9.8 and 0.6 mM $CaCl_2$ by incubating at 50°C for 15 min (Chakraborty et al., 2015). The digestion of EOP was carried out by using a mixture of *Ct*PME (8 µg/ml) and *Ct*PL1B (7 µg/ml) in 1 ml reaction mixture containing, 1% (w/v) EOP in 50 mM Tris-HCl buffer, pH 8.5 and 0.6 mM $CaCl_2$ by incubating at 50°C for 15 min.

6.2.2.15 TLC, HPLC and ESI-MS analysis of EOP pectic oligosaccharides

*Ct*PL1B, *Ct*PME or *Ct*PL1B along with *Ct*PME were used to cleave the EOP as mentioned in section 2.2.14. Each of 1 ml reaction was stopped by adding 2 ml of absolute ethanol to precipitate the un-lysed EOP. However, the reaction of *Ct*PME with EOP, leads to the formation of only de-esterified EOP and not POS. Therefore, the de-esterified EOP is differentiated from un-lysed EOP, by designating it as Pectic polysaccharide (PP). The precipitated un-hydrolyzed EOP, enzyme-hydrolyzed products and PP in the supernatant were separated by centrifugation at 13000g for 20 min. PP was washed with 1 ml of Milli-Q water for 4 times and dried in hot air oven to remove ethanol for further use. The supernatant containing the enzyme lysed products were further concentrated to 100 µl in hot air oven at 80°C. 1 µl sample of enzyme lysed products (pectic oligosaccharides, POS) and standards (1 mg/ml, D-galacturonic acid, di-galacturonic acid and tri-galacturonic acid) were loaded on the TLC plate. The TLC was run and the products were visualized as mentioned earlier by Chakraborty *et al*., (2015). The POS mixtures produced from *Ct*PL1B and *Ct*PL1B+*Ct*PME treatment were lyophilized. The lyophilized sample, 1 mg was dissolved in 1 ml of MilliQ water and filtered through 0.2 µm membrane. The samples were injected to the HPLC system as mentioned in section 2.2.7. The chromatogram was analysed by Lab solutions software

(Shimadzu, Japan). The enzyme lysed product samples were further analyzed by Electron Spray Ionization (ESI) mass spectrometer (Waters, Q-TOF Premier) in MS mode. The samples were analyzed by negative ion mode in ESI–MS. The N_2 gas was purged and the atmospheric pressure ionization and vent vacuum were maintained in ESI-MS mode. The parameters for ESI–MS analysis were capillary voltage 3 eV, collision energy 5 eV, ionization energy 1 eV, desolvation temperature 350°C and the source temperature 90°C.

6.2.2.16 Biocompatibility and Anticancer activity assay of PP, POS and mPOS

The normal human embryonic kidney (HEK293) cells and colon cancer (HT29) cells (procured from National Centre for Cell Science-Pune, India) were cultured in DMEM (low glucose medium) and RPMI-1640 medium, respectively. Both the media were supplemented with 10% (v/v) heat-inactivated fetal bovine serum (FBS) (Gibco, USA), 50 µg/ml streptomycin and 50 IU/ml penicillin (Gibco, USA). HT29 or HEK293 cells were incubated at 37°C, under 5% CO_2 with Relative Humidity, RH-95%. The effect of POS on viability of HEK293 and HT29 cells was analysed by MTT [3-(4,5-dimethylthiazol-2-yl)-2,5-diphenyltetrazolium bromide] reduction assay (Mosmann, 1983). 2×10^4 cells/well were seeded in a 96 well plate and incubated at 37°C in 5% (v/v) CO_2 with 95% relative humidity for 12 h for cell adherence. After incubation, the medium was completely removed and washed with 200 µl of 1X phosphate buffer saline (PBS, pH 7.4). The cells were treated with different concentrations (0.1 mg/ml to 1 mg/ml) of POS dissolved in serum-free DMEM medium. The serum free DMEM medium and RPMI 1640 without POS was used as negative control. The plates were incubated at 37°C in 5% CO_2 for 24 h and 48 h. The cell viability assay was performed by removing the medium and by adding 100 µl of MTT (0.5 mg/ml) to each well. The

plates were further incubated at 37°C in 5% CO_2 for 4 h. After the incubation, MTT was removed from the wells without disturbing the formazan crystals. The crystals were dissolved by adding 100 µl of dimethyl sulfoxide. The absorbance was monitored at 570 nm and 690 nm by a 96-well microplate reader (Tecan, Infinite 200 Pro, Switzerland). The cell viability (%) was calculated according to method of Rani *et al*., (2017). The cell morphology of HEK293 and HT29 cells after treatment with POS or PP were also observed under microscope (Nikon, TS100F, Japan) and photo images were taken and processed using imaging software (Nikon NIS-Element, NIS 40000) .

$$\text{Cell Viability (\%)} = (Nt/Nc) \times 100 \qquad \text{Eq 5}$$

Where,

Nt is the absorbance of treated cells and

Nc is the absorbance of untreated cells.

6.3 Results and Discussion

6.3.1 Extraction of pectin from orange peels

The pectin was extracted from orange peel waste by using the Ultrasound assisted extraction method (UAE) as shown in Fig. 6.1. The percentage yield of pectin obtained from 1st and 2nd extraction, were 9.8% and 23.3%, respectively. The increase in pectin yield in 2nd extraction as compared with the 1st extraction, was due to the structure loosening of the orange peel powder and destabilization due to the ultrasonic vibration. Similar results were reported in a previous study (Grassino et al., 2015). The 1st extraction gave thick solid flakes of EOP and its solubility was poor as compared with EOP obtained from the 2nd extraction. Therefore, the EOP from 1st extraction was discarded and EOP obtained from 2nd extraction was further characterized. The pectin yield depends on source material, extraction method and conditions (temperature, time and number of extraction) (Grassino et al., 2015). The digital images of OPP raw and after UAE treatment were showed colour change from light brown to dark brown (Fig. 6.2A & 6.2B). Similar pectin yields from other sources were reported. Pectin extraction from pomegranate peel and *Artocarpus heterophyllus* fruit peel by ultrasound-assisted extraction method yielded 23.9% and 14.5%, respectively (Moorthy et al., 2015, Moorthy et al., 2017). Pectin extracted from sweet lemon (*C. limetta*) at optimized pH 1.5 gave an yield of 16.7% (Aina *et al*., 2012). Another study showed that after statistical analysis and optimization of all parameters extraction of pectin from *Citrus limon* at pH 3.2 enhanced the yield to 32.4% (Kanmani *et al*., 2014). Extraction of pectin using microwave heating required lesser time and resulted in higher yield as compared with water based extraction (Fishman *et al*., 2003). Pectin extraction by microwave heating has higher anhydrogalacturonate content, degree of methylation and increased

viscosity (Fishman *et al*., 2000). The microwave heating during pectin extraction creates high pressure within the material. This modifies the physical properties of the tissue, disrupts cell structures and develops increased porosity. This facilitates easy entry of the extraction fluid to easily enter the material and thus resulting in an effective extraction process (Srivastava and Malviya, 2011).The microwave assisted extraction of pectin from orange peels yielded 19.3% (Maran et al., 2013). The extraction yield of 28% from sour orange peel was reported by UAE method (Hosseini et al., 2016).

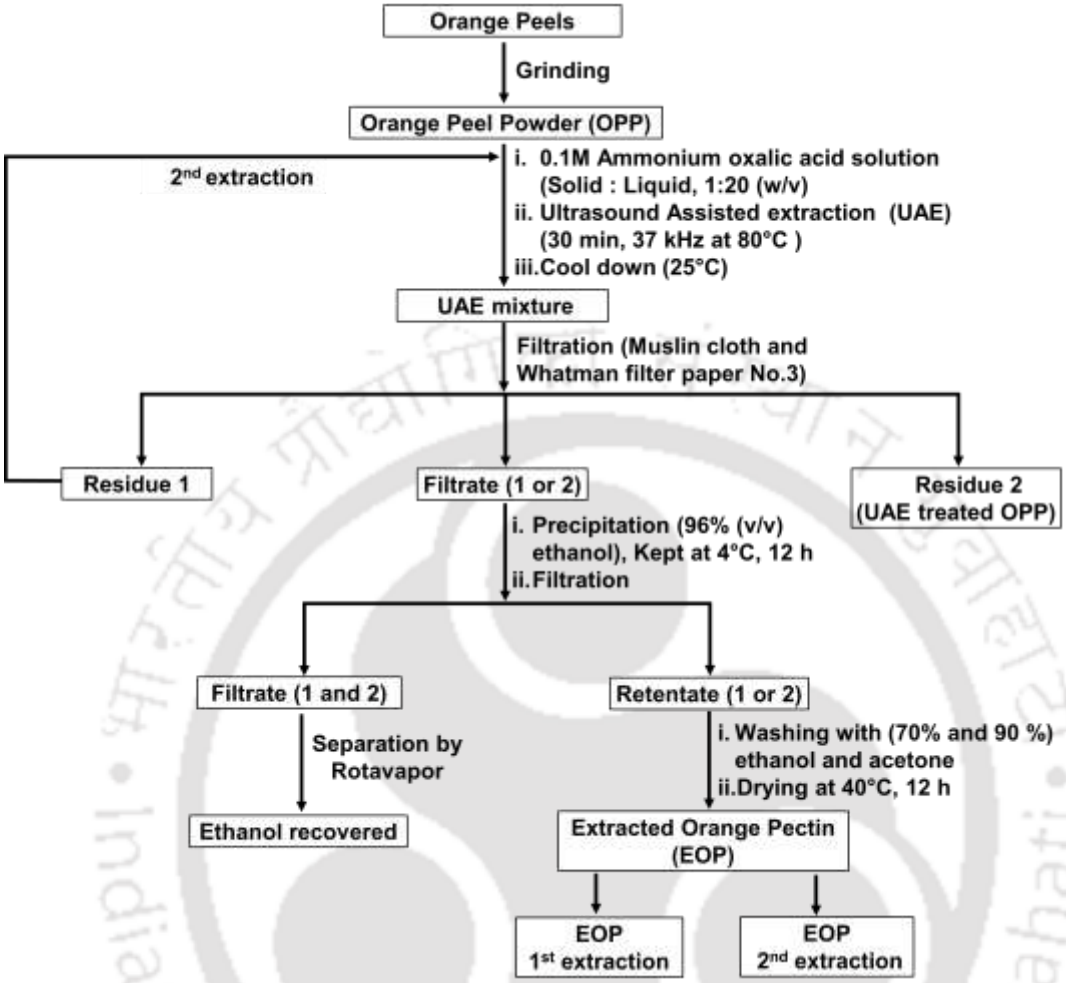

Fig. 6.1 Flow chart showing pectin extraction from orange peel by UAE method

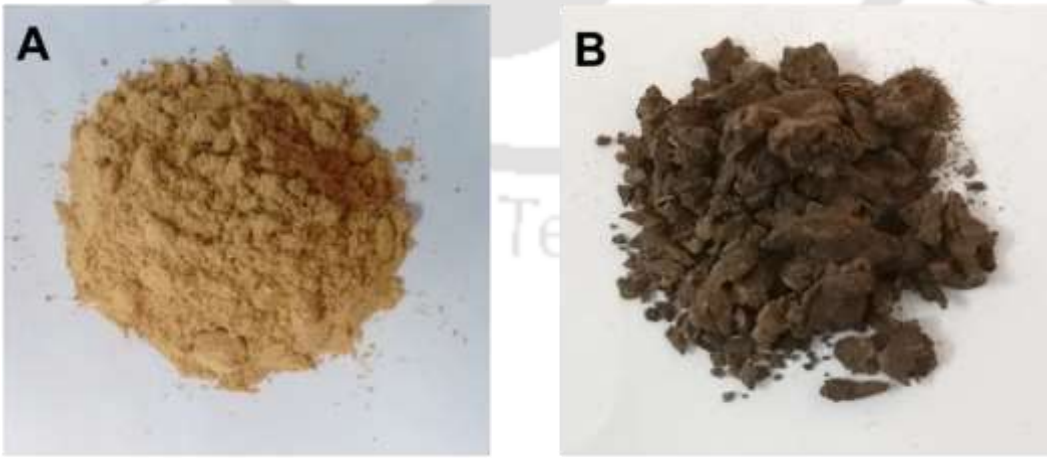

Fig. 6.2 Digital images orange peel powder (OPP). A) Untreated (Raw), B) UAE treated.

6.3.2 FESEM analysis of untreated OPP and UAE treated OPP

The FESEM analysis of untreated OPP showed smooth surface (Fig. 6.3A) while after UAE treatment OPP surface became more porous and rough (Fig. 6.3B). This indicated that UAE treatment destabilized and ruptured cell wall of OPP. Ponmurugan *et al*. (2017) reported similar results of UAE treatment from waste heads of *Helianthus annus.*

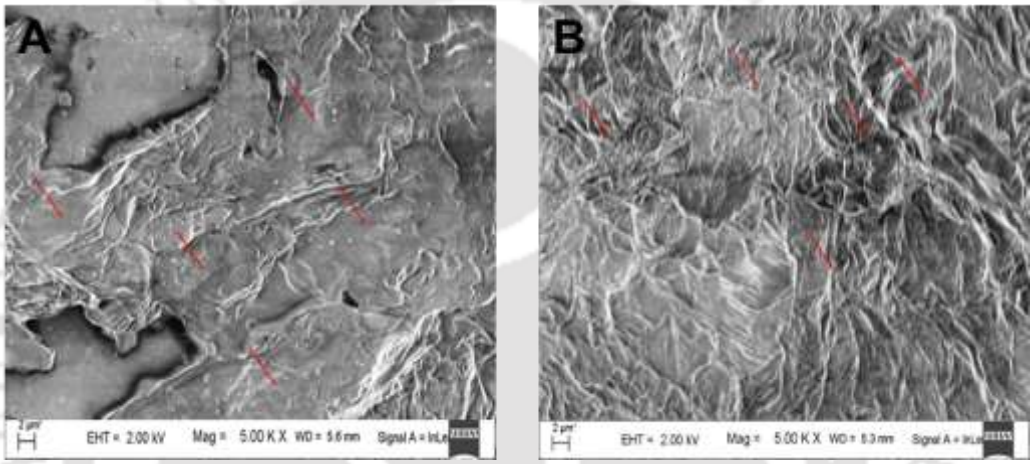

Fig. 6.3 FESEM surface images of OPP showing A) Untreated (Raw) at magnification 5.0 KX, B) UAE treated at magnification 5.0 kx.

6.3.3 FTIR analysis of untreated and UAE treated OPP

FTIR spectrum of UAE treated OPP shown in the Fig. 6.4. The intensity of broad band ranging from 3650 cm^{-1} - 3280 cm^{-1} corresponding to O-H stretching vibration, 3426 cm^{-1} was significantly increased, which is due to the hydroxyl groups of deformed hemicellulose as also reported earlier (Gnanasambandam and Proctor, 2000). The intensities of bands between 2850 cm^{-1} -3125 cm^{-1} (2983 cm^{-1} corresponding to C-H stretching), 450 cm^{-1} - 900 cm^{-1} attributing to C-C and C-O stretching of polysaccharides (cellulose and hemicellulose) and 1000 cm^{-1} - 1500 cm^{-1} (1353 cm^{-1} corresponding to -HC = O and C = C stretching of aldehyde and alkene) increased due

to destabilization OPP after UAE treatment as reported earlier also (Gnanasambandam and Proctor, 2000). The intensity of the bands at 1645 cm^{-1} for ester bonds C = O of pectin and hemicellulose and at 1133 cm^{-1} for the C-O-C stretching of the carbonyl of ester groups were also increased due to UAE treatment as compared to untreated OPP (Gnanasambandam and Proctor, 2000).. These results showed the UAE treatment is efficient for pectin extraction.

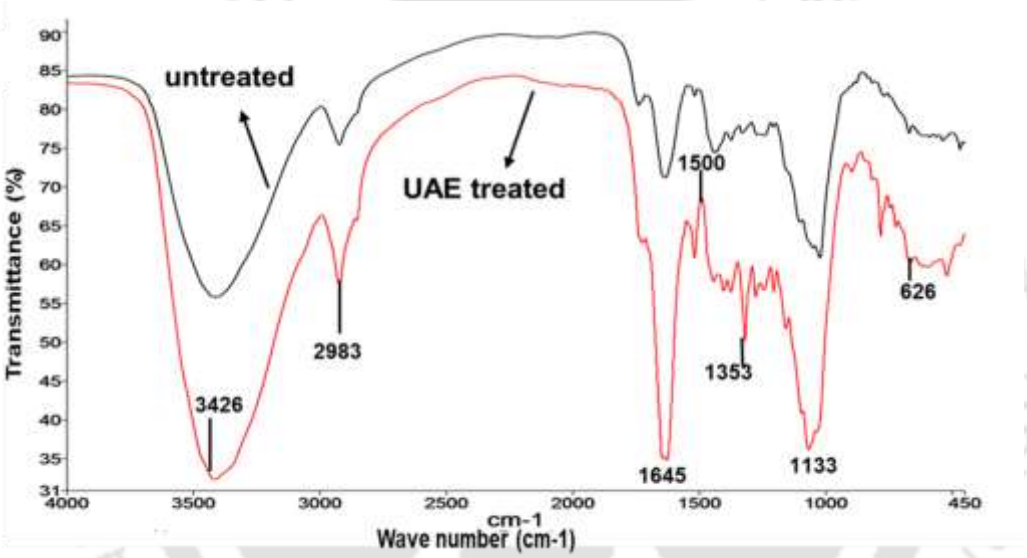

Fig. 6.4 FT-IR analysis of Untreated and UAE treated OPP.

6.3.4 Brunauer–Emmett–Teller analysis of OPP

The surface area and pore size of untreated or UAE treated OPP was analysed by BET. The UAE treated OPP showed more surface area and pore size as compared with untreated OPP. The specific surface area of UAE treated and untreated OPP were 5.6 m^2/g and 2.5 m^2/g, respectively. The average pore size of UAE treated and untreated OPP were 25.5 nm and 11.2 nm, respectively. Total pore volume of UAE treated and untreated OPP were 0.035 cc/g and 0.0072 cc/g, respectively. These results showed significantly increased surface area, pore size and pore volume of UAE treated OPP as

compared with untreated OPP (Table 6.1). These results also showed that the UAE treatment is efficient and suitable method for extraction of pectin from orange peel.

Table 6.1 BET analysis summary of untreated and UAE treated orange peel powder.

	BET analysis of OPP	
BET summary	Untreated OPP	UAE treated OPP
Surface area	2.5±0.2 m^2/g	5.6±0.3 m^2/g
Total pore volume	0.007±0.003 cc/g	0.035±0.001 cc/g
Average pore size diameter	11.2±0.12 nm	25.5±0.16 nm

6.3.5 FESEM and FESEM-EDX analysis of EOP

The extracted orange pectin (EOP) was obtained as pale yellow powder as shown in Fig. 6.5A. The FESEM analysis of EOP showed smooth surface and loosened heterogeneous wrinkled crystal structure (Fig. 6.5B). The pectin extracted from pamelo peel powder by UAE method showed similar surface as reported earlier (Liew et al., 2016). FESEM-EDX analysis gave the presence of significant elements. The EDX of EOP performed at 100 µm scale and element were C-44.8%, O-45.2%, N-9.1%, K-0.5% and 0.1% each of Mg, Na and Ca (Fig. 6.5C). The EOP contained minor trace elements which are due to the in bounded or based on extraction procedure these elements appeared. The EOP obtained from UAE treatment is compact in nature and distributed in small particle size, which may increase its solubility.

Fig. 6.5 A) Digital image of purified EOP, B) FESEM image of purified EOP at magnification 2.0 kx and C) EDX Elemental analysis of purified EOP.

6.3.6 AFM surface analysis of EOP

The AFM phase contrast analysis of EOP showed heterogeneous, net form and fibers structure throughout the surface. The 2D surface image showed net like structure with wrinkled fibers or thread like structures on scale, 5 µm X 5 µm (Fig. 6.6A) and 1 µm X 1 µm (Fig. 6.6C). The 3D view image showed the wrinkled rough surface of EOP pectin on scale of 5 µm X 5 µm (Fig. 6.6B) and 1 µm X 1 µm (Fig. 6.6D). The fibrous structure was observed due to the presence of multi-complex inter-molecule interaction of EOP pectin. Similar, structures were reported for sugar beet pectin and tomato pectin by Kirbay *et al*., (2008). The large variation in width of the structure could be due to the extraction method and buffer, which form aggregate fibers made up of EOP polysaccharide chain.

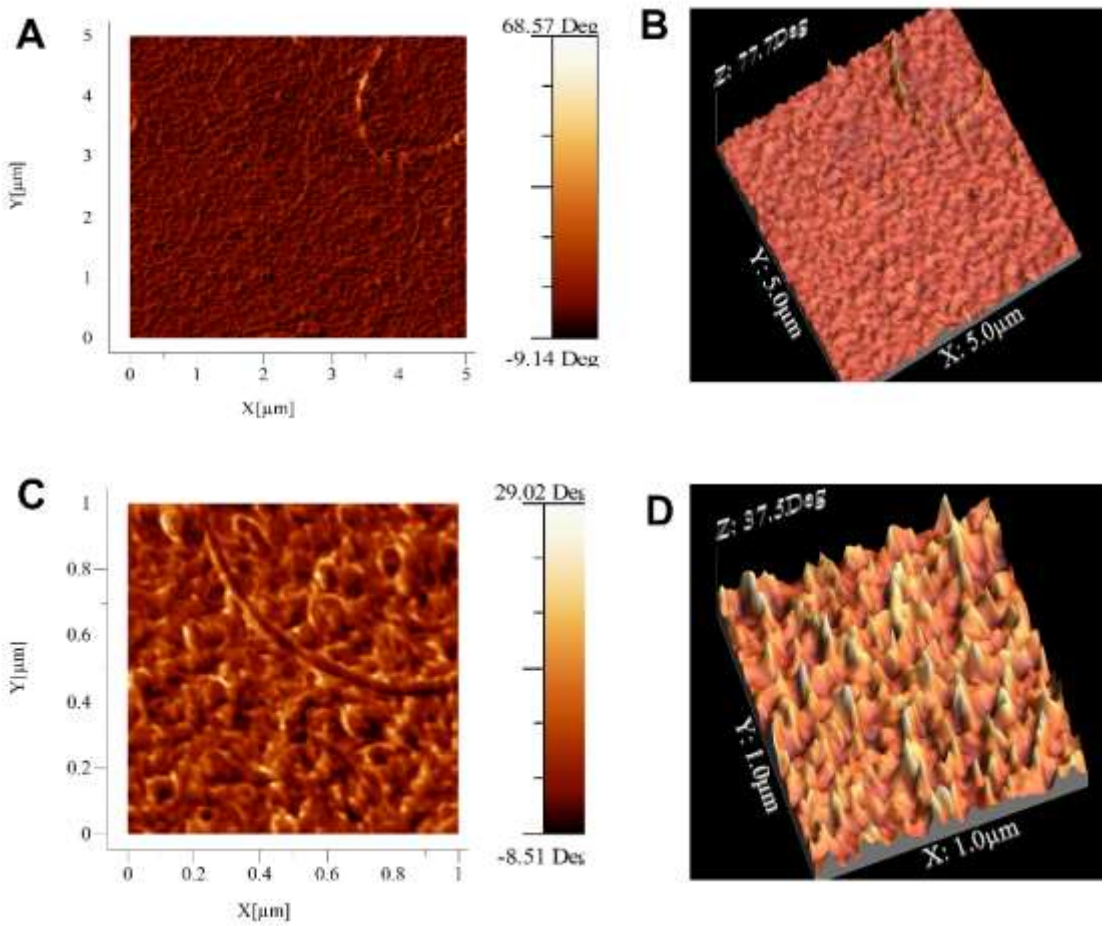

Fig. 6.6 AFM analysis of EOP showing A) 2D image view (5 µm x 5 µm), B) 3D image view (5 µm x 5 µm), C) 2D image view (1 µm x 1 µm) and D) 3D image view (1 µm x 1 µm).

6.3.7 Monosugar composition analysis of EOP

The neutral sugar composition of EOP was evaluated by TFA hydrolyzed. HPLC chromatogram of EOP hydrolyzed mono sugars are shown in Fig. 6.7. The chemical composition of EOP comprised galacturonic acid, galactose, rhamnose and arabinose as they showed the retention time of 13.5, 15.0, 15.6 and 16.4 min, respectively (Fig. 6.7). TFA hydrolysis of EOP produced di-galacturonic acid and tri-galacturonic acid, which showed retention time, 10.5 and 9.8 min, respectively (Fig. 6.7). These results corroborated with the standards, retention time.

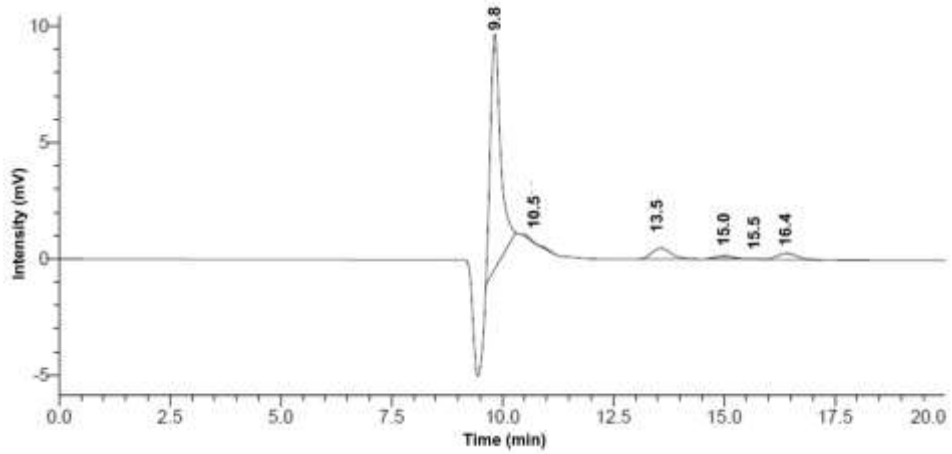

Fig. 6.7 HPLC analysis of EOP composition by TFA treatment.

6.3.8 Molecular mass determination and distribution of EOP by HPSEC

The molecular mass of polymer was determined by HPSEC. The EOP showed two peaks with the retention time 20.4 and 22.4 min (Fig. 6.8). The fractions for both peaks were collected separately and dialyzed against Milli-Q water. The EOP pectin showed two peaks of molecular masses, 92.3 kDa and 1.3 kDa, which was calculated by using the standard graph giving regression equation with R^2=0.9853. The major peak at 20.4 min (92.3 kDa) represented EOP. The peak at 22.4 min (1.3 kDa) was minor, which is small mass from hanging fragment of EOP polymer appearing owing to the UAE treatment.

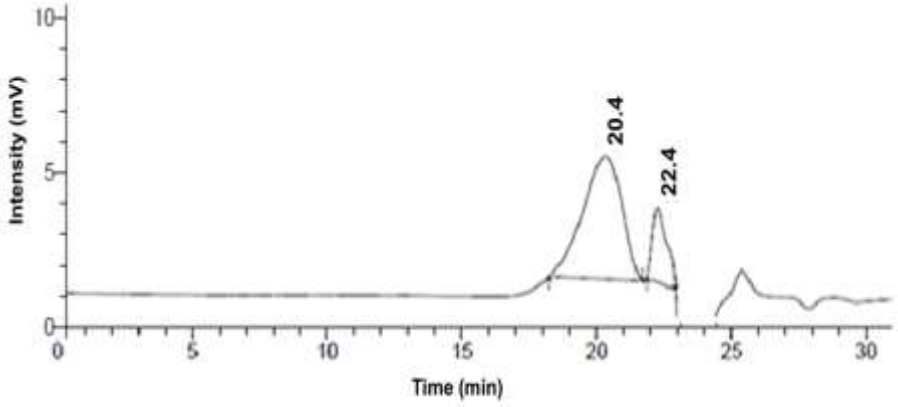

Fig. 6.8 Molecular mass determination of EOP by HPSEC.

6.3.9 DLS analysis of EOP

The particle size of EOP was determined by DLS. The particle size distribution vs intensity graph, statistical analysis of size distribution curve and cumulant fit (standard fitting curve in DLS) of correlation curves are show in Fig. 9A, 9B & 9C, respectively. The EOP polysaccharide showed polydispersity. The EOP pectin solution contained two peaks with hydrodynamic radius (R_h) of 864.9 nm and 196.0 nm, which might concur with the 92.3 kDa and 1.3 kDa polymers. The average hydrodynamic diameter of EOP was 329 nm by cumulants fit. The variation in the size measurements was less than 5% and repeated results distinguished from each other. The microwave-assisted extracted pectin from *Opuntia ficus indica*, showed average R_h of 110 nm (Lefsih et al., 2017). The microwave-assisted extracted pectin from lime flavedo average R_h was 321.8 nm (Fishman et al., 2007), which is similar to EOP of this study.

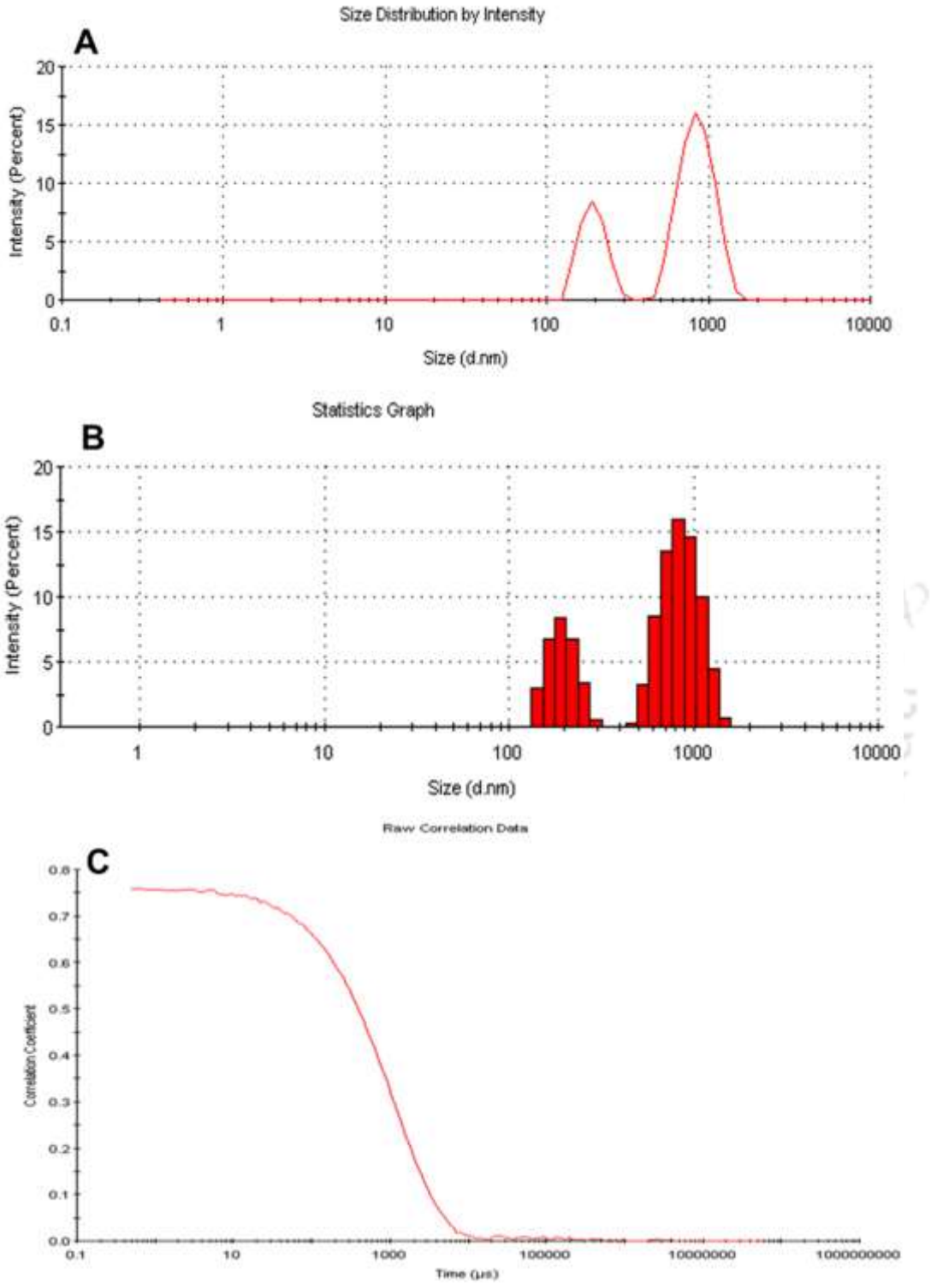

Fig. 6.9 DLS analysis of EOP pectin A) Size distribution plot, B) Statistical analysis and C) Cumulant curve fit,

6.3.10 FTIR analysis and DE of EOP pectin

The functional groups of EOP pectin were analysed by FTIR. FTIR spectrum of the EOP pectin showed a broad transmission peak at 3426 cm^{-1} due to the O-H stretching absorption of hydrogen bond (Fig. 6.10A) as also reported earlier (Kpodo et al., 2017). The peak in the range, 2890-2985 cm^{-1} is attributed to the C-H stretching vibration from CH_3, CH_2 and CH bonds in D-GalA chain as also described previously (Vriesmann and Petkowicz, 2014). The peaks at 1021, 1082 and 1353 cm^{-1} were assigned to -C-OH, -C-C- and -C-O- vibration, respectively (Fig. 6.10A). These three functional groups are represented by pectin polysaccharides, which was reported by Hosseini *et al*., (2016). The peaks at 1735 cm^{-1} and 1642 cm^{-1} are related to methyl esterified carboxylic group (-C=O) and carboxylate (-COO-), respectively. The carboxyl group or esterification is an important characteristics of pectin, which is different from other polysaccharides (Ponmurugan et al., 2017). The peaks between 1000 cm^{-1} and 650 cm^{-1} are due to the glycosidic linkages between the sugar units (Hosseini et al., 2016). Degree of esterification (DE) of EOP was 68% calculated by FTIR spectrum by using the Eq. (2) and Eq. (3). The DE of EOP was more than 50%, therefore, it falls under the category of high methylated pectin.

6.3.11 NMR analysis of EOP

The ^1H NMR spectrum of EOP was acquired at 600 MHz and analysed by TOPSPIN software (Fig. 10B). The proton chemical shift peaks were allocated according to the previous reports and compared. The ^1H NMR spectrum showed a sharp peak at 3.55 ppm, which protons corresponds to the esterification of D-galacturonic acid (GalA) units. The peak shift around at 1.02 and 1.15 ppm were showed due to the presence of methyl group on links of L-rhamnose (Al-Amoudi et al., 2019). The signals

of 4.85 (H-5) and 5.15 (H-1) ppm belong to non-esterified D-galacturonic acid units. The proton chemical shifts of H-1, H-2, H-3, and H-4 of D-galacturonate and methyl galacturonate residues were observed at 5.15, 3.50, 3.96 and 4.68 ppm, respectively. These results confirmed the presence of the pectin structure in EOP and corroborated with previous reports (Rosenbohm et al., 2003; Zhang et al., 2013; Grassino et al., 2016).

The ^{13}C NMR spectrum of the EOP is shown in Fig. 6.10C. The spectrum showed a chemical peak shift at 57.5 ppm, which is due to the methyl groups ($-CH_3$) bound to carboxyl groups of D-GalA, while its corresponding sharp proton singlet was detected at 3.55 ppm in ^{1}H NMR spectra. In ^{13}C NMR spectrum, the chemical shifts at 71.3, 77.8, 70.8, 65.2 and 99.9 ppm were related to C-5, C-4, C-3, C-2 and C-1 of carbon backbone of D-galacturonic unit, respectively. Peak shift at 175.4 and 168.9 ppm represent the C6 and C=O of D-galacturonic unit, respectively (Alba et al., 2015). Similar chemical shifts were reported by ultrasound method, extracted pectin from citrus peels (Kim et al., 2004), apple peels (Zhang et al., 2013) and tomato (Grassino et al., 2016). ^{1}H and ^{13}C NMR spectra revealed that the EOP contains esterified D-galacturonic acid units in the polysaccharide chain.

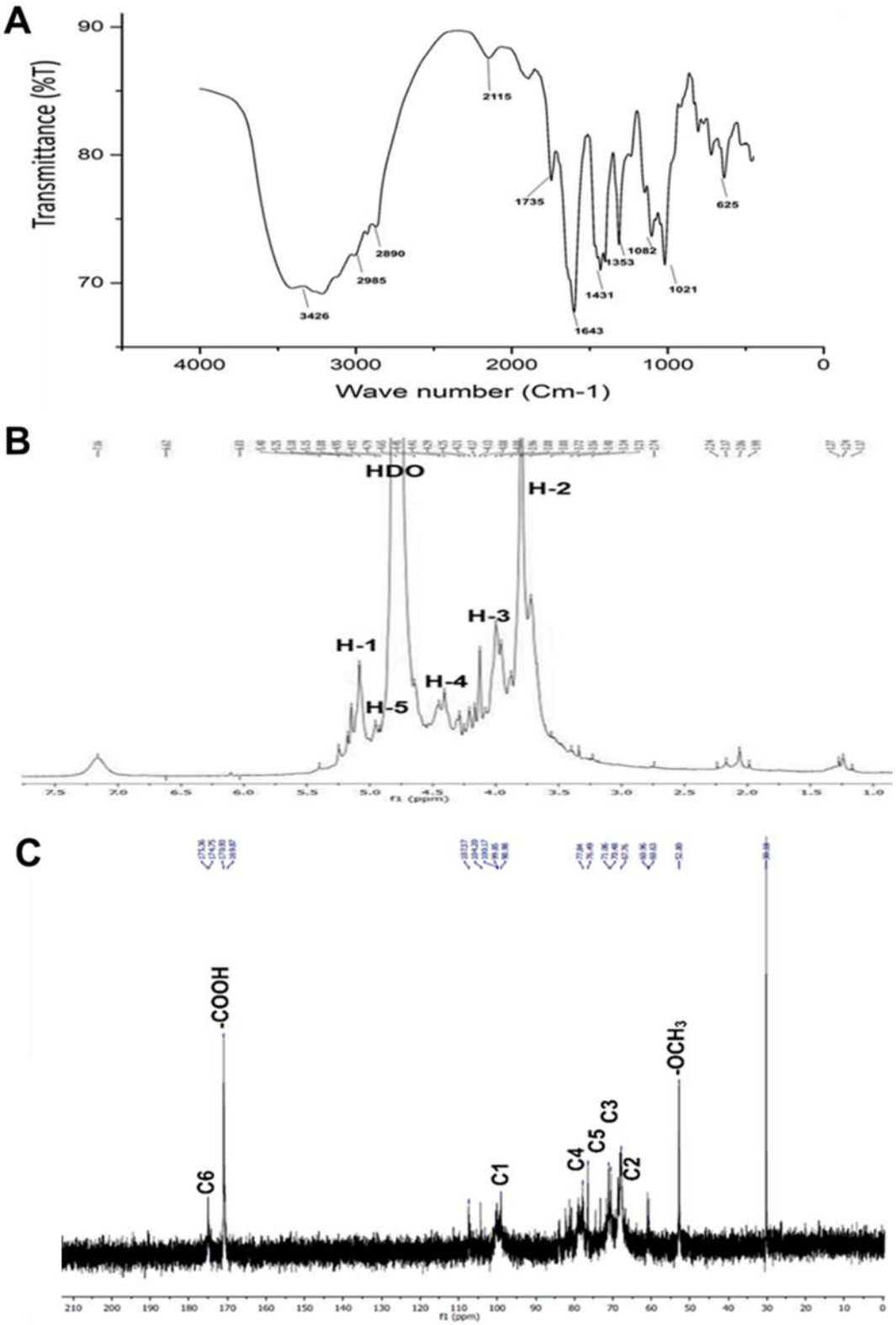

Fig. 6.10 A) FT-IR analysis of EOP, B) ^{1}H-NMR spectrum of EOP and C) ^{13}C-NMR spectrum of EOP

6.3.12 TGA and DSC analysis of EOP

The thermal degradation temperature and phase shift of EOP was analyzed by TGA-DSC thermal analyzer. Differential Thermogravimetric Analysis (DTG) was obtained from TGA graph (Fig. 6.11A). TGA and DTG curves showed the weight loss with respect to the increase in temperature. TGA of EOP curve is shown in the temperatures range, 25-900°C. The TGA curve showed significant changes in four temperature ranges (25-110°C, 110-280°C, 280-700°C and 700-900°C). The initial small change in weight loss (8%) occurred at 100-110°C, due to the heat water molecule from EOP was vaporized. The second stage, in temperature range, at 110-280°C, weight was drastically reduced from 8% to 54%, due to pyrolysis of the EOP polymer. In the third stage, the temperature range, 280-700°C, weight of EOP further decreased from 54% to 20% observed. In the final stage, in temperature range, 700-900°C, the weight loss of EOP was reduced from 20% to 12%, which is approximately, 0.75 mg of final residue as black color ash after the completion of experiment. Similar pattern was also observed in DTG curve and the degradation temperature was 225°C. Einhorn-Stoll *et al*., (2009) reported DTG of 250°C for citrus pectin, which similar to the EOP of present study.

The DSC analysis of EOP showed change of heat flow in system. The change glass transition state at 100°C, which is due to the initial stabilizing of EOP (Fig. 6.11B). The thermal scan of EOP showed a sudden decrease in curve at 200°C, signifying the occurrence of endothermic reaction. It could be due to loss of bound water molecule from the EOP polymer. However, the overall reaction was inferred to be exothermic in nature, by a continuous and gradual increase in curve. A careful observation of peak at 225°C also supports the semi-crystalline nature of EOP. Further, the EOP releases more

energy as form of exothermic reaction until end of the process. Einhorn-Stoll et al., (2007) explained similar pattern of endothermic and exothermic reactions using alkaline treated modified orange pectin.

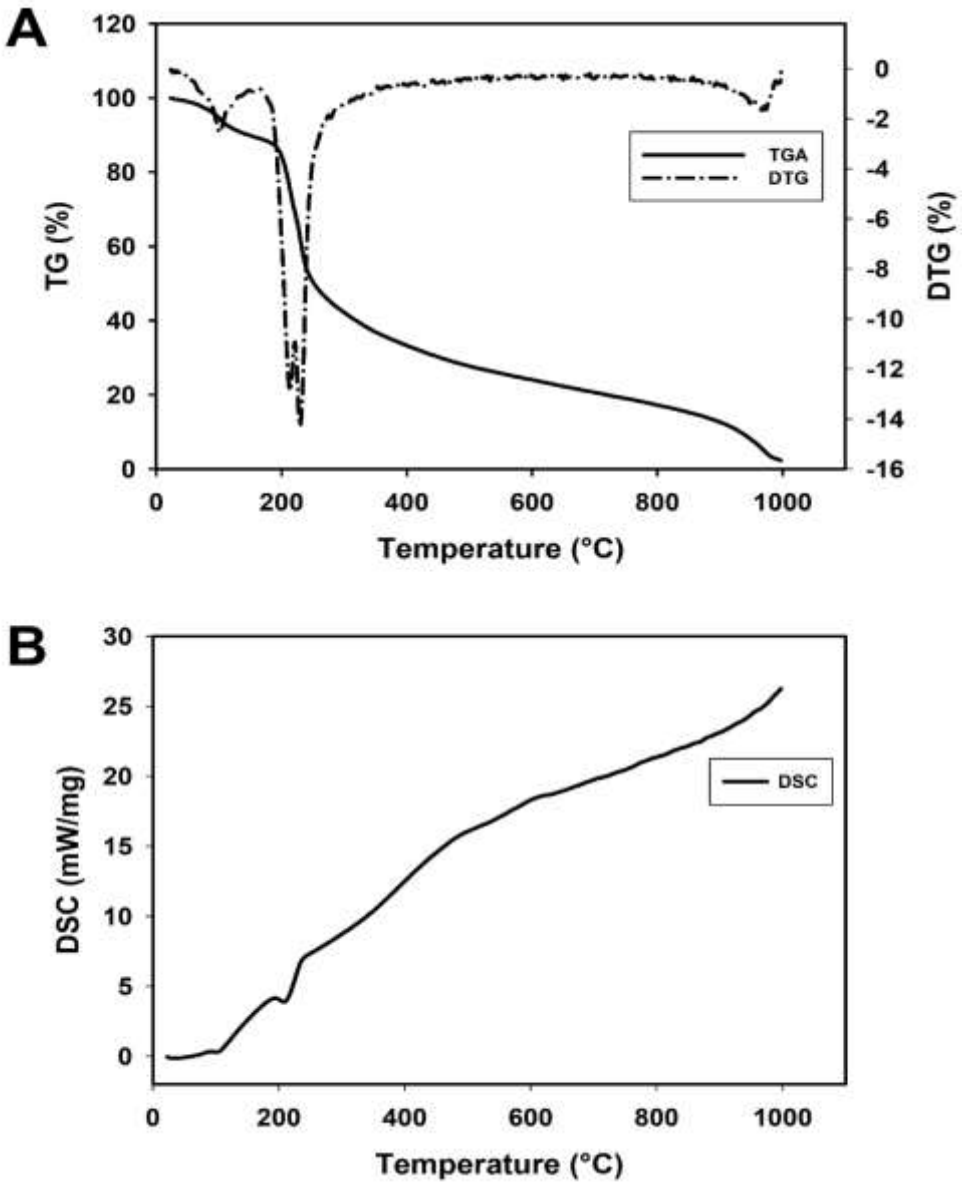

Fig. 6.11 A) TGA-DTG analysis of EOP and B) DSC analysis of EOP.

6.3.13 X-ray powder diffraction analysis of EOP

The XRD pattern of EOP was recorded by X-ray diffractometer. XRD analysis provides information on crystalline or amorphous form of the EOP pectin (Fig. 6.12). The XRD pattern of EOP pectin showed the intense sharp peaks at 13.9, 14.2, 17.2, 18.0, 19.4, 21.4, 22.0, 24.0, 27.2, 29.1, 31.3 and 36° (2θ) which are due to crystallinity of pectin polymer (Fig. 6.12). The Crystallinity Index (CrI) of EOP was 83%. The angles after 50° showed no significant peaks which indicated EOP also has the amorphous nature (Fig. 6.12). Therefore, the EOP had both crystalline and amorphous nature form in its structure. The results corroborated with the XRD result of pectin extracted by UAE method from *Citrus aurantium* (Hosseini et al., 2019).

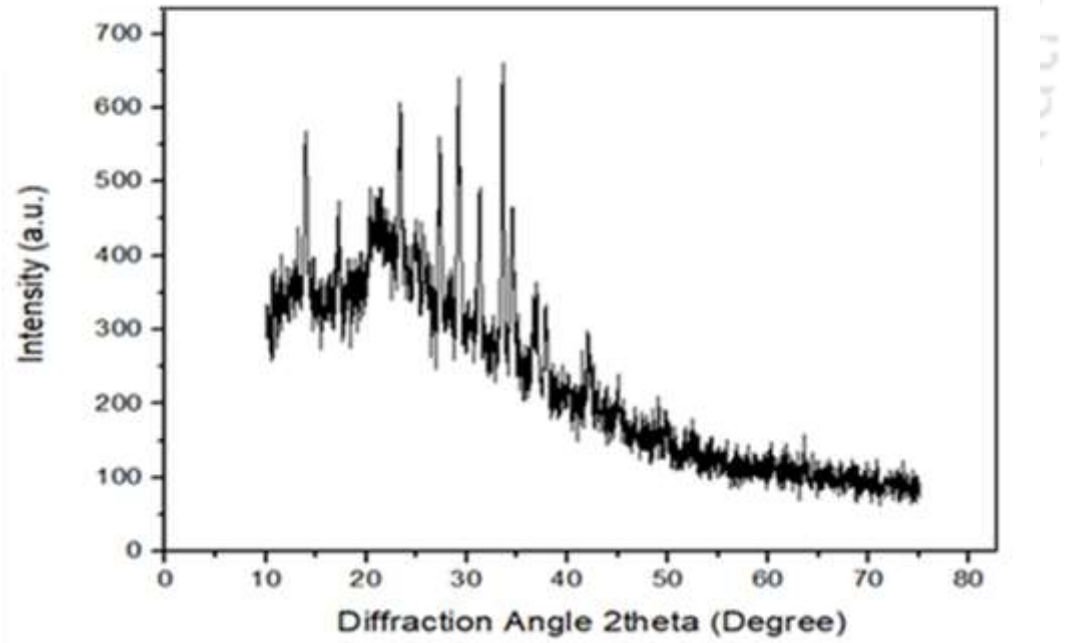

Fig. 6.12 XRD analysis of extracted orange pectin (EOP).

6.3.14 Enzyme activity assay against EOP

The enzyme activities of pectate lyase (*Ct*PL1B) and pectin methylesterase (*Ct*PME) activity against EOP were 6.9 U/mg and 9.5 U/mg, respectively. The EOP was also treated with mixture of *Ct*PME and *Ct*PL1B enzymes. The pectate lyase and pectin methylesterase activities of the mixture against EOP were 9.7 U/mg and 9.5 U/mg, respectively (Table 6.2). The individually used pectate lyase activity gave 6.9 U/mg whereas the same enzyme when used in combination with pectin methylesterase gave 9.7 U/mg, however there was no change in the of pectin methylesterase. This clearly showed 40% increase in the activity of *Ct*PL1B in the presence of *Ct*PME displaying lucidly that *Ct*PME removed the methyl groups from EOP thereby making it more accessible to *Ct*PL1B for de-polymerization. Thus, the combination of these two enzymes can be beneficial for applications in food and beverage industry.

Table 6.2 Enzyme activity against EOP.

Enzyme	Pectate lyase activity (U/mg)[¥]	Pectin methylesterase activity (U/mg) [¥]
*Ct*PL1B (7 µg/ml)	6.9±0.3	ND
*Ct*PME (8 µg/ml)	ND	9.5±0.2
*Ct*PME (8 µg/ml) and *Ct*PL1B (7 µg/ml)	9.7±0.1	9.5±0.2

[¥]*Values are in mean ± SD (n = 3).*
ND- No activity determined.

6.3.15 TLC, HPLC and ESI-MS analysis of lysed products of EOP

The TLC analysis results of lysed products of EOP released by *Ct*PME, *Ct*PL1B or mixture of *Ct*PME and *Ct*PL1B is shown in Fig. 6.13. *Ct*PME did not show any lysed

product, while *Ct*PL1B alone or mixture of *Ct*PME and *Ct*PL1B showed the presence of mono-galacturonate (DP1), unsaturated di-galacturonate (DP2) and unsaturated tri-galacturonate (DP3) (Fig. 6.13A and & 6.13B). The unsaturated di-galacturonate and tri-galacturonate were the major components produced in 12h. The lyophilized POS products of EOP by enzymes (*Ct*PL1B or *Ct*PME and *Ct*PL1B) were analysed. *Ct*PL1B treated EOP showed POS with DP1, DP2 and DP3 giving retention time of 13.9, 12.5 and 11.8 min, respectively (Fig. 6.13C). The enzyme mixture of *Ct*PME and *Ct*PL1B treated EOP showed POS with DP1, DP2 and DP3, giving retention time of 14.4, 13.1 and 12.3 min, respectively (Fig. 6.13D). The retention time of the standards *viz.* mono galacturonate, di-galacturonate and tri-galacturonate were 14.3, 13.0 and 12.1 min, respectively. The retention time of POS from *Ct*PL1B were different from the POS obtained from mixture of *Ct*PME and *Ct*PL1B was due to the methylation of unsaturated galacturonates in the case of *Ct*PL1B.

The molecular mass and degree of polymerization (DP) of POS from enzyme lysed EOP was also analyzed by ESI-MS. ESI-MS analysis of *Ct*PL1B lysed EOP showed peaks at *m/z* 198, *m/z* 383 and *m/z* 558 corresponding to mono galacturonate (DP1+ Na^+) with additive of Na^+ ion, unsaturated methyl-esterified di-galacturonate (DP2+Me) and unsaturated methyl-esterified tri-galacturonate (DP3+Me+H^+), respectively (Fig. 6.13E). ESI-MS analysis of POS produced from lysed EOP by mixture of *Ct*PME and *Ct*PL1B enzymes showed peaks at *m/z* 175, *m/z* 374 and *m/z* 551 corresponding to monogalacturonate (DP1+ H^+) with additive of H^+ ion, unsaturated di-galacturonate (DP2+ Na^+ + H^+) and unsaturated tri-galacturonate (DP3 + Na^+ + $3H^+$) with additive of Na^+ and H^+ ions (Fig. 6.13F). Chakraborty *et al*., (2018) also reported unsaturated di- and tri-galacturonate released from extracted pectin *Citrus Limetta* using

*Ct*PL1B hydrolysis. The action of *Ct*PME on EOP removed the methyl groups from EOP and produced the pectic polysaccharide (PP), which is a linear pectate. The *Ct*PL1B lysed EOP called methylated pectate oligosaccharides (mPOS) because its DP2 and DP3 are methylated. However, EOP lyzed by mixture of *Ct*PME and *Ct*PL1B released non-methylated oligosaccharides called pectate oligosaccharides (POS).

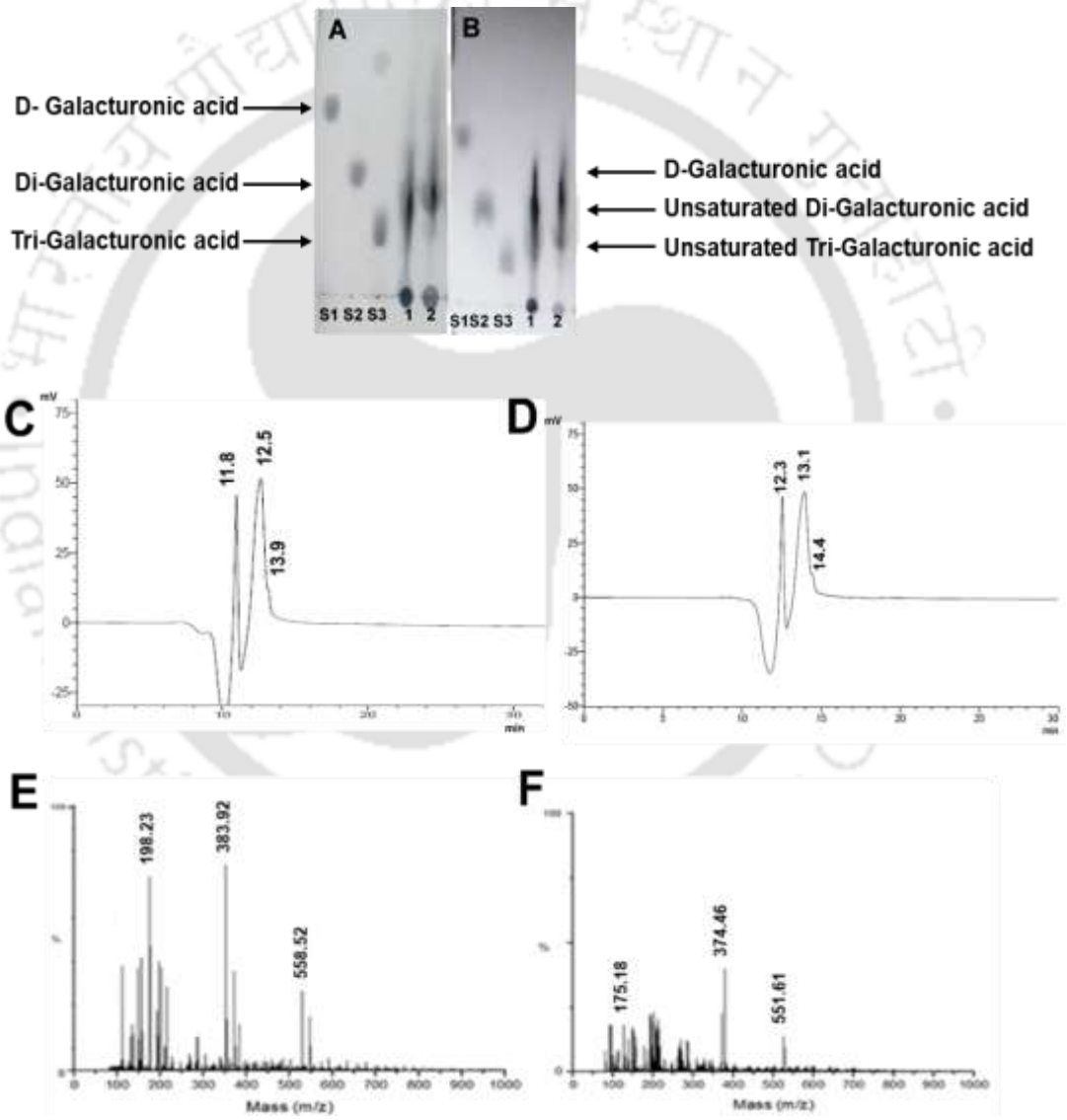

Fig. 6.13 TLC analysis of A) EOP treated by *Ct*PL1B Lane 1 and 2 (1:2 dilution), B) EOP treated by *Ct*PL1B and *Ct*PME. Lanes 1 and 2 (1:2 dilution); S1 -mono-, S2 -Di- and S3 -Tri-D-galacturonic acids. HPLC analysis of C) EOP treated by *Ct*PL1B (mPOS), D) EOP treated by *Ct*PME and *Ct*PL1B (POS) and ESI-MS analysis of EOP degradation products by E) *Ct*PL1B (mPOS) and F) *Ct*PL1B and *Ct*PME (POS).

6.3.16 Biocompatibility and Anticancer activity assay of PP, POS and mPOS

The effect of PP, POS and mPOS on the proliferation of HEK293 and HT29 cells was examined. The proliferation of HEK293 cells was not affected by the treatment of different concentrations (0.1 mg/ml to 1 mg/ml) of PP, POS and mPOS (Fig. 6.14) and showed cell viability in the range of 95-98% even after 48h. The microscopic analysis also showed that the morphology of HEK293 cells is not changed in the presence of PP, POS and mPOS (Fig. 6.14) clearly indicating that PP, POS and mPOS are biocompatible with human cells. The effect of PP, POS and mPOS was also examined for anticancer activity against HT29 cells. All of them reduced the proliferation rate of HT29 cells. PP, POS and mPOS showed reduced proliferation of HT29 cells by 18.4, 12 and 28.4%, respectively, in 24 h, while the 48 h treatment depicted higher reduction in proliferation, 22, 44.7 and 51.5%, respectively, of HT29 cells (Fig. 6.14). mPOS showed the maximum reduction of proliferation of HT29 cells as compared to POS or PP. Pectic oligosaccharide from tomato and swallow root also showed anticancer potential on a gastric cancer cell line by arresting of galectin-3 activity (Kapoor, & Dharmesh, 2017; Mallikarjuna, & Dharmesh, 2018). The role of POS is blocking the transcription factors mediated blockade of galectin-3 signaling cascade, which involves the down-regulation of galectin-3 gene (Zhang et al., 2016, Zhang et al., 2017). Metastasis is a necessary event for cancer cell survival, which involve several steps, such as increased cell–cell recognition, cell adhesion, cell invasion, proliferation and anti-apoptosis (Martin et al., 2000). Our study showed the presence of methyl group decorated on the pectic oligosaccharides showed reduction in HT29 cell proliferation. Microscopic analysis also showed that the presence of PP, POS and mPOS converted the undifferentiated HT29 cells into differentiated cells having

shrunk globular shape (Fig. 6.14). The mPOS displayed more differentiated and shrinkage of HT29 cells as compared to PP or POS. POS (2 mg/ml) produced from LMP1 and LMP2 from citrus showed anti-proliferative activity against MCF-7 cells, giving the inhibition 52% and 44%, respectively (Li et al., 2019). PP from citrus canning processing water showed 30% of antiproliferation MCF-7 (human breast adenocarcinoma) cells (Li et al., 2019). This study also showed that the methylated pectic oligosaccharides have the potential anticancer activity.

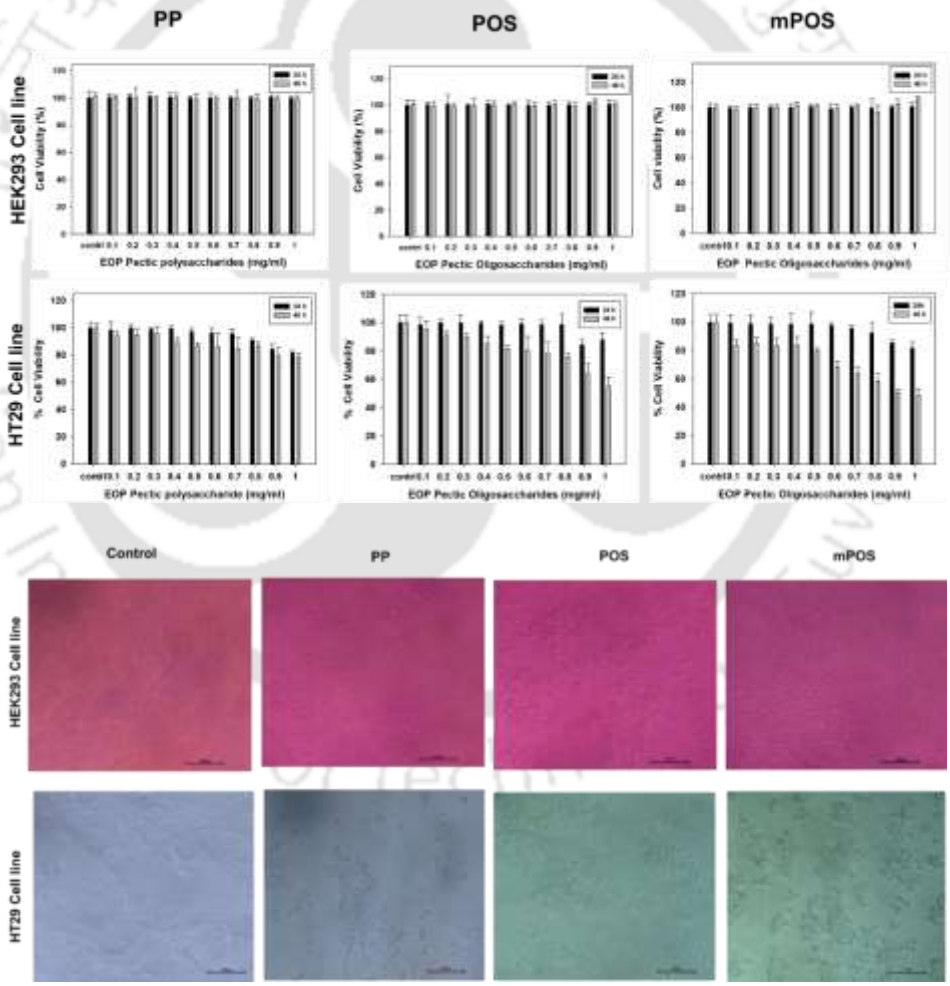

Fig. 6.14 MTT assay of normal HEK293 and cancer HT29 cells after treatment with 0.1-1.0 mg/ml of mPOS produced by *Ct*PL1B, POS produced by Mixture (*Ct*PL1B+*Ct*PME) and PP produced by *Ct*PME. Morphological analysis of HEK293 and of HT29 cells after treatment of 0.1-1.0 mg/ml of mPOS produced by *Ct*PL1B, POS produced by Mixture (*Ct*PL1B+*Ct*PME) and PP produced by *Ct*PME.

6.4 Conclusions

The pectin polysaccharide was extracted by UAE method from orange peels (*Citrus reticulate*). The yield of extracted orange pectin (EOP) obtained was 23.3%. FESEM analysis of UAE treated orange peel powder (OPP) showed more structural destabilization and porosity as compared with untreated OPP, which was also confirmed by BET analysis. FTIR spectrum showed the increased intensities of O-H, C=C and HC=O in UAE treated OPP as compared to untreated OPP displaying the disruption. These results showed that the UAE treatment is efficient and suitable for EOP extraction. The surface topology of EOP was globular particle like and wrinkled as shown by FESEM. The AFM depicted its fibrous and net-like structure. HPSEC analysis of EOP exhibited the molecular mass of 92.3 kDa. DLS analysis showed the average hydrodynamic diameter of 329.3 nm of EOP. FTIR and NMR spectra showed that EOP contains esterified D-galacturonic acid units. The degree of esterification of EOP was 68% as confirmed by FTIR. TGA-DTG showed the thermal degradation temperature of EOP to be 225°C and XRD analysis showed its semi-crystalline nature. *Ct*PL1B displayed 40% enhanced activity against EOP in the presence of *Ct*PME. The TLC analysis of lysed products of EOP released by *Ct*PL1B were majorly DP2 & DP3, which are methylated pectic oligosaccharides (mPOS) and by mixture of *Ct*PME and *Ct*PL1B, were non methylated pectic oligosaccharides (POS), which were confirmed by HPLC and ESI-MS. *Ct*PME hydrolysed the EOP and gave only the pectic polysaccharide (PP) and not POS. The effects of PP, POS and mPOS on proliferation of HEK293 and HT29 were studied. The proliferation of HEK293 cells was not affected even after 48 h in all the three case and the microscopic observation also showed no change in the cell morphology as compared with the untreated cells. All of them showed

reduced proliferation of HT29 cells, however, mPOS displayed maximum (51%) reduction of proliferation of HT29 cells as compared to POS or PP. The microscopic observation of mPOS treated HT29 cells revealed the reduced connection between the cells and change in cell morphology from undifferentiated to shrunk globular shape. The results displayed that mPOS, POS and PP are biocompatible and display anticancer properties. Therefore, these products generated from waste can be used for functional food applications for enriching their nutritional values. The orange peel, which is considered as waste can serve as source for potential healthcare products.

6.5 References

Aina, V.O., Barau, M.M., Mamman, O.A., Zakari, A., Haruna, H., Umar, M.S.H., Abba, Y.B. 2012 Extraction and characterization of pectin from peels of lemon (*Citrus limon*), grape fruit (*Citrus paradisi*) and sweet orange (*Citrus sinensis*). British Journal of Pharmacology and Toxicology, 3: 259–262.

Al-Amoudi, R. H., Taylan, O., Kutlu, G., Can, A. M., Sagdic, O., Dertli, E., Yilmaz, M. T. (2019) Characterization of chemical, molecular, thermal and rheological properties of medlar pectin extracted at optimum conditions as determined by Box-Behnken and ANFIS models. Food Chemistry, 271: 650-662.

Alba, K., Laws, A. P., Kontogiorgos, V. (2015) Isolation and characterization of acetylated LM-pectins extracted from okra pods. Food Hydrocolloids, 43: 726-735.

Boudart, G., Lafitte, C., Barthe, J. P., Frasez, D., Esquerre-Tugaye, M. T. (1998) Differential elicitation of defense responses by pectic fragments in bean seedlings. Planta, 206(1): 86-94.

Centelles, J. J. (2012) General aspects of colorectal cancer. ISRN Oncology, 2012, 1-19.

Chakraborty, S., Fernandes, V. O., Dias, F. M., Prates, J. A., Ferreira, L. M., Fontes, C. M., Goyal, A., Centeno, M. S. (2015) Role of pectinolytic enzymes identified in *Clostridium thermocellum* cellulosome. PloS One, 10(2): e0116787.

Chakraborty, S., Rani, A., Goyal, A. (2018) Pectic oligosaccharides produced from pectin extracted from waste peels of *Citrus limetta* using recombinant endo-pectate lyase (PL1B) inhibit colon cancer cells. Trends in Carbohydrate Research, 10(1).

Chaouch, M. A., Hafsa, J., Rihouey, C., Le Cerf, D., Majdoub, H. (2016b) Effect of pH during extraction on the antioxidant and antiglycated activities of polysaccharides from opuntia ficus indica. Journal of Food Biochemistry, 40(3): 316-325.

Chen, C.H., Sheu, M.T., Chen, T.F., Wang, Y.C., Hou, W.C., Liu, D.Z., Chung, T.C., Liang, Y.C. (2006) Suppression of endotoxin-induced proinflammatory responses by citrus pectin through blocking LPS signaling pathways. Biochemical Pharmacology, 72: 1001–1009.

Cheong, T. C., Shin, J. Y., Chun, K. H. (2010) Silencing of galectin-3 changes the gene expression and augments the sensitivity of gastric cancer cells to chemotherapeutic agents. Cancer Science, 101(1): 94-102.

Einhorn-Stoll, U., Kunzek, H. (2009) Thermoanalytical characterisation of processing-dependent structural changes and state transitions of citrus pectin. Food Hydrocolloids, 23(1): 40-52.

Einhorn-Stoll, U., Kunzek, H., Dongowski, G. (2007) Thermal analysis of chemically and mechanically modified pectins. Food Hydrocolloids, 21(7): 1101-1112.

Fishman, M. L., Chau, H. K., Hoagland, P. D., Hotchkiss, A. T. (2006) Microwave-assisted extraction of lime pectin. Food Hydrocolloids, 20(8): 1170-1177.

Fishman, M.L., Chau, H.K, Hoagland, P., Ayyad, K. (2000) Characterization of pectin, flash-extracted from orange albedo by microwave heating, under pressure. Carbohydrate Research, 323: 126–138.

Fishman, M.L., Walker, P.N., Chau, H.K., Hotchkiss, A.T. (2003) Flash extraction of pectin from orange albedo by steam injection. Biomacromolecules, 4(4): 880–889.

Fraser, G. E. (1994) Diet and coronary heart disease: beyond dietary fats and low-density-lipoprotein cholesterol. The American Journal of Clinical Nutrition, 59(5): 1117S-1123S.

Gardner, D. F., Schwartz, L., Krista, M., Merimee, T. J. (1984) Dietary pectin and glycemic control in diabetes. Diabetes Care, 7(2): 143–146.

Garg, G., Singh, A., Kaur, A., Singh, R., Kaur, J., Mahajan, R. (2016) Microbial pectinases: an ecofriendly tool of nature for industries. 3 Biotech, 6(1): 47.

Gnanasambandam, R., Proctor, A. (2000) Determination of pectin degree of esterification by diffuse reflectance Fourier transform infrared spectroscopy. Food Chemistry, 68: 327–332.

Grassino, A. N., Brnčić, M., Vikić-Topić, D., Roca, S., Dent, M., Brnčić, S. R. (2016) Ultrasound assisted extraction and characterization of pectin from tomato waste. Food Chemistry, 198: 93-100.

Greco, C., Vona, R., Cosimelli, M., Matarrese, P., Straface, E., Scordati, P., Giannarelli, D., Casale, V., Assisi, D., Mottolese, M., Moles, A., Malorni, W. (2004) Cell surface overexpression of galectin-3 and the presence of its ligand 90k in the blood plasma as determinants in colon neoplastic lesions. Glycobiology, 14: 783–792.

Hosseini, S. S., Khodaiyan, F., Kazemi, M., Najari, Z. (2019) Optimization and characterization of pectin extracted from sour orange peel by ultrasound assisted method. International Journal of Biological Macromolecules, 125: 621-629.

Hosseini, S. S., Khodaiyan, F., Yarmand, M. S. (2016a) Aqueous extraction of pectin from sour orange peel and its preliminary physicochemical properties. International Journal of Biological Macromolecules, 82: 920-926.

Hosseini, S. S., Khodaiyan, F., Yarmand, M. S. (2016b) Optimization of microwave assisted extraction of pectin from sour orange peel and its physicochemical properties. Carbohydrate Polymers, 140: 59-65.

Inohara, H., Raz, A. (1994) Effects of natural complex carbohydrate (citrus pectin) on murine melanoma cell properties related to galectin-3 functions. Glycoconjugate Journal, 11: 527–532.

Jackson, C.L., Dreaden, T.M., Theobald, L.K., Tran, N.M., Beal, T.L., Eid, M., Gao, M.Y., Shirley, R.B., Stoffel, M.T., Kumar, M.V., Mohnen, D. (2007) Pectin induces apoptosis in human prostate cancer cells: Correlation of apoptotic function with pectin structure. Glycobiology, 17: 805–819.

Johnson, E. J., Dorot, O., Liu, J., Chefetz, B., Xing, B. (2007) Spectroscopic characterisation of aliphatic moieties in four plant cuticles. Communication in Soil science and Plant Analysis, 38: 2461–2478.

Kanmani, P., Dhivya, E., Aravind, J., Kumaresan, K. (2014) Extraction and analysis of pectin from citrus peels: augmenting the yield from *Citrus limon* using statistical experimental design. Iranica Journal of Energy and Environment, 5 (3): 303-312.

Kapoor, S., Dharmesh, S. M. (2017) Pectic oligosaccharide from tomato exhibiting anticancer potential on a gastric cancer cell line: structure-function relationship. Carbohydrate Polymers, 160: 52-61.

Kermani, Z. J., Shpigelman, A., Pham, H. T. T., Van Loey, A. M., Hendrickx, M. E. (2015) Functional properties of citric acid extracted mango peel pectin as related to its chemical structure. Food Hydrocolloids, 44: 424-434.

Kim, W. C., Lee, D. Y., Lee, C. H., Kim, C. W. (2004) Optimization of narirutin extraction during washing step of the pectin production from citrus peels. Journal of Food Engineering, 63(2): 191-197.

Kirby, A. R., MacDougall, A. J., Morris, V. J. (2008) Atomic force microscopy of tomato and sugar beet pectin molecules. Carbohydrate Polymers, 71: 640-647.

Kpodo, F. M., Agbenorhevi, J. K., Alba, K., Bingham, R. J., Oduro, I. N., Morris, G. A., Kontogiorgos, V. (2017) Pectin isolation and characterization from six okra genotypes. Food Hydrocolloids, 72: 323-330.

Kratchanova, M., Pavlova, E., Panchev, I. (2004) The effect of microwave heating of fresh orange peels on the fruit tissue and quality of extracted pectin. Carbohydrate Polymers, 56(2): 181-185.

Kuwabara, I., Liu, F.T. (1996) Galectin-3 promotes adhesion of human neutrophils to laminin. Journal of Immunology, 156: 3939–3944.

Lefsih, K., Giacomazza, D., Dahmoune, F., Mangione, M. R., Bulone, D., San Biagio, P. L., Passantino, R., Costa, M.A., Guarrasi, V., Madani, K. (2017) Pectin from *Opuntia ficus indica*: Optimization of microwave-assisted extraction and preliminary characterization. Food Chemistry, 221: 91-99.

Li, J., Li, S., Liu, S., Wei, C., Yan, L., Ding, T., Linhardt, R. J., Liu, D., Ye, X. Chen, S. (2019) Pectic oligosaccharides hydrolyzed from citrus canning processing water by Fenton reaction and their antiproliferation potentials. International Journal of Biological Macromolecules, 124: 1025-1032.

Liew, S. Q., Ngoh, G. C., Yusoff, R., Teoh, W. H. (2016) Sequential ultrasound-microwave assisted acid extraction (UMAE) of pectin from pomelo peels. International Journal of Biological Macromolecules, 93: 426-435. .

Mallikarjuna, S. E., Dharmesh, S. M. (2018) Swallow root (*Decalepis hamiltonii*) pectic oligosaccharide (SRO1) induces cancer cell death via modulation of galectin-3 and survivin. Carbohydrate Polymers, 186: 402-410.

Maran, J. P., Sivakumar, V., Thirugnanasambandham, K., Sridhar, R. (2013) Optimization of microwave assisted extraction of pectin from orange peel. Carbohydrate Polymers, 97(2): 703-709.

Moorthy, I. G., Maran, J. P., Ilakya, S., Anitha, S. L., Sabarima, S. P., Priya, B. (2017). Ultrasound assisted extraction of pectin from waste *Artocarpus heterophyllus* fruit peel. Ultrasonics Sonochemistry, 34: 525-530.

Moorthy, I. G., Maran, J. P., Muneeswari, S., Naganyashree, S., Shivamathi, C. S. (2015) Response surface optimization of ultrasound assisted extraction of pectin from pomegranate peel. International Journal of Biological Macro molecules, 72: 1323-1328.

Murad, H. A., Azzaz, H. H. (2011) Microbial pectinases and ruminant nutrition. Research Journal of Microbiology, 6(3): 246-269.

Nangia-Makker, P., Honjo, Y., Sarvis, R., Akahani, S., Hogan, V., Pienta, K.J., Raz, A. (2000) Galectin-3 induces endothelial cell morphogenesis and angiogenesis. American Journal of Pathology, 156: 899–909.

Ponmurugan, K., Al-Dhabi, N. A., Maran, J. P., Karthikeyan, K., Moothy, I. G., Siva rajasekar, N., Manoj, J. J. B. (2017) Ultrasound assisted pectic polysaccharide extraction and its characterization from waste heads of *Helianthus annus*. Carbohydrate Polymers, 173: 707-713.

Rajulapati, V., Goyal, A. (2017) Molecular cloning, expression and characterization of pectin methylesterase (*Ct*PME) from *Clostridium thermocellum*. Molecular Biotechnology, 59(4-5): 128-140.

Rani, A., Baruah, R., Goyal, A. (2017) Physicochemical, antioxidant and biocompatible properties of chondroitin sulphate isolated from chicken keel bone for potential biomedical applications. Carbohydrate Polymers, 159: 11-19.

Rosenbohm, C., Lundt, I., Christensen, T. I., Young, N. G. (2003) Chemically methylated and reduced pectins: preparation, characterisation by ^{1}H NMR spectroscopy, enzymatic degradation, and gelling properties. Carbohydrate Research, 338(7): 637-649.

Sriamornsak, P. (2003) Chemistry of pectin and its pharmaceutical uses: A review. Silpakorn University International Journal, 3(1-2): 206-228.

Srivastava, P., Malviya. R. (2011) Source of pectin extraction, and its application in pharmaceutical industry. Indian journal of natural product and resources, 2: 10-18.

Voragen, A. G., Coenen, G. J., Verhoef, R. P., Schols, H. A. (2009) Pectin, a versatile polysaccharide present in plant cell walls. Structural Chemistry, 20(2): 263.

Vriesmann, L. C., de Oliveira Petkowicz, C. L. (2009) Polysaccharides from the pulp of cupuassu (*Theobroma grandiflorum*): Structural characterization of a pectic fraction. Carbohydrate Polymers, 77(1): 72-79.

Wang, M., Yuan, D., Gao, W., Li, Y., Tan, J., Zhang, X. (2013) A comparative genome analysis of PME and PMEI families reveals the evolution of pectin metabolism in plant cell walls. PLoS One, 8(8): e72082.

Wang, W., Ma, X., Xu, Y., Cao, Y., Jiang, Z., Ding, T., Ye, X. Liu, D. (2015) Ultrasound-assisted heating extraction of pectin from grapefruit peel: Optimization and comparison with the conventional method. Food Chemistry, 178: 106-114.

Wikiera, A., Mika, M., Starzyńska-Janiszewska, A., Stodolak, B. (2015) Application of Celluclast 1.5 L in apple pectin extraction. Carbohydrate Polymers, 134: 251-257.

Willats, W. G. T., Knox, J. P., Mikkelsen, J. D. (2006) Pectin: New insights into an old polymer are starting to gel. Trends in Food Science & Technology, 17(3): 97–104.

Zhang, D., Li, Y. H., Mi, M., Jiang, F. L., Yue, Z. G., Sun, Y., Fan, L., Meng, J., Zhang, X., Liu, L., Mei, Q. B. (2013) Modified apple polysaccharides suppress the migration and invasion of colorectal cancer cells induced by lipopolysaccharide. Nutrition research, 33(10): 839-848.

Zhang, L., Wang, P., Qin, Y., Cong, Q., Shao, C., Du, Z., Zhang, L., Wang, P., Qin, Y., Cong, Q., Shao, C., Du, Z., Ni, X., Li, P., Ding, K. (2017) RN1, a novel galectin-3 inhibitor, inhibits pancreatic cancer cell growth *in vitro* and in vivo via blocking galectin-3 associated signaling pathways. Oncogene, 36: 1297.

Zhang, L., Ye, X., Ding, T., Sun, X., Xu, Y., Liu, D. (2013) Ultrasound effects on the degradation kinetics, structure and rheological properties of apple pectin. Ultrasonics Sonochemistry, 20(1): 222-231.

Zhang, T., Zheng, Y., Zhao, D., Yan, J., Sun, C., Zhou, Y., Tai, G. (2016) Multiple approaches to assess pectin binding to galectin-3. International Journal of Biological Macromolecules, 91: 994-1001.

Abbreviations

UAE- Ultrasound Assisted Extraction

OPP- Orange Peel Powder

EOP- Extracted Orange Pectin

DE- Degree of Esterification

FESEM-Field Emission Scanning Electron Microscopy

BET-Brunauer–Emmett–Teller

FTIR-Fourier Transform Infrared Spectroscopy

FESEM-EDX-Field Emission Scanning Electron Microscopy-Energy-dispersive X-ray spectroscopic

HPLC-High Performance Liquid Chromatography

HPSEC-High-performance size exclusion chromatography

NMR-Nuclear magnetic resonance

DLS-Dynamic Light Scattering

TGA-Thermal Gravimetric Analysis

DTG- DSC-Differential Scanning Calorimetry

XRD-X-ray powder Diffraction

AFM-Atomic Force Microscopy

TLC-Thin Layer chromatography

ESI-MS-Electron Spray Ionization-Mass spectroscopy

POS-Pectic Oligosaccharides

PP-Pectic Polysaccharide

*Ct*PME-Recombinant Pectin Methylesterase

*Ct*PL1B- Recombinant Pectate Lyase

FUTURE PROSPECTS

Pectin methyl esterase (*Ct*PME) from *Clostridium thermocellum* characterized in this study displayed highest activity towards highly methyl esterified pectin polysaccharides. Owing to this fact, *Ct*PME can be used in various industrial processes involving degradation of pectin polysaccharides along with other pectinases such as clarification of fruit juice, stability of wine, degumming of plant fibers, extraction of citrus oils, bioscouring of cotton fabric etc.

*Ct*PME can be potential candidate for use in industrial operations. It can be used in combination with pectate lyase for degumming of jute and bioscouring of cotton fabric on large scale. *Ct*PME can be also with other pectinolytic enzymes like polygalacturonase and rhamnogalacturonan lyase for complete degradation of complex pectins for generation of value added products.

Pectin is the first layer of defense in plant cell wall. Therefore, *Ct*PME in combination with pectinolytic enzymes can be used prior to the pretreatment of hemicellulosic biomass that may provide improved yields of saccharification process. The immobilization of *Ct*PME on a suitable matrix can be useful for efficient reuse of the enzyme with enhanced thermostability and activity. This will also help in large-scale textile and food industry applications.

Pectic oligosaccharides has been identified as a potent inhibitor for colon cancer cells, hence it can be further used for targeted delivery to specific cancer cells by ligand-receptor interaction. This may increase the bioavailability of the pectic oligosaccharides and show reduction towards cancer cell proliferation. The extracted pectin from waste may also find potential polymer applications in tissue engineering and nano-material applications.

Publications from thesis

Accepted

1. **Rajulapati, V.,** Dhillon, A., kumar Gali, K., Katiyar, V., & Goyal, A. (**2020**). Green bioprocess of degumming of jute fibers and bioscouring of cotton fabric by recombinant pectin methylesterase and pectate lyases from *Clostridium thermocellum.* **Process Biochemistry.**
2. **Rajulapati**, **V**., Sharma, K., Dhillon, A., & Goyal, A. (**2018**) SAXS and homology modelling based structure characterization of pectin methylesterase a family 8 carbohydrate esterase from *Clostridium thermocellum* ATCC 27405. **Archives of Biochemistry and Biophysics**, 641, 39-49.
3. **Rajulapati, V**., & Goyal, A. (**2017**) Molecular cloning, expression and characterization of pectin methylesterase (*Ct*PME) from *Clostridium thermocellum*. **Molecular Biotechnology**, 59(4-5), 128-140.

Submitted

4. **Rajulapati**, V., Dhillon, A. & Goyal, A. Extraction and characterization of pectin from agro-waste of Orange (*Citrus reticulate*) peels and anti-cancer activity of produced pectic oligosaccharides). (submitted)

Other Publications

1. Rani, A., **Rajulapati, V**., & Goyal, A. (**2019**). Antitumor effect of chondroitin AC lyase (PsPL8A) from *Pedobacter saltans* on melanoma and fibrosarcoma cell lines by *in vitro* analysis. **Pharmacological Reports**, 71(1), 167-174.
2. Dhillon, A., **Rajulapati, V**., & Goyal, A. (**2019**). Bio-scouring of cotton fabric and enzymatic degumming of jute fibres by a thermo-alkaline recombinant rhamnogalacturonan lyase, ctrglf from *Clostridium thermocellum*. **The Canadian Journal of Chemical Engineering**, 97(5), 1043-1047.
3. Sharma, K., Antunes, I. L., **Rajulapati, V**., & Goyal, A. (**2018**). Low-resolution SAXS and comparative modeling based structure analysis of endo-β-1, 4-xylanase a family 10-glycoside hydrolase from *Pseudopedobacter saltans* comb. nov. **International Journal of Biological Macromolecules**, 112, 1104-1114.
4. Sharma, K., Antunes, I. L., **Rajulapati, V.,** & Goyal, A. (**2018**). Molecular characterization of a first endo-acting β-1, 4-xylanase of family 10 glycoside hydrolase (PsGH10A) from *Pseudopedobacter saltans* comb. nov. **Process biochemistry**, 70, 79-89.
5. Dhillon, A., Sharma, K., **Rajulapati, V.** & Goyal, A. (**2018**). The multi-ligand binding first family 35 Carbohydrate Binding Module (CBM35) of Clostridium thermocellum targets rhamnogalacturonan I. **Archives of Biochemistry and Biophysics**, 654, 194-208.
6. Balasubramaniam, K., Sharma, K., Rani, A., **Rajulapati, V.,** & Goyal, A. (**2018**). Deciphering the mode of action, structural and biochemical analysis of heparinase II/III (*Ps*PL12a) a new member of family 12 polysaccharide lyase from *Pseudopedobacter saltans*. **Annals of Microbiology**, 68(6), 409-418.
7. Gupta, A., **Rajulapati**, V. Das, D. & Goyal, A. (2017). Comparative analysis of bioethanol production involving saccharification by mixed recombinant clostridial enzymes using sugarcane leaves and kans grass as sustainable feed stocks from north-east India. **Indian Journal of Biotechnology**, 16, 199-210.

Conferences/Symposia/Meetings

1. **Vikky Rajulapati** and Arun Goyal (**2018**) Extraction, characterization and anti-cancer activity of pectic oligosaccharides produced from agro-waste of Orange (*Citrus reticulate*). 29th International Carbohydrate Symposium - ICS 2018, July 13-19, 2018, Faculty of Sciences, University of Lisbon, Portugal.
2. Ajit Kumar, Shweta Singh, **Vikky Rajulapati**, Arun Goyal (**2018**) Optimization of pretreatment of *Lantana camara* stem as lignocellulosic biomass for bioethanol. Indo-Japan Bilateral Symposium on Future Perspective of Bioresource Utilization in North-Eastern Region, February 1- 4, 2018, IIT Guwahati.
3. **Vikky Rajulapati**, Arun Dillon and Arun Goyal (**2017**) Application of recombinant pectinolytic enzymes from *Clostridium thermocellum* in textile industry. Society of Biological Committee (SBC) conference organizing by JNU Delhi, November 21-23, 2017, New Delhi, India.
4. Kedar Sharma, **Vikky Rajulapati**, Inês Lobo Antunes and Arun Goyal (**2017**) SAXS analysis and structure modelling of endo β-1,4 xylanase (*Ps*GH10A) from *Pedobacter saltans*. 86th Annual Meeting of Society for Biological Chemists, India, Nov. 16-19, Jawaharlal Nehru University, New Delhi, India.
5. **Vikky Rajulapati** and Arun Goyal (**2017**) A new family member of Carbohydrate Esterase 8, pectin methyl esterase (*Ct*PME) from *Clostridium thermocellum* and its food applications. 12th Carbohydrate Bioengineering Meeting, April 23 - 26, 2017, Audi Max, Augasse, Vienna, Austria.
6. **Vikky Rajulapati** and Arun Goyal (**2016**) Biochemical characterisation of recombinant a pectin methyl esterase (*Ct*PME), a family 8 Carbohydrate Esterase (CE8) from *Clostridium thermocellum*. International Conference on Current Trends in Biotechnology (BRSI-ICCB), December 8 - 10, 2016, VIT University, Vellore, Tamil Nadu, India.
7. **Vikky Rajulapati**, Arun Dillon and Arun Goyal (**2016**) Ultrasound assisted extraction of pectin polysaccharide from the waste fruit peels of *Citrus preticulate*, Malus domestica and Ananas comosus. 57th International Annual Conference of Association of Microbiologists of India (AMI), November 24-26, 2016, Gauhati University and the Institute of Advanced Study in Science and Technology (IASST), Assam, India.
8. Inês Lobo Antunes, **Vikky Rajulapati**, Kedar Sharma, Arun Goyal **(2015)** Cloning, expression and characeterization of a xylanase from family 10 glycoside hydrolase (GH10) from *Pedobacter Saltans* DSM12145. 56th International Annual Conference of Association of Microbiologists of India (AMI), December 7-10, 2015, Jawaher Lal Nehru University, New Delhi.
9. **Vikky Rajulapati** and Arun Goyal **(2015)** Cloning, expression and purification of recombinant pectin methyl esterase (*Ct*PME) a family 8 Carbohydrate Esterase (CE8) from *Clostridium thermocellum*.14th FAOBMB Congress 84th Annual Meeting of SBC (I) on Current Excitements in Biochemistry & Molecular Biology for Agriculture and Medicine, 24 - 30 November 2015, Hyderabad, India.
10. **Vikky Rajulapati**, Vania Fernandes, Arabinda Ghosh, Carlos M.G.A. Fontes and Arun Goyal **(2014)** Cloning and expression of novel thermostable multi-substrate specific family 81 glycoside hydrolase (GH81) from *Clostridium thermocellum* ATCC 27405. 55th Annual International Conference of AMI and National Conference on Empowering Mankind with Microbial Technologies (AMI-EMMT-2014), November 12-14, 2014, Tamil Nadu Agricultural University (TNAU), Coimbatore, Tamil Nadu, India.